A contribution to analysis and modeling of NO and N2O emissions during nitritation

Mathieu Poquet

Université Fédérale

Toulouse Midi-Pyrénées

THÈSE

En vue de l'obtention du

DOCTORAT DE L'UNIVERSITÉ DE TOULOUSE

Délivré par :

Institut National des Sciences Appliquées de Toulouse (INSA de Toulouse)

Présentée et soutenue par :
Mathieu Pocquet

le vendredi 23 janvier 2015

Titre :

A contribution to analysis and modeling of NO and N2O emissions during nitritation

---

École doctorale et discipline ou spécialité :

ED MEGEP : Génie des procédés et de l'Environnement

Unité de recherche :

Laboratoire d'Ingénierie des Systèmes Biologiques et des Procédés (LISBP Toulouse)

Directeur/trice(s) de Thèse :

Mathieu Spérandio, Professeur, INSA, Toulouse
Isabelle Queinnec, Directrice de recherche, LAAS, Toulouse

Jury :

Sylvie Gillot, Directrice de recherche, IRSTEA, Lyon - Rapporteur
Eveline Volcke, Professeur agrégé, Ghent University, Gand (Belgique) - Rapporteur
Peter A. Vanrolleghem, Professeur, Université Laval , Québec (Canada) - Président du jury

Remerciements

Les travaux qui font l'objet de ce mémoire ont été effectués au Laboratoire d'Ingénierie des Systèmes Biologiques et des Procédés (LISBP) à l'INSA de Toulouse.

Je suis très reconnaissant à Mathieu Spérandio et Isabelle Queinnec d'avoir encadré cette thèse et d'avoir rendu ces 3 années aussi agréables et enrichissantes.

Je suis également très reconnaissant à Etienne Paul qui m'a fait confiance et fut à l'origine de ma venue dans le laboratoire.

Je remercie Sylvie Gillot, Directrice de recherche à l'IRSTEA de Lyon et Eveline Volcke, Professeur agrégé à l'Université de Gent, d'avoir accepté de rapporter cette thèse et de leur investissement lors de l'analyse du manuscrit et de la soutenance. Je remercie également Peter A. Vanrolleghem, Professeur à l'Université Laval à Québec, d'avoir présidé le jury et de m'avoir accueilli au sein de son équipe pendant 3 mois.

Je remercie également les personnes qui ont contribué à ce travail : Ahlem Filali sur qui j'ai pu m'appuyer en début de thèse pour prendre en main la thématique « N_2O » ; Lisha Guo pour son aide lors de mon séjour à Québec ; Bing-Jie Ni et Zhiguo Yuan pour le travail collaboratif réalisé sur la comparaison et la calibration des modèles N_2O ainsi que Zhenjun Wu pour sa participation active à l'obtention des résultats expérimentaux de cette thèse.

Par ailleurs, je suis très reconnaissant envers l'équipe technique, Evrard Mengelle, Delphine Delagnes et Mansour Bounouba pour leur travail et leur implication. La qualité des pilotes et des appareils analytiques utilisés a été fondamentale au bon déroulement de ces travaux de recherche.

Merci également aux membres de l'équipe EAD9 qui rendent le quotidien au laboratoire si convivial et agréable : Etienne, Babeth, Claire, Mathieu, Yolaine, Evrard, Delphine, Mansour, Simon, Xav, Seb, Michel, Alexis, Anil, Hélène, Sandrine, Jillian….

Je remercie les collègues qui ont partagé de près cette expérience et qui, par leur présence au quotidien et leur amitié, tiennent une part importante dans le succès de ces travaux : Sophie, Yoan, Adèle, Matthieu et Laeti.

Enfin, je remercie ma famille, mes amis et Laure pour leur présence à mes côtés.

Scientific productions

Conferences

Analysis and modeling of process conditions influencing N_2O emission by aerobic granular sludge processes for N/DN treatment. Harbin, Chine, 23-25 Septembre 2012. *Oral presentation.* Pocquet Mathieu, Filali Ahlem, Bessière Yolaine, Guo Lisha, Queinnec Isabelle, Vanrolleghem Peter, Spérandio Mathieu. *IWA Nutrient Removal and Recovery 2012: Trends in NRR*

Modélisation de la production de protoxyde d'azote pendant les processus de nitrification / dénitrification : Application à un réacteur granulaire aérobie. Aix-en-Provence, France, 29-31 Octobre 2012. *Oral presentation.* Pocquet Mathieu, Filali Ahlem, Bessière Yolaine, Guo Lisha, Queinnec Isabelle, Vanrolleghem Peter, Spérandio Mathieu. *9^e congrès international GRUTTEE 2012*

Adaptation and identification of models for nitrous oxide (N_2O) production by autotrophic nitrite reduction. Narbonne, France, 18-20 Septembre 2013. *Oral presentation.* Pocquet Mathieu, Queinnec Isabelle, Spérandio Mathieu. *11th IWA Conference on Instrumentation Control and Automation*

Adaptation and identification of models for nitrous oxide (N_2O) production by autotrophic nitrite reduction. Lyon, France, 8-10 Octobre 2013. *Poster.* Pocquet Mathieu, Queinnec Isabelle, Spérandio Mathieu. *14^e congrès SFGP 2013*

Calibration of nitrous oxide production models with continuous long-term process data. Spa, Belgium, 30 Mars – 2 Avril 2014. *Oral presentation.* Mathieu Spérandio, Mathieu Pocquet, Lisha Guo, Peter A. Vanrolleghem, Bing-Jie Ni, Zhiguo Yuan. *4th IWA/WEF wastewater treatment (WWT) modeling*

A control system for nitrification / denitrification over nitrite in SBR with simultaneous mitigation of N_2O emissions. Kathmandu, Népal, 26-30 Octobre 2014. *Oral presentation.* M Pocquet, Z Wu, Y Bessiere, I Queinnec, X Lefebvre, M Mauret, M Spérandio. *Global Challenges: Sustainable Wastewater Treatment and Resource Recovery*

Research articles

Evaluation of different nitrous oxide production models with four continuous long-term wastewater treatment process data series. M Spérandio, M Pocquet, L Guo, B-J Ni, P A Vanrolleghem, Z Yuan. *In press, Bioprocess and Biosystems engineering*

Variation of the NO/N_2O ratio supports a two pathway model for N_2O emissions by ammonium oxidizing bacteria. M Pocquet, I Queinnec, M Spérandio. *In press, Water Research*

Patent

Method of treating an effluent by nitrification-denitrification

Inventors : *Mathieu Spérandio, Xavier Lefebvre, Michel Mauret, Evreard Mengelle, Zhenjun Wu, Mathieu Pocquet*

Résumé

L'oxyde nitreux ou N_2O est un gaz à effet de serre très puissant avec un pouvoir de réchauffement global 300 fois supérieur à celui du CO_2. L'oxyde nitrique ou NO est toxique pour les microorganismes et a un impact négatif sur l'environnement de par sa contribution à l'épuisement de la couche d'ozone. Il a récemment été reporté que, en 2010, le secteur du traitement des eaux usées était responsable de 0.22% des émissions totales de N_2O liées à l'activité humaine. Les émissions de ce secteur ont également augmenté de 25% en 20 ans et il est donc primordial de comprendre les mécanismes biologiques responsables de ces émissions dans le but de pouvoir les contrôler permettant ainsi de réduire l'impact environnemental des procédés de traitement des eaux usées.

Au niveau des stations d'épuration, le NO et le N_2O sont produits pendant l'élimination de l'azote, principalement pendant la nitrification par les bactéries ammonium oxydantes (AOB). Deux voies de production sont à l'origine de ces émissions par les AOB : (1) la voie de l'oxydation incomplète de l'hydroxylamine (notée NN) pendant l'oxydation de l'ammonium en nitrite et (2) la voie de la dénitrification autotrophe (ND) qui correspond à la réduction des nitrites en NO et N_2O. L'influence des paramètres opératoires sur ces deux voies de production constitue un sujet de recherche actuel. De plus, plusieurs modèles mathématiques décrivant soit la voie NN, soit la voie ND, ont été proposés et l'analyse de la pertinence de ces deux voies et le développement d'un modèle générique sont des enjeux majeurs.

Dans ce contexte, cette thèse se focalise sur l'étude des émissions de NO et N_2O pendant la nitrification dans un procédé SBR traitant des effluents fortement chargés en ammonium par nitrification/dénitrification. L'objectif général est d'améliorer la compréhension des mécanismes biologiques à l'origine des émissions de NO et N_2O en se basant sur une analyse des données expérimentales et leur confrontation aux modèles mathématiques. Cette confrontation a pour objectif d'évaluer les réactions biologiques mises en jeu dans ces émissions de NO et N_2O en lien avec les conditions expérimentales.

L'analyse des cycles du SBR a permis de mettre en évidence l'influence des conditions opératoires sur les émissions de NO et N_2O par les bactéries AOB. Le facteur d'émission de N_2O (N_2O-EF), qui correspond à la fraction d'ammonium éliminée qui a été transformée en N_2O, apparait être corrélé à la concentration en HNO_2. Les cycles du SBR avec les plus

grandes concentrations en HNO_2 (près de 0,9 $\mu gN.L^{-1}$) sont ceux qui ont les N_2O-EF les plus élevés (4-11%). A l'inverse, quand la concentration en HNO_2 ne dépasse pas 0,5 $\mu gN.L^{-1}$, les valeurs de N_2O-EF restent relativement faibles et inférieures à 1%.

La relation entre la concentration en oxygène dissous (DO) et le N_2O-EF montre que les N_2O-EF les plus faibles ont été obtenus à de hautes DO (entre 2,5 et 6,0 $mgO_2.L^{-1}$). Pour des DO plus faibles entre 1,0 et 2,0 $mgO_2.L^{-1}$ une variation importante du N_2O-EF entre 1% et 11% a été observée, les N_2O-EF les plus grands correspondant aux cycles avec une accumulation importante en HNO_2. En revanche, une faible corrélation a été observée entre le facteur d'émission de NO (NO-EF, calculé de façon similaire au N_2O-EF) et la concentration en HNO_2, de même qu'avec la DO. Ce facteur NO-EF varie entre 0.004% et 0.078% pour l'ensemble des cycles SBR. Ainsi, le ratio NO-EF/N_2O-EF n'est pas constant pour tous les cycles et diminue lorsque la concentration en HNO_2 augmente. Les valeurs les plus élevées de ce ratio ont été observées après injection d'hydroxylamine. Cette variation traduit une contribution différente des voies NN et ND en fonction des conditions opératoires avec une augmentation de la voie ND lorsque la concentration en HNO_2 augmente. A l'inverse, la contribution de la voie NN est maximale pour les cycles avec les ratios NO-EF/N_2O-EF les plus grands.

La confrontation de ces résultats expérimentaux aux modèles N_2O a montré que les émissions de N_2O étaient mieux décrites par les modèles basés sur la voie ND. Ces modèles permettent de décrire la relation entre le N_2O-EF et la concentration en HNO_2. En revanche, ces modèles décrivent mal les émissions de NO observées. Ces émissions de NO sont mieux décrites par le modèle basé sur la voie NN. Dans le système étudié, ces résultats suggèrent que les émissions de N_2O sont principalement associées à la voie de production ND et les émissions de NO à la voie NN. En se basant sur cette analyse, un nouveau modèle a été développé dans cette thèse. Ce modèle prend en compte les deux voies de production et permet de décrire les émissions de NO et N_2O obtenues expérimentalement. De plus, ce nouveau modèle arrive à décrire la variation du ratio NO-EF/N_2O-EF traduisant la contribution des deux voies de production en lien avec les conditions opératoires.

Abstract

Nitrous oxide (N_2O) is a key greenhouse gas (GHG) with a global warming potential 300 times stronger than carbon dioxide. Nitric oxide (NO) is toxic to micro-organisms and has a negative impact on the environment with contribution to ozone layer depletion. N_2O emissions from wastewater treatment have been reported to constitute 0.22% of the total anthropogenic N_2O emissions in 2010 and have increased for almost 25% in 20 years. It is thus important to understand the biological mechanisms involved in these emissions in order to control and reduce the environmental impacts of wastewater treatment systems.

In wastewater treatments plants, both NO and N_2O are produced during the nitrogen removal mostly by nitrification performed by ammonium oxidizing bacteria (AOB). Two production pathways are known to be responsible of these emissions by AOB: (1) the NN pathway which corresponds to the NO and N_2O production during the oxidation of ammonia to nitrite and (2) the ND pathway which corresponds to the reduction of nitrite to NO and N_2O. The influence of operating conditions on both NN and ND pathways is actually not fully elucidated. In addition, several N_2O models based on the NN or the ND pathway have been proposed and the development of a generic N_2O model is yet to be proposed.

In this context, this work aims at investigating NO and N_2O emissions during the nitrification performed in Sequencing Batch Reactors (SBR) treating ammonium rich effluents by nitrification/denitrification. The general objective of this thesis is to improve knowledge and understanding of the biological mechanisms involved in NO and N_2O production by AOB using mechanistic models coupled to designed experiments. The general strategy has consisted to confront experimental data to N_2O models based on a single pathway in order to identify AOB N_2O production pathways responsible of NO and N_2O emissions in response to environmental conditions.

The analysis of SBR cycles has highlighted the effect of operating conditions on NO and N_2O emissions during nitrification by AOB. The N_2O emission factor (N_2O-EF), which represents the fraction of nitrogen converted to N_2O during ammonium removal, appears to be correlated to the HNO_2 concentration. SBR cycles with the highest HNO_2 accumulation around 0.9 $\mu gN.L^{-1}$ are those with the highest N_2O-EF (from 4 to 11%). At a HNO_2 concentration lower than 0.5 $\mu gN.L^{-1}$ the N_2O-EF remained relatively low and below 1%.

The relation between DO and N_2O EF indicates that the lowest N_2O emission factors were obtained at high DO (from 2.5 to 6.0 $mgO_2.L^{-1}$) whereas a large variation from 1% to 11% was observed at DO between 1 and 2 $mgO_2.L^{-1}$ depending on the nitrite level. In this range, the highest N_2O emissions have been observed for cycles with the highest HNO_2 concentration. In contrast, no clear tendencies were observed for the variation of NO emission factor (NO-EF, calculated similarly to the N_2O-EF) neither with the DO nor the HNO_2 concentration. The NO-EF remained between 0.004% and 0.078% for all SBR cycles. The NO-EF/N_2O-EF ratio decreased with the increase of the HNO_2 whereas the highest value was observed after hydroxylamine injections. From these observations it comes that the decrease of this ratio reflects the increase of the ND pathway contribution on N_2O emissions with the increase of HNO_2 concentration (exacerbated at a low DO concentration). On the contrary, the contribution of the NN pathway increases for cycles with a high NO/N_2O ratio associated to a low HNO_2 accumulation.

The confrontation of these experimental observations to N_2O models based on a single pathway indicates that N_2O emissions are better described by models based on the ND pathway. These models are able to predict the relation between the N_2O-EF and the HNO_2 concentration. On the over hand, these models have difficulties to predict NO emissions observed in the SBR. These emissions are better described by the model based on the NN pathway. This suggests that the N_2O emissions are more related to the ND pathway and NO emissions to the NN pathway in the studied system. Based on these observations, a new model is proposed in this work. This model considers both the NN pathway and the ND pathway and is able to describe both NO and N_2O emissions. Moreover, this new model can catch the variation of the NO-EF/N_2O-EF ratio in relation to environmental conditions, reflecting the contribution of both NN and ND pathways on N_2O emissions.

Summary

List of figures

List of tables

Nomenclature

AMO	Ammonia monooxygenase
AOB	Ammonia-oxidizing bacteria
ASMN	Activated sludge model for Nitrogen
ASM3	Activated sludge model No. 3
AUR	Ammonia uptake rate
CH_4	Methane
CO_2	Carbon dioxide
COD	chemical oxygen demand
C/N	Ratio between organic carbon and nitrogen
DO	Dissolved oxygen
FA	Free ammonia
FNA	Free nitrous acid
GHG(s)	Greenhouse gas(es)
HNO_2	Free nitrous acid
HAO	Hydroxylamine oxidoreductase
HRT	Hydraulic retention time
IPCC	Intergovernmental Panel on Climate Change
K_La	Gas transfer coefficient
LCA	Life cycle assessment
N	Nitrogen
NOB	Nitrite-oxidizing bacteria
NH_3	Free ammonia
NH_2OH	Hydroxylamine
NH_4^+	Ammonia
NOH	Nytrosyl radical
NO_3^-	Nitrate
NO_2^-	Nitrite
NO	Nitric oxide
N_2O	Nitrous oxide
N_2	Nitrogen gas
N_2O_4	Dinitrogen tetroxide
NirK	Nitrite reductase
nirK	Nitrite reductase gene
Nor	Nitric oxide reductase
nor	Nitric oxide reductase gene
NN	Hydroxylamine pathway
ND	Nitrite reduction pathway
N_2OR	N_2O production rate
NO-EF	NO emission factor
N_2O-EF	N_2O emission factor
NO/N_2O	Instantaneous NO to N_2O ratio
$NO\text{-}EF/N_2O\text{-}EF$	NO-EF to N_2O-EF ratio
N/DN	Nitrification and denitrification
SBR	Sequencing batch reactor
SRT	Solid retention time
TSS	Total suspended solids
VSS	Volatile suspended solids
WWTP	Wastewater treatment plant

Chapter I Introduction

1 Context

Greenhouse gases (GHGs) are gaseous constituents of the atmosphere, both natural and anthropogenic, which absorb and emit radiation toward the surface of the earth increasing the mean earth surface temperature. Anthropogenic greenhouse gas emissions have increased since the pre-industrial era, driven largely by economic and population growth, and are now higher than ever impacting tragically the climate with the increase of land and ocean surface temperatures. From 2000 to 2010, GHG emissions have increased by 2.2% per year to reach 49 GtCO2eq/yr in 2010 (Blanco et al., 2014). Nitric oxide (NO) is not considered to affect significantly the global warming but contributes to ozone layer depletion (Crutzen, 1979). In contrast, nitrous oxide (N_2O) is one of the main contributors to the climate change with a global warming potential 310 times higher than carbon dioxide and an important lifetime in the atmosphere (121 years). In 2010, N_2O was the third anthropogenic greenhouse gas most emitted (6.2%) after carbon dioxide (CO_2, 76%) and methane (CH_4, 16%), mainly by agricultural and industrial activities (Krey et al., 2014).

For all sectors, the wastewater treatment activity contributes up to 1.58% of total anthropogenic GHGs emissions. These emissions are dominated by CH_4 (86%) followed by N_2O (14%). It results that N_2O emissions from the wastewater treatment activity accounted for 0.22% of total anthropogenic GHGs in 2010 (Fischedick et al., 2014). This contribution may seem minor but it is probably underestimated. Indeed, experts involved in the IPCC (2014) report have considered, based on a full-scale measurement campaign (Czepiel et al., 1995), that around 0.5% of the incoming nitrogen was converted to N_2O (Kampschreur et al., 2009; Krey et al., 2014). Recent measurement campaigns demonstrated the high temporal and spatial variability of this emission factor, reportedly in the range of 0.01 % to more than 10% (Ahn et al., 2010; Kampschreur et al., 2009). Moreover, (M. R. J. Daelman et al., 2013) have shown that an N_2O emission factor of 2.8% of the nitrogen load constitutes up to 78% of the total climate footprint of the plant. These emissions can be much higher for systems treating high-strength wastewater with shortcut nitrification and denitrification: from 2.2% to 11.2% (Desloover et al., 2011; Kampschreur et al., 2009; Pijuan et al., 2014). From now, there are no national or international rules which limit these emissions from wastewater treatment systems. Nevertheless, these emissions and their impacts on global warming are significant and must be reduced.

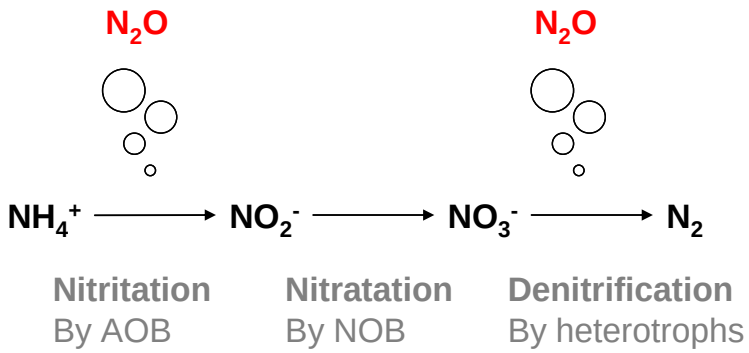

Figure 1. N_2O production during the biological nitrogen removal

N_2O is produced in wastewater treatment plants during the nitrogen removal by biological reactions. Ammonium (NH_4^+) is converted in three steps to nitrogen gas (N_2) further eliminated in the atmosphere. The first step called "nitritation" is the oxidation of ammonium to nitrite (NO_2^-) performed by ammonium oxidizing bacteria (AOB). Then nitrite is oxidized to nitrate by nitrite oxidizing bacteria (NOB) during the reaction called nitratation. These two reactions are performed under aerobic conditions and are called together "nitrification". Finally, nitrate is reduced to nitrogen gas by heterotrophs in absence of oxygen during the step called "denitrification". The production of N_2O can occur during both nitritation and denitrification. Recent studies supported the idea that nitritation contributes significantly more to N_2O production than heterotrophic denitrification in domestic wastewater treatment (Matthijs R.J. Daelman et al., 2013; Guo et al., 2013a; Kampschreur et al., 2009; Wunderlin et al., 2012), whereas heterotrophic denitrification may play also a role in the removal of N_2O produced by AOB (Guo and Vanrolleghem, 2013b).

In order to evaluate the influence of process configuration and operation on the N_2O emission, a significant effort has been recently devoted to N_2O modeling. For dynamic modeling of N_2O production, new model components have been proposed to enhance the commonly used nitrification and denitrification models at present to include various reaction intermediates such as nitrous oxide (N_2O), nitric oxide (NO) and hydroxylamine (NH_2OH). However, these models still need to be evaluated and compared. Concerning heterotrophic denitrification, N_2O and NO are known to be intermediate compounds. These compounds were included in the ASMN model proposed by (Hiatt and Grady, 2008) considering four successive steps in denitrification. In future, the combination of both nitrification and denitrification models coupled to life cycle assessments would be useful to evaluate the impact of various configuration of treatment plants on both N_2O emissions and overall GHGs emissions.

2 Research objectives and thesis organization

This thesis focuses on NO and N_2O emissions during nitritation by Ammonium-Oxidizing Bacteria (AOB) in Sequencing Batch Reactors (SBR) treating ammonium rich effluents by nitrification/denitrification. The general objective is to improve knowledge and understanding of the biological mechanisms involved in NO and N_2O production by AOB using mechanistic models coupled to designed experiments. These mechanisms are complex and the confrontation between mathematical models and experimental observations represents an appropriate approach. Concomitantly the study aims to optimize the operating conditions of the process for minimizing the N_2O emissions. The thesis is structured in five chapters, chapters 4; 5 and 6 written in the form of research publications. Specific objectives of these chapters are presented below.

Chapter II Mechanisms and models for N_2O emissions

This chapter presents the biological mechanisms involved in NO and N_2O production by AOB during nitritation and describes existing N_2O models. The objectives are (1) to present current knowledge on N_2O emissions and (2) present mathematical models used all along the document.

Chapter III Experimental and modeling material and methods

Experimental material and methods used in this work are presented in this chapter. Moreover, the calibration procedure proposed to calibrate N_2O models is presented and applied to two models based on AOB denitrification pathway. The growing concern about the dynamic modeling of N_2O production has lead to the development of new models enhancing conventional nitrification models with the consideration of intermediates such as nitrous oxide, nitric oxide and hydroxylamine (NH_2OH). The introduction of these new state variables induces new model components which can be difficult to measure or calibrate. In this context, this chapter presents the global strategy used to calibrate N_2O models and deals with potential parameters identification difficulties.

Chapter IV Evaluation of five candidate nitrous oxide production models with four continuous long-term wastewater treatment process data series

In this chapter, five N_2O models are calibrated, compared and confronted to four data sets. The objective of this study is to evaluate these models and reveal their limits and performances through their calibration using several sets of continuous long-term data collected from different systems under various process conditions. This part of the thesis is the result of an international collaboration involving the research groups model*EAU* from Université Laval in Canada with Lisha Guo and Peter Vanrolleghem and the Advanced Water Management Centre from the University of Queensland in Australia with Bing-Jie Ni and Zhiguo Yuan. Our contribution to this collaborative study corresponds to the obtention of experimental data collected in a lab-scale SBR treating an ammonium rich effluent by nitrification/denitrification over nitrite operated over 6 months and to the calibration of all N_2O models. The presentation of these data has been postponed in the chapter IV.

Chapter V Variation of the NO/N_2O ratio during nitrification: an indicator to track the N_2O production pathways

This chapter presents NO and N_2O emissions from the lab-scale SBR performing nitritation and denitrification. This chapter focuses on NO and N_2O emissions obtained under various conditions through dedicated batch experiments and various SBR operating conditions. The main objective is to understand the mechanisms of NO and N_2O emissions in such treatment process in relation with environmental conditions through the NO/N_2O ratio which could reflect the regulation between N_2O production pathways.

Chapter VI Variation of the NO/N_2O ratio supports a two-pathway model for N_2O emissions by ammonium oxidizing bacteria

The previously N_2O models calibrated are confronted to experimental data. Moreover, a new N_2O model combining the two major AOB pathways is presented and evaluated. The objective of this chapter is to evaluate if the new model is able to predict the variation of the NO/N_2O ratio in relation to environmental conditions.

Chapter II Mechanisms and models for NO and N_2O emissions

1 Introduction

The production of NO and N_2O by AOB is the result of several reactions occurring during the oxidation of ammonia to nitrite. This chapter presents first the biological reactions involved in the nitritation and details the mechanisms of NO and N_2O productions. The factors influencing these emissions are presented in the next part based on the analysis of major recent works from the literature. Finally the mathematical models developed to predict NO and N_2O emissions are presented and for some of them, errors in their original mathematical structure and highlighted and corrected.

2 Nitritation

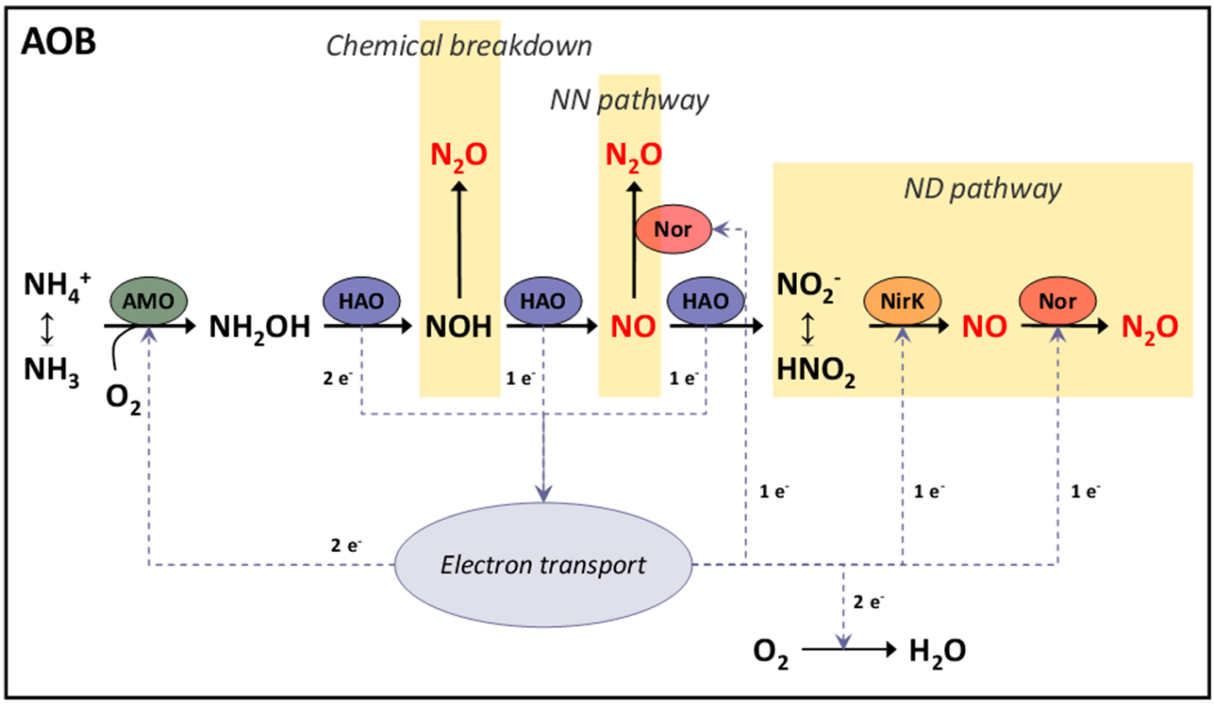

Figure 2. Schematic diagram of AOB pathways. Adapted from (Poughon et al., 2001; Ritchie and Nicholas, 1972; Schlegel and Bowien, 1989; Yu et al., 2010)

The nitrification is the process by which ammonia is oxidized to nitrite by Ammonia-Oxidizing Bacteria (AOB) (process called nitritation) further oxidized to nitrate by Nitrite-Oxidizing Bacteria (NOB) (process called nitratation). The nitritation is known to produce N_2O by AOB whereas NOB does not contribute to the N_2O production during nitrification (Colliver and Stephenson, 2000; Kampschreur et al., 2009; Law et al., 2012b).

The oxidation of ammonia to nitrite is realized thought successive enzymatic reactions by AOB represented in Figure 2. The true substrate of AOB during nitritation is ammonia (NH_3) (Suzuki et al., 1974). This unionized form is at equilibrium with ammonium (Equation 1). Ammonia is firstly oxidized to hydroxylamine (NH_2OH) by the membrane-bound enzyme ammonia monooxygenase (AMO) (Equation 2). This reaction requires 2 electrons which come from the further oxidation of hydroxylamine to nitrite. The second step corresponds to the oxidation of hydroxylamine to nitrite (Equation 3) catalyzed by the periplasmic enzyme hydroxylamine oxidoreductase (HAO) which releases 4 electrons. Two electrons are used for the ammonia oxidation and the two remaining electrons are used for energy production and reduction of oxygen to water (Equation 4).

Equation 1

$$NH_3 + H_2O \leftrightarrow NH_4^+ + OH^-$$

Equation 2

$$NH_3 + O_2 + 2H^+ + 2e^- \rightarrow NH_2OH + H_2O$$

Equation 3

$$NH_2OH + H_2O \rightarrow NO_2^- + 4e^- + 5H^+$$

Equation 4

$$\frac{1}{2}O_2 + 2H^+ + 2e^- \rightarrow H_2O$$

The oxidation of hydroxylamine to nitrite mediated by HAO is realized in 3 steps (Poughon et al., 2001; Ritchie and Nicholas, 1972), splitting the Equation 3 into three separate reactions (Equation 5, Equation 6 and Equation 7). Hydroxylamine is firstly oxidized to nitroxyl (NOH) releasing 2 electrons. Nitroxyl is then converted to NO further oxidize to nitrite. Both of these two last successive reactions release one electron. Equation 5 and Equation 6 can also be added to describe the oxidation of NH_2OH to NO in one step leading to the Equation 8.

Equation 5

$$NH_2OH \rightarrow NOH + 2e^- + 2H^+$$

Equation 6

$$NOH \rightarrow NO + e^- + H^+$$

Equation 7

$$NO + H_2O \rightarrow NO_2^- + e^- + 2H^+$$

Equation 8

$$NH_2OH \rightarrow NO + 3e^- + 3H^+$$

3 AOB NO and N_2O production pathways

During the nitritation by AOB, NO and N_2O can be produced by several enzymatic and non-enzymatic reactions. NO and N_2O can be produced during the oxidation of hydroxylamine to nitrite and by the reduction of nitrite by AOB. In addition, NO and N_2O can be produced by chemodenitrification (chemical decomposition of NH_2OH or HNO_2).

3.1 NO and N_2O production during NH_2OH oxidation

NO and N_2O can be produced during the oxidation of hydroxylamine to nitrite thought 2 reactions involving intermediates of this reaction.

First, the unstable intermediate nitroxyl (NOH) can form N_2O by chemical decomposition Equation 9 (Hooper and Terry, 1979; Poughon et al., 2001). This pathway is called “Chemical breakdown” in Figure 2.

Equation 9

$$NOH \rightarrow \frac{1}{2} N_2O + \frac{1}{2} H_2O$$

In addition, NO generated during the oxidation of hydroxylamine can be reduced to N_2O (Chandran et al., 2011; Stein, 2011). This reaction is attributed to the family of nitric oxide

reductases (Nor) (Chandran et al., 2011; Simon and Klotz, 2013). This pathway presented in Equation 10 is called "NN pathway" in Figure 2.

Equation 10

$$NO + e^- + H^+ \rightarrow \frac{1}{2} N_2O + \frac{1}{2} H_2O$$

3.2 Nitrifier denitrification

The dominant mode of energy generation by AOB is via aerobic metabolic pathways (Chain et al., 2003). However, AOB can utilize alternate electron acceptors such as nitrite or dimeric nitrogen dioxide (N_2O_4) (Anderson and Levine, 1986; Hooper et al., 1997; Kester et al., 1997; Shaw et al., 2006). The nitrifier denitrification or AOB denitrification corresponds to the reduction of nitrite to N_2O in two steps (via NO) (Poth and Focht, 1985; Wrage et al., 2001). This pathway is called "ND pathway" in Figure 2. The form HNO_2 instead of NO_2^- is considered to be the true substrate for the nitrite reduction to NO (Beaumont et al., 2004a; Shiskowski and Mavinic, 2006). Free nitrous acid (HNO_2) which is at equilibrium with NO_2^- (Equation 11) is first reduced to NO through the enzyme "nitrite reductase" (NirK) (Equation 12). Nitric oxide is subsequently reduced to N_2O through the "nitric oxide reductase" (Nor) (Equation 13). Both NirK and Nor reactions require one electron which comes from the hydroxylamine oxidation.

Equation 11

$$HNO_2 \leftrightarrow NO_2^- + H^+$$

Equation 12

$$HNO_2 + e^- + H^+ \rightarrow NO + H_2O$$

Equation 13

$$NO + e^- + H^+ \rightarrow \frac{1}{2} N_2O + \frac{1}{2} H_2O$$

3.3 Chemodenitrification

In addition to biological reactions, nitric and nitrous oxide can be produced, usually at low pH, by chemodenitrification which corresponds to the chemical decomposition of NH_2OH or HNO_2 to NO and N_2O and during a chemical reaction between NH_2OH and HNO_2 (Colliver and Stephenson, 2000; Kampschreur et al., 2009; Stüven et al., 1992; Wrage et al., 2001). These possible reactions are listed below:

Equation 14 $3HNO_2 \rightarrow HNO_3 + 2NO + H_2O$

Equation 15 $2HNO_2 \rightarrow NO + NO_2 + H_2O$

Equation 16 $NH_2OH + HNO_2 \rightarrow N_2O + 2H_2O$

Chemodenitrification is closely linked with nitritation so that it is often difficult to determine which process is involved when NO and N_2O are produced. However, the contribution of chemodenitrification was supposed to be negligible compared to the NO and N_2O produced during the NH_2OH oxidation or by AOB denitrification which are the main routes for NO and N_2O production by AOB (Kampschreur et al., 2009; Wunderlin et al., 2012).

4 Factors influencing N_2O production by AOB

Several factors have been reported to have an influence on N_2O production (Kampschreur et al., 2009; Law et al., 2012b). In contrast, the NO production by AOB in relation with operating conditions was poorly studied. It should be noted that the N_2O production is characterized in the literature by two parameters: the instantaneous N_2O production rate (N_2OR) and the N_2O emission factor (N_2O-EF) which corresponds to the fraction of nitrogen transformed to N_2O to the total amount of ammonium oxydized.

4.1 Process conditions

4.1.1 Aeration / Stripping

NO and N_2O are emitted in the gas phase and these emissions occur mostly during aerated periods (aerated compartments of a WWTP, aerobic periods of aerobic/anoxic systems) (Ahn et al., 2010; Kampschreur et al., 2009; Ye et al., 2014). N_2O is more soluble in water than NO

or O_2 with a Henry's law constant for solubility in water of 0.0240 $mol.kg^{-1}.bar^{-1}$ (at 25°C) which is more than ten times higher than those of NO and O_2 (0.0019 and 0.0013 $mol.kg^{-1}.bar^{-1}$ respectively) ("NIST Chemistry WebBook," 2005). Thus, N_2O could accumulate to higher levels in the liquid phase in the absence of active stripping in comparison to NO and O_2. It results that the N_2O produced during anoxic conditions by denitrification can be stripped during the next aerated period (Ahn et al., 2010; Law et al., 2012b; Ye et al., 2014).

4.1.2 Transition between anoxic and aerobic conditions

In biological systems using anoxic and aerobic compartments/periods to perform nitrification/denitrification, the mixed culture containing both nitrifiers and denitrifiers is exposed to repeatedly changes in aerobic and anoxic conditions leading to transient changes in the DO concentration. These transitions between anoxic and aerobic conditions can impact the NO and N_2O production by AOB (Chandran et al., 2011; Kampschreur et al., 2009; Yu et al., 2010). In addition to transient DO limitations which is known to enhance N_2O emissions by AOB (detailed below), these transitions have an impact on the gene expression of AOB, thus impacting NO and N_2O production by AOB (Chandran et al., 2011; Yu et al., 2010).

Using a pure culture of *Nitrosomonas europaea* in chemostat, (Yu et al., 2010) have investigated the effect of alternating anoxic/aerobic conditions on the expression of four genes involved in the ammonia oxidation and the NO and N_2O production by AOB. Authors have shown that the switch to anoxic conditions resulted in the cessation of ammonia oxidation (leading to the ammonia accumulation during anoxic period). The expression of the gene *NirK* increased during the anoxic period, but decreased to its previous level upon recovery to aerobic conditions. In contrast, the expression of *AMO*, *HAO*, and *Nor* uniformly decreased during the anoxic phase and recovered upon recovery to aerobic conditions, while both NO and N_2O are produced under aerobic conditions, only NO is produced by AOB under strictly anoxic conditions. Authors suggest that the presence of nitrite during the anoxic period may have resulted in the important expression of the gene *NirK*. Authors conclude that the transition to anoxia itself did not result in N_2O production by AOB, either in the absence or presence of ammonia. The N_2O is only produced upon recovery to aerobic conditions, when the reducing equivalents from NH_2OH oxidation are available again. From these observations, (Chandran et al., 2011) suggest that upon recovery to aerobic conditions in continuously ammonia fed systems, the oxidation of the accumulated ammonia results in a high substrate

consumption rate leading the transient NH_2OH accumulation. This oxidation of the accumulated NH_2OH leading to a transient important NO formation by the enzyme HAO further reduced to N_2O by the enzyme Nor (NN pathway). It can be also suggested that the imbalance between NirK and Nor enzymes upon recovery to aerobic conditions could lead to a more rapid production of NO than N_2O by the ND pathway in the presence of nitrite leading to the NO accumulation. Moreover, in the presence of heterotrophic bacteria, the NO produced by AOB during anoxic periods could be reduced to N_2O by denitrification.

4.2 Ammonia oxidation rate

As the two main N_2O production pathways of AOB occur during the oxidation of ammonia, it seems logical that the N_2OR is related to the ammonia oxidation rate (AOR) especially in a forward mechanism like the NN pathway. The relation between AOR and N_2O emission factor is less evident as the N_2OEF is related to the ratio between N_2OR and AOR. Operating conditions reported in the literature to have an influence on N_2O production such as pH, nitrite or DO concentration can also affect the AOR and it appears important to differentiate the direct or indirect effect of parameter on the N_2OR. In a recent study, (Law et al., 2012a) investigate the relation between N_2OR and the AOR using an enriched AOB culture acclimated in lab-scale SBR to high ammonium and nitrite concentrations (500 mg $N.L^{-1}$) and low DO concentration (0.5 - 0.8 $mgO_2.L^{-1}$). By varying the AOR with the ammonium concentration, ph and DO concentration, authors have found that the N_2OR was exponentially correlated to the AOR in the range of 0-300 $mgN.h^{-1}.gVSS^{-1}$. The N_2O-EF decreased from 1.0 % for the highest N_2OR to 0.2 % by reducing the maximum AOR by 20 %. Authors suggest that the culture conditions could suppress or reduce N_2O production by nitrifier denitrification and conclude that the chemical breakdown of NOH could be the dominant pathway but they also indicate that these observations could be unique to this AOB culture due to the operating conditions. However, the relation between the AOR, the N_2OR and the N_2O-EF remains unclear and following these results, the N_2OR appears to increase linearly from 0 to 0.3 $mgN\text{-}N_2O.h^{-1}.gVSS^{-1}$ with the increase of the AOR between 0 and 120 $mgN\text{-}NH_4^+.h^{-1}.gVSS^{-1}$. In that case the tendency could be also explained by the the NN pathway as the accumulation of intermediary compounds (hydroxylamine, NO) certainly increase with the AOR. If the AOR and N_2OR were linearly correlated, it would result that the N_2O-EF could be constant for this range of AOR, whereas an exponential correlation would mean that the N_2O-EF increases

with AOR. As a conclusion both the parameter N_2O-EF and the N_2OR should be calculated to analyze the positive or negative effect of operating conditions on N_2O emissions.

4.3 Nitrite and free nitrous acid NO_2^-/HNO_2

Nitrite can be used as terminal electron acceptor during the nitritation and be reduced to NO further reduced to N_2O by the ND pathway. The expression of the enzyme NirK involved in the reduction of nitrite to NO has been investigated in (Beaumont et al., 2004a) using a *Nitrosomonas europaea* batch culture with various environmental conditions. Authors have found that the nitrite concentration and the pH both affect the expressions of NirK. This expression is higher in cultures with a higher initial nitrite concentration and increases again for a similar culture performed at a lower pH (7.2 instead of 8.2). These results suggest that the HNO_2 concentration rather than the nitrite concentration could represent the main parameter which affects the expression of NirK in AOB during nitritation. More recently, (Yu and Chandran, 2010) have also demonstrated that an increase of the nitrite concentration constitute the principal trigger of the increase of the transcription of *NirK* and *Nor* genes in an AOB pure culture. In contrast, these two last studies indicate that the impact of DO on NirK and Nor expressions is not significant in comparison to the effect of nitrite. The effect of HNO_2 has also been investigated in (Shiskowski and Mavinic, 2006) and it appears that HNO_2 rather than nitrite should be considered as the electron acceptor for the ND pathway.

This difference between nitrite and HNO_2 is poorly considered in the literature and a majority of articles focus in the relation between N_2O production by AOB and the nitrite concentration rather than HNO_2. This relation is reported in several full-scale studies (Desloover et al., 2011; Kampschreur et al., 2009; Lemaire et al., 2011a; Sümer et al., 1995) and lab-scale studies using nitrifying cultures (Colliver and Stephenson, 2000; Marlies J Kampschreur et al., 2008). Some of these studies deal with the N_2O-EF and it seems clear now that an increase of the nitrite concentration (thus HNO_2 concentration) lead to an increase of the N_2O emission factor, at least in a "conventional" range of concentration from 0 to 50 mgN/L.

Recently, (Law et al., 2013) have explored a larger range of nitrite concentration between 0 and 1000 $mgN.L^{-1}$ and analyzed the effect of nitrite on the N_2OR using the similar culture of (Law et al., 2012a) presented in the previous section (Figure 3). Authors have shown that the N_2OR was highest at nitrite concentration below 50 $mgN.L^{-1}$. The increase of the nitrite

concentration from 50 to 500 mgN.L^{-1} resulted in a gradual decrease of the N_2OR until be maintained at a low value for nitrite concentrations between 500 and 1000 mgN.L^{-1}. In this last range the associated N_2O-EF was between 0.2 to 0.3% and highest N_2O-EF (0.8-1.4%) has been observed at a nitrite concentration lower than 50 mgN.L^{-1}. To explain these observations, authors suggest that the ND pathway activity is increased with the increase of the nitrite concentration until 50 mgN.L^{-1}. For nitrite concentrations higher than 50 mgN.L^{-1} they suggest the possible nitrite inhibition on the ND pathway rather than the ammonia oxidation as this rate seems unaffected in the whole range of nitrite considered. To our knowledge, this is the only article which mentions a possible inhibition of the ND pathway by an important nitrite concentration.

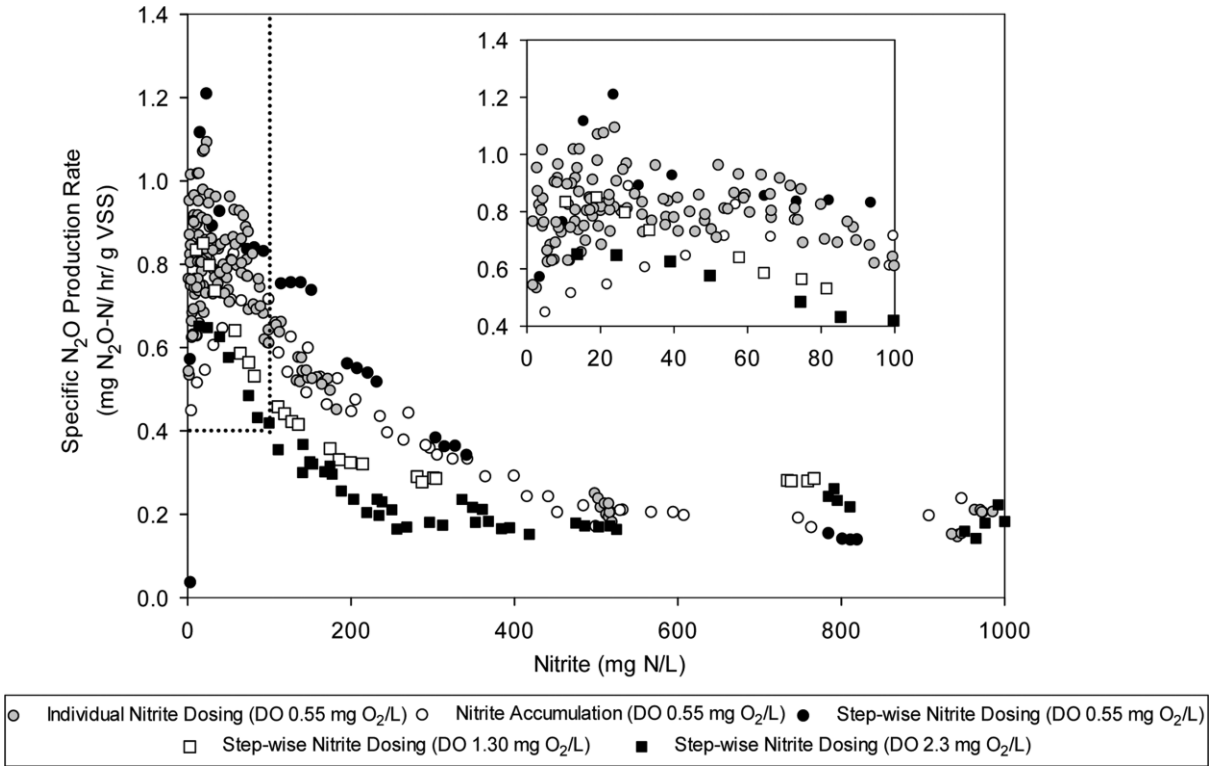

Figure 3. Experimental results of (Law et al., 2013)

The contribution of both NN and ND pathways to the N_2O emission in response to environmental conditions has been investigated with the help of isotopic methods (Sutka et al., 2006; Wunderlin et al., 2013). Using batch experiments with nitrifying activated sludge, (Wunderlin et al., 2013) have shown that the contribution of the ND pathway increased from 85% to 100% during the oxidation of 25 mgN-NH_4^+.L^{-1} at 2 mgO_2.L^{-1} in response to the progressive ammonia depletion and the accumulation of nitrite. Similar batch experiments were performed at different DO and the contribution of the ND pathway was higher for all the

conditions tested. These results confirm the key role of nitrite (thus HNO_2) on the ND pathway and highlight the influence of operating conditions on the pathways regulation.

4.4 Dissolved oxygen concentration

The effect of DO on N_2O production by AOB has been largely reported in the literature. Oxygen is used as terminal electron acceptor during the oxidation of ammonia to nitrite by AOB. Under oxygen stress, it has been shown that AOB were able to use simultaneously oxygen and nitrite as electron acceptors leading to the production of N_2O by ND pathway (Bock et al., 1995; Colliver and Stephenson, 2000; Goreau et al., 1980; Poth and Focht, 1985).

Recently, (Peng et al., 2014) have summarized different studies dealing with the effect of DO on N_2O production by nitrifying cultures and it appears that highest N_2O productions occurred at a low DO around 1.0 $mgO_2.L^{-1}$. From this analysis, authors have pointed out the difficulties to isolate the contribution of AOB to these N_2O productions as in this range of DO, heterotrophic activity could be significant leading the N_2O production and/or consumption by heterotrophic bacteria in both lab scale and full scale studies.

The effect of DO on the N_2O production by AOB during the oxidation of ammonia was investigated in (Peng et al., 2014; Wunderlin et al., 2013, 2012). Using batch experiments with an enriched nitrifying culture from a lab-scale SBR, (Peng et al., 2014) have investigated the effect of a DO range of 0.0 - 3.0 $mgO_2.L^{-1}$ on the N_2O production by AOB by quantifying both autotrophic and heterotrophic contributions. Batch experiments were performed with a similar and low nitrite accumulation allowing attributing the differences in N_2O production to the DO variation. The results of this work, mostly presented in Figure 4, revealed that for non-zero DO concentrations, the N_2OR increases with the increase of the DO similarly to the AOR which indicates a possible correlation of these two rates. However, the N_2O-EF decreases from 10.6% to 2.4% with the decrease of DO from 0.2 to 3.0 $mgO_2.L^{-1}$. It is explained by a higher N_2OR/AOR ratio at a low DO. Moreover, authors have investigated the contribution of both NN and ND pathways to the N_2O production using isotopic techniques. They have found that the ND pathway was dominant for all the batch experiments. The contribution of this pathway to the N_2O production by AOB decreases from 95% to 73% with the increase of the DO from 0.2 to 3.0 $mgO_2.L^{-1}$. Comparable results were obtained in

(Wunderlin et al., 2013, 2012) highlighting the negative effect of a low DO on the N_2O production by AOB and the contribution of both NN and ND pathways under low oxygen concentration. The 'inhibiting' effect of DO on the N_2O emissions by the ND pathway can be logically explained by the fact that there is a competition between oxygen and nitrite for accepting electrons. The role of DO on the NN pathway is still unknown and could be very different, possibly stimulated by the accelerating effect of DO on the AOR. As a consequence the effect of DO could depend on the contribution of each pathway.

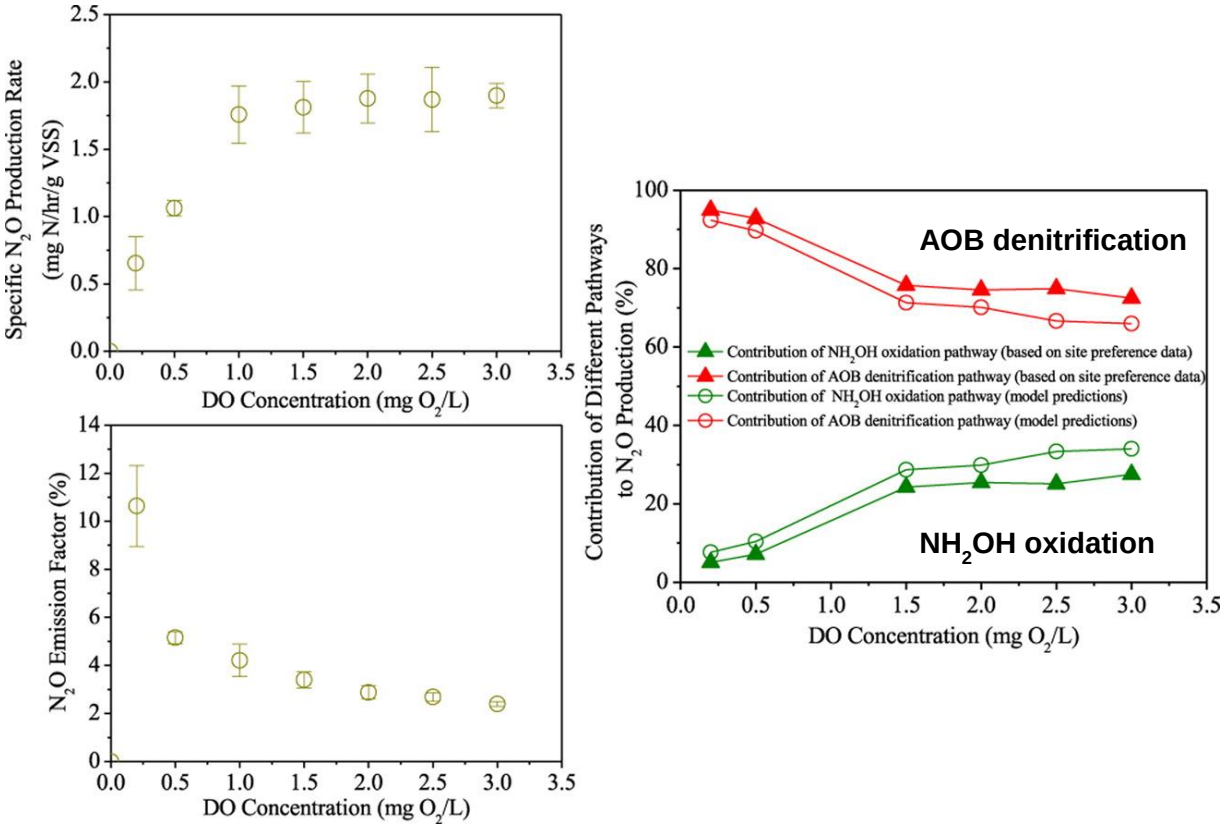

Figure 4. Experimental results of (Peng et al., 2014)

From this analysis, it can be suggested that the effect of DO is exacerbated with an important nitrite accumulation as this last parameter constitutes the main trigger in the expression of enzymes involved in the ND pathway as indicated in (Beaumont et al., 2004a; Yu and Chandran, 2010).

5 Mechanistic models for N_2O production by AOB

Several models have been proposed to describe NO and N_2O productions AOB pathways. The chemical breakdown pathway has been described by (Law et al., 2012a). The NN pathway has been described by the model of (Ni et al., 2013a). The ND pathway has been described by 4 models (Guo and Vanrolleghem, 2014; Mampaey et al., 2013; Ni et al., 2011; Pocquet et al., 2013). Recently, (Ni et al., 2014) has proposed a model which combines the NN pathway and the ND pathway. This model has been considered in the chapter VI of this thesis through its comparison to a new N_2O model developed in this work.

5.1 NN model – Model of Ni et al., 2013a

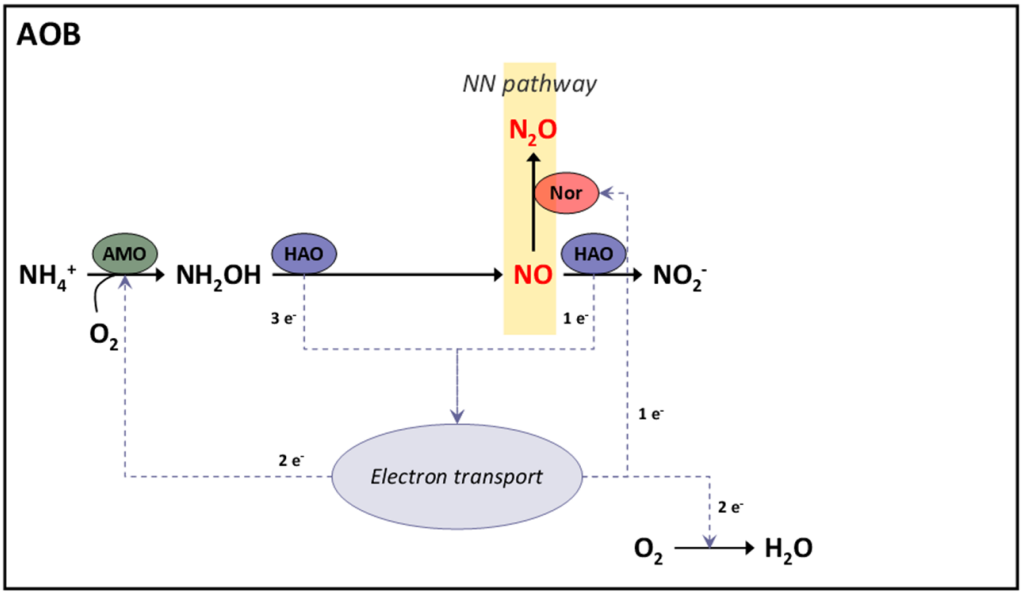

Figure 5. Schematic representation of reactions considered in the model (Ni et al., 2013a).

Table 1. Corrected stoichiometric matrix of the model (Ni et al., 2013a).

	Model Components – NN Pathway (Ni et al., 2013a)						
Process	S_{O_2}	S_{NH}	S_{NH_2OH}	S_{NO_2}	S_{NO}	S_{N_2O}	X_{AOB}
1	$-8/7$	-1	1				
2	$-\frac{12/7 - Y_{AOB}}{Y_{AOB}}$	$-i_{N,AOB}$	$-\frac{1}{Y_{AOB}}$		$\frac{1}{Y_{AOB}}$		1
3	$-4/7$			1	-1		
4			-1	1	-4	4	

Table 2. Kinetic rate equations of the model (Ni et al., 2013a).

Process	**Kinetic rate expressions – NN Pathway** (Ni et al., 2013a)
1	$\mu_{AOB,AMO} \cdot \frac{S_{O_2}}{K_{O_2,AOB,1} + S_{O_2}} \cdot \frac{S_{NH_4}}{K_{NH_4,AOB} + S_{NH_4}} \cdot X_{AOB}$
2	$\mu_{AOB,HAO,1} \cdot \frac{S_{O_2}}{K_{O_2,AOB,2} + S_{O_2}} \cdot \frac{S_{NH_2OH}}{K_{NH_2OH,AOB} + S_{NH_2OH}} \cdot X_{AOB}$
3	$\mu_{AOB,HAO,2} \cdot \frac{S_{O_2}}{K_{O_2,AOB,2} + S_{O_2}} \cdot \frac{S_{NO}}{K_{NO,AOB} + S_{NO}} \cdot X_{AOB}$
4	$\eta_{AOB} \cdot \mu_{AOB,HAO,1} \cdot \frac{S_{NH_2OH}}{K_{NH_2OH,AOB} + S_{NH_2OH}} \cdot \frac{S_{NO}}{K_{NO,AOB} + S_{NO}} \cdot X_{AOB}$

This model describes the N_2O produced by the NN pathway (i.e. via NO produced during the NH_2OH oxidation) and the nitritation in 3 steps. The ammonium form (considered as the substrate) is firstly oxidized to hydroxylamine (process 1). Then, hydroxylamine is oxidized to NO (process 2) which is further oxidized to nitrite (process 3). A fraction of NO produced by the process 2 is reduced to N_2O by the enzyme "Nor" considered in the process 4. This last process considers the oxidation of hydroxylamine to nitrite in one step and combines this oxidation with the reduction of NO to N_2O. Hydroxylamine is here considered to be the electron donor who released 4 electrons which are consumed by NO as terminal electron acceptor (one electron is necessary to reduce NO to N_2O, leading to the reduction of 4 NO to 4 N-N_2O during the oxidation of 1 NH_2OH to 1 NO_2^-). All process of this model consumed oxygen except the process 4. In the process 1, oxygen is consumed by the enzyme "AMO" to oxidize ammonia to hydroxylamine. In the processes 2 and 3, oxygen is used as terminal electron acceptor.

Errors from the original model published in (Ni et al., 2013a) have been corrected in this work. The growth of AOB was over-estimated in the original model, appearing in both process 2 and 3, thus involving that, for 1 gN-NH_4^+.L^{-1} oxidized, $2 \times Y_{AOB}$ gX_{AOB}.L^{-1} was produced. In this work, the growth of AOB has been considered to occur only during the oxidation of NH_2OH to NO (process 2) without major modifications (with "-$i_{N,AOB}$" instead of "$i_{N,AOB}$" for the state variable "S_{NH}"). In contrast, stoichiometry and kinetic of the process 3 are different as the growth of AOB has been removed from the original model of (Ni et al., 2013a). As a result, the rate in process 3 is now different to those of process 2 ($\mu_{AOB,HAO,2} = \mu_{AOB,HAO,1}/Y_{AOB}$).

5.2 Chemical breakdown model – Model of Law et al., 2012

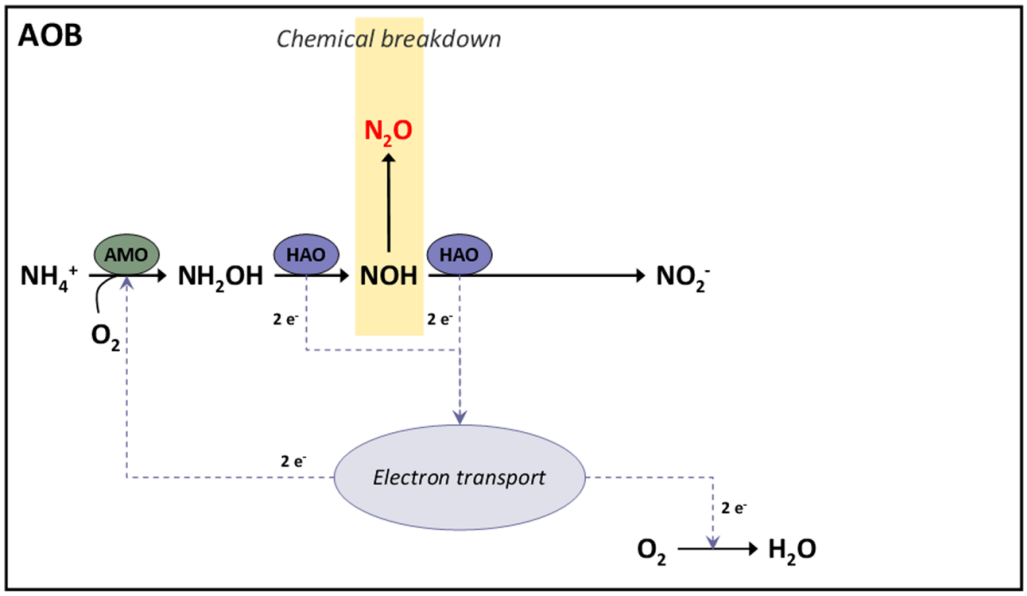

Figure 6. Schematic representation of reactions considered in the model (Law et al., 2012a).

This model considers the N_2O production from the chemical decomposition of the unstable intermediate NOH accumulated during the oxidation of NH_2OH to nitrite. In comparison to the previous model also based on the NH_2OH oxidation, this model does not consider the growth of AOB. In addition, the N_2O production rate is composed by a first order term on NOH whereas the model of (Ni et al., 2013a) considers a Monod term on NO reflecting the enzymatic reduction rate of NO to N_2O.

Recently, these models were compared in (Ni et al., 2013a) and the results of their confrontation to different set of experiments indicate that these models have similar capacities to predict N_2O emissions except for only one extreme condition. Indeed, only the NH_2OH/NOH pathway can explain N_2O productions of nitrification batch experiments (500 $mgN\text{-}NH_4^+.L^{-1}$) observed for AOR higher than 250 $mgN\text{-}NH_4^+.hr^{-1}.gVSS^{-1}$. However, authors underlined that these observations (obtained under extreme operating conditions very infrequent) could be unique to the culture used in this set of experimental data (Law et al., 2012a). For more "classic" conditions, the model based on the NN pathway (i.e. the NH_2OH/NO model) is recommended (Ni et al., 2013b). In this way, this thesis only considers

the NN pathway model proposed by (Ni et al., 2013a) for the description of N_2O emissions occurring during the oxidation of NH_2OH.

Table 3. Stoichiometric matrix of the model (Law et al., 2012a).

	Model Components – NOH chemical breakdown (Law et al., 2012a)					
Process	S_{O_2}	S_{NH}	S_{NH_2OH}	S_{NOH}	S_{NO_2}	S_{N_2O}
1	-1	-1	1			
2			-1	1		
3				-1	1	
4				-1		$\frac{1}{2}$
5	-1					

Table 4. Kinetic rate equations of the model (Law et al., 2012a).

Process	**Kinetic rate expressions – NOH chemical breakdown** (Law et al., 2012a)
1	$q_{AOB,1,\max} \cdot \frac{S_{O_2}}{K_{O_2,AOB,1} + S_{O_2}} \cdot \frac{S_{NH_4}}{K_{NH_4,AOB} + S_{NH_4}} \cdot X_{AOB}$*
2	$q_{AOB,2,\max} \cdot \frac{S_{O_2}}{K_{O_2,AOB,2} + S_{O_2}} \cdot \frac{S_{NH_2OH}}{K_{NH_2OH,AOB} + S_{NH_2OH}} \cdot X_{AOB}$
3	$q_{AOB,3,\max} \cdot \frac{S_{O_2}}{K_{O_2,AOB,3} + S_{O_2}} \cdot \frac{S_{NOH}}{K_{NOH,AOB} + S_{NOH}} \cdot X_{AOB}$
4	$q_{AOB,4,\max} \cdot S_{NOH} \cdot X_{AOB}$
5	$\frac{1}{2} R2 + R3 - R1$
	*if R1> R2 + R3 then R1 = R2 + R3

5.3 Nitrifier denitrification model (ND pathway)

Two major models have been proposed to describe the N_2O production by the AOB denitrification pathway (ND). The models proposed by (Ni et al., 2011) and (Mampaey et al., 2013) have been adapted in (Pocquet et al., 2013) and (Guo and Vanrolleghem, 2014) respectively.

5.3.1 Model of Ni et al., 2011

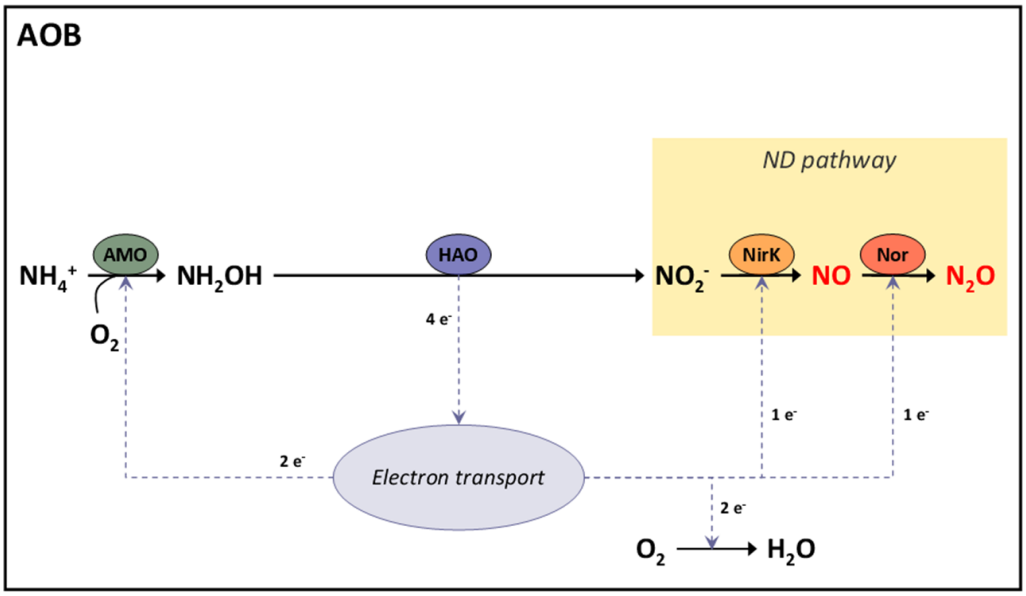

Figure 7. Schematic representation of reactions considered in the model (Ni et al., 2011).

Table 5. Stoichiometric matrix of the model (Ni et al., 2011).

	Model Components – ND Pathway (Ni et al., 2011)						
Process	S_{O_2}	S_{NH}	S_{NH_2OH}	S_{NO_2}	S_{NO}	S_{N_2O}	X_{AOB}
1	$-8/7$	-1	1				
2	$-\frac{16/7 - Y_{AOB}}{Y_{AOB}}$	$-i_{N,AOB}$	$-\frac{1}{Y_{AOB}}$	$\frac{1}{Y_{AOB}}$			1
3			-1	-3	4		
4			-1	1	-4	4	

Table 6. Kinetic rate equations of the model (Ni et al., 2011).

Process	**Kinetic rate expressions – ND Pathway** (Ni et al., 2011)
1	$\mu_{AOB,AMO} \cdot \frac{S_{O_2}}{K_{O_2,AOB,1} + S_{O_2}} \cdot \frac{S_{NH_4}}{K_{NH_4,AOB} + S_{NH_4}} \cdot X_{AOB}$
2	$\mu_{AOB,HAO} \cdot \frac{S_{O_2}}{K_{O_2,AOB,2} + S_{O_2}} \cdot \frac{S_{NH_2OH}}{K_{NH_2OH,AOB} + S_{NH_2OH}} \cdot X_{AOB}$
3	$\eta_{AOB} \cdot \mu_{AOB,HAO} \cdot \frac{K_{I,O_2,AOB}}{K_{I,O_2,AOB} + S_{O_2}} \cdot \frac{S_{NH_2OH}}{K_{NH_2OH,AOB} + S_{NH_2OH}} \cdot \frac{S_{NO_2}}{K_{NO_2,AOB} + S_{NO_2}} \cdot X_{AOB}$
4	$\eta_{AOB} \cdot \mu_{AOB,HAO} \cdot \frac{K_{I,O_2,AOB}}{K_{I,O_2,AOB} + S_{O_2}} \cdot \frac{S_{NH_2OH}}{K_{NH_2OH,AOB} + S_{NH_2OH}} \cdot \frac{S_{NO}}{K_{NO,AOB} + S_{NO}} \cdot X_{AOB}$

In this model, the nitritation is described in two steps. The first step corresponds to the oxidation of the ammonium form to hydroxylamine similarly to the NN pathway model of (Ni et al., 2013a). Then, hydroxylamine is oxidized to nitrite releasing 4 electrons which are consumed by oxygen as terminal electron acceptor (process 2). During this oxidation, this model considers the growth of AOB. The N_2O production by the ND pathway is described by 2 processes. Instead of oxygen, nitrite and NO are used as terminal election acceptor in processes 3 and 4. Nitrite is reduced in process 3 to NO by the enzyme "NirK". This process combines the oxidation of NH_2OH (electron donor) to NO_2^- which releases 4 electrons, and the reduction of NO_2^- (electron acceptor) to NO which consumes 1 electron. The process 4 describes the reduction of NO to N_2O by the enzyme "Nor". Note that, in contrast with the NN model (Ni et al., 2013a), the reduction of NO to N_2O by the enzyme "Nor" was here considered to be inhibited by oxygen. The oxygen is also considered to be an inhibitor to the first reduction of nitrite to NO by the enzyme "NirK".

5.3.2 Adaptation by Pocquet et al., 2013

Table 7. Kinetic rate equations of the model (Pocquet et al., 2013).

Process	**Kinetic rate expressions – ND Pathway** (Pocquet et al., 2013)
1	$\mu_{AOB,AMO} \cdot \frac{S_{O_2}}{K_{O_2,AOB,1} + S_{O_2}} \cdot \frac{S_{NH_3}}{K_{NH_3,AOB} + S_{NH_3}} \cdot X_{AOB}$
2	$\mu_{AOB,HAO} \cdot \frac{S_{O_2}}{K_{O_2,AOB,2} + S_{O_2}} \cdot \frac{S_{NH_2OH}}{K_{NH_2OH,AOB} + S_{NH_2OH}} \cdot X_{AOB}$
3	$\eta_{AOB} \cdot \mu_{AOB,HAO} \cdot \frac{S_{NH_2OH}}{K_{NH_2OH,AOB} + S_{NH_2OH}} \cdot \frac{S_{HNO_2}}{K_{HNO_2,AOB} + S_{HNO_2}} \cdot X_{AOB}$
4	$\eta_{AOB} \cdot \mu_{AOB,HAO} \cdot \frac{S_{NH_2OH}}{K_{NH_2OH,AOB} + S_{NH_2OH}} \cdot \frac{S_{NO}}{K_{NO,AOB} + S_{NO}} \cdot X_{AOB}$

This model is based on the ND model of (Ni et al., 2011). The stoichiometric matrix is unchanged in this adaptation and only the rates of processes have been modified. First, the true substrate NH_3 for AOB (Anthonisen et al., 1976) has been considered leading to a Monod term on the form NH_3 in the rate of the process 1 (in substitution to a Monod term on NH_4^+). Two others modifications have been brought to the description of NO and N_2O production

rates (processes 3 and 4). The form HNO_2 instead of NO_2^- has been considered to be the true substrate for the nitrite reduction to NO (Lemaire et al., 2011a; Shiskowski and Mavinic, 2006). It results in Monod term on HNO_2 in the rate of process 3. The last modification has consisted to not consider the inhibition terms of oxygen in the rates of processes 3 and 4 initially present in the model proposed in (Ni et al., 2011). This was initially supported by the fact that the model was used (chapter III and IV) for the description of responses obtained in aerobic conditions in a relatively small range of DO.

5.3.3 Model of Mampaey et al., 2013 (Assumption A)

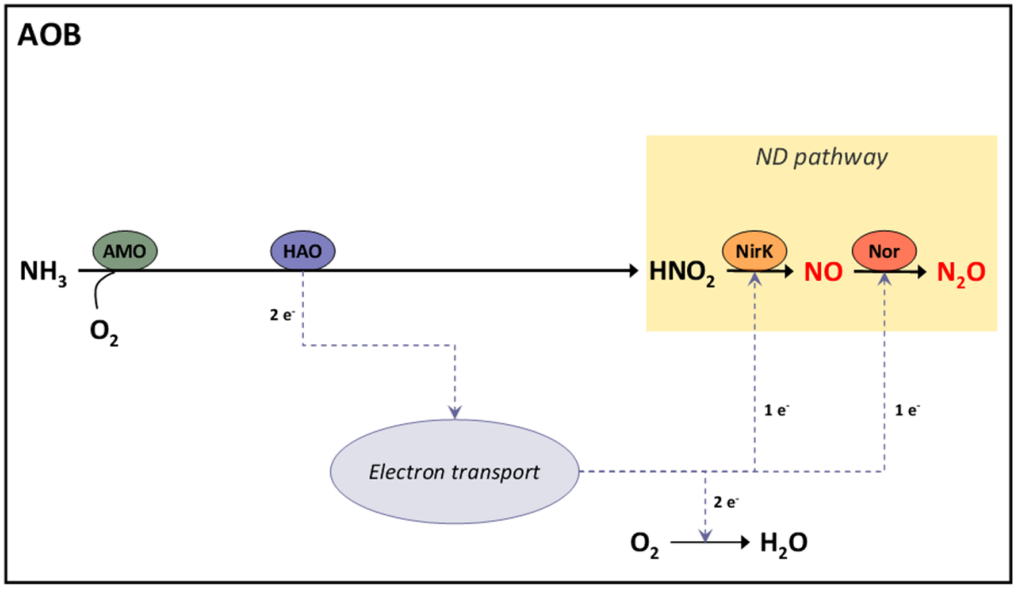

Figure 8. Schematic representation of reactions considered in the model (Mampaey et al., 2013).

Table 8. Stoichiometric matrix of the model (Mampaey et al., 2013).

	Model Components – ND Pathway (Mampaey et al., 2013)					
Process	S_{O_2}	S_{NH}	S_{NO_2}	S_{NO}	S_{N_2O}	X_{AOB}
1	$-\frac{24/7 - Y_{AOB}}{Y_{AOB}}$	$-\frac{1}{Y_{AOB}} - i_{N,AOB}$	$\frac{1}{Y_{AOB}}$			1
2	$-\frac{16/7 - Y_{AOB,den}}{Y_{AOB,den}}$	$-\frac{1}{Y_{AOB,den}} - i_{N,AOB}$	$-\frac{1}{Y_{AOB,den}}$	$\frac{2}{Y_{AOB,den}}$		1
3	$-\frac{16/7 - Y_{AOB,den}}{Y_{AOB,den}}$	$-\frac{1}{Y_{AOB,den}} - i_{N,AOB}$	$\frac{1}{Y_{AOB,den}}$	$-\frac{2}{Y_{AOB,den}}$	$\frac{2}{Y_{AOB,den}}$	1

Table 9. Kinetic rate equations of the model (Mampaey et al., 2013).

Process	**Kinetic rate expressions – ND Pathway** (Mampaey et al., 2013)
1	$\mu_{AOB} \cdot \frac{S_{O_2}}{K_{O_2,AOB} + S_{O_2}} \cdot \frac{S_{NH_3}}{K_{NH_3,AOB} + S_{NH_3}} \cdot X_{AOB}$
2	$\eta_{AOB} \cdot \mu_{AOB} \cdot \frac{S_{O_2}}{K_{O_2,AOB} + S_{O_2}} \cdot \frac{S_{NH_3}}{K_{NH_3,AOB} + S_{NH_3}} \cdot \frac{S_{HNO_2}}{K_{HNO_2,AOB} + S_{HNO_2}} \cdot X_{AOB}$
3	$\eta_{AOB} \cdot \mu_{AOB} \cdot \frac{S_{O_2}}{K_{O_2,AOB} + S_{O_2}} \cdot \frac{S_{NH_3}}{K_{NH_3,AOB} + S_{NH_3}} \cdot \frac{S_{NO}}{K_{NO,AOB} + S_{NO}} \cdot X_{AOB}$

This model considers the oxidation of ammonia to nitrite in one step (process 1). The growth of AOB is considered in this process which considers also the form NH_3 as the true substrate for AOB (leading to a Monod term on NH_3 in the process rate). The processes 2 and 3 describe the AOB denitrification pathway with the reduction of nitrite to NO in the process 2 and the reduction of NO to N_2O in the process 3. These two reactions occur in parallel with the oxidation of ammonia and the AOB growth is also considered in these processes. Both processes 2 and 3 combine the consumption of electron donor (NH_3) and consumption of electron acceptors HNO_2 and NO respectively. It results in two electrons from the oxidation of ammonia to nitrite leading to the reduction of 2 NO_2^- and 2 NO in processes 2 and 3. As in the model of (Ni et al., 2011) adapted by (Pocquet et al., 2013), this model considers also the form HNO_2 as the true substrate for the nitrite reduction.

5.3.4 Adaptation by Guo and Vanrolleghem 2014

The model of (Mampaey et al., 2013) has been adapted in (Guo and Vanrolleghem, 2014). In this adaptation, only the rates of the processes have been modified. First, inhibitions by NH_3 and HNO_2 have been introduced during the oxidation of ammonia to nitrite (process 1). The rates of processes 2 and 3 have been also modified by the introduction of the inhibition by oxygen, leading to the substitution of the Monod term by a modified Haldane term on DO. This modification of Haldane model allows setting 1 for its maximum value (which is not possible with a traditional Haldane expression).

Table 10. Kinetic rate equations of the model (Guo and Vanrolleghem, 2014).

Process	**Kinetic rate expressions – ND Pathway** (Guo and Vanrolleghem, 2014)
1	$\mu_{AOB} \cdot \frac{S_{O_2}}{K_{O_2,AOB} + S_{O_2}} \cdot \frac{S_{NH_3}}{K_{NH_3,AOB} + S_{NH_3} + S_{NH_3}^2 / K_{I,NH_3,AOB}} \cdot \frac{K_{I,HNO_2,AOB}}{K_{I,HNO_2,AOB} + S_{HNO_2}} \cdot X_{AOB}$
2	$\eta_{AOB} \cdot \mu_{AOB} \cdot \frac{S_{NH_3}}{K_{NH_3,AOB,den} + S_{NH_3}} \cdot \frac{S_{HNO_2}}{K_{HNO_2,AOB} + S_{HNO_2}} \cdot X_{AOB} \cdot DO_{Haldane}$
3	$\eta_{AOB} \cdot \mu_{AOB} \cdot \frac{S_{NH_3}}{K_{NH_3,AOB,den} + S_{NH_3}} \cdot \frac{S_{NO}}{K_{NO,AOB} + S_{NO}} \cdot X_{AOB} \cdot DO_{Haldane}$
	$DO_{Haldane} = \frac{S_{O_2}}{K_{O_2,AOB,den} + \left(1 - 2 \cdot \sqrt{K_{O_2,AOB,den} / K_{I,O_2,AOB}}\right) \cdot S_{O_2} + S_{O2}^2 / K_{I,O_2,AOB}}$

5.4 Modeling Liquid-Gas transfer

N_2O and NO liquid-gas transfer are considered in models. The liquid gas transfers rates for N_2O and NO are presented in Equation 17 and Equation 18 respectively (in mgN/h). The N_2O and NO coefficient transfer are linked to the oxygen coefficient transfer "Kla_{O2}" by the diffusivity coefficient ratio (Spérandio and Paul, 1997) (Equation 19 and Equation 20 respectively).

Equation 17

$$r_{N_2O} = Kla_{N_2O} \cdot \left(S_{N_2O} - KH_{N_2O} \cdot \rho_{N_2O}\right)$$

Equation 18

$$r_{NO} = Kla_{NO} \cdot \left(S_{NO} - KH_{NO} \cdot \rho_{NO}\right)$$

Equation 19

$$Kla_{N_2O} = Kla_{O_2} \cdot \left(\frac{D_{N_2O}}{D_{O_2}}\right)^{0.5}$$

Equation 20

$$Kla_{NO} = Kla_{O_2} \cdot \left(\frac{D_{NO}}{D_{O_2}}\right)^{0.5}$$

NO and N_2O concentrations in water at the equilibrium are defined by the product of Henry's law constants "KH_{NO}" and "KH_{N2O}" with partial pressures of NO and N_2O in the atmosphere

"ρ_{NO}" and "ρ_{N2O}" (representative to the air at the top of the reactor). Note that the state variable S_{N2O} (concentration of N_2O in the liquid phase) is expressed in "mgN-$N_2O.L^{-1}$". For homogeneity, "KH_{N2O}" and "ρ_{N2O}" are expressed in nitrogen in the form of N_2O ("mgN-$N_2O.L^{-1}.atm^{-1}$" and "atm N-N_2O" respectively). N_2O and NO concentrations into the gas phase (Equation 21 and Equation 22 respectively) are calculated at each time step. These concentrations are proportional to N_2O and NO liquid gas transfer rates and are expressed in "ppm" unit (ppm in volume).

Equation 21

$$N_2O_g(ppm) = Kla_{N_2O} \cdot \frac{V_{reactor} \cdot (T_{reactor} + 273.15) \cdot R \cdot 10^3}{Q_{air} \cdot 2 \cdot M_N} r_{N_2O}$$

Equation 22

$$NO_g(ppm) = Kla_{NO} \cdot \frac{V_{reactor} \cdot (T_{reactor} + 273.15) \cdot R \cdot 10^3}{Q_{air} \cdot M_N} r_{NO}$$

5.5 Modeling NH_4^+/NH_3 and NO_2^-/HNO_2 balances

In solution, NH_3 and HNO_2 are at equilibrium with ammonium (NH_4^+) and nitrite (NO_2^-) respectively

Equation 23

$$NH_4^+ + OH^- \longleftrightarrow NH_3 + H_2O$$

Equation 24

$$NO_2^- + H^+ \longleftrightarrow HNO_2$$

Concentrations of NH_3 and HNO_2 depend on pH and temperature of the solution (Anthonisen et al., 1976):

Equation 25

$$[NH_3] = \left[N - NH_4^+\right]_{tot} \cdot \frac{10^{pH}}{\frac{k_b}{k_w} + 10^{pH}}$$

Equation 26

with $$\frac{k_b}{k_w} = e^{(6344/(273+T))}$$

Equation 27

$$[HNO_2] = \left[N - NO_2^-\right]_{tot} \cdot \frac{1}{1 + k_a \times 10^{pH}}$$

Equation 28

with $k_a = e^{-(2300/(273+T))}$

The negative logarithm of the acid dissociation constant (*pKa*) is 9.24 for the pair NH_4^+/NH_3 and 3.3 for the pair NO_2^-/HNO_2. Thus, when pH is basic, the forms NH_3 and NO_2^- are predominant whereas with an acid pH, the predominant forms are NH_4^+ and HNO_2.

6 Conclusion and analysis of the model structure

In this chapter, the mechanisms involved in NO and N_2O emissions during nitritation have been presented as well as major factors impacting the production of these gases. NO and N_2O are mainly produced by two pathways:

The NN pathway corresponds to the oxidation of hydroxylamine to nitrite mediated by the enzyme HAO. During this oxidation, NO can be produced then reduced by the enzyme Nor to N_2O.

The ND pathway corresponds to the reduction of nitrite to NO by the enzyme NirK following by the reduction of this NO to N_2O.

The increase of nitrite concentration was observed to stimulate N_2O emissions in a given range of concentrations, logically explained by the ND pathway. N_2O emission was also observed to be inhibited at very high nitrite level (up to 1000 mgN.L-1). Several works has reported that a low DO exacerbated N_2O emissions, but this observation was not systematically observed with full scale data. Different models have been proposed to describe these observations. In this study four models based on the ND pathway and one model based on the NN pathway will be considered in the following results. Recent findings have highlighted the regulation of these pathways in relation with environmental conditions. The ND pathway appears to be the dominant pathway in most cases and can be stimulated with the nitrite at small nitrite concentration but could be inhibited at high level. The variation of the contribution of NN and ND models can probably explain the variable effect of DO on N_2O emissions.

The models presented in this chapter were based on coupling both consumptions of electron acceptors and donors. An easy way to understand the matrix structure of each model is presented in Figure 9 associated to the Table 11 where AOB reactions which are coupled in each process are presented.

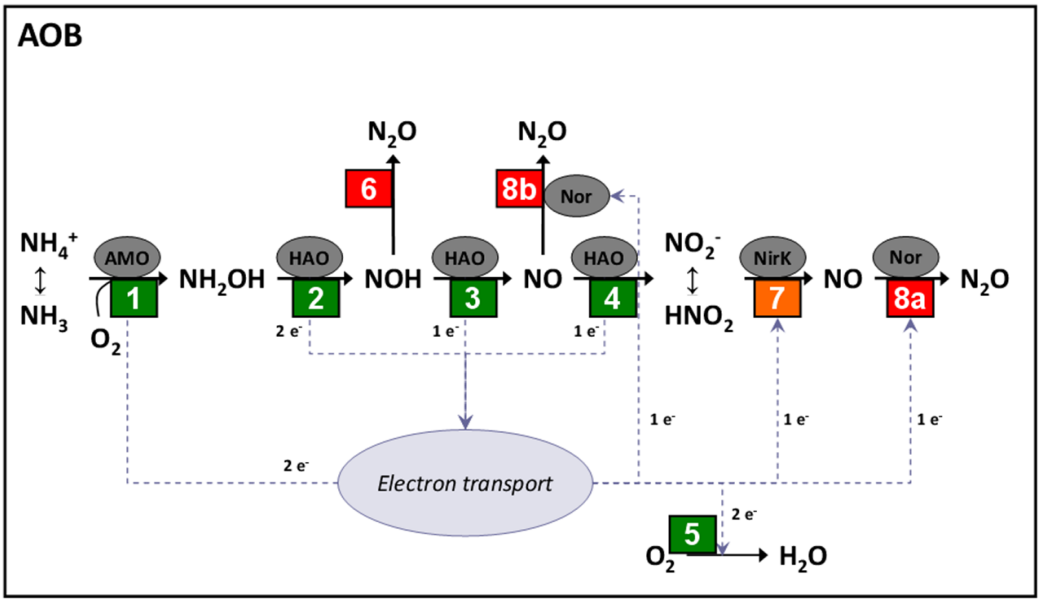

Figure 9. AOB reactions considered in AOB N_2O models

Table 11. AOB reactions considered in models processes

Model composition		
NH_2OH models		
Process	**Ni et al., 2013a**	**Law et al., 2012a**
1	1	1
2	2-3-5	2
3	4	3-4
4	1-2-3-4-8b	6
5		5
ND pathway models		
Process	**Ni et al., 2011 & Pocquet et al., 2013**	**Mampaey et al., 2013 & Guo and Vanrolleghem, 2014a**
1	1	1-2-3-4-5
2	2-3-4-5	1-2-3-4-7
3	2-3-4-7	1-2-3-4-8a
4	2-3-4-8a	

Chapter III Experimental and modeling materials and methods

1 Introduction

This chapter addresses materials and methods both in terms of experimental devices and of mathematical tools used for model calibration. The chapter is then decomposed in two parts. The first part concerns the description of the reactor used for providing experimental data, the measurements methods and apparels and briefly presents the types of experiments realized in this thesis. Details of the experiments are postponed in each chapter to facilitate the reading of the other chapters.

The second part concerns the mathematical tools used for model calibration and aims at providing a procedure for model calibration which is further used throughout the manuscript. The aspects related to the unification of two of the models based on the ND pathway presented in Chapter II are also addressed in the chapter.

2 Experimental set-up

2.1 Reactor

All experiments considered in this thesis were performed in a lab-scale bioreactor (2 litres). The reactor was equipped with mechanical mixing (Rushton type), aeration system (fine bubble), temperature regulation with water jacket (maintained at 28 ± 0.5°C) and probes in the liquid phase for pH (H8481HD from Schott) and dissolved oxygen (DO) (Visiferm DO Arc 120 from Hamilton). The air flow rate was controlled with a mass flowmeter. The off-gas was sampled at the top of the reactor at a constant flow rate of 0.2 $L.min^{-1}$ (much lower than the off-gas flow rates used in this study) for the online monitoring of NO (NGA 2000 CLD from Emerson; range 0-30 ppm; minimum detectable level: 0.1 ppm) and N_2O (X-STREAM X2GP from Emerson; range: 0-100 ppm; minimum detectable level: 0.1 ppm). Chemical species were monitored by ion chromatography (IC25, 2003, DIONEX, USA). Ammonium, VSS, and COD were determined using standard methods. A control panel connected to a computer allowed managing stirring, aeration and all inputs and outputs of the reactor. The complete experimental device is illustrated in Figure 10.

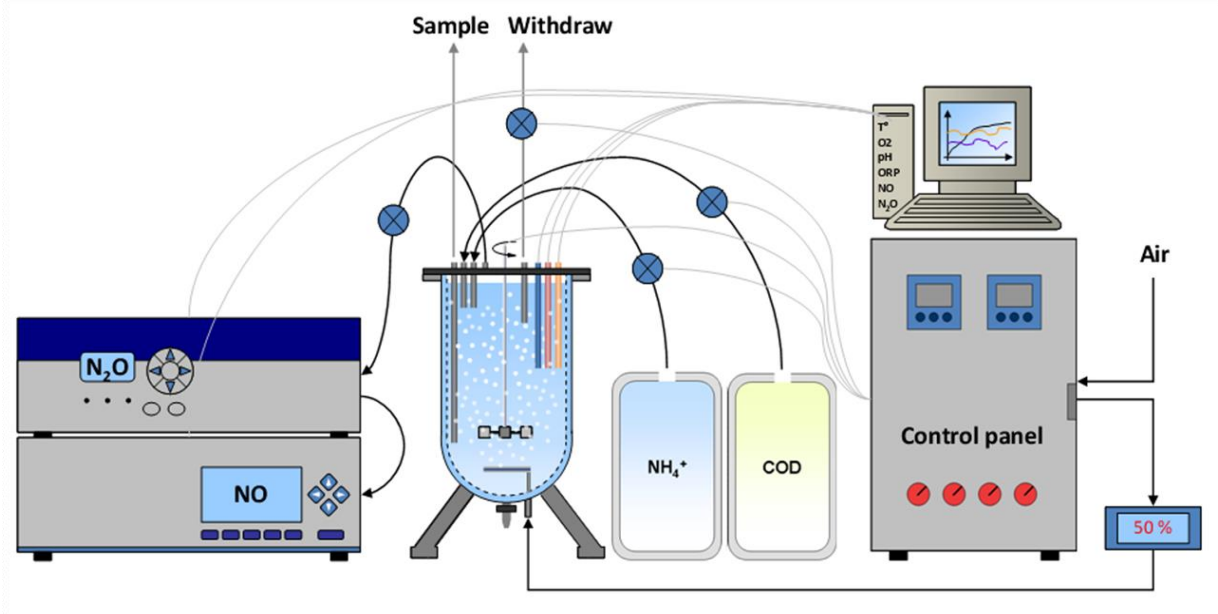

Figure 10. Experimental device for the lab-scale SBR pilot

2.2 Calculation

For each NO and N_2O gas phase concentration monitored the corresponding NO and N_2O emission rates (N_2O-ER in gN-N_2O.L^{-1}.h^{-1}, and NO-ER in gN-NO.L^{-1}.h^{-1}) were calculated:

Equation 29

$$N_2O\text{-}ER = N_2O \cdot 10^{-6} \cdot Q_{gas} \cdot Vm^{-1} \cdot 2 \cdot M_N \cdot V^{-1}$$

Equation 30

$$NO\text{-}ER = NO \cdot 10^{-6} \cdot Q_{gas} \cdot Vm^{-1} \cdot M_N \cdot V^{-1}$$

with

N_2O: N_2O gas phase concentration (ppmv)

NO: NO gas phase concentration (ppmv)

Q_{gas}: Air flow rate ($L.h^{-1}$)

Vm: Molar volume of gases ($L.mol^{-1}$)

M_N: Molar mass of nitrogen ($g.mol^{-1}$)

V: Volume of the reactor (L)

The total amounts of NO and N_2O emitted during a cycle were obtained by integration of the emission rates. Emission factors NO-EF and N_2O-EF were calculated by dividing the total amounts of NO and N_2O by the amount of ammonium removed.

3 Experimental conditions and data sets

All experimental data presented in this work have been obtained under aerobic conditions. In this study, 3 sets of experimental data obtained with two microbial cultures have been considered and detailed below as well as summarized when they are used in the next chapters.

3.1 Batch experiments – set 1

This set of experimental data corresponds to nitrification batch experiments performed with a first enriched nitrifying culture initially collected in a SBR process (300L) treating a high strength wastewater (digestate). The mixed liquor volatile suspended solid concentration of the batch experiments was 5.4gVSS.L^{-1}. The pH has varied (described later) and the temperature was controlled at 20 ± 0.5 °C. No measurement of NO was available.

The data set 1 was considered in this chapter only to set up the model calibration procedure presented later in this chapter. For each experiment, different amounts of ammonium and nitrite were imposed with different feeds of synthetic solutions: 10.50 gN-NH_4^+.L^{-1} (NH_4Cl), 11.55 gN-NO_2^-.L^{-1} ($NaNO_2$) (diluted concentrations). Conditions are presented in Table 12.

Table 12. Experimental conditions of the batch experiments.

Batch Number	N-NH_4^+ oxidized (mgN.L^{-1})	N-NO_2^- (mgN.L^{-1}) (start-max - end)	pH (start-min)	DO ($mgO_2.L^{-1}$) (start-min)	N_2O-EF (%)
1	9.4	0 - 6.3 - 0	7.86 - 7.26	7.9 - 4.5	0.18
2	9.8	0 - 6.7 - 0	7.76 - 7.15	7.9 - 4.4	0.20
3	0.0	7.6 - 7.6 - 0	7.60 - 7.60	7.9 - 7.3	0.00
4	10.3	7.7 - 12.2 - 0	7.65 - 7.03	7.9 - 4.4	0.72
5	10.6	18.6 - 18.6 -0	7.46 - 6.90	7.9 - 4.7	1.24
6	11.1	39.6 - 39.6 - 0	7.29 - 6.75	8 - 5.2	1.82

In this data set, N_2O emissions were attributed to AOB activity. Heterotrophic biomass was present but the contribution of denitrification was expected to be negligible as DO was higher than 4.4 $mgO_2.L^{-1}$ and no organic substrate was added.

3.2 SBR – sets 2 & 3

The reactor described above was operated over 6 months in sequencing batch mode (SBR) and inoculated with a sludge sample from a WWTP with stable nitrification (Graulhet, France, 50 000 PE; sludge retention time of 20 d). During all the study, the sludge retention time (SRT) was maintained at 15 d with daily wasting and the mixed liquor volatile suspended solid concentration of the SBR was maintained at approximately 4 $gVSS.L^{-1}$. The initial mixed culture volume was 1.43 L for all cycles. The pH was not controlled and the average pH for all cycles varied between 7.8 and 8.8. The SBR managed to treat an ammonium rich influent by nitrification and denitrification. The composition of this synthetic wastewater was 403.3 to 563.6 $mgN\text{-}NH_4^+.L^-$ (NH_4Cl), 4356 $mgHCO_3^-.L^{-1}$ ($NaHCO_3$), 70 $mgCa^{2+}.L^{-1}$ ($CaCl_2.2H_2O$), 45 $mgMg^{2+}.L^{-1}$ ($MgSO_4.7H_2O$), 30$mgP\text{-}PO_4^{3-}.L^{-1}$ ($Na_2HPO_4.12H_2O$ + KH_2PO_4). The second effluent rich in organic carbon used for full denitrification was a solution of whey at 18.8 $gCOD.L^{-1}$. Ammonia and COD solutions were supplied to the reactor at 20 $mL.min^{-1}$ and 6.25 $mL.min^{-1}$ respectively. The SBR cycles were composed by aerobic and anoxic periods with constant or variable lengths. Two cycle's configurations were used in this study:

Table 13. SBR cycle: Configuration 1

Action	Description	Aerated	Length (minutes)
1	Ammonia feeding	YES	10
2	Nitrification	YES	100 or controlled
3	COD feeding	NO	2.5 – 7.5
4	Denitrification	NO	180 or controlled
5	Settling	NO	20
6	Withdrawal	NO	8

Table 14. SBR cycle: Configuration 2

Action	Description	Aerated	Length (minutes)
1	Aerobic period	YES	15
2	Ammonia feeding	YES	10
3	Nitrification	YES	Controlled
4	Aerobic period	YES	20 – 40
5	COD feeding	NO	2.5 – 7.5
6	Denitrification	NO	Controlled
7	Settling	NO	20
8	Withdrawal	NO	8

The periods with variable lengths were controlled using a system allowing the automatic detection of the end of nitrification and denitrification (detailed in Appendix A with a SBR cycle operated with the configuration 1 as example). This control system is based on DO and ORP signals. The first derivative of DO and the second derivative of ORP are used to detect the end of nitrification and the end of denitrification, respectively. During nitrification, the exhaustion of ammonium induces an increase of the DO in the liquid medium which leads to an increase of $dDO.dt^{-1}$. When this rate reaches a threshold value (value defined manually), the system automatically moves to the next period of the cycle, thereby detecting the end of nitrification. At the end of denitrification, when nitrite and/or nitrate are depleted, sulfate-reducing bacteria use sulfate as final electron acceptor for the carbon consumption. As a consequence, sulfate (SO_4^{2-}) is reduced to sulfide (HS^-, H_2S) which have a strong influence on ORP. Thus, the inhibitory effect of oxygen, nitrite and nitrate on the sulfate-reducing activity allows observing a bending point on the ORP curve at the end of denitrification. In the same way, when $d^2ORP.dt^{-2}$ reaches a threshold value, the system moves to the next period. The fact that the sensor derivatives were used as an indicator makes the system insensitive to signal drift and calibration error. The first and second derivatives were calculated with linear regression associated to the "n" last data. A monitoring period of 20 seconds was used in this study with a number of data (n) for the derivative calculations of 15.

Two experimental data sets come from the SBR:

Set 2. The aerobic period of the SBR cycles has been analyzed. These cycles have been classified according to three different operating periods, depending on the cycle configuration and the phase length control being activated or not. These three periods have been analyzed in chapter V and consist of 290 cycles. This set of experimental data is also considered in chapter VI.

Set 3. This set corresponds to batch experiments using the SBR mixed culture (similar conditions of sludge concentration, pH and temperature). During the operation period of the SBR, cycles were stopped in order to perform dedicated batch experiments. This set of experimental data is considered in chapters IV, V and VI.

4 Model calibration procedure using two ND models

4.1 Models incorporating N_2O production by the ND pathway

Several models describing the N_2O production by the ND pathway have been presented in Chapter II. We consider now the two matrix structures of these ND models, the model of (Ni et al., 2011) adapted in (Pocquet et al., 2013) (noted model 1) and the model of (Mampaey et al., 2013) (noted model 2), stoichiometry and kinetics being presented in Chapter II.

Moreover, some adaptations and additional processes were considered for models extensions and homogenisation:

- Oxidation of nitrite to nitrate by NOB was included

- Assumptions were homogenized concerning the influence of pH and temperature on AOB and NOB growth. Temperature dependence has been introduced with Arrhenius-type functions for AOB and NOB growth rates. The influence of pH was considered with the dissociation of ionic and neutral forms for ammonia (NH_3) and free nitrous acid (HNO_2), which were assumed to be the true substrates for AOB and NOB. Equilibrium with ammonium (NH_4^+) and nitrite (NO_2^-) in respect with pH and temperature were included in

both models. To take into account the large range of pH variation in this set of experimental data, inhibitions of nitritation and nitratation by both NH_3 and HNO_2 were included (Anthonisen et al., 1976; Vadivelu et al., 2007, 2006).

- In model 1 (Pocquet et al., 2013), inhibition terms have been added during the oxidation of free ammonia to hydroxylamine as AMO rather than HAO is most commonly identified as the target of inhibitors during nitritation (Juliette et al., 1993; Stein and Arp, 1998).

- In model 2 (Mampaey et al., 2013), as NO and N_2O are produced during the oxidation of ammonia to nitrite, NH_3 and HNO_2 inhibition terms have been included in all processes.

- According to Activated Sludge Model 3 (ASM3) (Henze, 2000), endogenous respiration of heterotrophic and autotrophic biomass have been considered.

- Finally liquid-gas transfer for oxygen, nitric oxide and nitrous oxide was also included.

Both models have been implemented and solved with the software AQUASIM version 2.1g (Reichert, 1998). All the optimisations were also performed with AQUASIM using the parameter estimation of the software based on the minimum chi-square estimation.

4.2 Sensitivity analysis and model calibration procedure

A preliminary sensitivity analysis has been performed comparing the simulation of all batch experiments with respect to available experimental data. All state variables were considered in the analysis although only some of them were measured: nitrite, ammonium, DO and nitrate in the liquid phase, and N_2O concentration in the gas phase. In the results and discussions presented above, the N_2O and NO considered are the liquid form, but similar results can be obtained with the gaseous variables as both are linked by a transfer coefficient. The root mean square of the absolute-relative sensitivity function for each parameter was normalized by the average value of the state variable. This criterion allowed obtaining the relative influence of parameters on each state variable.

All the results are summarized in Table 15. In accordance with the examination of the models structure involving successive reaction steps, the sensitivity analysis exhibits that the parameters can be classified into three groups:

- The first group (parameters in italic in Table 15) corresponds to parameters which influence all state variables, because they directly influence the nitritation rates (μ_{AOB}; $\mu_{AOB,AMO}$; Y_{AOB} ; K_{NH3} ; $K_{O2,AOB,1}$; $K_{O2,AOB}$; $K_{O2,AOB,2}$). On the other hand, only the parameters of this group influence the dynamics of ammonia in both models and of hydroxylamine in the case of model 1.

- The second group (parameters underlined in Table 15) involves the parameters which influence nitrite, nitrate, nitric and nitrous oxide ($\underline{Y_{NOB}}$; $\underline{\mu_{NOB}}$; $\underline{K_{HNO2,NOB}}$; $\underline{\mu_{AOB,HAO}}$; $\underline{K_{O2,NOB}}$; $\underline{K_{NH2OH}}$).

- The third group (parameters in bold in Table 15) corresponds to parameters which influence the dynamics of NO and N_2O, but not significantly the other variables ($\boldsymbol{\eta_{AOB}}$; $\boldsymbol{K_{HNO2,AOB}}$; $\boldsymbol{K_{NO}}$).

Table 15. Sensitivity analysis on soluble state variables. Parameters in italic are associated to group 1, parameters underlined to group 2 and in bold to group 3. Notations "M1" and "M2" correspond to model 1 and model 2 respectively.

		Influence (%)					
State variable	**Model**	**5-50**	**50-100**	**100-150**	**150-200**	**200-250**	**250-300**
S_NH	M1	K_{NH3} Y_{AOB} $K_{O2,AOB,1}$				$\mu_{AOB,AMO}$	
	M2	K_{NH3} $K_{O2,AOB}$	μ_{AOB}		Y_{AOB}		
S_NH_2OH	M1	K_{NH3} $K_{O2,AOB,2}$ $K_{O2,AOB,1}$		K_{NH2OH}		Y_{AOB} $\mu_{AOB,HAO}$ $\mu_{AOB,AMO}$	
S_NO_2	M1	$\mu_{AOB,AMO}$ $K_{O2,NOB}$ $\mu_{AOB,HAO}$ Y_{AOB} K_{NH2OH}	$K_{HNO2,NOB}$ μ_{NOB}			Y_{NOB}	
	M2	Y_{AOB} $K_{O2,NOB}$ μ_{AOB} K_{NH3}	$K_{HNO2,NOB}$ μ_{NOB}		Y_{NOB}		
S_NO_3	M1	Y_{NOB} $K_{HNO2,NOB}$ μ_{NOB}					
	M2	Y_{NOB} $K_{HNO2,NOB}$ μ_{NOB}					
S_NO	M1	$K_{HNO2,NOB}$ $\mu_{AOB,HAO}$ **K_{NO}** K_{NH2OH} K_{NH3} $K_{O2,NOB}$	**η_{AOB}** μ_{NOB} Y_{AOB}	**$K_{HNO2,AOB}$** $\mu_{AOB,AMO}$ Y_{NOB}			
	M2	μ_{AOB} $K_{HNO2,NOB}$ **K_{NO}** K_{NH3} $K_{O2,NOB}$ $K_{O2,AOB}$	Y_{NOB} **η_{AOB}** μ_{NOB} Y_{AOB}	**$K_{HNO2,AOB}$**			
S_N_2O	M1	$K_{HNO2,NOB}$ K_{NH3} **K_{NO}** $K_{O2,AOB,2}$ $K_{O2,AOB,1}$ $K_{O2,NOB}$	$\mu_{AOB,HAO}$ μ_{NOB} Y_{NOB} K_{NH2OH}	**$K_{HNO2,AOB}$**		Y_{AOB} $\mu_{AOB,AMO}$	**η_{AOB}**
	M2	K_{NH3} $K_{HNO2,NOB}$ $K_{O2,AOB}$ **K_{NO}** $K_{O2,NOB}$	μ_{NOB} Y_{NOB}	Y_{AOB} μ_{AOB} **$K_{HNO2,AOB}$**			**η_{AOB}**

Based on this classification, a 3-steps procedure was defined, which has been systematically used for calibration of the most sensitive parameters, summarized in Table 16. The first step consists to estimate the most sensitive parameters of group 1 on the ammonia measurement. Then the most sensitive parameters of group 2 are calibrated on the nitrite and nitrate concentration. Finally, in the last step, major parameters associated to the group 3 are calibrated with N_2O analysis. Parameters with low sensitivity and parameters well known in the literature were fixed at a given value.

Specific attention has to be given to sensitive parameters for N_2O modeling which are poorly described in the literature. Above all, the reduction factor η_{AOB} for AOB denitrification rate and the half saturation constant for free nitrous acid $K_{HNO2,AOB}$ are clearly the most sensitive parameters in both model 1 and 2 for N_2O prediction. For this reason a focus on the identifiability and the sensitivity of the parameter estimates is presented in the next section.
Attention should also be paid to affinity parameters associated to intermediary compounds hydroxylamine and nitric oxide which were not measured in this work, i.e. K_{NO} and K_{NH2OH}. Their low influence on the measured variables of the experimental set 1 led us to keep the values of (Ni et al., 2011) but the uncertainty is high considering the poor literature concerning these parameters.

Considering the homogenisation of the models, the main idea is to consider, as much as possible, the same numerical values for parameters of both models with the same significance. Actually, thanks to similarities in the models formulation most of the parameters values (especially in group 1 and 2) may be considered to have a similar value for both models. On the other hand considering or not the hydroxylamine as intermediary compound makes a difference in the limitation functions introduced in the expression of N_2O production rates. Indeed the N_2O production rate is related to ammonia in model 2 but to hydroxylamine in model 1 and the limitation degree imposed by these different electron donors in the kinetic rate is then different. For this reason the estimation value of the parameter ηAOB is allowed to be different in model 1 and 2.

Table 16. Model calibration steps and parameters calibrated at each step. Parameters in italic are associated to group 1, underlined to group 2 and in bold to group 3.

Calibration steps	Experimental data	Parameters calibrated		
		Model 1 & 2	Model 1	Model 2
1	$N\text{-}NH_4^+$	K_{NH3}	$\mu_{AOB,AMO}$	
2	$N\text{-}NO_2^-$ $N\text{-}NO_3^-$	$\underline{K_{HNO2,NOB}}$	$\underline{\mu_{AOB,HAO}}$	
3	$N\text{-}N_2O$	$\mathbf{K_{HNO2,AOB}}$	$\boldsymbol{\eta_{AOB}}$	$\boldsymbol{\eta_{AOB}}$

4.3 Parameter identifiability

Because of the high sensitivity of N_2O simulation to the parameters η_{AOB} and $K_{HNO2,AOB}$, their identifiability was evaluated. First a multi-start approach was chosen for optimisation. 25 different initialization values were used for these parameters and the final reproducibility of the estimations was evaluated. Model 2 was firstly calibrated and parameters η_{AOB} and $K_{HNO2,AOB}$ were estimated using all batch experiments (Table 12). Then, η_{AOB} was estimated in model 1 using the value of $K_{HNO2,AOB}$ estimated in model 2. The multi-start estimation was realised for each model using initial η_{AOB} and $K_{HNO2,AOB}$ values corresponding to +/- 50% and +/- 25% to those estimated. In addition, these parameter estimations were compared to those obtained by considering each batch experiment independently or with a group of experiments.

Figure 11 presents the parameter estimation results obtained with model 2 and considering all batch experiments or only one batch experiment. In this example, initial values of η_{AOB} and $K_{HNO2,AOB}$ did not impact the final values for these parameters. In contrast, these final values are different considering one experiment or all experiments. Using all experiments, optimal values for η_{AOB} and $K_{HNO2,AOB}$ have been estimated to 0.025 and 0.008 $mgN\text{-}HNO_2.L^{-1}$ respectively. These values are higher if we consider only the experiment 6 with optimal values estimated at 0.07 and 0.046 $mgN\text{-}HNO_2.L^{-1}$ respectively.

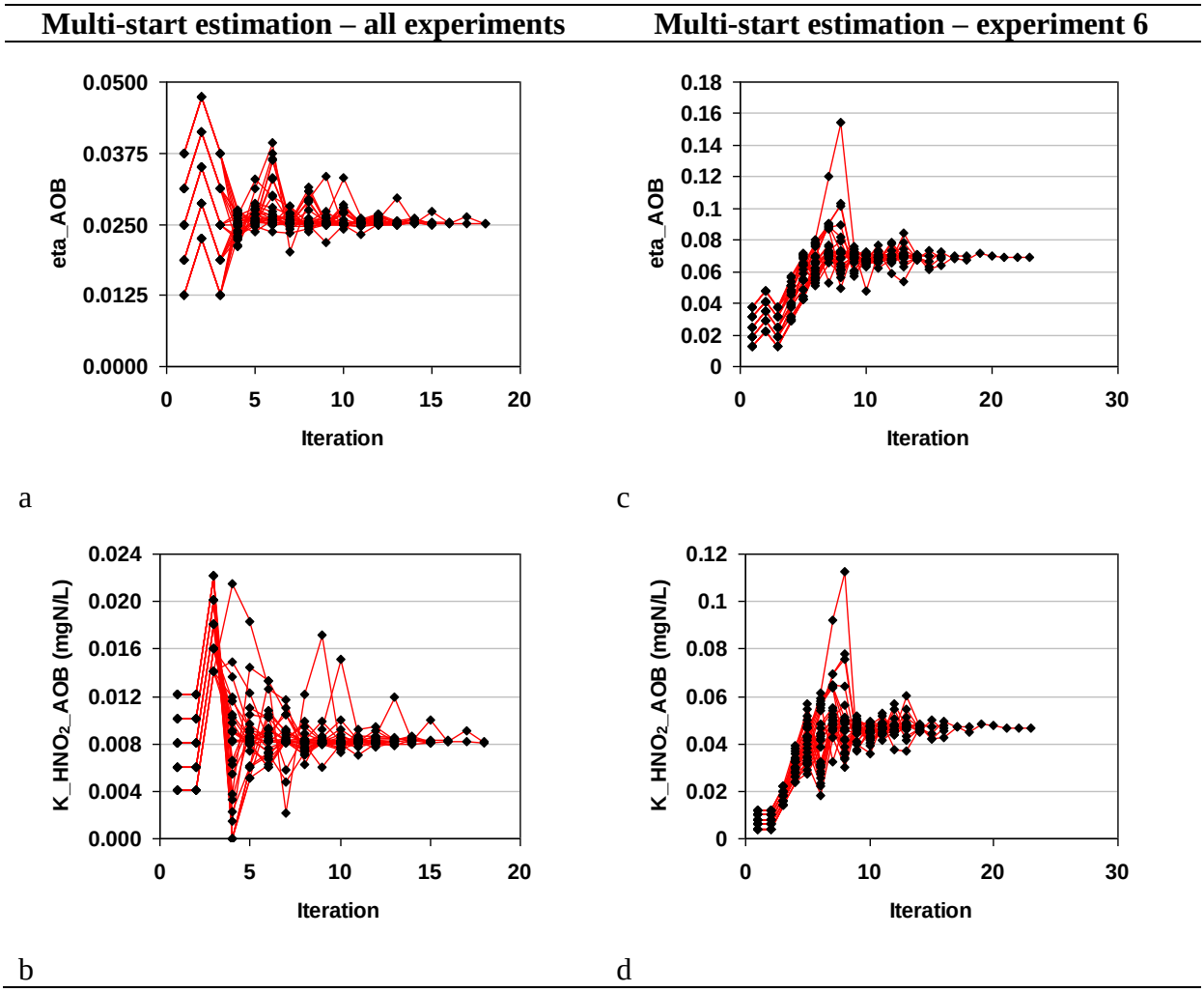

Figure 11. Multi-start parameter estimations function of the number of iterations obtained with the model 2 and considering all batch experiments (a and b) or only the batch experiment 6 (c and d).

Figure 12 presents optimal η_{AOB} and $K_{HNO2,AOB}$ values estimated for both models 1 (Figure 12.a) and 2 (Figure 12.b) and considering a unique experiment (2, 4, and 6), couples of experiment (2-4, 2-6, 4-6) or all the six batch experiments simultaneously (noted "all"). For each optimisation the multi-start method leads to very similar optimal parameters, which indicates that estimations for both models are highly reproducible. However the values obtained with different groups of experiments may differ significantly from the overall optimum. For both models, parameter estimations obtained with only one cycle are not able to fit with accuracy the entire experiments. Finally only the estimations obtained with couple of cycle 4-6 or with all the experiments provide the best global optimums. This is explained by the range of nitrite concentration obtained in these experiments: if the nitrite concentration is too low ($[HNO_2] < K_{HNO2,AOB}$) and if the concentration does not vary significantly, a strong correlation is observed between parameters η_{AOB} and $K_{HNO2,AOB}$ and only the ratio is actually identifiable. It is then recommended to use at least two batch tests with a variation of at least

50% of the HNO_2 concentration in a range of concentrations not far from the $K_{HNO2,AOB}$ value in order to obtain representative values for these parameters. Note also that a similar problem (and recommendation) could be stated with respect to the affinity constants for NO or hydroxylamine.

Here HNO_2 concentration variation from 2.3 and 10.6 $\mu gN.L^{-1}$ allowed a good identifiability of the couple η_{AOB}-$K_{HNO2,AOB}$ (nitrite reduction rate varying by 78% and 43% respectively for models 1 and 2). On the one hand the range of optimal values for $K_{HNO2,AOB}$ was similar for both models between 0.005 and 0.01 $mgN\text{-}HNO_2.L^{-1}$ with a global optimal value of 0.008 and 0.006 $\mu gN.L^{-1}$ for model 2 and model 1 respectively. On the other hand optimal values for η_{AOB} were different for both models. For model 1, optimal value is located between 0.062 and 0.077 whereas it ranges from 0.021 to 0.031 for model 2. The main difference between models 1 and 2 is that model 1 has a Monod term on NH_2OH whereas model 2 has a Monod term on NH_3 in the rate of nitrite reduction. As the value of the Monod term on NH_3 is less limiting than that of the Monod term on NH_2OH the value of η_{AOB} value is higher in model 1 than in model 2.

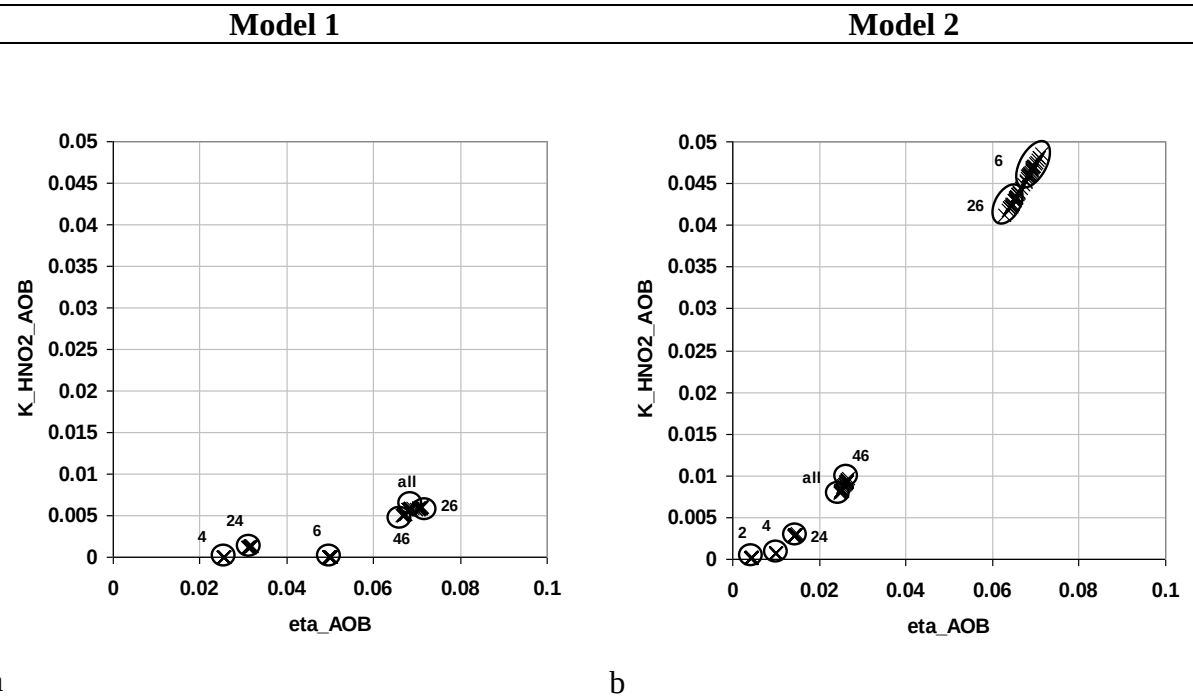

Figure 12. Final values of η_{AOB} and $K_{HNO2,AOB}$ estimated with model 1 (a) and model 2 (b) considering different combinations of batch experiment.

In addition, the error function dependence on the parameters was also evaluated by calculating the deviation between data and simulations. For each model, 12500 simulations were performed with different η_{AOB} and $K_{HNO2,AOB}$ values (η_{AOB} from 0.001 to 0.1 with a step of 0.001, $K_{HNO2,AOB}$ from 0.0002 to 0.0498 mgN-HNO_2.L^{-1} with a step of 0.0004 mgN-HNO_2.L^{-1}). For each intersection in the grid defined by η_{AOB} and $K_{HNO2,AOB}$ ranges, the average deviation between simulation and data has been calculated (Figure 13). This deviation corresponds to the difference between N_2O experimental data and N_2O simulated with the corresponding η_{AOB} and $K_{HNO2,AOB}$ pair values. This difference is calculated for each simulation step, and then averaged considering all batch experiments. It results in a unique deviation for each point of the grid. The minimum zone is clearly visible for each model without local minima. However the curves show a minima "valley" corresponding to roughly similar values for the $\eta_{AOB}/K_{HNO2,AOB}$ ratio. In that zone, the N_2O production rate is relatively comparable with different couples of values.

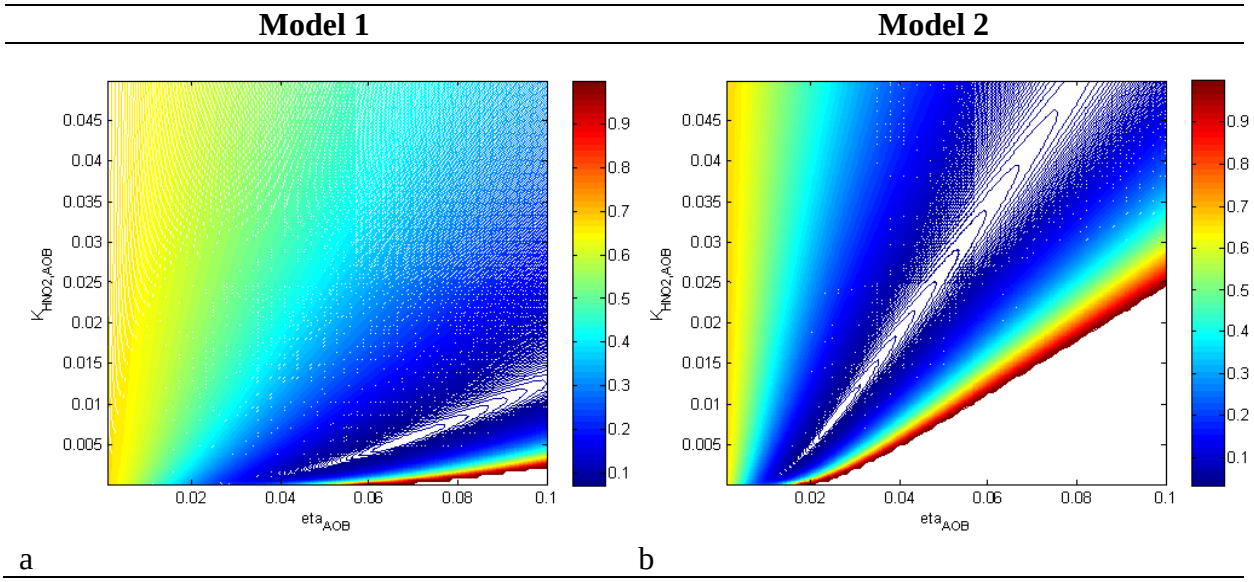

Figure 13. Normalized deviation function value obtained for the 12500 simulations performed for both models (η_{AOB} from 0.001 to 0.1 with a step of 0.001, $K_{HNO2,AOB}$ from 0.0002 to 0.0498 mgN-HNO_2.L^{-1} with a step of 0.0004 mgN-HNO_2.L^{-1}).

5 Modeling batch experiments with models 1 and 2

The six successive batch experiments with different nitrite and ammonia concentrations have been simulated using models 1 and 2 with the set of parameters given in Table 17 issued from the calibration procedure above described. Parameters related to heterotrophs and gas transfer are presented in

Appendix B and considered for all simulations in this thesis. This set of parameter values is related to the set of experimental data 1.

Table 17. Set of parameters related to the set of experimental data 1

Name	Description	Unit	Value M-1	Value M-2	Source
μ_{AOB}	Maximum AOB growth rate	h^{-1}	0.0325	-	(Hiatt and Grady, 2008)
$\mu_{AOB,AMO}$	Maximum AOB growth rate - AMO reaction	h^{-1}	-	0.216	Calculated
$\mu_{AOB,HAO}$	Maximum AOB growth rate - HAO reaction	h^{-1}	-	0.062	Estimated
μ_{NOB}	Maximum NOB growth rate	h^{-1}	0.0325	0.0325	(Hiatt and Grady, 2008)
Y_{AOB}	AOB growth yield	$mgCODX.mgN^{-1}$	0.15	0.15	(Ni et al., 2013a)
Y_{NOB}	NOB growth yield	$mgCODX.mgN^{-1}$	0.09	0.09	(Ni et al., 2013a)
η_{AOB}	N_2O emission factor	Dimensionless	0.025	0.079	Estimated
K_{NH3}	AOB affinity constant for NH_3	$mgN.L^{-1}$	0.0051	0.0051	Estimated
$K_{HNO2,AOB}$	AOB affinity constant for HNO_2	$mgN.L^{-1}$	0.0081	0.0081	Estimated
$K_{HNO2,NOB}$	NOB affinity constant for HNO_2	$mgN.L^{-1}$	0.00125	0.00125	Estimated
K_{NH2OH}	AOB affinity constant for NH_2OH	$mgN.L^{-1}$	-	2.4	(Ni et al., 2011)
K_{NO}	AOB affinity constant for NO	$mgN.L^{-1}$	0.0084	0.0084	(Ni et al., 2011)
$K_{O2,AOB}$	AOB affinity constant for O_2	$mgO_2.L^{-1}$	0.25	0.25	(Houweling et al., 2011)
$K_{O2,AOB,1}$	AOB affinity constant for O_2 (AMO reaction)	$mgO_2.L^{-1}$	0.25	0.25	(Houweling et al., 2011)
$K_{O2,AOB,2}$	AOB affinity constant for O_2 (HAO reaction)	$mgO_2.L^{-1}$	0.25	0.25	(Houweling et al., 2011)
$K_{O2,NOB}$	NOB affinity constant for O_2	$mgO_2.L^{-1}$	0.5	0.5	(Houweling et al., 2011)
$i_{N,BM}$	Nitrogen content of biomass	$mgN.mgCODX^{-1}$	0.07	0.07	(Henze, 2000)

Figure 14 presents dynamic modeling results obtained with these models for all successive batch experiments (noted 1 to 6 in this figure) previously used for the calibration of the models. An injection close to 10 $mgN\text{-}NH_4^+.L^{-1}$ has been realised for each test except for test 3 (without ammonia). Injection of ammonia only (experiments 1 and 2) led to small transitory nitrite accumulation and a small N_2O production. Nitrite injection without ammonia did not generate N_2O emissions (cycle 3). Then increasing amounts of N_2O were produced when ammonia and nitrite were injected simultaneously with increasing nitrite concentrations from 15 to 40 $mgN\text{-}NO_2^-.L^{-1}$ (cycles 4, 5 and 6). Considering the online pH measurements (varying

from 6.44 to 7.86) free nitrous acid concentration was calculated and ranged from 0.0 to 10.6 $\mu gN.L^{-1}$. A final experiment (not shown) similar to the first one was realised at the end with the same injections as the first and second tests in order to verify the reproducibility. A very similar N_2O peak was obtained with only 0.04% of difference in term of N_2O emission factor with the first test. This confirms a good reproducibility and also demonstrated that the increased production of N_2O during the test is not correlated to the time but to the ammonia and nitrite level imposed in the tests. In addition these experiments confirm the correlation between nitrite accumulation in the soluble phase and N_2O production even in condition of relatively high dissolved oxygen concentration ($DO>4.4\ mgO_2.L^{-1}$).

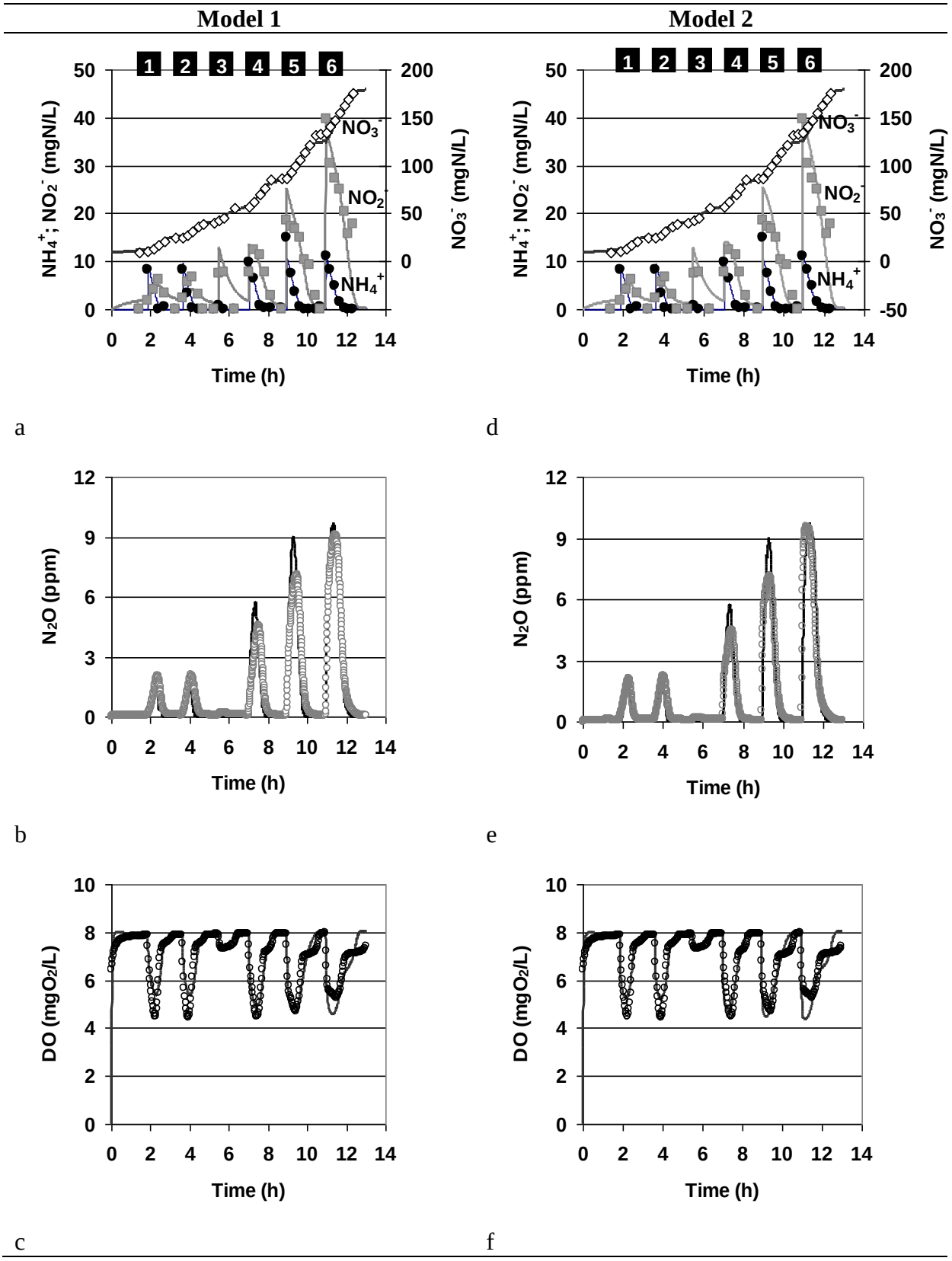

Figure 14. Modeling results of the batch experiments. Evolution of ammonium, nitrite and nitrate (a for model 1, d for model 2). Evolution of N_2O (b for model 1, e for model 2). Evolution of oxygen (c for model 1, f for model 2). Legend: (■) N-NO_2^-, (◊) N-NO_3^-, (●) N-NH_4^+, (○) N_2O, (○) O_2.Points correspond to experimental data and lines to modeling results.

Both models predict correctly the dynamics of nitrogen species in liquid and gas phase (i.e. ammonia, nitrite, nitrate and nitrous oxide) during the successive injections. Considering the test 3, it is also demonstrated that the absence of ammonium, in presence of nitrite, leads to the absence of N_2O production. In that case, both models similarly predict this absence of N_2O compared to other cycles, confirming that assumptions of ammonium or hydroxylamine as the electron donors for AOB denitrification give simulations in very good accordance with the observations.

Moreover, both models are able to catch the effect of free nitrous acid concentration on the dynamics of N_2O production (tests 4, 5, 6, 7). Some slight differences in the dynamic profile are still observed (tests 4, 5) but this can be considered satisfying considering the experimental uncertainties. In addition, if we consider the global N_2O production integrated for each cycle, the change in N_2O emission factor is also well predicted by both models (Table 18).

Table 18. Comparison of experimental and simulated N_2O emission factor calculated for each batch experiment.

		N_2O emission factor (%) $gN\text{-}N_2O/gN\text{-}NH_4^+$ removed		
Batch experiment	**HNO_2 range ($\mu gN.L^{-1}$)**	**Experimental**	**Model 1**	**Model 2**
1	0-0.8	0.185	0.267	0.266
2	0-0.8	0.203	0.276	0.272
3	0-0.8	0.000	0.000	0.000
4	0-2.3	0.712	0.850	0.872
5	0-5.0	1.226	1.400	1.440
6	0-10.6	1.779	1.756	1.815

6 Conclusion

In addition to the classical materials and methods elements given in the first part of the chapter, one main aspect of this part of the manuscript was to propose a 3-step calibration procedure of the parameters involved in the models incorporating N_2O production by the ND pathway. This procedure shows the general strategy used for all parameter estimations of N_2O models considered in this manuscript. This 3-steps procedure was based on a preliminary sensibility and identifiability analysis, which allows the identification of different groups of parameters and also identify the most sensitive model components. The most sensitive parameters are calibrated using the considered set of experimental data. The value of the less sensitive parameters is defined following the literature.

In the set of experimental data 1 used to present the calibration procedure, the NOB activity was significant and an accurate calibration of the NOB related parameters was important to describe the dynamic of nitrite, thus the dynamic of N_2O production. In the following chapters, the NOB activity was negligible as no nitrate was observed in set of experimental data 2 and 3. In contrast the NO measurement was available in sets 2 and 3 making possible the identification of the model parameters associated to NO production by AOB.

Two models with different mathematical structure but with similar hypothesis have been considered, and parameters with the same significance in both models have been set to the same value. Only the N_2O reduction factor η_{AOB} has been calibrated at two different values in models 1 and 2, which can be explained by the different mathematical model structures. Actually, in model 1, the N_2O production is realised during the oxidation of hydroxylamine whereas in model 2, N_2O is produced during the oxidation of ammonia. In order to balance the Monod term on hydroxylamine that is lower than the Monod term on ammonia in model 2, the N_2O reduction factor appears to be higher in model 1 than in model 2.

The calibration of these models was performed using the set of experimental data 1 obtained from batch experiments with various initial additions of ammonia and/or nitrite. Simulation results with the set of parameter values identified showed that both models were able to represent both the dynamic of nitrification and N_2O production and the N_2O emission factors of each experiment. On the other hand, it has to be kept in mind that parameter values could be different considering other operating conditions or mixed culture.

The variability in the parameter estimations may come from three main causes: (1) the experiment which has to cover an enough range of operating conditions (such as HNO_2 concentration) to avoid identifiability problems, (2) the dynamic of enzymatic pool in response to environmental conditions (the enzymes NirK and Nor responsible of NO and N_2O production are more or less produced depending on the nitrite accumulation (Beaumont et al., 2004b; Yu and Chandran, 2010)) and (3) the model structure which does not considers enough processes to describe experimental observations (such as the NN pathway which can have a significant contribution to N_2O production under specific conditions).

Chapter IV Evaluation of five candidate nitrous oxide production models with four continuous long-term wastewater treatment process data series

This chapter is the result of an international collaboration involving research groups model*EAU* from Université Laval in Canada with Lisha Guo and Peter Vanrolleghem and the Advanced Water Management Centre from the University of Queensland in Australia with Bing-Jie Ni and Zhiguo Yuan.

Abstract

Five activated sludge models describing N_2O production by ammonium oxidising bacteria (AOB) were compared to four different long-term process data sets. Each model considers one of the two known N_2O production pathways by AOB, namely the AOB denitrification pathway and the hydroxylamine oxidation pathway, with specific kinetic expressions. Satisfactory calibration could be obtained in most cases but none of the models was able to describe all the N_2O data obtained in the different systems with a similar parameter set. Variability of the parameters can be related to difficulties related to undescribed local concentration heterogeneities, physiological adaptation of micro-organisms, a microbial population switch, or regulation between multiple AOB pathways. This variability could be due to a dependence of the N_2O production pathways on the nitrite (or free nitrous acid - FNA) concentrations and other operational conditions in different systems. This work gives an overview of the potentialities and limits of single AOB pathway models. Indicating in which condition each single pathway model is likely to explain the experimental observations, this work will also facilitate future work on models in which the two main N_2O pathways active in AOB are represented together.

1 Introduction

N_2O is a powerful greenhouse gas that can be emitted from wastewater treatment plants (WWTP). The emission varies with the design and operation of a WWTP. Measurement campaigns demonstrated high temporal and spatial variability in the fraction of influent nitrogen load emitted as N_2O, reportedly in the range of 0.01 % to more than 10% (Ahn et al., 2010; Kampschreur et al., 2009). Both denitrification and nitrification processes can produce N_2O. However, recent measurement campaigns have conclusively shown that ammonium oxidising bacteria (AOB) in most cases contribute significantly more to N_2O production than heterotrophic denitrification (Matthijs R.J. Daelman et al., 2013; Guo et al., 2013a; Wunderlin et al., 2012), whereas heterotrophic denitrification may play an important role in the removal of N_2O produced by AOB (Castro-Barros et al., 2015; Guo and Vanrolleghem, 2013b).

In order to evaluate the influence of process configuration and operation on the N_2O emission, a significant effort has been recently devoted to N_2O modelling. For dynamic modelling of N_2O production, new model components have been proposed to enhance the commonly used nitrification and denitrification models at present to include various reaction intermediates such as nitrous oxide (N_2O), nitric oxide (NO) and hydroxylamine (NH_2OH).

Concerning heterotrophic denitrification, N_2O and NO are known to be intermediate compounds. These compounds were included in the ASMN model proposed by (Hiatt and Grady, 2008) considering four successive steps in denitrification. The accumulation rate of NO and N_2O depends on the relative rates of the successive steps. More recently (Pan et al., 2013) proposed a new model, which considers the electron competition between the different electron acceptors.

The mechanisms responsible for N_2O production by AOB are more controversial. The two widely accepted mechanisms are the AOB denitrification pathway, through which AOB produce N_2O via NO by reducing nitrite (Chandran et al., 2011), and the hydroxylamine-related pathway. In this second mechanism, incomplete oxidation of hydroxylamine could form NO or NOH (nitroxyl radical) as intermediates for N_2O production (Chandran et al., 2011; Stein, 2011). Several mathematical models have been proposed based on these hypothesized pathways (Mampaey et al., 2013; Ni et al., 2011, 2013a, 2013b). (Ni et al., 2013a) evaluated four different models by calibrating these models with literature data

obtained in batch experiments with activated sludge samples. As none of the models tested could reproduce all results, (Ni et al., 2013a) suggested that a regulation between the two main pathways probably occurs, and called for more work to further identify the specific conditions under which each of the models would be applicable, and to also develop a generic model by integrating various pathways. Moreover, one issue related to model calibration with batch experiments is that the sludge history may impact the physiological state of the sludge. This is potentially leading to transient behaviour due to metabolic regulation, especially after a sudden change from biomass cultivation conditions to the batch condition. For this reason it appeared essential that the models be confronted to long term operational data measured in situ to better establish the characteristics of such generic model. Additionally a model combining the two main AOB pathways responsible of N_2O production was recently proposed by (Ni et al., 2014). It was based on a new approach which included intracellular metabolic variables and involved electrons transport for uncoupling oxidation and reduction. Before implementing this new type of multiple pathway model, it is here proposed to provide a state of the art in term of predicting N_2O emissions with the current and more conventional AOB models based on a single pathway.

Therefore, the objective of this study is to evaluate different models through their calibration with several sets of continuous long-term data collected from different systems, to reveal the performance of these models under various process conditions. This work gives an overview of the potentialities and limits of using these models based on single AOB pathway to real sewage systems.This sheds light on the conditions under which each of the models are suitable, helping the practitioners to define the actual boundaries of current modelling approaches. Finally indicating in which condition each single pathway model is likely to explain the experimental observations, this work will also facilitate the development and the future calibration of a generic model by combining different pathways.

2 Material and methods

2.1 Experimental data

As detailed in Table 19, four different continuous biological systems were considered in this study: a UCT (University of Cape Town) process, an oxidation ditch, and two sequencing batch reactors (SBR). Detailed descriptions of each system and measurement campaigns summarized in Table 20 can be found in dedicated articles and communications (Guo and Vanrolleghem, 2014; Ni et al., 2013b).

The SBR1 is a lab-scale pilot which was operated during more than six months. It was fed with a nitrogen rich wastewater (500 mgN-NH_4^+ L^{-1}). Cycles consisted of five phases, i.e. feeding, aerobic reaction, anoxic reaction, settling, and withdrawal. A complement in organic carbon for denitrification was provided by a lactose-rich solution (whey). An average volumetric loading rate of 2.79 kgCOD m^{-3} d^{-1} was obtained. This carbon source was provided during a short period at the beginning of the anoxic period to maintain a suitable COD:N ratio (from 3.5 to 5). Various volumetric exchange ratios were imposed in order to adapt the ammonium concentration in the reactor. The system was operated in view of shortcut nitrogen removal over nitrite by controlling the duration of aeration. This strategy consists in stopping aeration as soon as ammonia is depleted which limits the oxidation of nitrite to nitrate. The process was operated at a high ammonia loading rate (0.267 kgN m^{-3} d^{-1}) and exhibited nitrite accumulation during aerobic periods. The average hydraulic retention time (HRT) is 35 hours. The solids retention time (SRT) is 15 d.

The full-scale oxidation ditch (OD) plant receives domestic wastewater at approximately 4000 m^3 per day (approx. 20000 population equivalent noted PE). The plant consists of a primary clarifier and an activated sludge system with surface aerators. After primary sedimentation, wastewater is introduced into the activated sludge unit with a working volume of 8750 m^3. The average hydraulic retention time (HRT) in the OD is 34 h. The solids retention time (SRT) is approximately 12 d. More details about data collection are given by (Ni et al., 2013b).

Data collected from a full-scale SBR plant (SBR2) is also considered. The average daily flow of the plant is 120000 m^3 per day (approx. 600000 PE). The plant consists of a primary

sedimentation tank followed by secondary treatment. The biological nutrient removal component of the plant comprises a circular tank that is evenly quartered into four basins. Each basin operates as a separate SBR. At the time of this study, each SBR cycle consisted of the following phases in sequence: 90 min continuous feeding and aeration, 35 min settling and 55 min decanting. The average exchange volume per cycle in each SBR was approximately 5000 m^3. Each SBR had a working volume of 28000 m^3, and hence the average HRT was 17 h. The total airflow to the three SBRs was fixed at 45000 m^3 h^{-1} throughout the aeration phase with equal distribution among the three reactors. The SRT was maintained at 19 days.

The Eindhoven WWTP, in the Netherlands, has a capacity of 750000 PE. It treats wastewater using a University Cape Town (UCT) process, implemented with three rings. The inner ring is an anaerobic tank, the middle ring is an anoxic tank and the outer ring is a partially aerated tank. The outer ring is equipped with two aeration zones. The so-called summer aeration zone functions all year round, but the winter aeration zone is only turned on in winter conditions and occasionally under certain conditions, e.g. under rain events. The SRT was 10 days and the overall hydraulic retention time was 19 h. More details can be found in (Guo and Vanrolleghem, 2014).

Long-term and/or intensive measurement campaigns for quantification of N_2O were performed on each system (Table S1). The detailed procedures used on each plant can be found also in associated publications (Guo and Vanrolleghem, 2014; Ni et al., 2013b; Pocquet et al., 2013) with several key technical aspects underlined in this work. A special effort was dedicated to the development of an accurate quantification of N_2O emissions in oxidation ditch (Ni et al., 2013b), particularly for the emissions from the surface aerator zone which cannot be easily captured by floating hoods. Because liquid is recirculating in a plug flow regime in the oxidation ditch dissolved N_2O was measured in liquid samples using gas chromatography (GC) at different times and in different zones. It was thus possible to clearly differentiate the emissions in anoxic and aerobic zone considering both liquid accumulation and gas emissions.

The N_2O concentration in the off-gas was monitored using online continuous infrared (IR) spectroscopy for three of these systems (UCT and the two SBRs). Floating hood methods were used for measuring N_2O in the gas phase for full scale UCT and SBR2. The N_2O was

measured at different surface locations with a specific protocol (Guo and Vanrolleghem, 2014). Sampling of the off gas was used for the lab-scale SBR1 (covered reactor). In addition the NO concentration in the off-gas was also measured in SBR1 using an IR analyser.

In these systems the daily average N_2O emission factors were quantified in gN-N_2O/gTN removed (Table 1). It varied from 0.12 to 3.1% for the UCT, 1 to 5% for the SBR1, 0.36 to 0.68% for the OD, 1 to 1.5% for the SBR2. The highest emission was obtained with the SBR1 working at the highest loading rate (0.267 kgN m^{-3} d^{-1}) with the highest nitrite variation (0-50 mgN L^{-1}).

Table 19. Comparison of the experimental systems and operating conditions

Process type	AS – UCT	SBR1	AS –Oxidation ditch	SBR2
Country	Netherlands	France	Australia	Australia
Wastewater type	Domestic	Agro-industry	Domestic	Domestic
COD/N (gCOD/gN)	9	5	10	10
SRT (d)	10	15	10	19
HRT (h)	19	35	48	17
DO aerobic (mgO_2/L)	0.1-5.4	2–6.0	0.1–8.0	0.1-4.0
Aerobic fraction (of time or volume)	0.2-0.5	0.55	<0.5*	0.5
Temperature during campaign (°C)	21+/-0.5	28+/-0.5	25+/-0.5	25+/-0.5
MLSS (g/L)	2.5-3.5	5.3-6.3	2.9-3.7	4-4.5
Reactor N-NH_4^+ (mgN/L)	0-45	0-45	0-5	0-25
Reactor N-NO_2^- (mgN/L)	0-0.1	0-50	0-0.5	0-2.5
Reactor N-NO_3^- (mgN/L)	0-6.5	0-10	0-1	0-5
Nitrogen load (kgN/m^3/d)	0.070	0.267	0.045	0.074
N_2O emission factor (gN-N_2O/gTN)	0.12%-3.10%	1.0%-5%	0.36%-0.68%	1.0%-1.5%
Measurment campaign (month)	1	6	1	1

*Not precisely determined

Table 20. Information concerning the full scale process modeling.

Oxidation ditch	
Hydrodynamic properties and mass balance	The OD reactor was modelled using 10 CSTR reactors in series. (Volumes= 1×370 m^3; 4×980 m^3; and 5× 950 m^3) The gas-liquid oxygen transfer at different locations along the OD is considered in the model. The rates of gas-liquid oxygen transfer are assumed to be proportional to the difference in oxygen concentration between gas and liquid interface, and the proportionality factor is the volumetric oxygen transfer coefficient.
Average wastewater characteristics	COD= 573 mgO_2/L, TSS= 156 mg/L, TKN= 60 mgN/L Influent COD composition (mg/L): Ss= 197, Xs= 325, Xi= 36, Si= 15 (constant fractionation percentage)
SBR2	
Hydrodynamic properties and mass balance	The SBR reactor was modelled using a CSTR reactor. (Volume= 28 ML) The gas-liquid oxygen transfer is modelled by assuming the rates of gas-liquid oxygen transfer are proportional to the difference in oxygen concentration between gas and liquid interface, and the proportionality factor is the volumetric oxygen transfer coefficient.
Wastewater characteristics	COD= 615 mgO_2/L, TSS= 125 mg/L, TKN= 59 mgN/L Influent COD composition (mg/L): Ss= 254, Xs= 289, Xi= 59, Si= 13 (constant fractionation percentage)
UCT	
Hydrodynamic properties and mass balance	The UCT process was modelled by 14 CSTRs. The first 4 CSTRs, each with a volume of 2799 m3, make anaerobic tank (the inner ring), the following 2 CSTRs, each with a volume 14375 m3, construct anoxic tank (the middle ring) and the rest 8 CSTRs are built into partially aerated tank (the outer ring). The total volume of outer ring is 50311 m3. The summer package in the outer ring is divided into 3 CSTRs and each has a volume of 5367 m3. The gas stripping of N_2, N_2O and NO, as well as the aeration, is modelled following Henry's law. The oxygen transfer coefficient (k_La) is calculated from an aeration model and the gas transfer coefficients of N2, N2O and NO are calculated from k_La and gas diffusion coefficients.
Average wastewater characteristics	Inflow=137786 (m^3/d) COD= 624 mgO_2/L, TSS= 355 mg/L, TKN= 45.5 mgN/L Influent COD composition (mg/L): S_I=42.37; S_F=71.85; S_A= 70.01; X_I=237.23; X_S=198.19; X_H=5; S_{NH}=29.90;

2.2 Mathematical models

In this study mathematical models, all based on the ASMN framework (Hiatt and Grady, 2008), were used with additions for considering production of NO and N_2O by AOB. As nitrification was supposed to be the main producer of N_2O and because of the different possible pathways involved, different AOB models were compared. The reaction stoichiometry and kinetics of the five N_2O models related to AOB are summarized in Table 21. These models have been fully described in chapter II. Some key elements are briefly recalled here.

Table 21. Processes stoechiometry and kinetics of the models for AOB.

Process	Model components							Kinetic rate expressions
	S_{O_2}	S_{NH}	S_{NH_2OH}	S_{NO_2}	S_{NO}	S_{N_2O}	X_{AOB}	
Model A – Ni et al. (2011)								
1	$-\frac{8}{7}$	-1	1					$\mu_{AOB,AMO} \cdot \frac{S_{O_2}}{K_{O_2,AOB,1}+S_{O_2}} \cdot \frac{S_{NH_4}}{K_{NH_4,AOB}+S_{NH_4}} \cdot X_{AOB}$
2	$-\frac{\frac{16}{7}-Y_{AOB}}{Y_{AOB}}$	$-i_{N,AOB}$	$-\frac{1}{Y_{AOB}}$	$\frac{1}{Y_{AOB}}$			1	$\mu_{AOB,HAO} \cdot \frac{S_{O_2}}{K_{O_2,AOB,2}+S_{O_2}} \cdot \frac{S_{NH_2OH}}{K_{NH_2OH,AOB}+S_{NH_2OH}} \cdot X_{AOB}$
3			-1	-3	4			$\eta_{AOB} \cdot \mu_{AOB,HAO} \cdot \frac{K_{I,O_2,AOB}}{K_{I,O_2,AOB}+S_{O_2}} \cdot \frac{S_{NH_2OH}}{K_{NH_2OH,AOB}+S_{NH_2OH}} \cdot \frac{S_{NO_2}}{K_{NO_2,AOB}+S_{NO_2}} \cdot X_{AOB}$
4			-1	1	-4	4		$\eta_{AOB} \cdot \mu_{AOB,HAO} \cdot \frac{K_{I,O_2,AOB}}{K_{I,O_2,AOB}+S_{O_2}} \cdot \frac{S_{NH_2OH}}{K_{NH_2OH,AOB}+S_{NH_2OH}} \cdot \frac{S_{NO}}{K_{NO,AOB}+S_{NO}} \cdot X_{AOB}$
Model A1 – Pocquet et al. (2013)								
1								$\mu_{AOB,AMO} \cdot \frac{S_{O_2}}{K_{O_2,AOB,1}+S_{O_2}} \cdot \frac{S_{NH_3}}{K_{NH_3,AOB}+S_{NH_3}+S_{NH_3}^2/K_{I,NH_3,AOB}} \cdot X_{AOB}$
2								$\mu_{AOB,HAO} \cdot \frac{S_{O_2}}{K_{O_2,AOB,2}+S_{O_2}} \cdot \frac{S_{NH_2OH}}{K_{NH_2OH,AOB}+S_{NH_2OH}} \cdot X_{AOB}$
3								$\eta_{AOB} \cdot \mu_{AOB,HAO} \cdot \frac{S_{NH_2OH}}{K_{NH_2OH,AOB}+S_{NH_2OH}} \cdot \frac{S_{HNO_2}}{K_{HNO_2,AOB}+S_{HNO_2}} \cdot X_{AOB}$
4								$\eta_{AOB} \cdot \mu_{AOB,HAO} \cdot \frac{S_{NH_2OH}}{K_{NH_2OH,AOB}+S_{NH_2OH}} \cdot \frac{S_{NO}}{K_{NO,AOB}+S_{NO}} \cdot X_{AOB}$
Model B – Mampaey et al. (2013)								
1	$-\frac{\frac{24}{7}-Y_{AOB}}{Y_{AOB}}$	$-\frac{1}{Y_{AOB}}-i_{N,AOB}$		$\frac{1}{Y_{AOB}}$			1	$\mu_{AOB} \cdot \frac{S_{O_2}}{K_{O_2,AOB}+S_{O_2}} \cdot \frac{S_{NH_3}}{K_{NH_3,AOB}+S_{NH_3}} \cdot X_{AOB}$
2	$-\frac{\frac{16}{7}-Y_{AOB,den}}{Y_{AOB,den}}$	$-\frac{1}{Y_{AOB,den}}-i_{N,AOB}$		$-\frac{1}{Y_{AOB,den}}$	$\frac{2}{Y_{AOB,den}}$		1	$\eta_{AOB} \cdot \mu_{AOB} \cdot \frac{S_{O_2}}{K_{O_2,AOB}+S_{O_2}} \cdot \frac{S_{NH_3}}{K_{NH_3,AOB}+S_{NH_3}} \cdot \frac{S_{HNO_2}}{K_{HNO_2,AOB}+S_{HNO_2}} \cdot X_{AOB}$
3	$-\frac{\frac{16}{7}-Y_{AOB,den}}{Y_{AOB,den}}$	$-\frac{1}{Y_{AOB,den}}-i_{N,AOB}$		$\frac{1}{Y_{AOB,den}}$	$-\frac{2}{Y_{AOB,den}}$	$\frac{2}{Y_{AOB,den}}$	1	$\eta_{AOB} \cdot \mu_{AOB} \cdot \frac{S_{O_2}}{K_{O_2,AOB}+S_{O_2}} \cdot \frac{S_{NH_3}}{K_{NH_3,AOB}+S_{NH_3}} \cdot \frac{S_{NO}}{K_{NO,AOB}+S_{NO}} \cdot X_{AOB}$
Model B1 – Guo et al. (2013b)								
1								$\mu_{AOB} \cdot \frac{S_{O_2}}{K_{O_2,AOB}+S_{O_2}} \cdot \frac{S_{NH_3}}{K_{NH_3,AOB}+S_{NH_3}+S_{NH_3}^2/K_{I,NH_3,AOB}} \cdot \frac{K_{I,HNO_2,AOB}}{K_{I,HNO_2,AOB}+S_{HNO_2}} \cdot X_{AOB}$
2								$\eta_{AOB} \cdot \mu_{AOB} \cdot \frac{S_{NH_3}}{K_{NH_3,AOB,den}+S_{NH_3}} \cdot \frac{S_{HNO_2}}{K_{HNO_2,AOB}+S_{HNO_2}} \cdot X_{AOB} \cdot DO_{Haldane}$
3								$\eta_{AOB} \cdot \mu_{AOB} \cdot \frac{S_{NH_3}}{K_{NH_3,AOB,den}+S_{NH_3}} \cdot \frac{S_{NO}}{K_{NO,AOB}+S_{NO}} \cdot X_{AOB} \cdot DO_{Haldane}$
								$DO_{Haldane} = \frac{S_{O_2}}{K_{O_2,AOB,den}+\left(1-2\cdot\sqrt{K_{O_2,AOB,den}/K_{I,O_2,AOB}}\right)\cdot S_{O_2}+S_{O2}^2/K_{I,O_2,AOB}}$
Model C – Ni et al. (2013b)								
1	$-\frac{8}{7}$	-1	1					$\mu_{AOB,AMO} \cdot \frac{S_{O_2}}{K_{O_2,AOB,1}+S_{O_2}} \cdot \frac{S_{NH_4}}{K_{NH_4,AOB}+S_{NH_4}} \cdot X_{AOB}$
2	$-\frac{\frac{12}{7}-Y_{AOB}}{Y_{AOB}}$	$-i_{N,AOB}$	$-\frac{1}{Y_{AOB}}$		$\frac{1}{Y_{AOB}}$		1	$\mu_{AOB,HAO,1} \cdot \frac{S_{O_2}}{K_{O_2,AOB,2}+S_{O_2}} \cdot \frac{S_{NH_2OH}}{K_{NH_2OH,AOB}+S_{NH_2OH}} \cdot X_{AOB}$
3	$-\frac{4}{7}$			1	-1			$\mu_{AOB,HAO,2} \cdot \frac{S_{O_2}}{K_{O_2,AOB,2}+S_{O_2}} \cdot \frac{S_{NO}}{K_{NO,AOB}+S_{NO}} \cdot X_{AOB}$
4			-1	1	-4	4		$\eta_{AOB} \cdot \mu_{AOB,HAO,1} \cdot \frac{S_{NH_2OH}}{K_{NH_2OH,AOB}+S_{NH_2OH}} \cdot \frac{S_{NO}}{K_{NO,AOB}+S_{NO}} \cdot X_{AOB}$

Two models were based on the AOB denitrification pathway: namely the Ni et al. (Ni et al., 2011) model which does include NH_2OH as an intermediate in ammonium oxidation (Model A), and the Mampaey et al. (Mampaey et al., 2013) model, which does not (Model B). Another key difference between these two models is the influence of oxygen: Model A only includes DO inhibition of N_2O production whereas oxygen is only a limiting substrate in Model B. The third model was based on the hydroxylamine oxidation pathway (Model C). In this model NO is considered as an intermediary compound during the oxidation of NH_2OH to nitrite(Ni et al., 2011, 2013a, 2013b). N_2O is then produced by reduction of NO with the same reaction as in Model A. Note that Model C contains a modification compared to the initial model (Ni et al., 2011, 2013a, 2013b): originally growth was considered to occur in two processes, but here biomass production was removed from process 3 in order to use the

conventional value for the growth yield (Y_{AOB}). Consequently the value of the new maximal rate $\mu_{AOB,HAO,2}$ is here calculated as $\mu_{AOB,HAO,1}/Y_{AOB}$.

Two modifications of the original AOB denitrification models (A and B) have also been considered (Guo and Vanrolleghem, 2014; Pocquet et al., 2013) (Models A1 and B1). In Model A1 the oxygen inhibition of the AOB reduction pathway was not considered. In addition free ammonia (FA) and free nitrous acid (FNA) were considered as the substrate for the AOB reactions, in order to explicitly consider the effect of pH variation. In Model B1, oxygen limitation and inhibition was considered through a Haldane function in both the kinetics of NO_2^- reduction and NO reduction (Guo and Vanrolleghem, 2014, 2013b). Inhibition by FA was also considered in Model A1 and both inhibition by FA and FNA were included in Model B1.

The gas liquid transfers of oxygen, NO and N_2O were also included. The transfer coefficients (K_La) for both NO and N_2O were calculated with the measured oxygen transfer coefficient and respective diffusivity ratio (Ye et al., 2014). In addition the phosphorus removal and the influence of temperature were also considered for UCT process modelling including phosphorus accumulating organisms with the ASM2d framework (Guo and Vanrolleghem, 2014). Simulations were performed using AQUASIM (Reichert, 1998) and WEST (Vanhooren et al., 2003).

2.3 Parameter calibration

Simulation methodologies for each system were similar to well-accepted protocols for dynamic activated sludge models calibration with long term data and were detailed elsewhere (Guo and Vanrolleghem, 2014; Ni et al., 2013b; Pocquet et al., 2013). Physical and hydrodynamic characteristics were also considered for modelling the full scale oxidation ditch and UCT process with appropriate combination of in-series reactors (Guo and Vanrolleghem, 2013b; Ni et al., 2013b). Wastewater characteristics were collected and solid mass balance were checked. Wastewater characteristics and COD fractionation are given in Table 20 with some key information on hydraulic description. Oxygen transfer rate was assessed in each reactor or zone. Variables initialisation was obtained from steady state simulations related to average mass balances. The steady state biomass concentrations are given in Table 22. Simulated MLVSS were in agreement with experimental data without adaptation of the central model parameters: default values for heterotrophs decay rate and growth yield were used (ASMN: Y_{OHO}=0.6gCOD/gCOD, b_{OHO}=0.41d^{-1}). Parameter calibration was then

performed in two steps, first considering the major rates and components (ammonia, nitrate, and nitrite) and then the N_2O and NO data. All the parameters of the models are given in Table 24 and in Appendix D, Appendix E, Appendix F and Appendix G. Whenever possible, our approach has been to use typical parameter values reported in literature (Hiatt and Grady, 2008) for most of heterotrophic and autotrophic processes (for instance, yields, decay rates, and hydrolysis rates). Concerning NOB related parameters, the prediction of nitrite concentration is very important for N_2O models and must be predicted with accuracy. For example, in the case of UCT process the NOB parameters had to be adapted in order to predict more accurately the nitrite level in the system. Parameter estimation was basically realised manually and in a second time for a limited number of parameters, mathematical minimisation of the root mean squared error was tested for better adjustment (Newton-Raphson method). For the different systems the data and the simulation indicated that denitrification process was not responsible of N_2O emissions and can even consume N_2O. This is related to the presence of sufficient readily biodegradable COD for denitrification. The affinity constant dedicated to reduction of each electron acceptor (NO_3, NO_2, NO, N_2O) were slightly adapted for process SBR1 and UCT to match with that observation (no emission in anoxic periods).

Table 22. Steady State Biomass concentrations obtained for different processes.

X concentration mgCOD.L^{-1}	SBR 1	AS – OD	SBR 2	AS – UT
Simulations				
AOB	320	160	210	56
NOB	0	100	130	9
OHO (+PAO)	4500	1600	2100	343+304
Total MLVSS	5775	3100	4000	4003
Experimental				
Total MLVSS	5830	3103	4073	3309

Sensitivity analysis was performed in order to identify the most influential parameters on N_2O and NO emissions. As an example the results of the sensitivity analysis on N_2O and NO for parameters involved in the AOB models are illustrated in supplementary information (Table 23) for the case of the SBR1. Basically for all the models and for all the systems studied the most influential parameter related to N_2O processes was the reduction factor (η_{AOB}) which impacts both the emission rate and the emission factor. Moreover the emission rate was indirectly sensitive to core parameters which influence the nitritation rate (Y_{AOB}, μ_{AOB}, $K_{NH4,AOB}$) but these parameters did not influence the N_2O emission factor. Depending on the feeding regime (batch or continuous) the prediction of N_2O responses and emission factors is

more or less influenced by the affinity constant (K_{NH2OH}, K_{NO2}, K_{NO}). Identifiability of η_{AOB} and K_{HNO2} has been evaluated by (Pocquet et al., 2013) for models based on AOB denitrification. These parameters were estimated independently as soon as the explored range of nitrite concentration was sufficiently large (situation of SBR1 for instance).

Parameters influencing ammonium, nitrite, nitrate (and indirectly NO and N_2O) were calibrated during the first step (e.g.$\mu_{AOB,AMO}$, μ_{AOB}, $K_{NH4,AOB}$). Secondly the parameters influencing only the N_2O emission and NO emission (with very low impact on ammonia, nitrite or nitrate) were adapted, in this way maintaining the model fit to the ammonium, nitrate and nitrite data. In this second phase the reduction factor η_{AOB} as well as the affinity constant $K_{NO2,AOB}$ were focused upon due to their significant influence. The NO emission is also very sensitive to the parameter $K_{NO,AOB}$ which was estimated with the NO measurements performed on SBR1.

Table 23. Sensitivity of state variables NO and N_2O (in liquid) to stoichiometric and kinetic parameters for the five models (example of SBR1). The classification is related to the root mean square of the Absolute-Relative function expressed in mgN-N_2O.L^{-1} for N_2O and in mg N-NO.L^{-1} for NO.

	A-R function range (mgN-NXO.L^{-1})	Models A	A1	B	B1	C
N_2O	>0.01	$\mu_{AOB,AMO}$ η_{AOB} Y_{AOB} $K_{NO2,AOB}$ $K_{NH4,AOB}$	$\mu_{AOB,AMO}$ η_{AOB} Y_{AOB}	η_{AOB} Y_{AOB}	η_{AOB} Y_{AOB} μ_{AOB} $K_{I,O2,AOB}$	$\mu_{AOB,AMO}$ Y_{AOB} η_{AOB}
	0.0025 - 0.01	$K_{I,O2,AOB}$ $K_{NH2OH,AOB}$ $K_{O2,AOB,2}$ $\mu_{AOB,HAO}$	$K_{I,NH3,AOB}$ $K_{NH3,AOB}$ $K_{O2,AOB,2}$ $K_{NH2OH,AOB}$	μ_{AOB} $K_{NH3,AOB}$ $K_{O2,AOB}$	$K_{NH3,AOB}$ $K_{O2,AOB}$	$K_{O2,AOB,2}$ $K_{NH4,AOB}$ $\mu_{AOB,HAO}$ $K_{NH2OH,AOB}$
	<0.0025	$K_{O2,AOB,1}$ $K_{NO,AOB}$	$\mu_{AOB,HAO}$ $K_{O2,AOB,1}$ $K_{HNO2,AOB}$ $K_{NO,AOB}$	$K_{HNO2,AOB}$ $K_{NO,AOB}$	$K_{HNO2,AOB}$ $K_{NO,AOB}$	$K_{O2,AOB,1}$ $K_{NO,AOB}$
NO	>1.10^{-4}	$K_{NO2,AOB}$ $\mu_{AOB,AMO}$ $K_{NO,AOB}$ $K_{NH4,AOB}$	$\mu_{AOB,AMO}$ $K_{NO,AOB}$	$K_{NO,AOB}$ Y_{AOB}	$K_{NO,AOB}$ Y_{AOB}	$\mu_{AOB,AMO}$ Y_{AOB} $\mu_{AOB,HAO}$ $K_{O2,AOB,2}$ $K_{NH4,AOB}$ $K_{NH2OH,AOB}$ η_{AOB}
	$2.5.10^{-5}$ - 1.10^{-4}	Y_{AOB} η_{AOB} $K_{NH2OH,AOB}$ $K_{I,O2,AOB}$	$K_{NH3,AOB}$ Y_{AOB} $K_{I,NH3,AOB}$	μ_{AOB} $K_{NH3,AOB}$	μ_{AOB} $K_{NH3,AOB}$ $K_{O2,AOB}$	$K_{O2,AOB,1}$
	<$2.5.10^{-5}$	$\mu_{AOB,HAO}$ $K_{O2,AOB,2}$ $K_{O2,AOB,1}$	$K_{NH2OH,AOB}$ η_{AOB} $\mu_{AOB,HAO}$ $K_{HNO2,AOB}$ $K_{O2,AOB,2}$ $K_{O2,AOB,1}$	$K_{O2,AOB}$ $K_{HNO2,AOB}$ η_{AOB}	$K_{I,O2,AOB}$ η_{AOB} $K_{HNO2,AOB}$	$K_{NO,AOB}$

Table 24. Parameters of the models A, A1, B, B1, and C calibrated with four case studies.

Name	Description	Unit	SBR1					OD exp			SBR2			UCT		
			A	A1	B	B1	C	A	B	C	A	B	C	A1	B1	C
η_{AOB}	N_2O emission factor	Dimensionless	0.35	0.2	0.08	0.1	0.06	0.082	0.63	0.285	0.096	0.56	0.337	0.5	0.3	0.3
$\mu_{AOB,AMO}$	Maximum AOB growth rate - AMO	h^{-1}	0.216	0.216	-	-	0.216	0.122	-	0.205	0.122	-	0.205	0.154	-	0.103
$\mu_{AOB,HAO}$	Maximum AOB growth rate - HAO	h^{-1}	0.062	0.062	-	-	-	0.105	-	-	0.109	-	-	0.032	-	-
$\mu_{AOB,HAO,1}$	Maximum AOB growth rate - HAO1 (C)	h^{-1}	-	-	-	-	0.062	-	-	0.085	-	-	0.091	-	-	0.032
$\mu_{AOB,HAO,2}$	Maximum AOB growth rate - HAO2 (C)	h^{-1}	-	-	-	-	0.413	-	-	0.567	-	-	0.607	-	-	0.178
μ_{AOB}	Maximum AOB growth rate	h^{-1}	-	-	0.035	0.035	-	-	0.045	-	-	0.052	-	-	0.032	-
$K_{HNO2,AOB}$	AOB affinity constant for HNO_2	$mgN.L^{-1}$	-	0.002	0.002	0.002	-	-	2^{E-05}	-	-	2^{E-05}	-	1^{E-06}	1^{E-06}	-
$K_{NO2,AOB}$	AOB affinity constant for NO_2^-	$mgN.L^{-1}$	150	-	-	-	-	0.14	-	-	0.14	-	-	-	-	-
$K_{I,NH3,AOB}$	AOB inhibition constant for NH_3	$mgN.L^{-1}$	-	16	-	16	-	-	-	-	-	-	-	0.5	0.1	-
$K_{I,HNO2,AOB}$	AOB inhibition constant for HNO_2	$mgN.L^{-1}$	-	-	-	0.4	-	-	-	-	-	-	-	-	0.001	-
$K_{NH2OH,AOB}$	AOB affinity constant for NH_2OH	$mgN.L^{-1}$	2.4	2.4	-	-	2.4	2.4	-	2.4	2.4	-	2.4	0.01	-	0.1
$K_{NH3,AOB}$	AOB affinity constant for NH_3	$mgN.L^{-1}$	-	0.4575	0.4575	0.4575	-	-	1.2	-	-	0.9	-	0.001	0.005	-
$K_{NH3,AOB,den}$	AOB affinity constant for NH_3 for AOB den	$mgN.L^{-1}$	-	-	-	0.4575	-	-	-	-	-	-	-	-	0.002	-
$K_{NH4,AOB}$	AOB affinity constant for NH_4^+	$mgN.L^{-1}$	5	-	-	-	5	2.4	-	2.4	2.4	-	2.4	-	-	0.1
$K_{NO,AOB}$	AOB affinity constant for NO	$mgN.L^{-1}$	0.004	0.004	0.004	0.004	0.004	0.0084	0.0084	0.0084	0.0084	0.0084	0.0084	0.01	0.1	0.07
$K_{O2,AOB,1}$	AOB affinity constant for O_2 - AMO	$mgO_2.L^{-1}$	0.043	0.043	-	-	0.043	0.043	-	0.4	0.043	-	0.4	0.4	-	0.28
$K_{O2,AOB,2}$	AOB affinity constant for O_2 - HAO	$mgO_2.L^{-1}$	0.6	0.6	-	-	0.6	0.76	-	0.073	0.65	-	0.058	0.4	-	0.2
$K_{O2,AOB}$	AOB affinity constant for O_2	$mgO_2.L^{-1}$	-	-	0.25	0.25	-	-	0.56	-	-	0.41	-	-	0.4	-
$K_{O2,AOB,den}$	AOB affinity constant for O_2 for AOB den	$mgO_2.L^{-1}$	-	-	-	0.25	-	-	-	-	-	-	-	-	3.59	-
$K_{I,O2,AOB}$	AOB inhibition constant for O_2 for AOB den	$mgO_2.L^{-1}$	2	-	-	2	-	1.24	-	-	1.76	-	-	-	5.01	-
$i_{N,BM}$	Nitrogen content of biomass	$mgN.mgCODX^{-1}$	0.07	0.07	0.07	0.07	0.07	0.07	0.07	0.07	0.07	0.07	0.07	0.07	0.07	0.07
Y_{AOB}	AOB growth yield	$mgCODX.mgN^{-1}$	0.15	0.15	0.15	0.15	0.15	0.15	0.15	0.15	0.15	0.15	0.15	0.18	0.18	0.18
$Y_{AOB,den}$	AOB growth yield for AOB denitrification	$mgCODX.mgN^{-1}$	0.15	0.15	0.15	0.15	0.15	0.15	0.15	0.15	0.15	0.15	0.15	0.18	0.15	0.18

3 Results

3.1 SBR1

All five models were examined with the data collected from SBR1. In this system more than 97% of the ammonia was converted to nitrite during the aerobic period and only a very low level of nitrate was detected. For the five models Figure 15 shows examples of simulated and experimental data (NH_4^+, NO_2^-, DO, NO and N_2O) during the aerobic periods obtained after calibration. Depending on the cycle oxygen varied from 2 to 6 mg O_2 L^{-1}, initial ammonium from 10 to 40 mg N L^{-1}, and final nitrite ranged from 30 to 135 mg NL^{-1}. N_2O and NO peaks were only observed during the aerobic period whereas no emission was observed during the anoxic phase (even with nitrogen gas injection). The five models were calibrated on a series of data (5 cycles) and model predictions were also validated with other cycles collected at different times in different conditions. For all models the predicted profiles of ammonium, nitrite and DO match the observed experimental trends. The four models based on nitrite denitrification (Models A, A1, B, B1) also describe the observed N_2O peak well. In contrast, Model C could not predict the variation of N_2O peaks for the different cycles, with high discrepancies at high nitrite concentrations. In those conditions with relatively high DO, simulations indicate that N_2O was mainly related to AOB processes with an insignificant contribution by heterotrophic denitrification.

For all models the predicted profiles of ammonium, nitrite and DO match the observed experimental trends. The four models based on the ND pathway (Models A, A1, B, B1) also describe the observed N_2O peak well. In contrast, Model C could not predict the variation of N_2O peaks for the different cycles, with high discrepancies at high nitrite concentrations. In those conditions with relatively high DO, simulations indicate that N_2O was mainly related to AOB processes with an insignificant contribution by heterotrophic denitrification.

The order of magnitude of NO peaks was reasonably predicted by the four models based on AOB denitrification but the increase of NO with HNO_2 was over estimated. In comparison model C could not predict this order of magnitude. Based on simultaneous monitoring of N_2O and NO calibration of the K_{NO} value was possible. However, despite significant calibration effort model C was unable to predict the experimentally observed change in the NO to N_2O

ratio (Table 25). Overall, the best predictions for NO and N_2O were observed with models A, A1, B and B1, basically because they are based on the AOB denitrification concept. Corrections made on the oxygen effect (inhibition) could also impact the simulation, but in the data used the DO was relatively high and the constant for oxygen inhibition was thus not identifiable. It should be pointed out that this system exhibits high transient nitrite accumulation and the data indicates a correlation between nitrite and the N_2O production rate (Figure 15). It was possible to predict this phenomenon with AOB denitrification models but not with the concept of incomplete hydroxylamine oxidation which is not related to nitrite (Model C).

Figure 16 compares the predicted and experimental emission factors (EF) for N_2O and NO for 11 different cycles (calibration and validation). These results confirm that Models A1, B and B1 show the best prediction of N_2O and NO emissions, Model A also being relatively good. The predictions of NO fluctuations are less accurate than for N_2O but the ratio between both gases is relatively well predicted by the models based on the ND pathway (Table 25). The model C based on the NN pathway could not predict the experimental data as it is unable to predict the effect of nitrite accumulation on N_2O and NO production. This leads to an underestimation of N_2O emission at high HNO_2 concentrations whereas NO emission is overestimated.

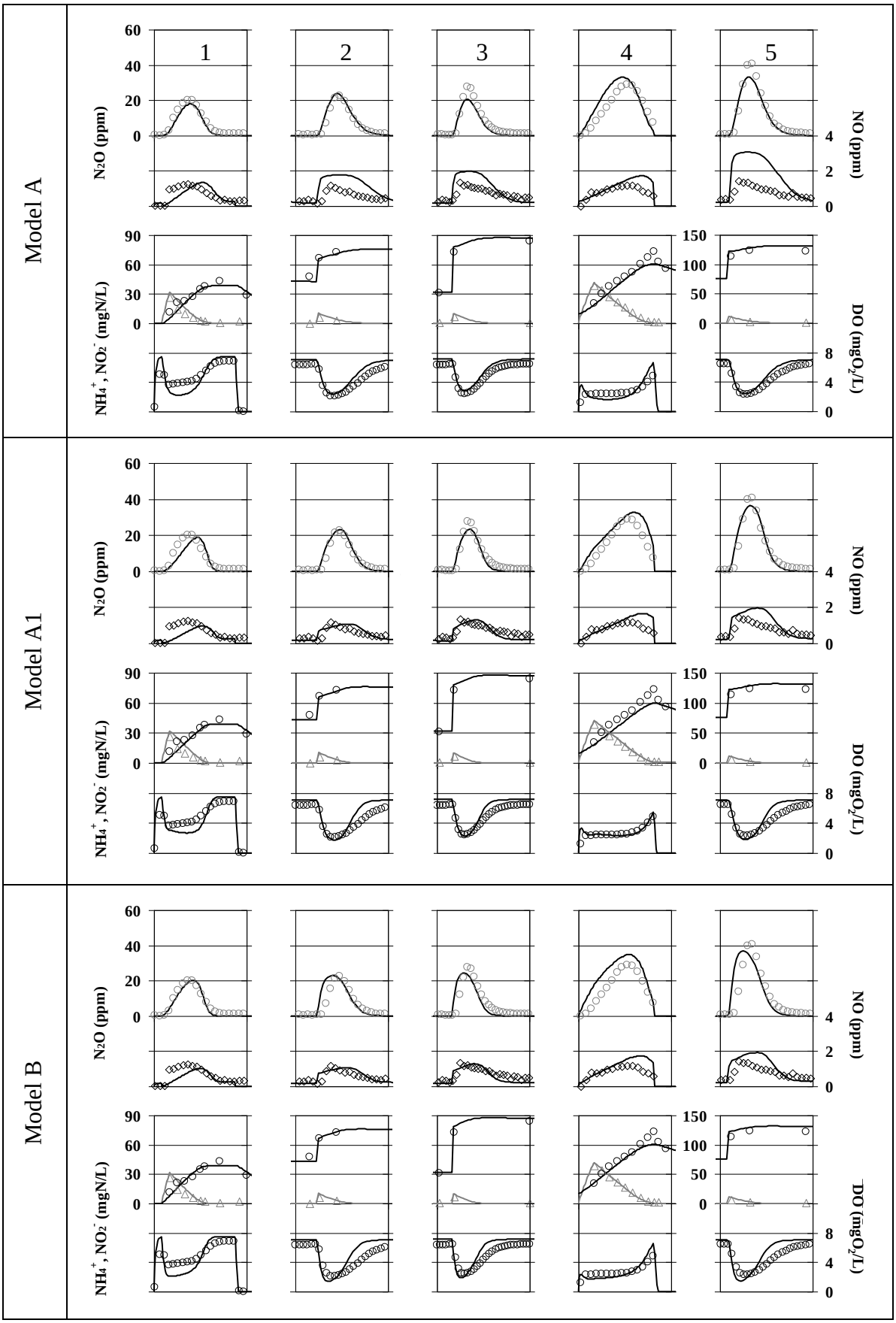
Model A
Model A1
Model B
1
2
3
4
5
N2O (ppm)
NO (ppm)
NH4+ , NO2- (mgN/L)
DO (mgO2/L)

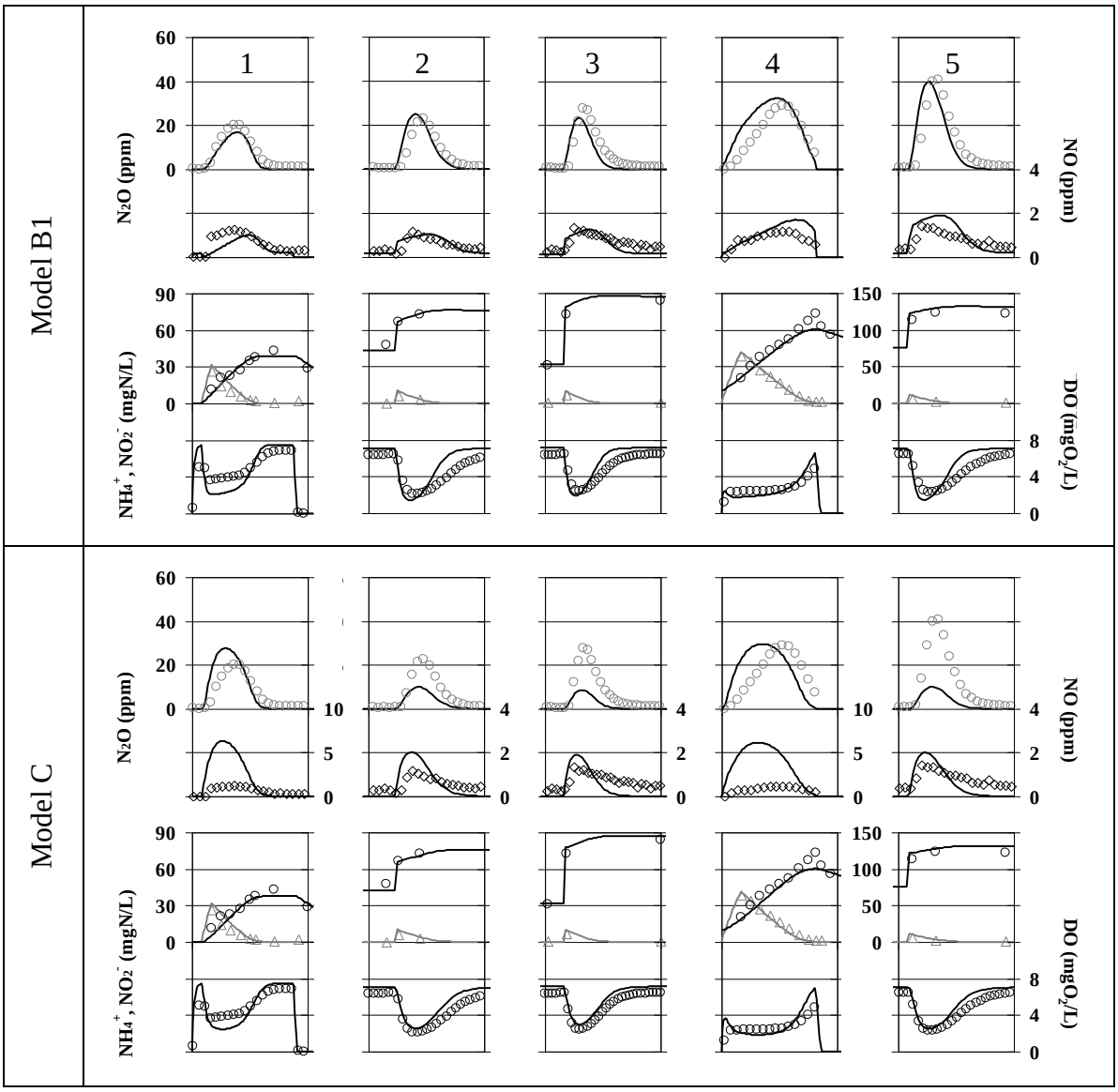

Figure 15. Dynamic of nitrification and NO and N_2O production for 5 experiments obtained with the SBR. Experimental results (in points) are confronted to modeling results (in line) for the five models. The dynamic of NO (◊) (secondary axis) and N_2O (○) (primary axis) production are presented in the first line of each models whereas ammonium (Δ), nitrite (○) (primary axis) and dissolved oxygen (○) (secondary axis) are presented in the second line. Duration of experiment 1 to 5 : 1h, 0.4h, 0.4h, 1h, 0.4h. Experimental N_2O emission factor for experiment 1 to 5 (in gN-N_2O/gN-NH_4^+ removed): 1.39 %, 2.58%, 3.86%, 1.83%, 4.52%.

Table 25. Comparison between experimental and simulated NO to N_2O ratio from SBR1.

	NO/N_2O ratio (gN-NO/gN-N_2O)				
Experiment/cycle	**1**	**2**	**3**	**4**	**5**
Data	4.4 %	4.6 %	4.9 %	2.9 %	3.5 %
Model A	5.3 %	7.5 %	9.2 %	2.9 %	8.6 %
Model A1	3.6 %	4.2 %	4.9 %	2.5 %	4.6 %
Model B	3.5 %	4.2 %	4.7 %	2.4 %	2.4 %
Model B1	4.1 %	4.2 %	5.2 %	2.7 %	4.5 %
Model C	12.0 %	10.7 %	11.6 %	10.5 %	10.8 %

N_2O emission factor (gN-N_2O/gN-NH_4^+ removed)	**NO emission factor (gN-NO/gN-NH_4^+ removed)**

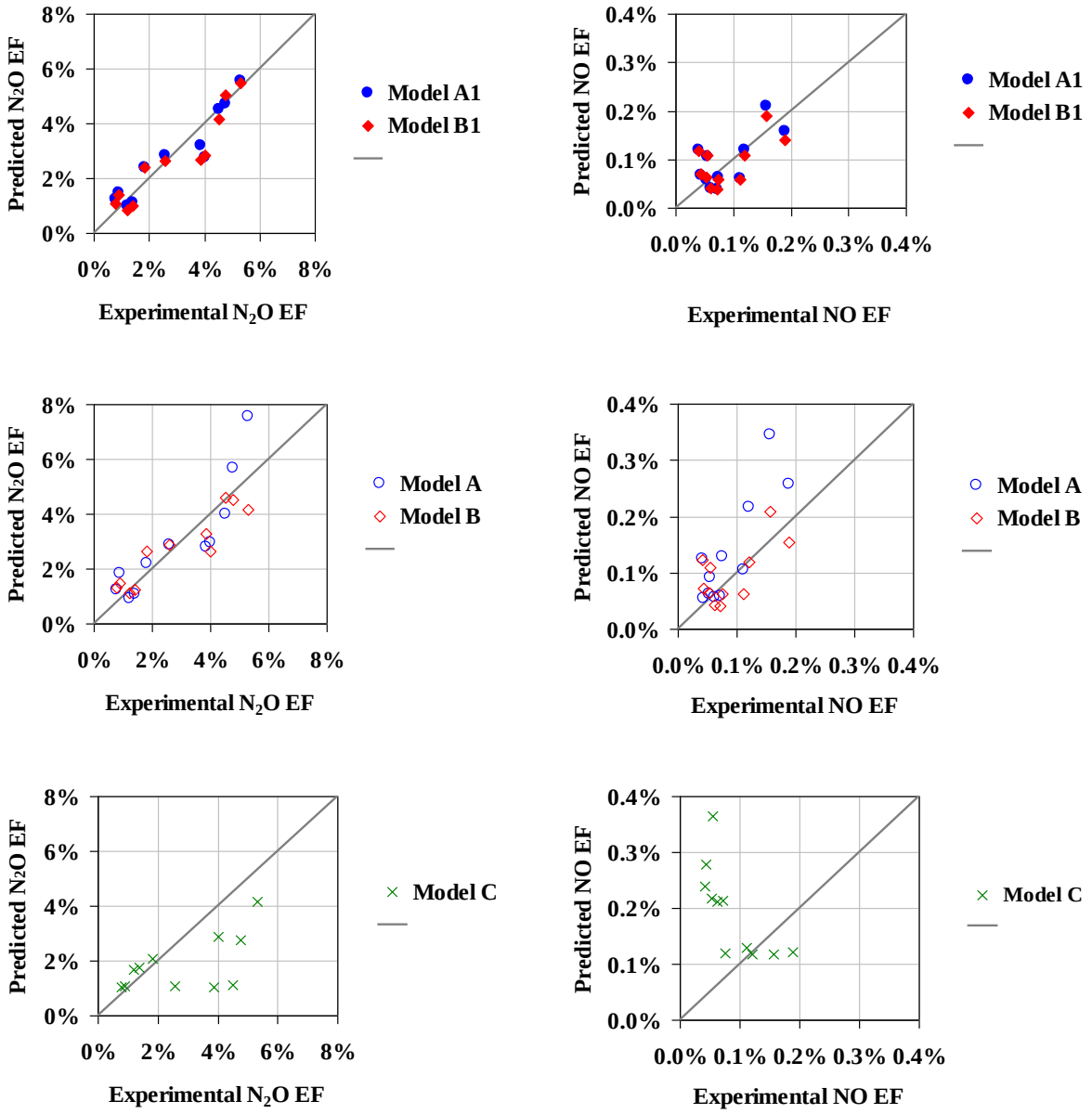

Figure 16. Comparison between experimental and predicted N_2O and NO emission factors for different cycles (11) obtained with the SBR1.

3.2 Oxidation ditch

The original AOB denitrification models (Models A and B) and the NH_2OH/NO model (Model C) were examined with the experimentally observed continuous N_2O data from the full-scale oxidation ditch (OD).The models were calibrated using the extensive monitoring data from a three-day intensive sampling campaign at three different locations (OD4-aeration zone, OD5-aerobic zone near the propulsor and OD2-anoxic zone) of the ditch. Figure 17

shows the simulated and experimental data (NH_4^+, NO_2^-, NO_3^- and N_2O) at the three locations along the ditch. The N_2O emissions occurred mainly in aerobic zones (OD4) with high ammonium concentrations but low nitrite accumulation.

For the three models (A, B and C) the predicted profiles of ammonium, nitrite and nitrate match the observed experimental trends. However, the results indicate that Model A cannot predict the N_2O data. Indeed, Model A predicts a dependency of N_2O production on DO that is opposite to that observed at the OD plant (Figure 17A-F). Conversely, the kinetic structure of Model B ensures that the N_2O production rate is dependent on oxygen availability, resulting in a N_2O dynamic trend similar to that shown by the experimental data (Figure 17G-L). However, for Model B to reasonably predict the N_2O production rate when nitrite accumulation in the OD system is very low (<0.67 mgN/L), a relatively high anoxic reduction factor (0.63) has to be employed due to the fact that the N_2O production rate is dependent on nitrite concentrations (this point is discussed below). In contrast, Model C achieves a good fit between the model-predicted and measured N_2O data. The NH_2OH pathway of Model C captures all observed trends.

3.3 SBR2

The original Models A, B and C were also evaluated with the experimentally observed N_2O data from a full-scale SBR plant (SBR2). The models were calibrated using the monitoring data collected from SBR2 during a three-cycle continuous intensive sampling campaign. Figure 18 shows the simulated and experimental data (effluent NH_4^+, NO_2^-, NO_3^- and N_2O) during the three cycles. Similar to the OD system, SBR2 also has low nitrite accumulation. In SBR2, N_2O emissions occurred mainly during aerated periods. The N_2O production rate increased with the increase of DO concentration during the SBR2cycles.

Again, for the three models the predicted profiles of ammonium, nitrite and nitrate match the observed experimental trends. As before, Model A predicts an N_2O trend opposite to that observed, while Models B and C achieve a good fit between the model-predicted and measured N_2O data. For Model B again, based on nitrite reduction pathway, a high reduction factor η_{AOB} (0.56) has to be used as the N_2O production rate is related to nitrite concentrations which was low in the SBR2.

Model A – ND pathway (Ni et al., 2011)

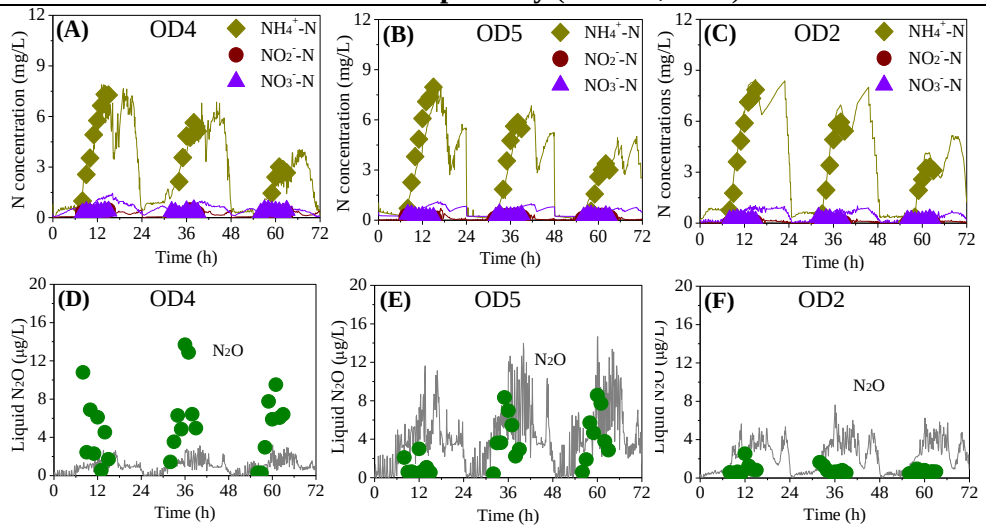

Model B – ND pathway (Mampaey et al., 2013)

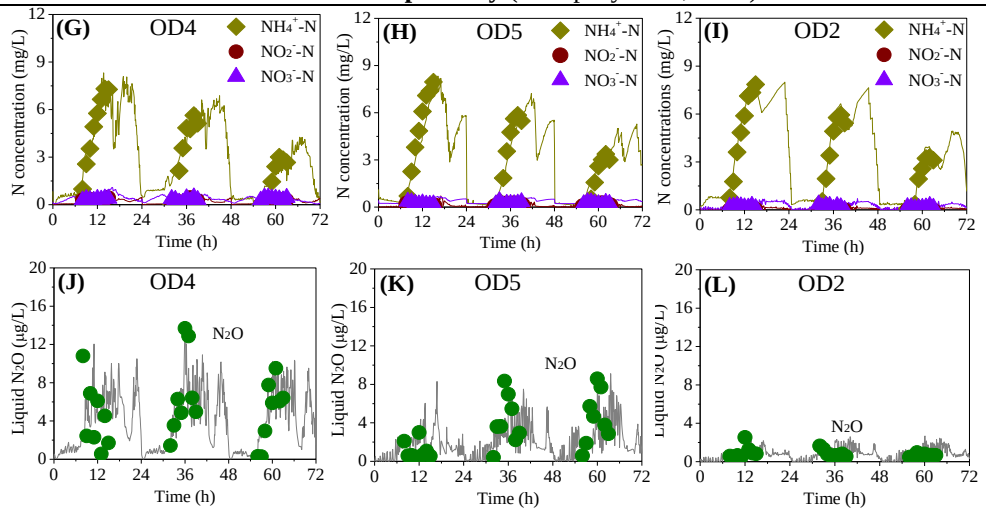

Model C – NN pathway (Ni et al., 2013a)

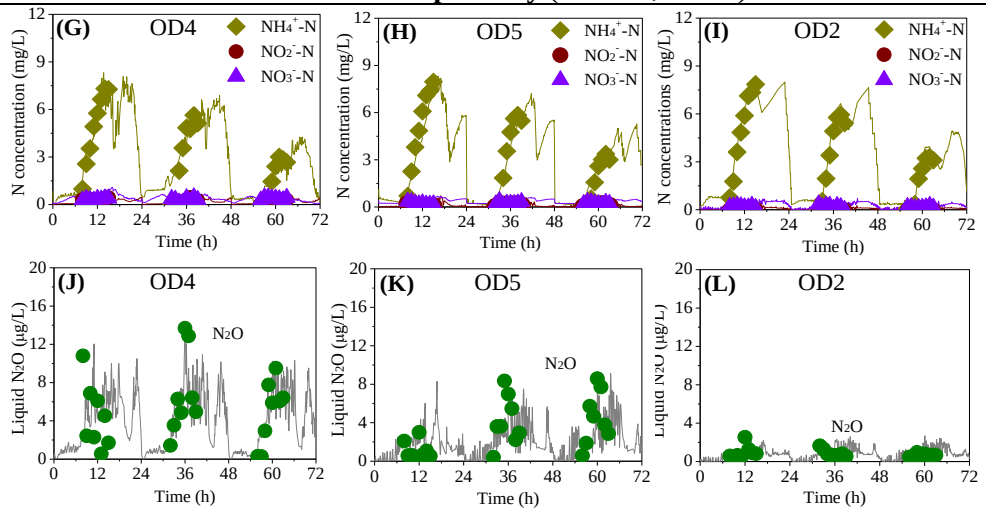

Figure 17. Model evaluation results of the three-day N_2O production data from the Oxidation Ditch WWTP (experimental data: symbols; model predictions: lines) with ammonium, nitrite, nitrate, and liquid phase N_2O profiles at the different sampling locations (OD4, OD5 and OD2): (A-F) Model A; (G-L) Model B; and (M-R) Model C.

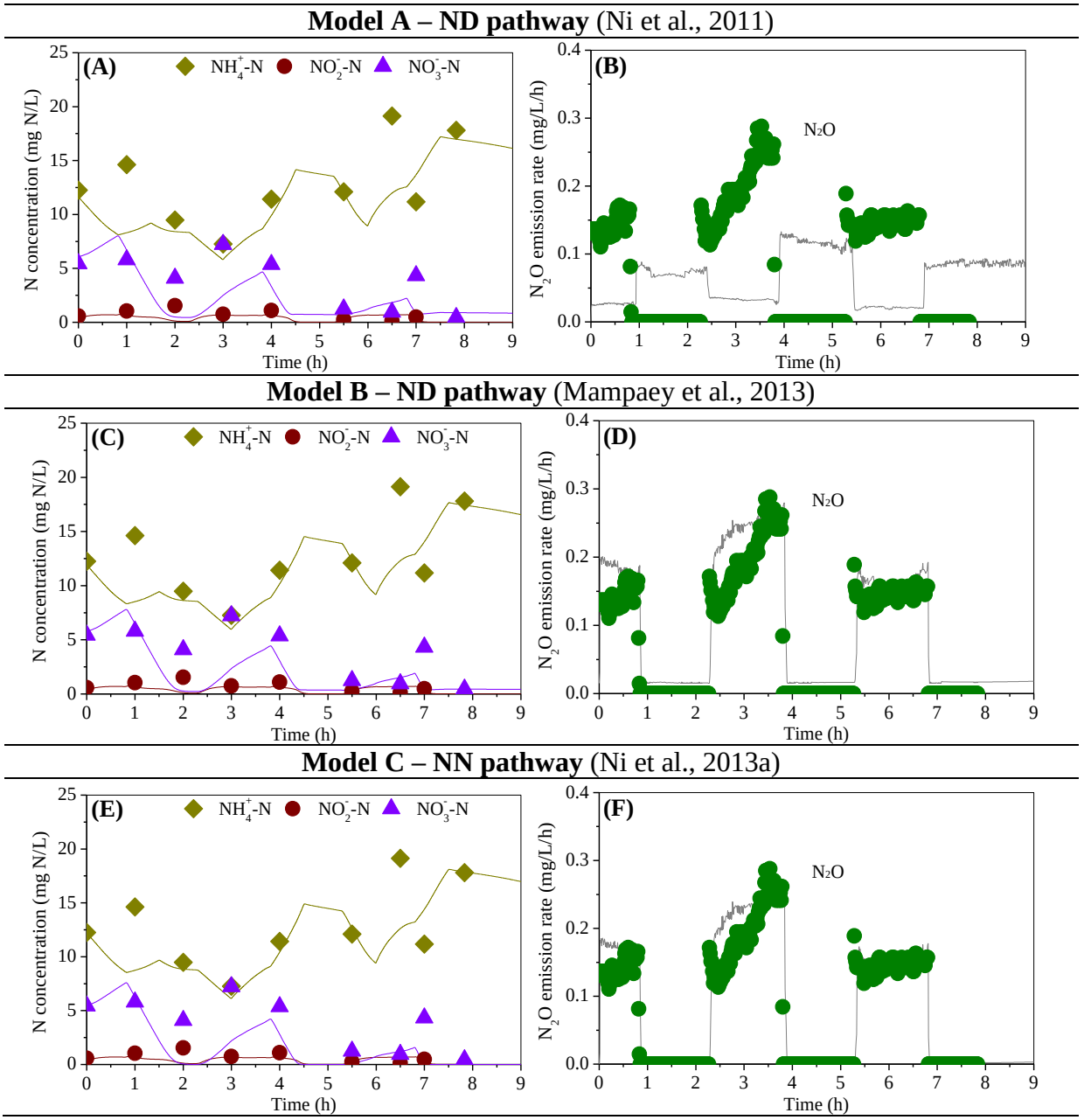

Figure 18. Model evaluation results of the N_2O production data from SBR2 WWTP (experimental data: symbols; model predictions: lines) with ammonium, nitrite, nitrate, and N_2O emission rate profiles: (A-B) Model A; (C-D) Model B; and (E-F) Model C.

3.4 UCT process

Dynamic simulations were confronted to the data collected on the UCT process from the Eindhoven plant. Model A1, Model B1 and Model C were implemented for this plant and their parameters were calibrated using date collected in a 1-month measurement campaign. Figure 19 compares the simulated NH_4^+, NO_3^- and DO concentrations with the on-line sensor data near the outlet of the summer aeration zone. Figure 20 compares the simulation and the measurement data of N_2O emissions at three different locations along the summer aeration

zone. The conclusion is that all models can be calibrated to the same level of fit. They have similar performance and can follow the dynamic variations in the measurement data. There was a rain event on August 25th - 26th. All models showed better simulation performance under dry-weather conditions than wet-weather conditions (Figure 19). Results show that there was less N_2O emission under wet-weather conditions compared to dry-weather conditions (Figure 20).

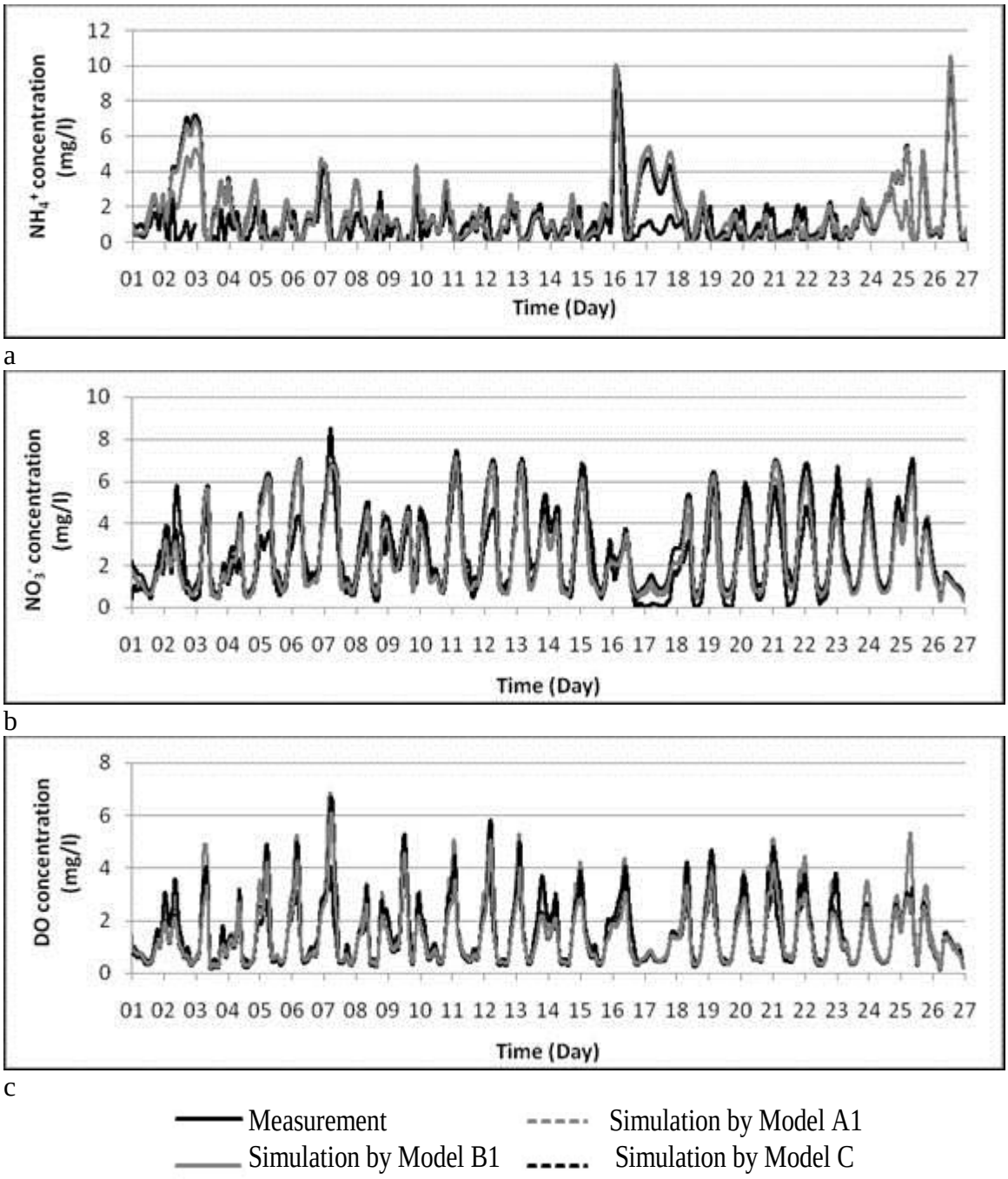

Figure 19. Comparison of the measurement results with the simulation results of NH_4^+ (a), NO_3^- (b) and DO (c) near the outlet of the summer aeration package

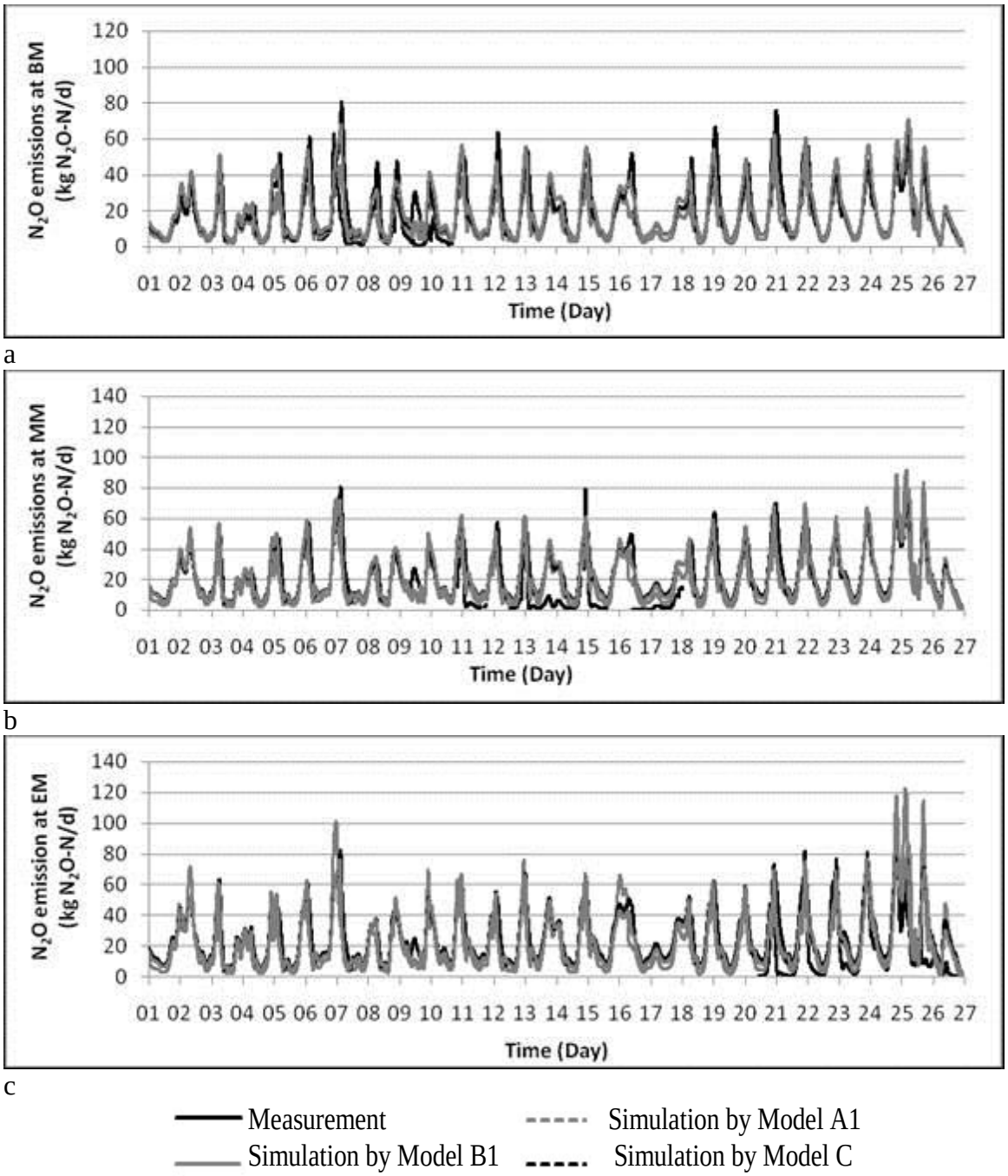

Figure 20. Comparison of simulated and measured N_2O emissions at the beginning (BM) (a), the middle (MM) (b) and the end section (EM) (c) of the summer aeration package

4 Discussion

4.1 Observed N_2O emissions and capabilities of the models

The data monitored on the four continuous systems considered in this study confirm that the N_2O emission factors varied very significantly from 0.1 to 5.2% of the nitrogen removed. Data and simulations also confirmed that nitrification is the major contributor to N_2O production. For instance, N_2O emissions were negligible in SBR1 during anoxic periods (checked with punctual nitrogen insufflation) probably thanks to a sufficient COD:N ratio for complete denitrification. In contrast 0.5 to 5% of nitrogen was converted to N_2O during aerobic nitrification depending on the FNA concentration (DO from 2 to 6 $mg.L^{-1}$). In OD the overall N_2O emission factor over a full month was 0.52% of the nitrogen load to the plant, with over 90% contribution from the aeration zone (DO of over 5 $mg.L^{-1}$). These data were issued from both liquid mass balance and gas emissions. Similarly, the N_2O emission factor of the SBR2 over the month is around 1.0-1.5 % of the nitrogen load, with N_2O emissions occurring mainly during aerated periods. Simulation of the UCT process (with Model B1) was used for quantifying the average contribution of heterotrophs and autotrophs to the N_2O production. This analysis shows that N_2O is mainly produced through the AOB pathway but it is to a significant extent consumed by heterotrophic denitrification. Overall, the total N_2O production by AOB is 290% of the net production while the heterotrophs contribute by -190% (Guo and Vanrolleghem, 2013b) i.e. for every 3 molecules of N_2O produced by AOB, 2 are removed by heterotrophs. These results thus clearly confirm the need of a good prediction for AOB-related N_2O production as well as heterotrophic denitrification by N_2O. Another important factor in such system when using AOB denitrifying models is that a good NOB growth model is needed to be able to predict nitrite concentrations which impact N_2O production by AOB (Houweling et al., 2011). This means that the ratio between AOB and NOB maximal growth rates as well as respective values of affinity constants for oxygen should be appropriately calibrated, which would determine the quality of nitrite prediction during daily peak loads and concomitantly the N_2O productions.

Table 26 summarizes the models capabilities for the different case studies. The simulations indicate that all five models can correctly describe the ammonium, nitrite and nitrate measurements. Concerning N_2O emissions all the experimental data can be correctly described by at least one (or several) models. Satisfying predictions were observed with AOB

denitrification models for SBR1 in which the nitrite concentration varied significantly, the best results being obtained with models considering FNA instead of total nitrite as the substrate for AOB denitrification (A1, B, B1). On the contrary it was not possible to predict the data with Model C based on incomplete oxidation of hydroxylamine, as the effect of nitrite (or FNA) was not considered in this model. In addition, NO emissions were also predicted more accurately with the AOB denitrification model (see data from SBR1). For the OD and SBR2 systems in which nitrite did not accumulate, the simulations with model B and C were in agreement with the observations whereas the other model based on AOB denitrification (Model A) failed. Finally, for the UCT system, Models A1, B1 and C could not be discriminated given the data set collected, all performed adequately.

Table 26. Comparison of models capabilities after calibration on the different case-studies

	Systems			
Models	**SBR1**	**OD**	**SBR2**	**UCT**
Model A	+/-	-	-	
Model A1	+			+
Model B	+	+	+	
Model B1	+			+
Model C	-	+	+	+

Overall it can be stated that the model based on the hydroxylamine pathway was able to match most of the data except for the system with important transient nitrite accumulation (SBR1). On the other hand the models based on AOB denitrification were able to fit most of the data, either those using hydroxylamine as a state variable (A, A1) or those which do not (B, B1). Concerning the effect of DO, for the systems well described by the AOB denitrification concept (SBR1, UCT) the functions used to reduce N_2O emissions when oxygen increases slightly improved the predictions (model B1, A). The use of the Haldane expression in model B1 (instead of the inhibition term only in model A) allows to predict more accurately the data obtained in the UCT process which exhibited large variation of DO from 0.4 mgO_2/L to more than 6 mgO_2/L. However, it must be stated that Models A1 and C were also able to reasonably fit the same data without this oxygen inhibition term. In the SBR working with high nitrite accumulation (SBR1) the DO was not very influential in the range presented here (from 2 to 6 mgO_2/L) and for this reason the models which do not consider DO

inhibition (A1, B) were able to describe the observations as well as the model B1 with Haldane expression (with relatively high inhibition constant). Hence it is not possible here to conclude definitively on the benefit of considering inhibition by oxygen. Moreover higher N_2O production (measured in the liquid phase) was observed in the OD process in zones with higher dissolved oxygen, which further supports a positive correlation between N_2O emissions and DO in this system. It is important to note that the influence of oxygen differs among the predominant pathways. The model based on the hydroxylamine pathway describes the observations of the oxidation ditch better because N_2O is positively related to oxygen in that pathway, assumed to be predominant in that system (due to the low nitrite concentration). On the other hand a slight decrease of N_2O emission with increased DO was observed in SBR1. In that systems the predominant pathway is likely to be the ND pathway which is logically reduced by increasing the oxygen concentration. In conclusion, the available data were not sufficiently discriminant for this question regarding the oxygen effect but it is suggested to evaluate in the future a multiple pathway model with different effect of oxygen on the emission depending on the pathway.

4.2 Comparison of parameter sets

It should be noted that these properties of the five different models were obtained after significant calibration efforts, and thus the key parameter variations as well as their physical significance are also highly relevant when discussing the validity of the models. All the parameters of the models are given in Table 24 and in Appendix D, Appendix E, Appendix F and Appendix G. Table 27 presents the range of variation of the set of AOB parameter values obtained after calibration of each model to the different case studies. Some of the parameters exhibit a large variation among the case studies (more than 100%), which means that they need to be significantly modified from one case to another. The reduction factor η_{AOB}, the half saturation constant for nitrite or FNA (for models A, A1, B, B1), and the half saturation constant for NO (model C) are at the same time highly variable among the case studies and very influential on N_2O and NO emission results. For instance for different systems which were correctly predicted, the reduction factor varied from 0.08 to 0.63 for model B and similar variations were observed for the other models based on denitrification pathway. For model C, based on the other concept, the calibration needed important adjustment of the affinity constant (K_{NO} from 8.4 10^{-3} to 7 10^{-2} mg/L, K_{NH2OH} from 0.1 to 2.4 mg/L). None of

the models was able to predict all measured N_2O data sets without significant parameter adjustment. On the one hand this agrees with the finding of (Ni et al., 2013a) through model evaluation with batch data that it is difficult to predict data obtained under various operating conditions with models based on a single pathway. On the other hand this comparison using long-term data provides new information which allows evaluating the range of application of each model.

Concerning the models based on the AOB denitrification pathway (e.g., A1 and B1) the large variation of some parameters among the case studies seemed to be related to the range of nitrite (or FNA) concentrations observed in each system. This can be illustrated by two case studies with important difference in the nitrite concentration range: the SBR1 and the UCT process. In Figure 21, the influence of the FNA concentration on the simulated NO production rate is represented for these two models (A1 and B1) calibrated for the SBR1 and UCT systems respectively. It should be pointed out that the N_2O production rate is correlated to the NO production rate as NO is the precursor for N_2O in these models. In the system with low nitrite concentration (UCT), a high value for η_{AOB} (0.3-0.5) and a low value for $K_{HNO2,AOB}$ (10^{-5}-10^{-6}) are obtained in order to fit the observed NO and N_2O emission data. In such situation, the accuracy and the physical significance of the parameters must be evaluated with caution. Indeed the factor η_{AOB} defined originally as a reduction factor for (anoxic) AOB denitrification becomes very high and the affinity constant for FNA is poorly identifiable. With these parameter values the N_2O production rate is little affected by the nitrite concentration, except for very low concentrations. In comparison, a lower value for η_{AOB} (0.1-0.2) and a higher value for $K_{HNO2,AOB}$ (2.10^{-3}) were obtained during the calibration of the models on the SBR1 process. With those parameters a variation of the FNA concentration influences the NO and N_2O production rates significantly.

These large variations of parameters from one system to another could be explained by different reasons: micro-organisms history and adaptation, defaults in the structure of the models, undescribed local heterogeneities in reactor. The nitrifying bacteria are indeed able to acclimatize in different ways to the environmental situations, substrate or inhibitors levels. Adaptation of enzymatic activity (NirK for instance) possibly occurs in these systems. Considering this physiological adaptation the problem with actual model structures is that model constants should actually be treated as model variables. The observed differences could be also due to different nitrifying communities. Based on the observation of Terada et al.

(Terada et al., 2013) the *Nitrosospira* could be adapted to continuously fed process (UCT, OD) and *Nitrosomonas* in SBRs for instance. This would mean that the calibration realised at low nitrite concentrations (and low loaded process) is not valuable in a system with high nitrite accumulation in high loaded process (and vice-versa).

Alternatively, it could be that the second pathway based on hydroxylamine incomplete oxidation is also present in parallel to the denitrification pathway. In that case a model that considers both pathways would have potential as it could possibly describe a larger range of experimental conditions with a single parameter set, a desirable property as it reduces the calibration effort (Ni et al., 2014). In case further experiments confirm that adaptation actually occurs, calibration will remain to be required.

Finally a limit of the modelling exercise with full scale processes is to not consider the non-ideality nature of mixing and diffusion within the mixed liquor such that measurements of ammonia and nitrite at the macro-scale (in the bulk) solution may not be representative of what the bacteria are actually experiencing at the micro-scale. In case of significant heterogeneities the values of parameters lump biochemical and physical phenomenon. This could be also an explanation for the differences in parameter values observed for a perfectly mixed reactor lab-scale reactor (SBR1) and full scale reactors (OD, UCT, SBR2).

Table 27. Relative standard-deviation of parameters for all the different case-studies

model A		**model A1**		**model B**		**model B1**		**model C**	
	$\sigma_y/\bar{y}$		**$\sigma_y/\bar{y}$**		**$\sigma_y/\bar{y}$**		**$\sigma_y/\bar{y}$**		**$\sigma_y/\bar{y}$**
$K_{NO2,AOB}$	173%	$K_{HNO2,AOB}$	141%	$K_{HNO2,AOB}$	168%	$K_{HNO2,AOB}$	141%	$K_{NO,AOB}$	139%
η_{AOB}	86%	$K_{NH3,AOB}$	141%	η_{AOB}	71%	$K_{NH3,AOB,den}$	140%	$K_{O2,AOB,2}$	109%
$K_{NH4,AOB}$	46%	$K_{NH2OH,AOB}$	140%	$K_{NH3,AOB}$	44%	$K_{NH3,AOB}$	138%	$K_{NH4,AOB}$	81%
$K_{NO,AOB}$	37%	$K_{I,NH3,AOB}$	133%	$K_{O2,AOB}$	38%	$K_{NO,AOB}$	131%	$K_{NH2OH,AOB}$	63%
$\mu_{AOB,AMO}$	35%	$K_{O2,AOB,1}$	114%	$K_{NO,AOB}$	37%	$K_{O2,\ AOB,den}$	123%	$K_{O2,AOB,1}$	60%
$\mu_{AOB,HAO}$	28%	η_{AOB}	61%	μ_{AOB}	19%	η_{AOB}	71%	η_{AOB}	51%
$K_{I,O2,AOB}$	23%	$K_{NO,AOB}$	61%	$i_{N,AOB}$	-	$K_{I,O2,AOB}$	61%	$\mu_{AOB,HAO,1}$	40%
$K_{O2,AOB,2}$	12%	$\mu_{AOB,HAO}$	45%	Y_{AOB}	-	$K_{O2,AOB}$	33%	$\mu_{AOB,HAO,2}$	40%
$K_{O2,AOB,1}$	-	$\mu_{AOB,AMO}$	24%	$Y_{AOB,den}$	-	Y_{AOB}	13%	$\mu_{AOB,AMO}$	29%
$i_{N,AOB}$	-	$K_{O2,AOB,2}$	28%			μ_{AOB}	6%	Y_{AOB}	10%
$K_{NH2OH,AOB}$	-	Y_{AOB}	13%			$i_{N,AOB}$	-	$Y_{AOB,den}$	10%
Y_{AOB}	-	$Y_{AOB,den}$	13%			$Y_{AOB,den}$	-	$i_{N,AOB}$	-
$Y_{AOB,den}$	-	$i_{N,AOB}$	-						

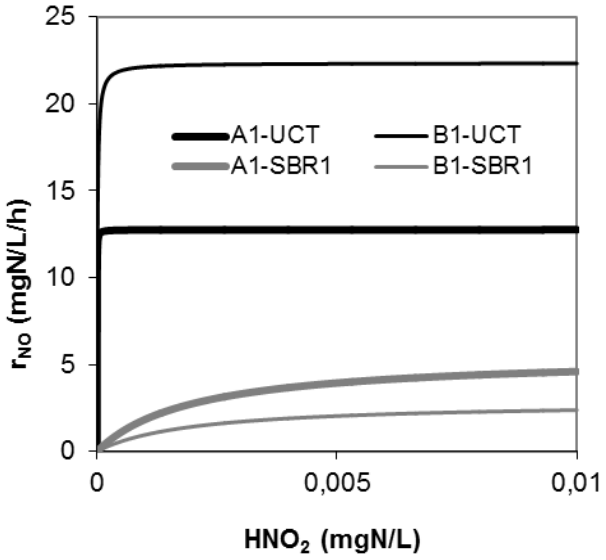

Figure 21. Relation between NO production rate and HNO_2 concentration with AOB denitrification models (A1, B1) calibrated on different data (example of UCT and SBR1).

4.3 Relation between N_2O pathways and nitrite (or HNO_2) concentration

From the model comparison it can be concluded that the AOB denitrification models are able to describe N_2O emissions from the SBR process with high nitrite variation whereas the NH_2OH/NO model (C) is not able to predict this system. For all the other systems with low nitrite concentration, the model based on the hydroxylamine pathway (C) fits well with the observations, as well as the models based on AOB denitrification after critical adaptation of some parameters. This supports the assumption that regulation of the N_2O production pathway could be influenced by the free nitrous acid (FNA) concentration. For example, the maximal nitrite concentration in the OD and SBR2 are respectively around 0.67 mgN/L and 1.53 mgN/L, with pH close to 7.1. This corresponds to 0.16 and 0.32 µgN-FNA/L respectively at 15°C. It was also observed that in SBR1 the production of N_2O decreases very significantly when the FNA concentration was lower than 0.5 µgN-FNA/L. It could be speculated that this value could be the limit below which the AOB denitrification processes become less significant compared to the hydroxylamine oxidation pathway. On the other hand, in the UCT system the highest observed nitrite concentration was only 0.11 mgN/L and the Models A1, B1 and C were able to describe the observed trends. Obviously as discussed previously for full scale processes the measurements of FNA in bulk solution may be not representative of what the bacteria actually experience transiently in some local zone where

nitrite can accumulate punctually. In contrast the pilot SBR can be considered as a perfectly mixed system. In this reactor the analysis of the variation of NO:N_2O ratio and N_2O emissions also supported the idea that nitrite stimulated the AOB denitrification pathway (Pocquet et al., 2013).

Indeed it seems logical that the pathway based on nitrite denitrification was favoured when nitrite accumulates. As it is related to a competition for electrons between nitrite and oxygen as electron acceptors, this competition process should be more intensive at a high FNA:DO ratio, or in case of alternating anoxic-aerobic phases. Considering the model structures, models based on AOB denitrification correlate the N_2O production rate to nitrite, whereas the NH_2OH oxidation models correlate the N_2O production to the ammonium uptake rate. This should be considered for future applications when selecting one of these models. In addition these observations may help the future development of a generic model involving both the AOB denitrification and the NH_2OH pathways. Finally, it is good to mention that these results are in accordance with the results of the quantification of the origin of N_2O during nitrification based on isotope signatures (Rathnayake et al., 2013; Toyoda et al., 2011; Wunderlin et al., 2013). (Wunderlin et al., 2013) demonstrated that the nitrite reduction pathway was the major mechanism responsible for N_2O production during batch feeding with ammonium and nitrite. In contrast, the hydroxylamine oxidation pathway became the major process as soon as hydroxylamine accumulated or was injected. The contribution of N_2O reduction was also observed to increase with the nitrite accumulation over time (Rathnayake et al., 2013; Wunderlin et al., 2013). A recent study also indicated that very high nitrite concentration can also inhibit the AOB denitrification pathway (Law et al., 2013). Given the role of nitrite and FNA in determining N_2O emissions and pathways in some of the systems, the ability of AOB/NOB growth models to predict nitrite buildup would be also a key point for future modelling exercises.

5 Conclusion

The continuous long-term data sets collected from four different biological processes and the calibration results obtained for different model structures compiled in this paper lead to the following conclusions:

- All the collected N_2O data can be described by at least one (or several) model(s) tested in this study and the results allow evaluating the most appropriate N_2O model for each system and operational condition.
- Concerning the two different model concepts for N_2O production by AOB: the hydroxylamine pathway model can describe most of the data except for those obtained from a system with transient high accumulation of nitrite; the models based on AOB denitrification can fit most of the data except with critical values for some parameters for DO inhibition.

- None of the models were able to describe with similar parameter sets the data obtained in systems with high and low nitrite concentrations. A significant calibration effort is necessary for each system, in some cases leading to extreme and controversial values for parameters. Variability of the parameters can be related to physiological adaptation of micro-organisms, a microbial population switch, regulation between multiple AOB pathways or difficulties related to undescribed local concentration heterogeneities.

- The regulation between the N_2O production pathways is likely correlated with (variation of) the nitrite concentration in the system. Future efforts will be deployed to evaluate a more generic model in which the enzymatic regulation and/or the interaction between both AOB pathways are described, and it will be necessary to evaluate whether such approach could extend the model validity and reduce calibration effort.

Chapter V Variation of the NO/N_2O ratio during nitrification: an indicator to track N_2O production pathways

Abstract

The variation of NO and N_2O emissions during nitritation under aerobic conditions was investigated with a mixed culture developed in a sequencing batch reactor (SBR). The stimulating effect of free nitrous acid (HNO_2) on N_2O emission was shown both during dedicated batch experiments with various levels of nitrite and during SBR operation in different periods. For all the experiments, the NO/N_2O ratio measured during aerobic ammonium oxidation decreased from 0.5 gN-NO/gN-N_2O to 0.02 gN-NO/gN-N_2O as HNO_2 increased (in the range 0-1.77 $\mu gN.L^{-1}$) reflecting the stimulation of the nitrifier denitrification (ND) pathway. These observations confirmed the key role of HNO_2 level in the pathway regulation. During batch experiments performed with hydroxylamine, which is known to stimulate the NN pathway (hydroxylamine oxidation pathway), the highest values were obtained for NO/N_2O, i.e. 0.4-0.5 gN-NO/gN-N_2O. These observations suggest that the value of NO/N_2O ratio depends on the respective contribution of each N_2O production pathway, the ND pathway resulting in a lower NO/N_2O ratio than the NN pathway. Measurement of NO/N_2O ratio in the off-gas could be an appropriate indicator to track N_2O production pathways.

1 Introduction

Ammonia oxidizing bacteria (AOB) have been identified as significant contributors to N_2O emissions in WWTP (Kampschreur et al., 2009; Law et al., 2012b). Two major pathways were recently investigated: NN and ND pathways (Figure 22). The contribution of each N_2O production pathway and the effect of operating conditions on their regulation were recently evaluated by isotope techniques.(Peng et al., 2014; Toyoda et al., 2011; Wunderlin et al., 2013). (Wunderlin et al., 2013) demonstrated that the contribution of the NN pathway was dominant when hydroxylamine was used as the nitrogen source, whereas the ND pathway predominated during ammonia oxidation (batch experiments). It was also observed that the contribution of the ND pathway increased with time during the oxidation of ammonia as the nitrite accumulated. (Peng et al., 2014) found that the ND pathway was the main contributor to N_2O production during ammonia oxidation (73% - 95% of N_2O from the ND pathway). This work also indicated that, for similar operating conditions, the increase of the dissolved oxygen (DO) concentration from 0.2 to 3 $mgO_2.L^{-1}$ led to an increase of the NN pathway contribution from 5 % to 27%.

The existence of a regulation among the different pathways can explain some contradictory observations concerning the effect of operating parameters on N_2O emissions. N_2O emission rate is known to increase with increasing nitrogen load during nitrification (Marlies J Kampschreur et al., 2008; Kim et al., 2010; Law et al., 2012a; Tallec et al., 2006). A confounding effect of nitrite has recently been reported. (Law et al., 2013) observed a decrease of the specific N_2O production rate at very high nitrite concentration, whereas N_2O emissions were observed to be proportional to nitrite accumulation in previous studies (Foley et al., 2010; Kim et al., 2010; Shiskowski and Mavinic, 2006; Tallec et al., 2006). It was suggested that the ND pathway was inhibited at very high nitrite level and the NN pathway became predominant. The influence of dissolved oxygen on each production pathway could also be different. DO limitation is thought to encourage N_2O emission by the ND pathway but such a correlation has not been demonstrated for the NN pathway. In practice, DO limitation resulted in higher N_2O emission factors (Goreau et al., 1980; Marlies J Kampschreur et al., 2008; Peng et al., 2014; Pijuan et al., 2014; Tallec et al., 2006) but the N_2O production rate decreased with the decrease of the DO (Ni et al., 2013a; Peng et al., 2014). Consequently no single pathway model could describe all these observations as previously highlighted in the previous chapter and also in (Ni et al., 2013a). Recently a two-pathway model for N_2O

emissions was proposed by (Ni et al., 2014) but the validation and calibration of this model is still limited as only the isotopes technique has been proposed for experimental assessment of each pathway.

The aim of the present chapter is to investigate NO and N_2O emissions during ammonia and hydroxylamine oxidation. Its main originality is to reveal a possible relation between the variation of NO/N_2O ratio and the regulation between N_2O production pathways. In particular, the influence of the free nitrous acid concentration is evaluated using both dedicated batch experiments and long-term data collected in a sequencing batch reactor (SBR).

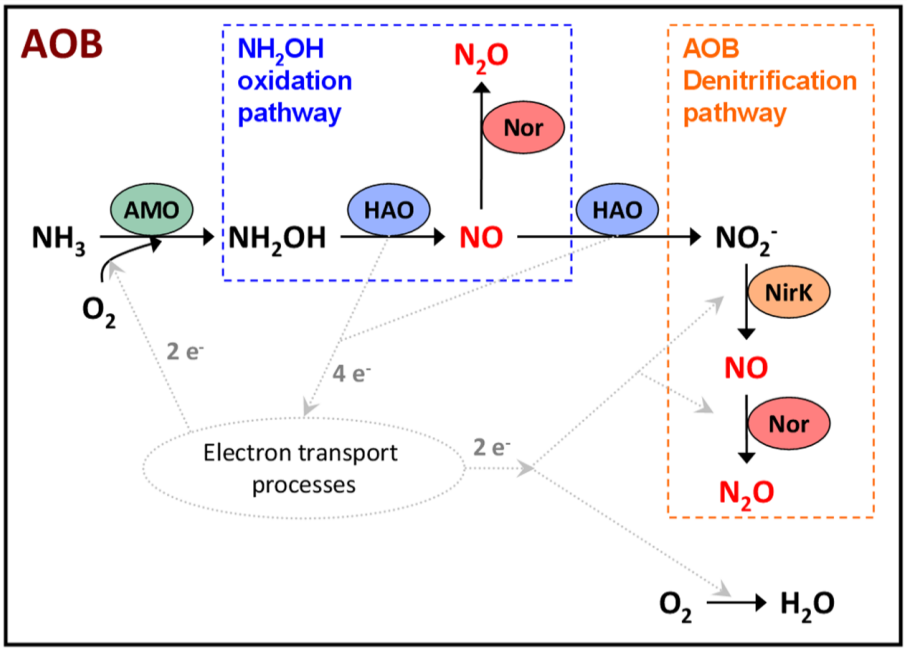

Figure 22. Schematic description of enzymatic pathways in ammonium oxidizing bacteria.(Ni et al., 2014; Poughon et al., 2001; Ritchie and Nicholas, 1972; Schlegel and Bowien, 1989; Yu et al., 2010)

2 Experimental data

The experimental set-up and the operating conditions of the SBR are described in chapter III. In this chapter, experimental data sets 2 and 3 are analyzed and correspond respectively to the aerobic period of SBR cycles and batch experiments using the SBR mixed culture with similar pH and temperature conditions. These sets of experimental data are detailed below.

2.1 Aerobic period of SBR cycles – set 2

The aerobic period of cycles monitored during three different operational periods of the SBR were selected for this study. Operating conditions are summarized in Table 28. The duration of the nitrification and denitrification phases were fixed during period II (32 days), at 100 minutes and 180 minutes respectively. The nitrogen load was 0.286 $gN\text{-}NH_4^+.L^{-1}.d^{-1}$ during this period. In contrast, an adaptive control of phase length was used during periods I (16 days) and III (13 days). This control system was based on DO and ORP bending point detection (by derivative calculation), which indicated the end of nitrification or denitrification respectively. The optimal times for switching off aeration and ending the reaction phase were determined. The nitrogen load varied in the 0.218-0.926 $gN\text{-}NH_4^+.L^{-1}.d^{-1}$ range during periods I and III. The configuration 1 was used during the periods II and III (Table 29) and the configuration 2 for the period I (Table 30). At the beginning of each cycle, the total initial ammonia concentration imposed in the reactor was between 35.8 and 55.0 $mgN\text{-}NH_4^+.L^{-1}$. At the time experiments were started, the SBR had been running for approximately two months and was showing stable performance. For all the cycles monitored in this study, ammonium was totally removed during the aerobic phase and was almost fully converted to nitrite (>95%). Nitrite and nitrate were completely removed during the anoxic phase.

Table 28. Characteristics of three periods of SBR operation.

Period	Automatic Control	Cycle configuration	Initial NH_4^+ ($mgN.L^{-1}$)	DO ($mgO_2.L^{-1}$)	N load ($gN\text{-}NH_4^+.L^{-1}.d^{-1}$)
I	Yes	2	36.0 - 51.0	1.4 – 5.3	0.253 – 0.605
II	No	1	55.0	1.5 – 5.7	0.286
III	Yes	1	55.0	0.9 – 5.3	0.218 – 0.926

Table 29. SBR cycle composition: Configuration 1

Action	Description	Aerated	Length (minutes)
1	Ammonia feeding	YES	10
2	Nitrification	YES	100 or controlled
3	COD feeding	NO	2.5 – 7.5
4	Denitrification	NO	180 or controlled
5	Settling	NO	20
6	Withdrawal	NO	8

Table 30. SBR cycle composition: Configuration 2

Action	Description	Aerated	Length (minutes)
1	Aerobic period	YES	15
2	Ammonia feeding	YES	10
3	Nitrification	YES	Controlled
4	Aerobic period	YES	20 – 40
5	COD feeding	NO	2.5 – 7.5
6	Denitrification	NO	Controlled
7	Settling	NO	20
8	Withdrawal	NO	8

This study focused on nitrification and the NO and N_2O emissions were attributed to AOB activity. Heterotrophic biomass was present but it was checked that its contribution to NO and N_2O emission was negligible. In the SBR, no significant amounts of NO or N_2O were emitted during anoxic phases (checked by punctual injection of nitrogen gas into the reactor) so only the emissions during aerobic phases were collected. During the batch tests, the contribution of denitrification was expected to be negligible as DO was higher than 2 $mgO_2.L^{-1}$ and no organic substrate was added. In order to confirm this assumption, tests were also carried out in pure anoxic conditions with constant nitrogen gas flow: ammonia, hydroxylamine and nitrite were injected and the levels of NO and N_2O emissions were not detectable.

2.2 Batch kinetics – set 3

With the same volume of sludge (1.43 L), dedicated batch kinetics tests were carried out. All experiments were performed with pH and temperature similar to those imposed in the SBR. It was first verified that ammonium, nitrite and nitrate had been initially completely removed from the bulk. Then different amounts of ammonium, nitrite, and hydroxylamine were imposed with different feeds of synthetic solutions: 15 $gN\text{-}NH_4^+.L^{-1}$ (NH_4Cl), 15 $gN\text{-}NO_2^-.L^{-1}$ ($NaNO_2$), 14.3 $gN\text{-}NH_2OH.L^{-1}$ (NH_2OH solution – Sigma-Aldrich). Conditions are presented in Table 31. All tests were performed with a constant aeration rate and, for all experiments, the minimal value of DO during the nitrogen oxidation (NH_4^+ or NH_2OH) was between 2.0 and 5.4 $mgO_2.L^{-1}$. A first series of tests was performed for ammonium oxidation with ammonium concentration varying from 10.5 to 54.8 $mgN.L^{-1}$, and initial nitrite concentration

from 0 to 100.5 mgN.L^{-1}. A second series of tests was carried out with hydroxylamine (10.5-21.1 mgN.L^{-1}), with or without nitrite initially present (0-10.5 mgN.L^{-1}).

Table 31. Summary of batch experiments using ammonium or hydroxylamine as substrate.

Experiment	N injected (mgN.L^{-1})	NO_2^- (mgN.L^{-1})		HNO_2 (µgN.L^{-1})		EF (gN-NxO/gN-NHx)		
		Start	End	Start	End	N_2O	NO	NO/N_2O (gN/gN)
NH_4^+ addition								
	10.49	10.5	21.0	0.07	0.15	0.16%	0.081%	0.516
	10.49	22.5	33.0	0.11	0.16	0.12%	0.048%	0.405
	10.49	20.5	31.0	0.15	0.22	0.83%	0.080%	0.097
	10.49	36.5	47.0	0.22	0.28	0.89%	0.047%	0.053
	54.8	0.0	53.8	0.00	0.70	1.84%	0.049%	0.027
	48.6	52.8	100.0	0.70	1.32	2.87%	0.080%	0.028
	35.3	100.5	134.6	1.32	1.77	3.19%	0.121%	0.038
NH_2OH addition (aerobic)								
	10.5	0.0	10.5	0.00	0.04	0.80%	0.055%	0.068
	10.5	0.0	10.5	0.00	0.05	0.76%	0.078%	0.102
	21.1	0.0	20.7	0.00	0.10	1.53%	0.192%	0.126
	10.5	10.5	20.6	0.04	0.08	3.54%	0.287%	0.081
	10.5	0.0	10.3	0.00	0.04	1.85%	0.126%	0.068

3 Results

3.1 NO and N_2O emissions during ammonia oxidation in aerobic batch tests

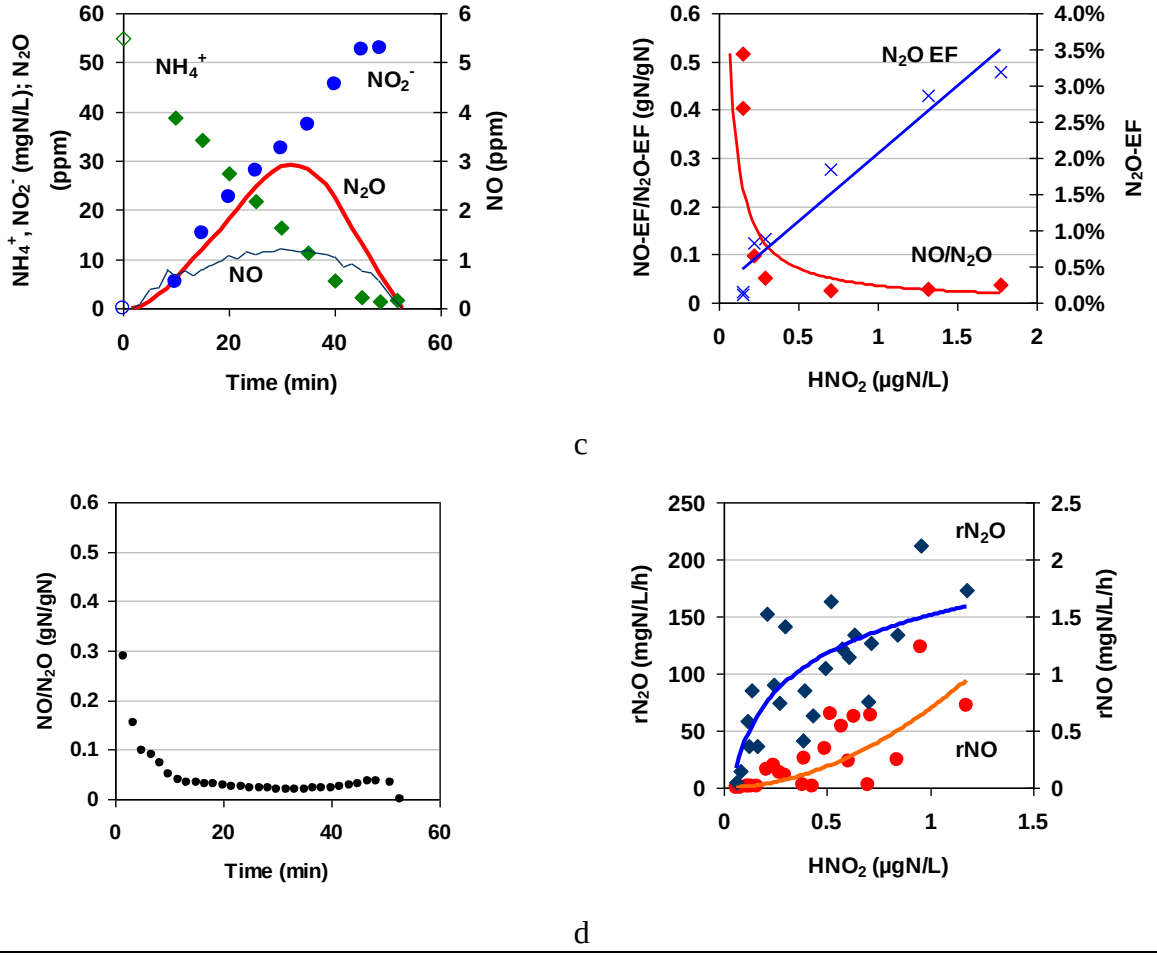

Figure 23. Batch experiments with ammonia as substrate: dynamics of ammonia, nitrite, NO and N_2O concentration in gas phase with theoretical ammonia and nitrite concentrations at initial time (a), dynamics of the NO/N_2O ratio (b). NO/N_2O ratio and N_2O EF in relation to HNO_2 concentration (c), instantaneous NO and N_2O emission rates (rNO, rN_2O) in relation to HNO_2 concentration for all batch experiments using ammonia as nitrogen source (d).

Figure 23 shows a typical example of aerobic batch kinetics. The first ten minutes corresponded to the feeding of ammonia (theoretically up to 54.8 mgN-NH_4^+.L^{-1}, but this value was never reached as the nitritation started during feeding). The nitrate concentration was negligible and ammonia was fully converted to nitrite, indicating that NOB activity was very small compared to AOB. The evolution of NO and N_2O in the gas phase is also presented in Figure 23.a and the ratio NO/N_2O in Figure 23.b. A few minutes after the

beginning of the aerobic period, NO and N_2O concentrations started to increase in the gas phase, reaching a maximum after about 30 minutes of nitritation (1.2 ppm and 29.1 ppm respectively). NO and N_2O concentrations rapidly became negligible at the end of nitritation.

The NO/N_2O ratio was initially high (> 0.2 gN-NO/gN-N_2O) but rapidly decreased as NO and N_2O accumulated in the gas phase. It stabilized around 0.02 gN-NO/gN-N_2O when the maximal NO and N_2O concentrations were reached. Similar tendencies were observed for all experiments using ammonia as the nitrogen source (Table 31). In the example presented in Figure 23.a, NO and N_2O emission factors were respectively 1.84% and 0.049%, leading to an overall NO to N_2O ratio of 0.027 gN-NO/gN-N_2O. But considering all ammonia oxidation batch tests, this ratio varied significantly depending on the nitrite concentration reached during the experiment.

For all ammonia oxidation batch experiments, the effect of free nitrous acid (HNO_2) concentration on both the N_2O-EF and the NO-EF/N_2O-EF ratio is shown in Figure 23.c. HNO_2 concentration is considered here instead of nitrite concentration as much better correlations were observed with the acid form. The N_2O-EF appears to be correlated with the HNO_2 level for all the experiments. This factor was around 0.0014 gN-N_2O/gN-NH_4^+ (0.14%) for the lowest HNO_2 concentration and increased to 0.0319 gN-N_2O/gN-NH_4^+ (3.19%) for the highest HNO_2 level at 1.77 µgN.L^{-1}. The differences in the HNO_2 level at the end of each test were attributed to the variation of initial ammonia or nitrite level imposed and also to the small pH variation.

In contrast, such a clear trend was not observed between NO-EF and HNO_2 concentration. NO emission factor ranged from 0.048% to 0.121%, presenting a lower variation than N_2O-EF. As a result, the NO-EF/N_2O-EF ratio clearly decreased with increasing HNO_2 concentration (Figure 23.c). This ratio decreased from 0.516 to 0.053 gN-NO/gN-N_2O for an HNO_2 rise from 0.15 to 0.29 µgN.L^{-1}. The ratio was even lower, in the range 0.027-0.038 gN-NO/gN-N_2O, for HNO_2 higher than 0.5 µgN.L^{-1}.

Figure 23.d shows the instantaneous NO and N_2O emission rates versus the HNO_2 concentration (calculated when the ammonia utilization rate is maximal for all experiments using ammonia as the nitrogen source). The NO emission rate increased more rapidly than the N_2O emission rate for low levels of HNO_2, whereas the increase of N_2O emission rate was

more pronounced at high levels (HNO_2>0.5 µgN.L^{-1}). This led to a decrease of NO/N_2O ratio with the increase of HNO_2 concentration. To conclude, this correlation between the ratio NO/N_2O and HNO_2 was observed both on the average value collected for each experiment (Figure 23.c) and dynamically during each experiment as nitrite accumulated with time.

3.2 NO and N_2O emissions during hydroxylamine oxidation in batch tests

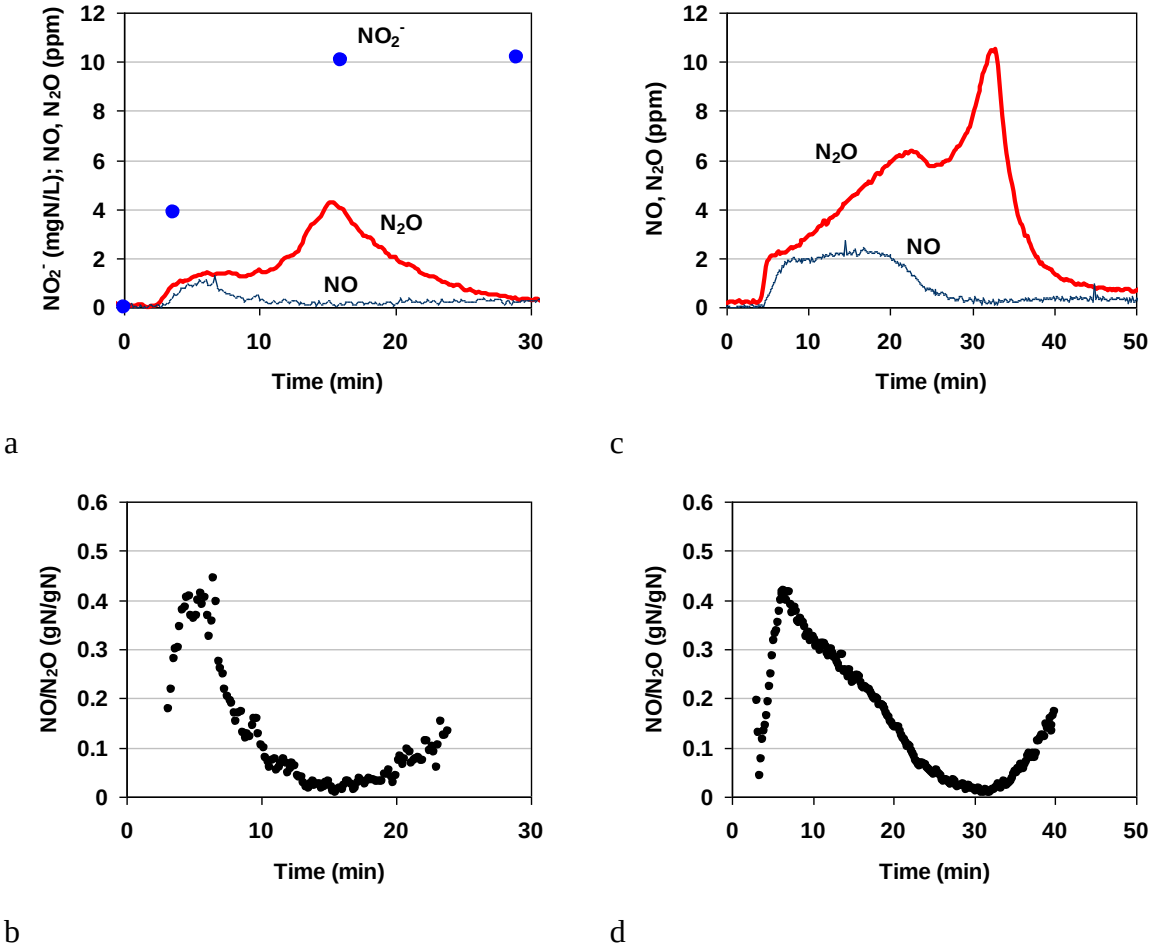

Figure 24. Batch experiments with hydroxylamine as substrate (injection of 10.5 mgN-$NH_2OH.L^{-1}$ for figures a and b at t=2 min 30s; injection of 21.1 mgN-$NH_2OH.L^{-1}$ for figures c and d at t=4 min 30s): dynamics of nitrite, NO and N_2O concentration in gas phase (a, c), dynamics of the NO/N_2O ratio (b, d).

The results from experiments using hydroxylamine as the nitrogen source are summarized in Table 31. Figure 24.a and c present typical dynamic profiles obtained for an injection of 10.5 and 21.1 mgN-$NH_2OH.L^{-1}$ respectively (initially without nitrite). The dynamics of NO and N_2O emissions during the oxidation of hydroxylamine were very different from those observed during ammonia oxidation. NO and N_2O emissions started simultaneously as soon

as NH_2OH were injected and were very well correlated in the first few minutes, during which the NO/N_2O ratio rapidly reached a maximal value around 0.40 gN-NO/gN-N_2O. This value was similar for the two experiments presented in Figure 24. After that, the ratio decreased progressively to a low value around 0.01 gN-NO/gN-N_2O for both experiments (Figure 24.b and d) when the N_2O concentration was maximum. In these cases, the NO/N_2O ratio profile was similar for injections of 10.5 or 21.1 mgN-$NH_2OH.L^{-1}$. The more NH_2OH was injected, the more NO and N_2O were produced (higher concentrations during a longer period). Another important difference with experiments using ammonia as the nitrogen source was that the N_2O concentration continued to increase even if the NO concentration decreased during the NH_2OH oxidation. In these experiments, NO-EF and N_2O-EF were respectively 0.078% and 0.76% for an injection of 10.5 mgN-$NH_2OH.L^{-1}$, leading to an overall NO/N_2O ratio of 0.102 gN-NO/gN-N_2O. The increase in the amount of NH_2OH injected led to the increase of these emission factors with an NO-EF of 0.192% and an N_2O-EF of 1.53% for an overall NO/N_2O ratio of 0.126 gN-NO/gN-N_2O. The highest N_2O-EF (3.54%) was obtained for the test with simultaneous presence of hydroxylamine and nitrite at the initial time. In comparison with previous tests with ammonia, the NO emission factor was generally higher for the tests with hydroxylamine, ranging from 0.055% to 0.287%.

3.3 NO and N_2O emissions during different operating periods of SBR

NO and N_2O emission factors were determined for 290 different cycles during the SBR operation. Statistical distributions of NO-EF, N_2O-EF, NO-EF/N_2O-EF ratio and HNO_2 concentration are summarized in Figure 25 (more than 81 cycles for each period). The lowest N_2O emission factor (median at 0.45%) was observed during period I, which corresponded to the period with low HNO_2 accumulation (median at 0.40 µgN.L^{-1}). Higher N_2O emission was observed during period II (median at 2.74%) and the highest emissions were observed during period III (median at 4.69%, maximal N_2O-EF of 11.6%), which corresponds to the period with highest HNO_2 accumulation (median at 0.87 µgN.L^{-1}).

In contrast, NO emissions were observed to be of a similar order of magnitude for each period. From period I to period III, the median of the NO-EF decreased slightly from 0.053% in period I, to 0.042% in period II and 0.037% in period III. As in batch kinetics experiments, this resulted in a significant variation of the NO-EF/N_2O-EF ratio between periods. The

median decreased from 0.094 gN-NO/gN-N_2O in period I to 0.0123 gN-NO/gN-N_2O in period II and 0.007 gN-NO/gN-N_2O in period III. Highest NO-EF/N_2O-EF ratios corresponded to cycles with the lowest N_2O-EF and lowest HNO_2 concentration, whereas lowest NO-EF/N_2O-EF ratios corresponded to cycles with highest N_2O-EF and highest HNO_2 level.

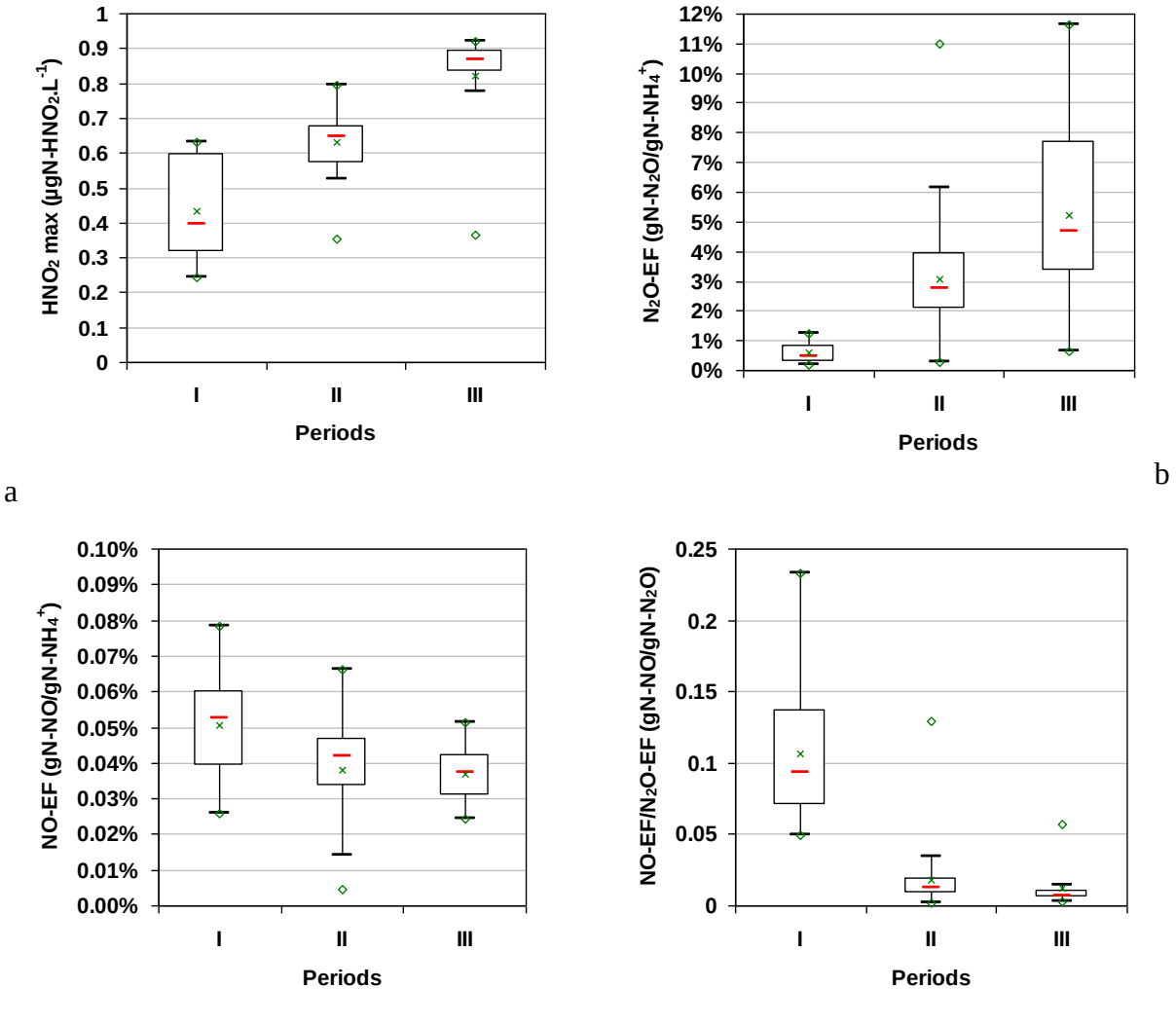

Figure 25. Statistical distributions of the maximum HNO_2 concentration (a), the N_2O-EF (b), the NO-EF (c) and the NO-EF/N_2O-EF ratio (d) during the three periods of the SBR. The medians are represented with thick red lines, the averages with green crosses, extreme values with green triangles and whiskers with vertical black lines delimited with horizontal black lines at top and bottom.

3.4 Effect of environmental conditions on NO and N_2O emissions

Figure 26 summarizes the emission factors and the NO-EF/N_2O-EF ratio in all the SBR cycles versus DO and HNO_2. The N_2O-EF appeared to be exponentially correlated with the

maximum HNO_2 concentration reached during the aerobic period (Figure 26.a). At HNO_2 concentrations lower than 0.50 $\mu gN.L^{-1}$, the N_2O-EF remained relatively low (below 1% for 95.2% of the cycles). Higher HNO_2 concentration resulted in a significant increase of N_2O-EF. At the maximum HNO_2 tested (around 0.87 $\mu gN.L^{-1}$), the N_2O-EF varied from 3% to 11%. In contrast, NO emissions did not increase with HNO_2 (Figure 26.b). NO-EF varied from 0.004% to 0.078% and no clear trend was detected, except a slight decrease of the mean value for each period with increasing HNO_2.

The NO-EF/N_2O-EF ratio showed a clearly decreasing trend with increasing HNO_2 concentration. The maximal NO-EF/N_2O-EF value (around 0.20 gN-NO/gN-N_2O) was observed for the lowest HNO_2 concentrations and a very low value (around 0.002 gN-NO/gN-N_2O) was obtained for the highest HNO_2 concentrations (Figure 26.c). This result confirmed the observations obtained during dedicated batch tests. Both sets of experiments showed significant variations of HNO_2 levels, related to the evolution of ammonium and pH in both the SBR cycles and the batch experiments. Very similar correlations were obtained between maximal HNO_2 concentration and N_2O or NO emission factors. Consequently, for both SBR cycles and batch tests, an increase of HNO_2 concentration led to a decrease of the NO-EF/N_2O-EF ratio.

The relation between DO and N_2O-EF is also presented in Figure 26. The lowest N_2O emission factors (<1%) were observed at high DO (from 2.5 to 6 $mgO_2.L^{-1}$) whereas a large variation from 1% to 11% was observed at DO between 1 and 2 $mgO_2.L^{-1}$ (Figure 26.d). In fact, the highest N_2O emissions were observed for cycles having the highest HNO_2 concentration and the lowest DO concentration simultaneously (period III). For cycles with a low HNO_2 accumulation (lower than 0.63 $\mu gN.L^{-1}$, i.e. for cycles of period I), the impact of low DO was limited when N_2O-EF was around 1%. The effect of nitrite on N_2O emissions was observed to be similar for a range of DO from 2.5 to 5.5 $mgO_2.L^{-1}$ but it was exacerbated when the oxygen concentration became lower than 2 $mgO_2.L^{-1}$. This observation matches with the assumption that during the N_2O production by the ND pathway the competition between oxygen and nitrite is assumed, as both act as electron acceptor. In contrast, NO-EF versus DO did not show such a clear tendency (Figure 26.e). The variation of the NO-EF/N_2O-EF ratio with DO was different depending on the cycles (Figure 26.f). The highest values of NO-EF/N_2O-EF ratio (0.05 to 0.2) were obtained during period I (at low levels of

HNO_2) but variation seemed poorly correlated with the DO. In contrast, very low ratios (<0.01) were obtained for low DO and high nitrite levels.

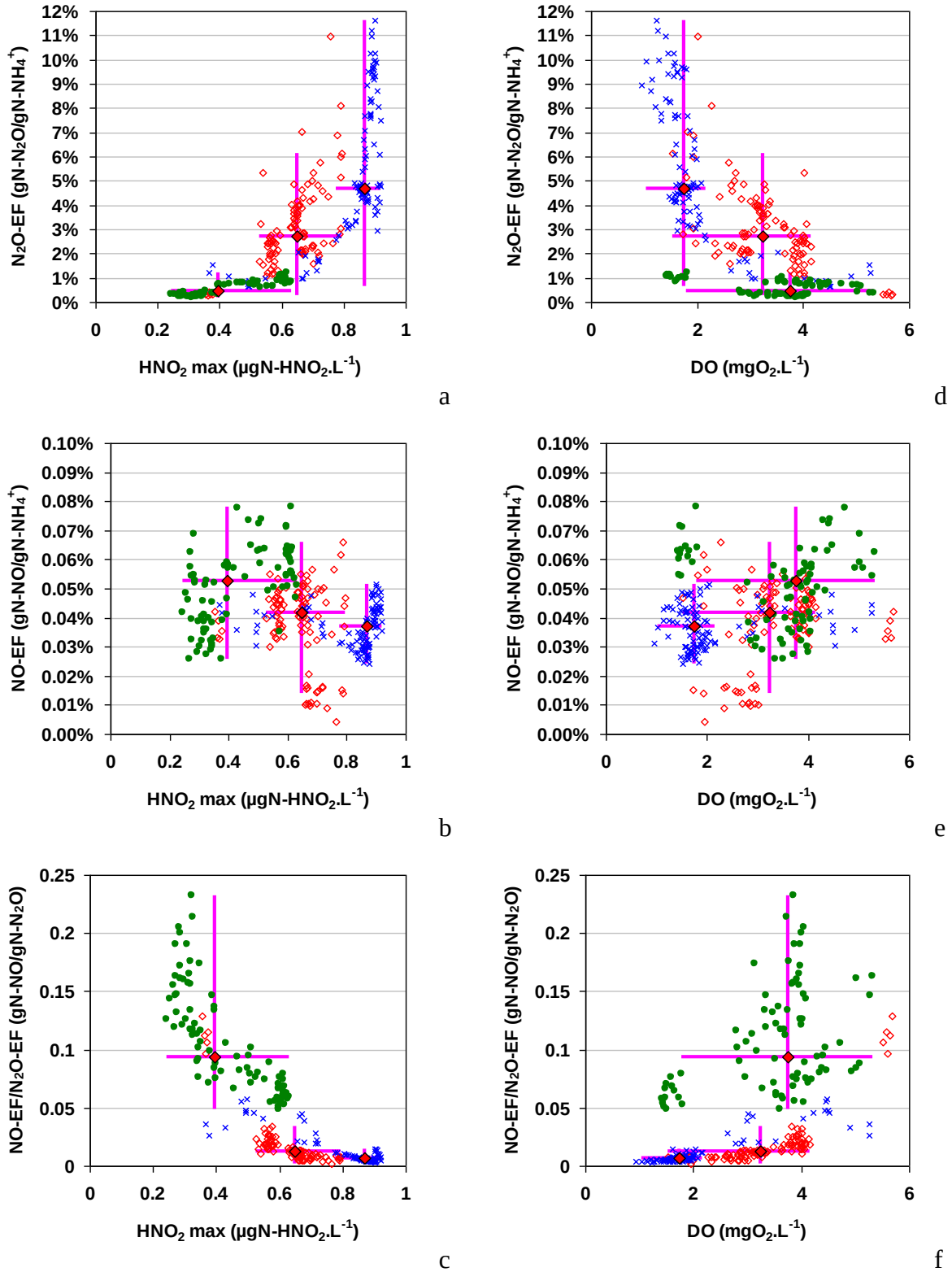

Figure 26. SBR experiments – Relation between HNO_2 maximum concentration during nitrification and N_2O-EF (a), NO-EF (b) and the NO-EF/N_2O-EF ratio (c). Relation between DO and N_2O-EF (d), NO-EF (e) and the NO-EF/N_2O-EF ratio (f). Cycles of periods of the SBR are represented as follows: Period I (●), period II (◊), period III (×). Each point corresponds to a cycle. Horizontal and vertical lines represent the range between minimum and maximum whiskers of the associated parameters (i.e. horizontal for the abscissa and vertical for the ordinate) for each period. One SBR cycle = one dot.

4 Discussion

4.1 The stimulating effect of HNO_2 on N_2O emissions and the NO/N_2O ratio

Under aerobic conditions, the presence of nitrite was shown to induce N_2O production by the nitrifier denitrification (ND) pathway in pure culture (Anderson et al., 1993). The relation between N_2O emission and nitrite was previously observed during nitrification in AOB enriched culture or mixed cultures (Houweling et al., 2011; Marlies J Kampschreur et al., 2008; Kim et al., 2010; Law et al., 2012a; Tallec et al., 2006). In this study, the N_2O emission rate and emission factor were correlated with the HNO_2 concentration, with much better accuracy than with nitrite. The HNO_2 concentration range explored in this work is the result of different nitrite levels, but also of different pH with similar nitrite concentrations.

During both ammonium and hydroxylamine oxidation, the accumulation of HNO_2 resulted in an increase in N_2O production. The two phases observed on NO and N_2O profiles during hydroxylamine oxidation (Figure 24.a and c) can be explained by a progressive switch from the NN pathway to the ND pathway, the ND pathway being induced when HNO_2 reached a certain value. Initially, N_2O emission by NN was the major pathway due to high hydroxylamine levels and the absence of nitrite. Then the ND pathway was progressively activated with the accumulation of HNO_2 and NO stimulating the NirK and Nor activities (with the increase of the substrate concentrations or of the expression of the NirK gene (Beaumont et al., 2004b)).

(Law et al., 2013) recently observed an inhibition of the specific N_2O production rate at very high nitrite concentrations (50-1000 $mgN.L^{-1}$). These authors assumed that the ND pathway was inhibited for such high concentrations, the hydroxylamine oxidation becoming the major pathway for nitrite concentrations higher than 500 $mgN.L^{-1}$. Such a high concentration was not attained in our study and this potential inhibition was not observed. The stimulation of the N_2O emission rate was observed for HNO_2 accumulation from 0 to 1.77 $\mu gN.L^{-1}$. In addition, the increase of N_2O emission was exacerbated when HNO_2 increased to over 0.5 $\mu gN.L^{-1}$. A comparable threshold value was reported by (Lemaire et al., 2011b).

The combined effect of a high HNO_2 concentration and a low DO concentration was also observed in the SBR data set. As the nitrite and the oxygen compete to accept electrons (Figure 22) the activation of N_2O emission by nitrite is logically higher at low DO in the ND pathway (Anderson et al., 1993; Sutka et al., 2006). For low HNO_2 levels (<0.5 $\mu gN.L^{-1}$), only a small variation of N_2O emission factor was observed with decreasing DO. In that situation, the contribution of the ND pathway is probably lower resulting in the increase of the NN pathway contribution. In contrast, for higher HNO_2 concentrations, the N_2O emission increased at low DO (especially between 1 and 2 $mgO_2.L^{-1}$) (Figure 26). This confirms the recent results of (Peng et al., 2014) showing a significant increase in N_2O emission factor for DO lower than 1 $mgO_2.L^{-1}$ but only a slight increase of N_2O EF for a DO decrease from 3 to 1 $mgO_2.L^{-1}$. As observed by (Peng et al., 2014), the pure effect of DO without the presence nitrite is difficult to assess as a small amount of nitrite always accumulates in theirs batch experiments. Overall, the effect of HNO_2 on N_2O emission was observed even at high DO but was exacerbated at very low DO.

As the HNO_2 concentration stimulated the N_2O production by the ND pathway, the NO/N_2O ratio decreased as HNO_2 increased during ammonium or hydroxylamine oxidation. In batch tests with ammonium, the ratio decreased from 0.5 to 0.02 gN-NO/gN-N_2O as HNO_2 was imposed at different levels from 0 to 1.77 $\mu gN.L^{-1}$. During hydroxylamine oxidation, the ratio decreased from 0.45 gN-NO/gN-N_2O to less than 0.02 gN-NO/gN-N_2O as HNO_2 accumulated with time. Based on 290 SBR cycles monitored, the NO-EF/N_2O-EF ratio decreased from 0.2 to 0.005 gN-NO/gN-N_2O as the maximum HNO_2 varied from 0.25 to 0.87 $\mu gN.L^{-1}$. Such variations of NO-EF/N_2O-EF ratio have never been reported before and suggest the importance of HNO_2 both in the enzyme activation and in the pathway regulation.

4.2 Potential relation between NO/N_2O ratio and AOB pathway regulation

The results of this study support the idea that the variation of the NO/N_2O ratio under aerobic conditions is related to the respective contribution of the two main AOB pathways involved in the production of N_2O. Thus it is suggested here that the respective emissions of NO and N_2O can be different depending on whether N_2O is produced by the NN or ND pathways. As illustrated in Figure 22, which presents the different AOB pathways, the NO is an intermediary product whereas N_2O is a final compound. The NO accumulation in the cell and

the NO emission depend on the different enzymatic production and consumption rates. This Production can be linked to the incomplete hydroxylamine oxidation by HAO (NN pathway) and the HNO_2 reduction by NirK (ND pathway), whereas its consumption is possibly due to the oxidation to nitrite by HAO and the reduction to N_2O by Nor. During the hydroxylamine oxidation, four electrons are released and two of them are consumed by terminal electron acceptors (nitrite and nitric oxide) during the reduction of nitrite to N_2O in two steps (ND pathway).

Based on isotopic techniques (Site Preference or SP method) the contributions of each pathway to the N_2O emissions according to operating conditions have recently been quantified (Peng et al., 2014; Toyoda et al., 2011; Wunderlin et al., 2013). (Wunderlin et al., 2013) demonstrated that the contribution of the NN pathway was the main pathway when hydroxylamine was injected, whereas the ND pathway was predominant in ammonia oxidation batch tests. It was also observed that the contribution of ND increased with time as the nitrite accumulated, confirming the stimulation role of nitrite (or HNO_2). For hydroxylamine injections similar to those used in this study (Wunderlin et al., 2013) found that the contribution of NN was close to 100% (97-100%) initially and decreased to around 20% at the end when nitrite accumulated. In our case the NO/N_2O ratio was initially around 0.4 gN-NO/gN-N_2O and progressively decreased to 0.02 gN-NO/gN-N_2O during similar experiments. When ammonia was used as the substrate in (Wunderlin et al., 2013), ND was the major pathway: it was initially responsible for 80% of N_2O emission and progressively increased to 100% at the end as nitrite accumulated. For similar experiments, our data showed that the NO/N_2O ratio decreased from 0.3 to 0.02 gN-NO/gN-N_2O. The preponderance of the ND pathway when ammonium and nitrite were both present has been confirmed by various authors using isotopes (Peng et al., 2014; Sutka et al., 2006; Toyoda et al., 2011; Wunderlin et al., 2013). Consequently, our results suggest that N_2O production via the NN pathway leads to a relatively high NO/N_2O ratio (0.4 gN-NO/gN-N_2O) whereas production by the ND pathway results in a low NO/N_2O ratio (<0.05 g/g).

During batch tests with hydroxylamine, the constant NO and N_2O emission observed during the first minutes can be attributed mainly to the NN pathway. At that time, the NO/N_2O ratio measured (0.4 gN-NO/gN-N_2O) corresponded to about 0.8 mole of NO per mole of N_2O. The comparison of nitrite accumulation rate (thus hydroxylamine oxidation rate) and NO and N_2O emission rates indicated that 0.0008 to 0.0018 gNO/gN-NH_2OH and 0.0019 to 0.0036 gN-

N_2O/gN-NH_2OH were produced (0.08 to 0.18% of N-NH_2OH oxidized converted to NO and 0.19 to 0.36% to N_2O). This could be the NO and N_2O emitted solely by the NN pathway before nitrite accumulated and ND started. In contrast, very low NO/N_2O ratios were observed in periods with significant HNO_2 concentration, for which ND is assumed to be the major process.

The variation of the NO/N_2O ratio could be explained by a lower NO accumulation when ND is the pathway, compared to that generated by the NN pathway. In other words, the amount of NO accumulated to produce the same amount of N_2O should be higher in the NN pathway than in the ND pathway. This could be related to different fluxes of NO depending on the activity and affinity constants of HAO, NirK and Nor enzymes. The presence of nitrite (or HNO_2) stimulating NirK and Nor activities would increase the amount of NO reduced to N_2O, whether it originated from hydroxylamine oxidation or was produced by HNO_2 reduction. This would lead to a decrease of NO loss comparatively to N_2O loss as the ND pathway increased. It suggests that the NO produced by NirK is very rapidly consumed by the enzyme Nor in the ND pathway and probably that the NO produced by the ND pathway is poorly consumed by HAO but directly used by Nor. Obviously, more information about enzyme activity and affinity constants for NO would be necessary to explain this phenomenon.

Finally it can be concluded that the experimental measurement of the NO/N_2O ratio in the gas phase is a relatively simple technique to track N_2O production pathways in lab-scale or full-scale systems. Further work would be necessary to confirm this theory and to compare these methodologies. Another approach that could support this theory would be to confront a two-pathway model with the experimental data. As the operating parameters have different impacts on the N_2O emissions by the different pathways, tracking the N_2O production pathways would be very useful to calibrate models and select an appropriate strategy for N_2O emission mitigation.

5 Conclusion

In this chapter, the variation of NO and N_2O emissions during nitritation has been investigated. The main conclusion is that the variation of NO/N_2O ratio appears to be related to the contribution of each N_2O production pathway. Indeed data and theory suggest that the NN pathway results in higher NO/N_2O ratio in the off-gas compared to the ND pathway. The variation of the NO/N_2O ratio gives similar conclusions concerning the contribution of ND and NN pathways in different conditions to those obtained from isotopes signature techniques. The measurement of NO/N_2O ratio constitutes an interesting alternative, easier to implement than isotopic techniques, to evaluate pathways involved in N_2O emissions. Obviously it is not yet a quantification method like isotopic method is, but this new insight could open possibility to track N_2O production pathways and would probably help further models validation.

Chapter VI Variation of the NO/N_2O ratio supports a two-pathway model for N_2O emissions by ammonium oxidizing bacteria

Abstract

In this chapter, a new model for nitritation combining two N_2O emission pathways was confronted with both NO and N_2O measurements during nitrification. The model was calibrated with batch experiments and validated with long-term data collected in a sequencing batch reactor (SBR). A good prediction of the evolution of N_2O emissions for a varying level of nitrite was demonstrated. The NO/N_2O ratio was shown to vary during nitritation depending on the nitrite level. None of the models based on a single pathway could describe this variation of the NO/N_2O ratio. In contrast, the 2 pathway model was capable of describing the trends observed for the NO/N_2O ratio and gave better predictions of N_2O emission factors. The model confirmed that the decrease of the NO/N_2O ratio can be explained by an increase of the ND pathway to the detriment of the NN pathway. The ND pathway was systematically the predominant pathway during nitritation. The combined effect of nitrite (or free nitrous acid) and dissolved oxygen (DO) on the contribution of each pathway was in agreement with practical observations and the literature.

1 Introduction

Mathematical dynamic modeling of N_2O emission is of great importance in the search for mitigation strategies based on optimal design and control. Among the different possible mechanisms for N_2O production by AOB, two pathways are now considered to be the major processes responsible for the emissions during nitrification (Chandran et al., 2011; Wunderlin et al., 2012). The first major pathway corresponds to the autotrophic denitrification of nitrite (noted "ND") (Kim et al., 2010), i.e. the reduction of nitrite to NO by the NirK enzyme, followed by the reduction of NO to N_2O by the Nor enzyme. The second pathway (noted "NN") is incomplete hydroxylamine oxidation by the HAO enzyme (Chandran et al., 2011; Law et al., 2012a; Stein, 2011), resulting in the accumulation of NO, which is then reduced to N_2O by the Nor enzyme.

At least four different models based on single pathways have been proposed and confronted with different lab-scale or full-scale N_2O measurements (Ni et al., 2013a; Spérandio et al., 2015) leading to satisfactory descriptions in various cases. However the conclusions of these calibration exercises, with either batch results (Ni et al., 2013a) or continuous long-term data (Spérandio et al., 2015), were that it was not possible to find a single model structure based on a single pathway that could describe all the data published in the literature. The main assumption formulated was that both NN and ND pathways can occur at the same time and the contribution of each of them would depend on the operating conditions. The regulation between the two main N_2O production pathways of AOB has been partially elucidated by recent works based on isotope signature measurements (Peng et al., 2014; Wunderlin et al., 2013). These works show that the nitrite (or the free nitrous acid) and the dissolved oxygen both play key roles in this regulation. During ammonium oxidation in batch experiments, the ND pathway is dominant and increases with time. The contribution of ND has been shown to increase as DO decreases under 1 mgO_2/L whereas the contribution of NN pathway increases with the DO (Peng et al., 2014). The contribution of the ND pathway also increases with nitrite accumulation at low DO level (Wunderlin et al., 2013). However it has also been supposed that the ND pathway is inhibited at very high nitrite concentrations, from 50 to 1000 $mgN.L^{-1}$ (Law et al., 2013). Finally a comparative calibration work indicated that models based on the NN pathway matched the data from systems with relatively low nitrite accumulation (< 1 $mgN.L^{-1}$), whereas ND pathway models were more suitable for systems with strong nitrite peaks (Spérandio et al., 2015).

Recently, a unified model describing the two main pathways has been proposed by (Ni et al., 2014). The originality of this model is to include the description of electron transport by means of new intracellular variables. Electron donors are oxidized and produce mediated electron, then the different electron acceptors (NO, O_2, HNO_2) can compete to consume this mediated electron pool. Oxidation and reduction reactions are thus described separately (whereas they are commonly coupled in conventional activated sludge models). Consequently, in that model, the predictions depend on kinetic parameters related to intracellular variables (electron carriers) which could be difficult to assess. In contrast, the simultaneous consumption of different electron acceptors for the same donor (and the competition between them) was previously modelled using switching function. Recently (Guo and Vanrolleghem, 2014) proposed to use a new expression to describe the inhibition of the nitrite reduction by oxygen, considering that oxygen plays a role in the ND pathway regulation. Finally there is not one single way to consider two AOB pathways simultaneously in a unified approach, which still need to be confronted with experimental observations. Moreover, single or multiple pathway models have, so far, never been simultaneously confronted with NO and N_2O emissions for their validation or calibration.

Therefore the objective of this study was to evaluate a new model combining the two main AOB pathways (noted 2-P model) with the measurements of NO and N_2O emissions, placing special emphasis on the variation of the NO/N_2O ratio. Emissions were measured in aerobic batch tests and a sequencing batch reactor (SBR), in which full nitritation and denitrification were achieved.

2 Materials and methods

2.1 Experimental data sets 2 and 3 for model evaluation

In this chapter, experimental data sets 2 and 3 (see chapter III) were considered for the model evaluation. The set 2 corresponds to NO and N_2O emissions during the aerobic period of SBR cycles. The maximum HNO2 concentration reached during the aerobic and the average DO have been calculated for each SBR cycle. In this chapter 187 cycles have been considered. The set 3 corresponds to batch experiments using the SBR mixed culture (similar conditions

of sludge concentration, pH and temperature). In this chapter, batch experiments with the same initial concentration of ammonium are considered (Table 32).

Table 32. Summary of batch experiments using ammonium as substrate

Experiment	N injected ($mgN.L^{-1}$)	NO_2^- ($mgN.L^{-1}$)		HNO_2 ($\mu gN.L^{-1}$)		EF (gN-NxO/gN-NHx)		NO/N_2O (gN/gN)
		Start	End	Start	End	N_2O	NO	
NH_4^+ addition								
	10.49	10.5	21.0	0.07	0.15	0.16%	0.0811%	0.516
	10.49	22.5	33.0	0.10	0.16	0.12%	0.0484%	0.405
	10.49	20.5	31.0	0.15	0.22	0.83%	0.0805%	0.097
	10.49	36.5	47.0	0.22	0.28	0.89%	0.0475%	0.053
	10.49	68.5	79.0	0.50	0.57	2.61%	0.0814%	0.031
	10.49	112.5	123.0	0.87	0.95	4.58%	0.0770%	0.017

2.2 2-Pathway model description

The mathematical model for AOB was developed considering both NN and ND production pathways (2-P model). A schematic description of the reactions considered is presented in Figure 27 and the stoichiometry and kinetics are presented in Table 33 and Table 34 respectively.

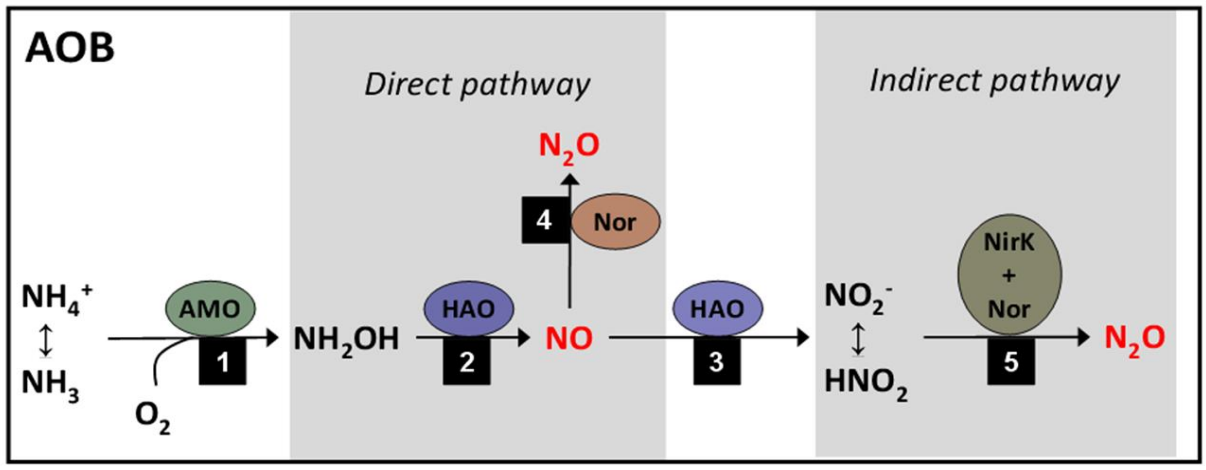

Figure 27. Schematic representation of the five enzymatic reactions considered in the model.

Table 33. Stoichiometry of the 2 pathways model.

	Model Components – 2-P model						
Process	S_{NH}	S_{NH_2OH}	S_{NO}	$S_{NO_2^-}$	S_{N_2O}	S_{O_2}	X_{AOB}
1	-1	1				$-8/7$	
2	$-i_{N,BM}$	$-1/Y_{AOB}$	$1/Y_{AOB}$			$-\left(12/7 - Y_{AOB}\right)/Y_{AOB}$	1
3			-1	1		$-4/7$	
4		-1	-4	1	4		
5		-1		-1	2		

Table 34. Kinetics of the 2 pathway model.

Process	**Kinetic rate expressions – 2-P model**
1	$q_{AOB,AMO}\frac{S_{O_2}}{S_{O_2}+K_{O_2,AOB,1}}\frac{S_{NH_3}}{S_{NH_3}+K_{NH_3,AOB}}X_{AOB}$
2	$\mu_{AOB,HAO}\frac{S_{O_2}}{S_{O_2}+K_{O_2,AOB,2}}\frac{S_{NH_2OH}}{S_{NH_2OH}+K_{NH_2OH,AOB}}X_{AOB}$*
3	$q_{AOB,HAO}\frac{S_{O_2}}{S_{O_2}+K_{O_2,AOB,2}}\frac{S_{NO}}{S_{NO}+K_{NO,AOB,HAO}}X_{AOB}$
4	$q_{AOB,N_2O,NN}\frac{S_{NH_2OH}}{S_{NH_2OH}+K_{NH_2OH,AOB}}\frac{S_{NO}}{S_{NO}+K_{NO,AOB,Nor}}X_{AOB}$
5	$q_{AOB,N_2O,ND}\frac{S_{NH_2OH}}{S_{NH_2OH}+K_{NH_2OH,AOB}}\frac{S_{HNO_2}}{S_{HNO_2}+K_{HNO_2,AOB}}X_{AOB}$

* In the rate of process 2, an ammonium limitation for growth is mathematically imposed with $S_{NH}/(S_{NH}+10^{-12})$

The assumptions for the description of NN and ND pathways are based on previous single pathway models (Ni et al., 2011, 2013a). The continuity of this new model was verified based on (Hauduc et al., 2010) and five processes were included in the model, corresponding to the following five enzymatic reactions:

(1) NH_3 oxidation to hydroxylamine (NH_2OH) with oxygen consumption,

(2) NH_2OH oxidation to nitric oxide (NO) coupled with oxygen reduction,

(3) NO oxidation to nitrite (NO_2^-) coupled with oxygen reduction,

(4) NO reduction to N_2O by the enzyme "Nor" coupled with the hydroxylamine oxidation to nitrite (N_2O from NN pathway),
(5) HNO_2 reduction to N_2O coupled with NH_2OH oxidation to nitrite (N_2O from ND pathway).

Reactions 2 and 4 describe the production of NO and N_2O respectively by the NN pathway with small corrections compared to the original model of (Ni et al., 2013a) (growth takes place in reaction 2). Reaction 5 describes the N_2O production by the ND pathway. Two successive processes were considered in the original ND model (Mampaey et al., 2013; Ni et al., 2011): nitrite reduction to NO (NirK enzyme) followed by the reduction of NO to N_2O (Nor enzyme). In the present work, the decision was made to lump these two reactions together in a single process (5) corresponding to the direct reduction of nitrite to N_2O in one step. This modification was necessary to avoid the NO loop, i.e. the fact that the NO produced by the ND pathway would be rapidly oxidized to nitrite by the nitritation process (3), as this last process has a much higher rate (Ni et al., 2014). In other words, it was assumed that the Nor enzyme rapidly consumed the nitric oxide produced by the NirK. In some situation this assumption of the amount of NO accumulated by the ND pathway was not significant (thus ignored) compared to that emitted by the NN pathway could be critical for the prediction of NO emissions. For example Kampschreur et al. (2007) reported some change in NO emission (with nitrite) which was attributed to ND pathway. In that case NO emitted by NirK could be considered (as a different state variable to avoid the NO loop). However in the present study, this was not necessary as the prediction of NO emissions was in accordance with the experimental observation, probably because at high nitrite level (case of this study) the Nor enzymes are highly synthetized and rapidly consume the intermediary NO of the ND pathway.

The ammonia oxidation rate was related to the concentration of free ammonia, which was assumed to be the true substrate of AOB (Anthonisen et al., 1976) and nitrite reduction rate was similarly related to free nitrous acid concentration. Inhibitions of AOB growth by NH_3 and HNO_2 were not considered in this work (concentrations were relatively low). A possible extension could naturally be to consider the inhibitions observed at high concentration (Law et al., 2013). The effect of dissolved oxygen on the ND pathway was considered in reaction 5 by an inhibition term as proposed by (Guo and Vanrolleghem, 2013b). This term describes the increase of the specific N_2O production rate with the decrease of DO, up to a maximum

production rate, beyond which the rate decreases when DO is close to zero (Peng et al., 2015a). Note that the model was initially tested without DO inhibition (option 1), with a conventional uncompetitive inhibition term $K_i/(K_i+S)$ (option 2) and finally with the modified inhibition term (option 3). Significant improvement was observed with the third option especially for the prediction of long term data (SBR) at relatively low DO (1-2 mg/L). However it should be noted that this is not a generic conclusion as the experimental design was more focused on the nitrite effect in this study. Such assumption would need more strong evidence with future work dedicated to DO effect. The gas liquid transfers of oxygen, NO and N_2O were also included in the models. The transfer coefficients (K_La) for NO and N_2O were calculated with the measured oxygen transfer coefficient and the respective diffusivity ratio (Ye et al., 2014).

2.3 Model simulation, calibration and sensitivity analysis

All the simulations, sensitivity analysis and calibration were performed with AQUASIM software (Reichert, 1998). A relative-relative sensitivity function was determined for each parameter and measured variable in order to assess the identifiability of model parameters (identifiability analysis). Furthermore, the derivatives calculated in sensitivity analyses allowed to estimate the uncertainty in parameter estimates considering experimental uncertainty (5% for ammonia, nitrite, dissolved oxygen, 10% for gas measurements). Analysis was performed considering the simulations of batch experiments presented in Table 32 simultaneously.

In this study the 2-P model was compared to other models developed previously. Above all, the main goal was to find out which model was able to simultaneously describe the variation of N_2O and the variation of the tendency of NO/N_2O ratio. Different single pathway models based on the ND (Guo and Vanrolleghem, 2014; Mampaey et al., 2013; Ni et al., 2011; Pocquet et al., 2013) or NN pathway (Ni et al., 2013a) were tested. The components and kinetic rates of ND models considered in this chapter have been presented in the chapter II and only results obtained with the model of (Mampaey et al., 2013) are presented in this study. The NN model (Ni et al., 2013a), was slightly modified with the distinction of two affinity constants for NO: one for the HAO reaction and one for the Nor reaction. Indeed, in the original model the affinity constant for NO was considered similar in both reactions.

These adaptations are presented in Table 35 and encircled in red. The set of parameter values is presented in

Appendix C for NN and ND models. In this table, according to the chapter IV the model of (Ni et al., 2011) is noted A, (Pocquet et al., 2013) A1, (Mampaey et al., 2013) B, (Guo and Vanrolleghem, 2014) B1, (Ni et al., 2013a) C.

Table 35. Kinetic rate equations of the adapted NN model

Process	**Kinetic rate expressions – NN Pathway** (Ni et al., 2013a)
1	$\mu_{AOB,AMO} \cdot \frac{S_{O_2}}{K_{O_2,AOB,1} + S_{O_2}} \cdot \frac{S_{NH_4}}{K_{NH_4,AOB} + S_{NH_4}} \cdot X_{AOB}$
2	$\mu_{AOB,HAO,1} \cdot \frac{S_{O_2}}{K_{O_2,AOB,2} + S_{O_2}} \cdot \frac{S_{NH_2OH}}{K_{NH_2OH,AOB} + S_{NH_2OH}} \cdot X_{AOB}$
3	$\mu_{AOB,HAO,2} \cdot \frac{S_{O_2}}{K_{O_2,AOB,2} + S_{O_2}} \cdot \frac{S_{NO}}{K_{NO,AOB,HAO} + S_{NO}} \cdot X_{AOB}$
4	$\eta_{AOB} \cdot \mu_{AOB,HAO,1} \cdot \frac{S_{NH_2OH}}{K_{NH_2OH,AOB} + S_{NH_2OH}} \cdot \frac{S_{NO}}{K_{NO,AOB,Nor} + S_{NO}} \cdot X_{AOB}$

Finally the 2-P model developed in this study was also compared to the unified model proposed by Ni et al. (2014). The same approach was used for all the models tested. First the model was calibrated on batch tests (Table 32). Then the calibrated model was evaluated and possibly validated by simulating the long-term data collected on the SBR, i.e. for 187 cycles. During the whole experimental period (6 months), variations of ammonia feeding conditions and pH led to a variation of the nitrite and free nitrous acid accumulated in the reactor. Moreover the dissolved oxygen concentration also varied (from 1 to 5.5 mg/L) depending on both nitrification rate and air flow rate.

The 2-P model includes fourteen independent parameters. The maximum kinetic rates noted "q" (for processes without growth 1, 3, 4, 5) were not determined independently but related to the maximum growth rate 'μ' (related to process 2). Indeed maximum rates are potentially linked to the same specific enzymes (reactions 2, 3, 4, 5, are linked to HAO coupled with different electron acceptors). The value of $q_{AOB,HAO}$ was calculated as the growth rate $\mu_{AOB,HAO}$ divided by Y_{AOB}, leading to a similar substrate utilization rate for reactions 2 and 3 both related to the HAO oxidation activity with oxygen as electron acceptors. The maximum rates of reactions 4 and 5 are related to HAO coupled with nitric oxide and nitrite reduction

respectively. Thus the maximum rates $q_{AOB,N2O,NN}$ and $q_{AOB,N2O,ND}$ were calculated by multiplying $q_{AOB,HAO}$ by two different reduction factors noted $\eta_{AOB,NN}$ and $\eta_{AOB,ND}$ respectively. Note that these coefficients are not called "anoxic" reduction factors as the reactions are still active in presence of oxygen. Note also that the values of these reduction factors cannot be compared directly to those of previous models by (Ni et al., 2011) and (Ni et al., 2013b) as they were originally applied to the growth rate.

3 Results

3.1 Parameter calibration and sensitivity analysis

The results from sensitivity analysis are presented in Table 36. The set of parameter values (and uncertainties) identified for the two pathway model is presented in Table 37. Three parameters were directly implemented with values from literature (Y_{AOB}, $i_{N,BM}$, μ_{AOB}). The other parameters were estimated by successive calibrations with the different measured variables. Based on sensitivity analysis, the parameters influencing ammonium uptake rate and oxygen consumption were firstly calibrated (i.e. parameters related to AMO and HAO reactions) with NH_4^+, NO_2^- and O_2 measurements. Then the parameters influencing specifically the N_2O and NO emissions (related to both rate 4 and rate 5) were adjusted based on experimental N_2O and NO measurements in the gas phase. Based on the sensitivity analysis, it was found that N_2O emission was more specifically influenced by the factors related to rate 5 ($\eta_{AOB,ND}$, $K_{O2,AOB,ND}$, $K_{I,O2,AOB,ND}$, $K_{HNO2,AOB}$) which seems logical as the ND was the major pathway contributing to N_2O emissions in this study. A previous analysis (Pocquet el al., 2013) demonstrated that the correlation between the key parameters of ND pathway ($\eta_{AOB,NN}$ and K_{HNO2}) during the estimation was minimized thanks to the use of data obtained in a large range of nitrite concentration, as applied in this study. The predicted NO was very sensitive to parameters related to HAO ($K_{NH2OH,AOB}$, $K_{O2,AOB,2}$, $K_{NO,AOB,HAO}$) and slightly sensitive to parameter related to NN pathway i.e. rate 5 ($\eta_{AOB,NN}$). Thus the use of NO measurement for calibration logically improved the identifiability of those parameters. Finally efficient parameter identification was obtained by calibrating the model successively on the different type of measurements (soluble compounds, NO and N_2O) using simultaneously a relatively high number of data. Most of the estimated parameters showed a satisfying accuracy (Table 37) except those with poor influence of the simulations.

Table 36. Result from sensitivity analysis. Parameters with sensitivity function higher than 5% (relative-relative).

Processes	Measured variables				Other variables		
	S_{NH}	S_{O2}	NO_{gas}	N_2O_{gas}	S_{NH2OH}	N_2O_{NN}	N_2O_{ND}
General	μ_{AOB} Y_{AOB}	μ_{AOB} Y_{AOB}	μ_{AOB} Y_{AOB}	μ_{AOB} Y_{AOB}	μ_{AOB} Y_{AOB}	μ_{AOB} Y_{AOB}	μ_{AOB} Y_{AOB}
AMO	$K_{O2,AOB,1}$ $K_{NH3,AOB}$	$K_{O2,AOB,1}$	$K_{O2,AOB,1}$ $K_{NH3,AOB}$	$K_{O2,AOB,1}$ $K_{NH3,AOB}$	$K_{O2,AOB,1}$ $K_{NH3,AOB}$	$K_{O2,AOB,1}$ $K_{NH3,AOB}$	$K_{O2,AOB,1}$ $K_{NH3,AOB}$
HAO	$K_{NH2OH,AOB}$	$K_{NH2OH,AOB}$	$K_{NH2OH,AOB}$ $K_{O2,AOB,2}$ $K_{NO,AOB,HAO}$	$K_{NH2OH,AOB}$ $K_{O2,AOB,2}$	$K_{NH2OH,AOB}$ $K_{O2,AOB,2}$	$K_{NH2OH,AOB}$ $K_{O2,AOB,2}$ $K_{NO,AOB,HAO}$	$K_{NH2OH,AOB}$ $K_{O2,AOB,2}$
NN pathway			$\eta_{AOB,NN}$			$\eta_{AOB,NN}$ $K_{NO,AOB,NN}$	
ND pathway				$\eta_{AOB,ND}$ $K_{O2,AOB,ND}$ $K_{I,O2,AOB,ND}$ $K_{HNO2,AOB}$		$\eta_{AOB,ND}$ $K_{I,O2,AOB,ND}$	$\eta_{AOB,ND}$ $K_{O2,AOB,ND}$ $K_{I,O2,AOB,ND}$ $K_{HNO2,AOB}$

Table 37. Parameters values of the 2-P model and specific kinetic rates (at 20°C, considering Arrhenius equation with θAOB=0.094 for growth rate).

Name	Description	Unit	Value	Source
μ_{AOB}	Maximum AOB growth rate	h^{-1}	0.0325	(Hiatt and Grady, 2008)
Y_{AOB}	AOB growth yield	$mgCODX.mgN^{-1}$	0.15	(Ni et al., 2013a)
$i_{N,BM}$	Nitrogen content of biomass	$mgN.mgCODX^{-1}$	0.07	(Henze, 2000)
$\eta_{AOB,ND}$	Reduction factor applied for the ND pathway	Dimensionless	0.250 ±0.011	Estimated
$\eta_{AOB,NN}$	Reduction factor applied for the NN pathway	Dimensionless	0.0015 ±0.001	Estimated
$K_{NH3,AOB}$	AOB affinity constant for NH_3	$mgN.L^{-1}$	0.20 ±0.08	Estimated
$K_{NH2OH,AOB}$	AOB affinity constant for NH_2OH	$mgN.L^{-1}$	0.90 ±0.11	Estimated
$K_{HNO2,AOB}$	AOB affinity constant for HNO_2	$mgN.L^{-1}$	0.004 ±0.003	Estimated
$K_{NO,AOB,HAO}$	AOB affinity constant for NO (from HAO)	$mgN.L^{-1}$	$3\ 10^{-4}$ $\pm 2.10^{-5}$	Estimated
$K_{NO,AOB,NN}$	AOB affinity constant for NO (from NirK)	$mgN.L^{-1}$	0.008 ±0.006	Estimated
$K_{I,O2,AOB}$	N_2O constant for production inhibition by O_2	$mgO_2.L^{-1}$	0.8 ±0.09	Estimated
$K_{O2,AOB,ND}$	AOB constant for O_2 effect on ND (rate 5)	$mgO_2.L^{-1}$	0.5 ±0.09	Estimated
$K_{O2,AOB,1}$	AOB affinity constant for O_2 (AMO reaction)	$mgO_2.L^{-1}$	1.0 ±0.14	Estimated
$K_{O2,AOB,2}$	AOB affinity constant for O_2 (HAO reaction)	$mgO_2.L^{-1}$	0.6 ±0.16	Estimated
$q_{AOB,AMO}$	Maximum rate for AMO reaction	$mgN.mgCODX^{-1}.h^{-1}$	0.2167	μ_{AOB}/Y_{AOB}
$q_{AOB,HAO}$	Maximum rate for HAO reaction	$mgN.mgCODX^{-1}.h^{-1}$	0.2167	μ_{AOB}/Y_{AOB}
$q_{AOB,N2O,ND}$	Maximum N_2O production rate by ND pathway	$mgN.mgCODX^{-1}.h^{-1}$	0.0542	$q_{AOB,HAO} . \eta_{AOB,ND}$
$q_{AOB,N2O,NN}$	Maximum N_2O production rate by NN pathway	$mgN.mgCODX^{-1}.h^{-1}$	$3.25\ 10^{-4}$	$q_{AOB,HAO} . \eta_{AOB,NN}$

3.2 Modeling batch experiments with the 2-P model

The 2-P model was initially calibrated with a series of batch tests with similar ammonia concentrations but different initial nitrite concentrations. Figure 28 presents typical results obtained during four experiments (ammonia injection at 1 minute). Figure 29 shows the experimental data and simulations obtained for the emission factor N2O-EF and the NO/N2O ratio for all batch experiments presented in

Table 37. During all experiments, nitrate concentration was negligible and ammonia was fully converted to nitrite. The SBR process had been operating for 3 months before these tests with appropriate aeration phase control to eliminate the NOB activity. The ammonium, nitrite and dissolved oxygen concentrations were correctly described by the 2-P model. Before calibrating the NO and N_2O productions, a good prediction of DO and nitrite was crucial considering their combined effect.

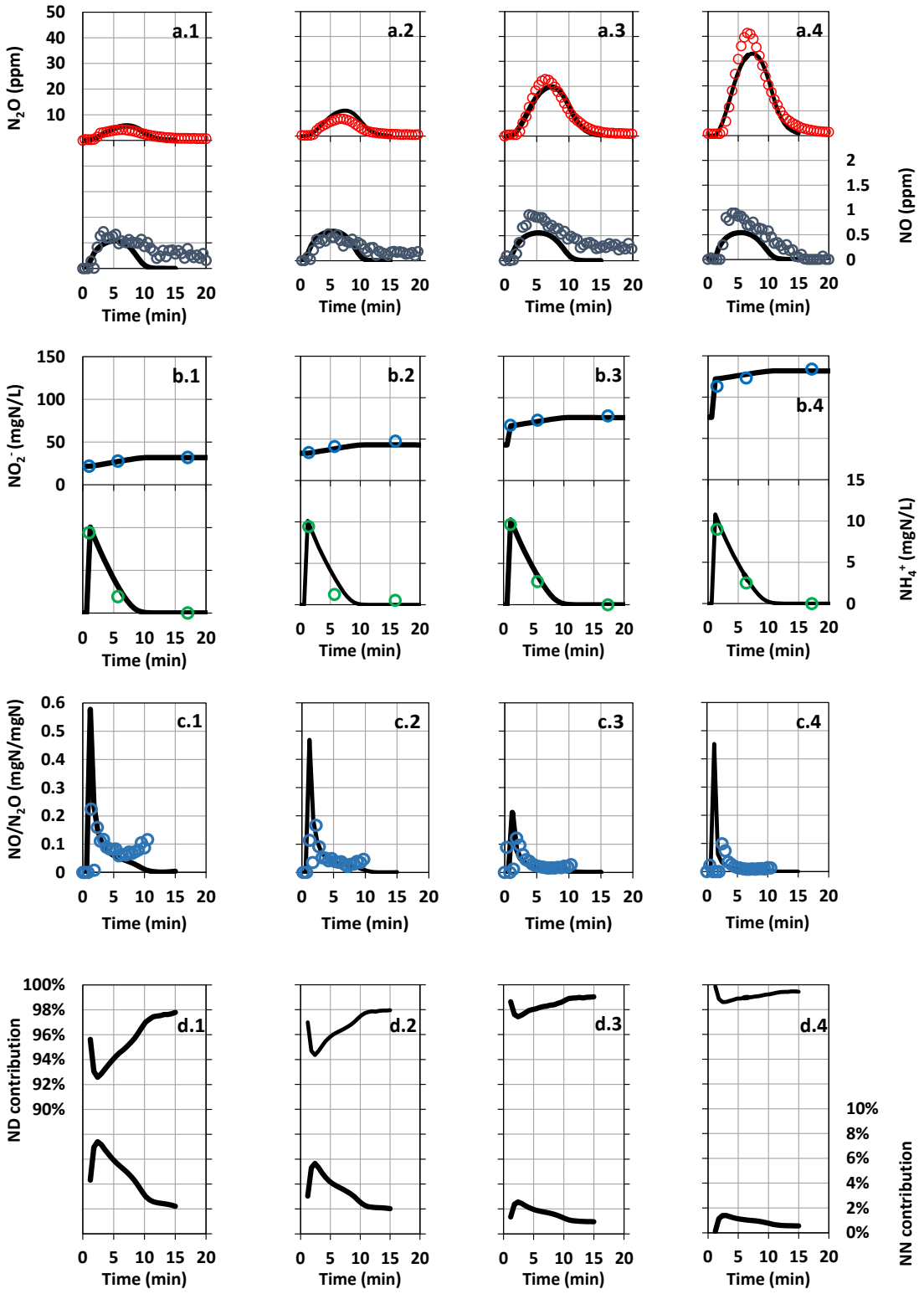

Figure 28. Experimental data (points) and simulation with the 2-P model (lines) for four aerobic batch tests with ammonia injections (10 mgN/L) and oxidation to nitrite for different initial nitrite concentrations. (a) NO and N_2O concentration in the gas phase (ppm); (b) Ammonia and nitrite concentrations; (c) NO/N_2O ratio; Simulated relative contributions of NN and ND pathways to N_2O emission (d).

As shown in Figure 28, the 2-P model accurately predicted the dynamics of N_2O emissions, and the effect of nitrite on the emissions. By comparing the different responses on Figure 28 (a, b and c), in the beginning 2 min, N_2O (ppm) is very small, only NO is produced increasingly, resulting in a sharp increase of NO/N_2O ratio in the beginning. After 2 min, N_2O production starts and its production rate is faster than NO (Figure 28a), which causes a sudden decrease of NO/N_2O ratio. This phenomenon was especially observed when nitrite concentration was low or null initially. Then, when ammonia was depleted, N_2O starts to decrease and gets zero after a few minutes (NO/N_2O ratio was not calculated in that final zone due to high uncertainty). As indicated by Figure 28d (NN and ND contribution to N_2O emission), the model predicted that ND was the major pathway responsible for N_2O emission, and the N_2O emission rate was stimulated by the increase of free nitrous acid (HNO_2) concentration (or nitrite). Hence the agreement between simulated N_2O and experimental N_2O was mainly related to the ND pathway prediction (process 5). In contrast, NO emissions were quantitatively much lower than N_2O emissions and NO reached its maximum concentration before N_2O. The 2-P model gave an acceptable prediction of NO emissions and the prediction of NO/N_2O matched experimental data well. In the 2-P model, the variation of the NO/N_2O ratio was basically related by the variation of ND and NN contributions to the N_2O emissions. NO was rapidly emitted by hydroxylamine oxidation (process 2), and N_2O was firstly produced by process 4 (NN pathway) independently of the presence of nitrite. Then N_2O was produced by process 5 (ND pathway) consuming hydroxylamine and nitrite, which led to the decrease of the NO/N_2O ratio. This progressive stimulation of the ND pathway during batch kinetics was in agreement with the data from isotope signature analysis reported in literature (Wunderlin et al., 2013).

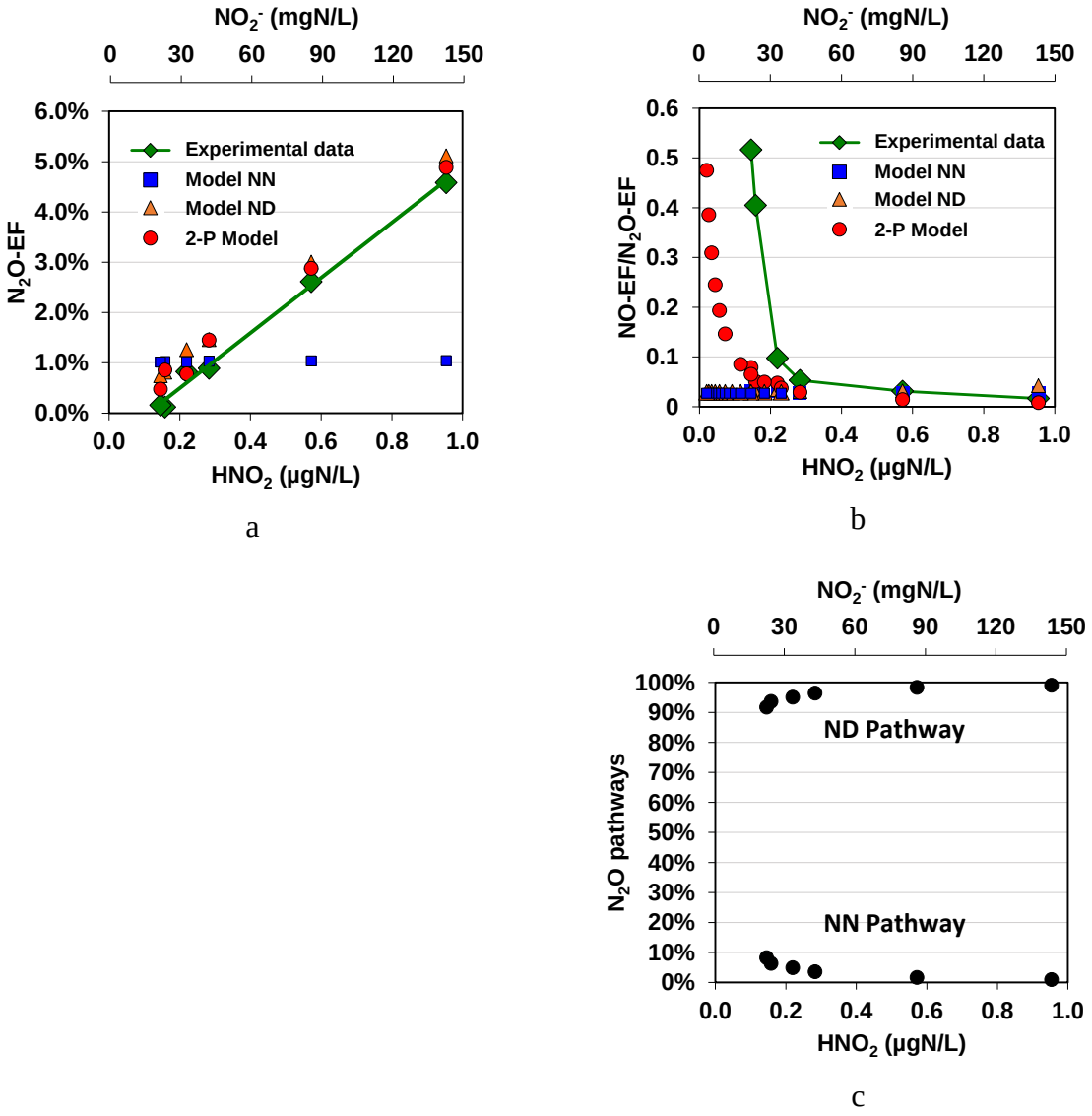

Figure 29. N_2O emission factor (EF) as a function of HNO_2 or nitrite concentration (a); NO-EF/N_2O-EF ratio as a function of HNO_2 or nitrite concentration (b); Simulated relative contributions of NN and ND pathways (c).

As shown in Figure 29a, the N_2O emissions clearly increased proportionally to nitrite concentration (the same correlation was observed with free nitrous acid as the pH was similar during these tests). It was checked that this increase was completely reversible by repeating a test at low nitrite level at the end of the series. In contrast, the variations of NO emission factors were not statistically significant. Consequently, the NO/N_2O ratio decreased with the increase of nitrite (Figure 29b). For these different experiments the two pathway model predicted the increase of the N_2O emission factor and the decrease of the NO-EF/N_2O-EF ratio, consistently with experimental observations (Figure 29a and Figure 29b respectively). The predictions of the 2-P model indicate that the increase of free nitrous acid or nitrite stimulated N_2O emission by the ND pathway and consequently the decrease of the NO/N_2O

ratio. The level of HNO_2 for which the decrease of the NO-EF/N_2O-EF ratio was observed was slightly underestimated by the model. However, except for this small discrepancy, the trend of the simulation was comparable to observations. The NO-EF/N_2O-EF ratio decreased from 0.5 to less than 0.02 for the range of HNO_2 explored (0.02 – 0.95 µgN.L^{-1}). The highest ratio was obtained when the contribution of the NN pathway was maximum (at low HNO_2) whereas the lowest ratio was predicted when ND was the major contributing pathway (at the highest HNO_2). Basically the ability of the model to describe NO emission uncorrelated to nitrite accumulation was due to the fact that NO was considered to be only emitted by hydroxylamine oxidation, neglecting the possible contribution of the ND pathway. Even if this assumption is a simplification of the reality it enabled the observations to be reasonably well described. However this assumption should not be considered as a general statement (it probably depends on the level of activation of NirK and Nor enzymes). And it should be noted that the model was not confronted to a system with important variation of NO emission.

3.3 Validation of the 2-P model with long-term data set from SBR process

Simulations were compared with the long-term data set collected in the SBR (Figure 30). N_2O-EF, NO-EF and NO-EF/N_2O-EF ratio were calculated for each cycle based on the off-gas measurements during the aerated phase. The data are represented in Figure 30 versus the maximum HNO_2 concentration reached during the aerated period of the cycle, variation of HNO_2 resulting in both nitrite and pH variations. The time evolution during the long-term validation with N_2O-EF, NO-EF, HNO_2 concentration and DO variations are presented in Figure 31. In Figure 30 and Figure 31, each dot corresponds to one cycle (187 cycles). The dynamic evolution of NO and N_2O gas phase concentrations are presented in Figure 32 for nine successive cycles.

The data confirmed the correlation between N_2O emissions and HNO_2 accumulation (Figure 30a). For HNO_2 concentrations below 0.60 µgN.L^{-1} the N_2O-EF remained lower than 1% for most of the cycles. The N_2O-EF increased significantly up to 3% for an HNO_2 concentration of 0.8 µgN.L^{-1}. Values ranging from 4% to more than 11% were finally observed for HNO_2 accumulation close to 0.9 µgN.L^{-1} and it should be noted that the dissolved oxygen was observed to vary during the corresponding period. The highest emission factors were observed for relatively low DO (1-1.5 mg/L) in that period. For comparison, in a previous

batch test, the emission factor was 4.5% at similar HNO_2 level with DO higher than 2-2.5 mgO_2/L (Figure 29). In contrast NO emission varied from 0.024% to 0.078% but was not correlated with HNO_2 concentration (Figure 30b). In consequence, the NO-EF/N_2O-EF ratio decreased from 0.20 to 0.002 gN-NO/gN-N_2O for an HNO_2 concentration increase from 0.24 to 0.92 $\mu gN.L^{-1}$ (Figure 30c). This result is thus similar to those previously observed for specific batch experiments (Figure 29).

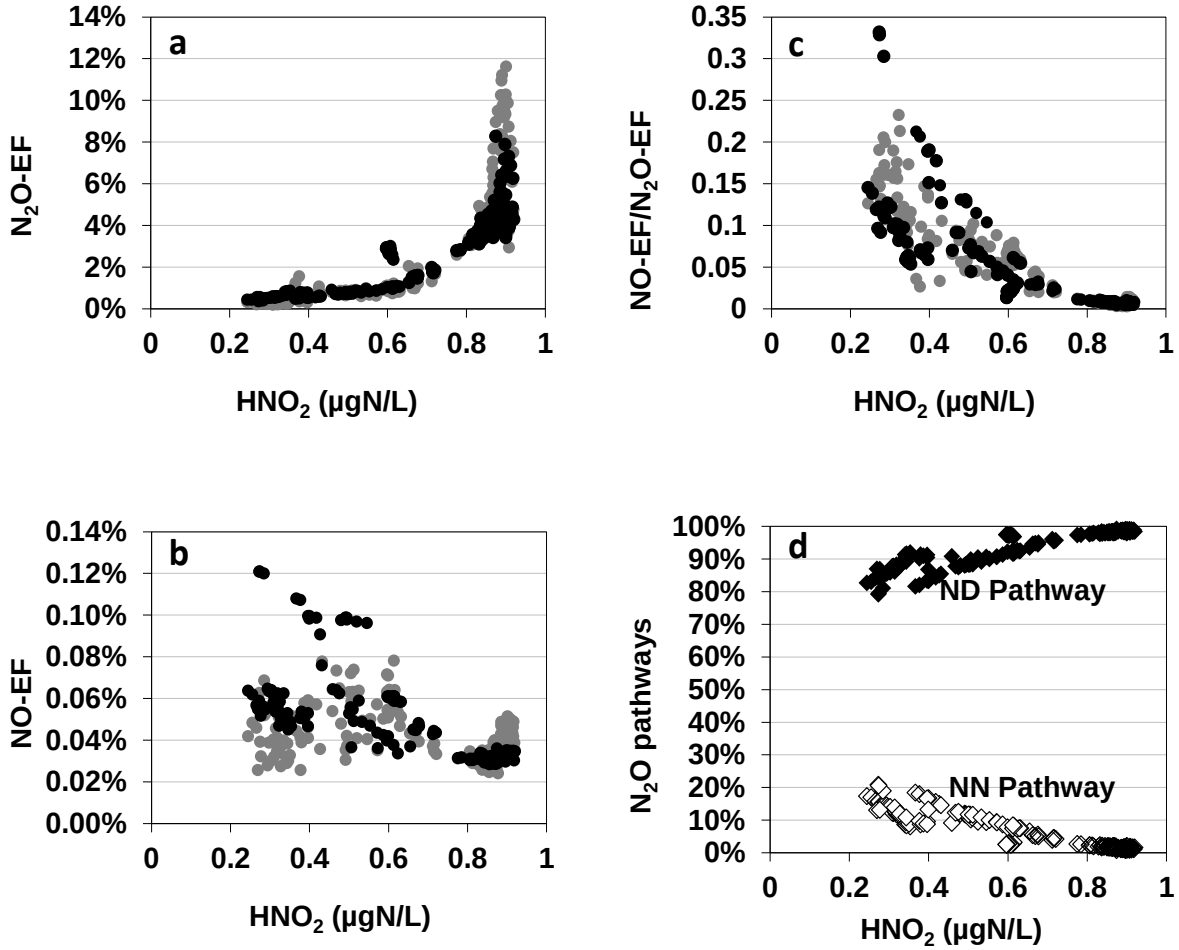

Figure 30. Simulated results (black) and experimental data (grey) for 187 cycles of the SBR (One dot = one cycle). N_2O (a), NO (b), the NO-EF/N_2O-EF ratio (c), versus the HNO_2 concentration. Simulated relative contributions of NN and ND pathways (d).

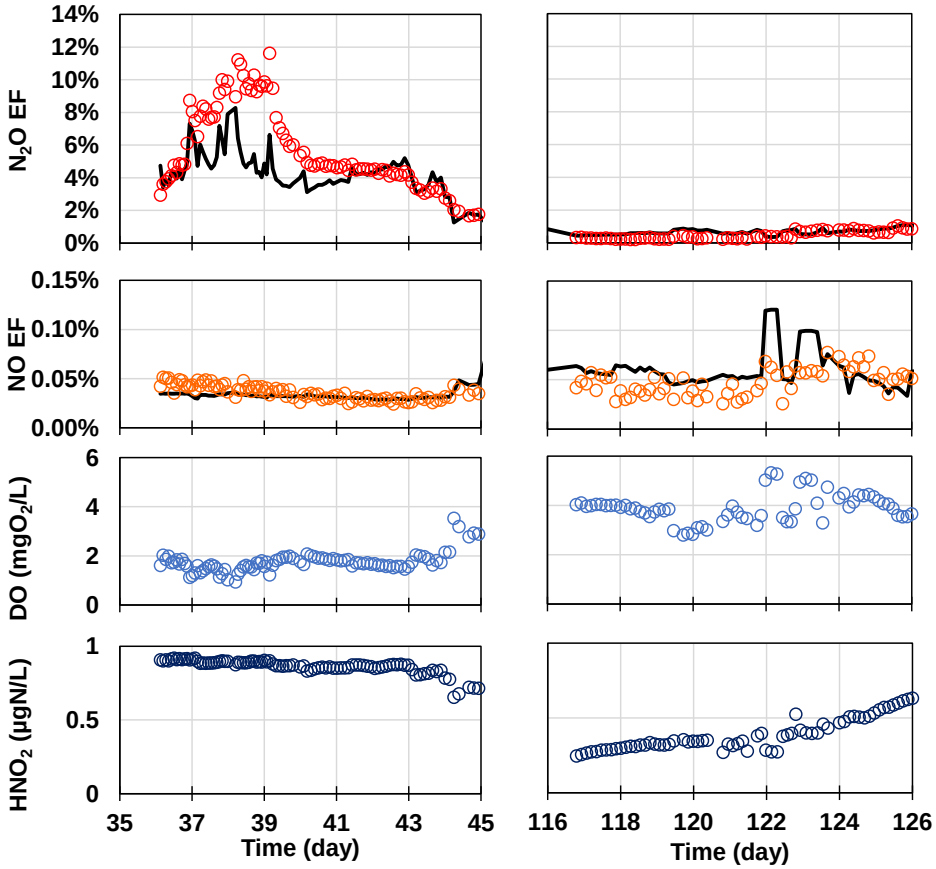

Figure 31. Evolution of N_2O EF, NO EF, DO and HNO_2 during long term operation of SBR. Each point corresponds to one SBR cycle. The average DO concentration and the average HNO_2 concentration have been calculated for each cycle.

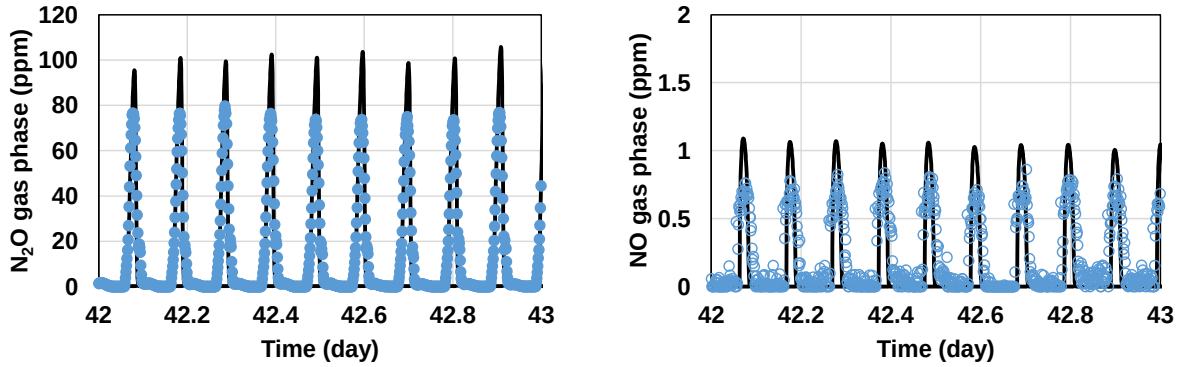

Figure 32. Evolution of the N_2O and NO gas phase concentrations during successive SBR cycles.

The simulations obtained with the 2-P model were in agreement with the experimental observations for N_2O-EF, NO-EF and NO-EF/N_2O-EF ratio. The calibrated model was capable of predicting most of the data collected during 6 months on the SBR, with a large range of N_2O emissions factors from 0.1% (at low nitrite, high DO) to 8% (at high nitrite, low DO). The model slightly underestimated the N_2O emissions for a 4 day period with rapid aerobic-anoxic alternance (at low DO), this high frequency may have generated an additional emission during anoxic period that we did not consider in the model. The increase of the N_2O emission factor as a function of HNO_2 was predicted very correctly (only the highest N_2O-EF obtained during those 4 days were slightly under-estimated). In addition the N_2O production was exacerbated when high nitrite and low DO were maintained simultaneously. This effect of DO was described by the model thanks to the modified inhibition term on DO. It is important to note, here, that the 2-P model predicted a 6 month period with 187 cycles obtained at different pH and different DO (1 to 6 mg/L). Compared to batch experiments, the variation of HNO_2 resulted from simultaneous variations of pH and nitrite. This result validates the choice of using free nitrous acid in the kinetic expressions of the model.

Basically, the 2-P model has similar predictive capacities as the NN pathway model for NO-EF (Figure 33). Finally, the 2-P model made it possible to explore the relative contribution of both NN and ND pathways to the N_2O emissions (Figure 30d). The model predicted a major contribution of the ND pathway, which increased from 80% to 99% with the increase of the HNO_2 concentration from 0.24 to 0.92 $\mu gN.L^{-1}$.

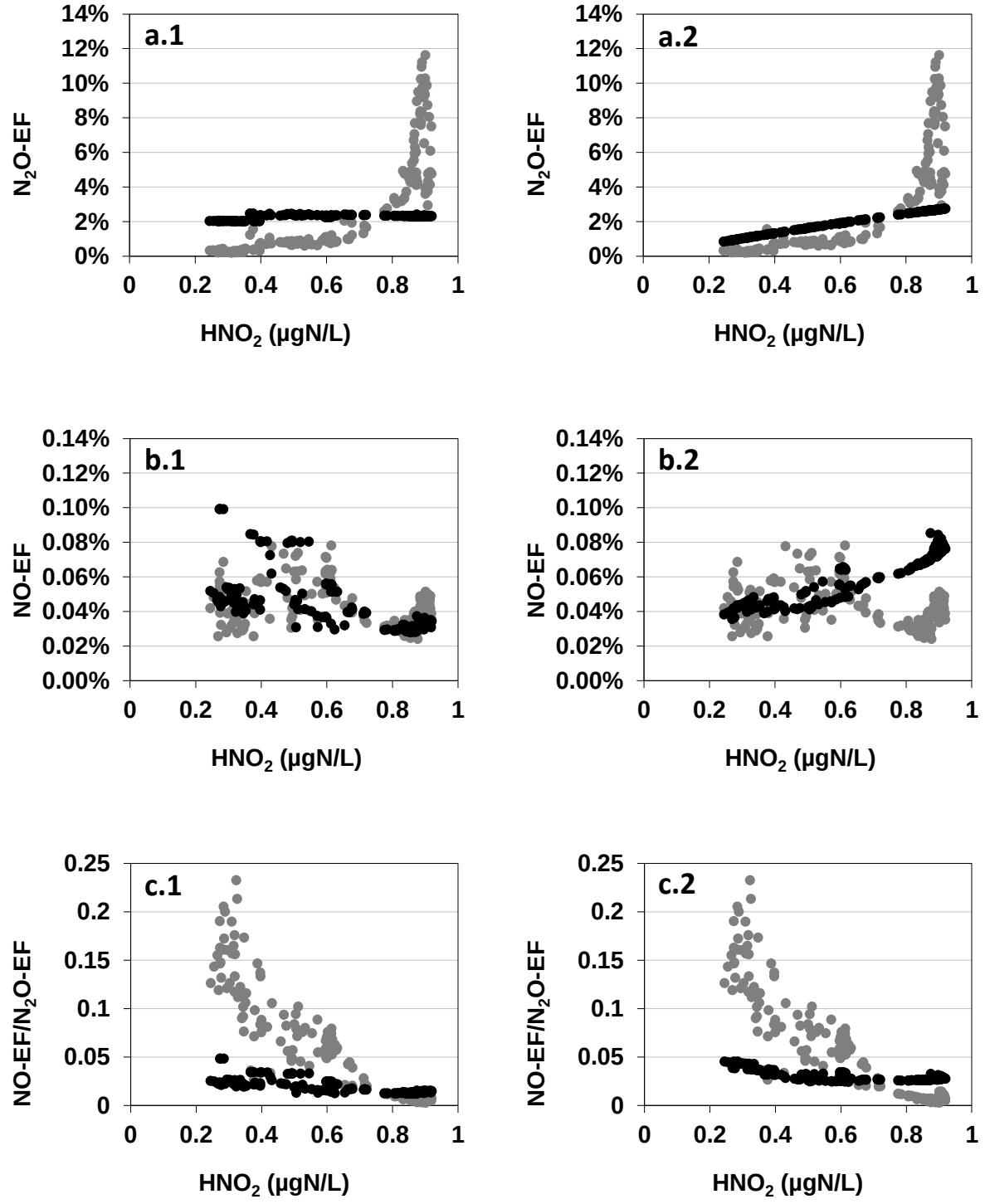

Figure 33. Comparison on two single pathway models (NN and ND) calibrated independently. Simulated (black) and experimental (grey) emission factors in relation with the HNO_2 concentration for N_2O (a), NO (b), and the NO-EF/N_2O-EF ratio (c).

3.4 Simulations with other existing models

The predictions of different single pathway models were also confronted with both NO and N_2O emissions collected in this study. The main conclusions were that single pathway models were not able to predict NO and N_2O profiles simultaneously. The ND pathway model gave a satisfactory description of N_2O but did not capture NO trends. Conversely, the model based on the NN pathway correctly described NO emissions but did not match the N_2O trend (see Figure 34 and Figure 35). As shown by Figure 29a, for different batch experiments at various nitrite concentrations, the ND model correctly predicted the increase of N_2O emission whereas the NN model was not able to predict any influence of nitrite. In addition, both NN and ND models predicted a constant ratio between NO and N_2O, which was not confirmed by experimental observations (Figure 29b). Basically, the NO and N_2O productions are structurally related in single pathway model and it is not possible to predict a significant variation of NO/N_2O ratio. Finally, only the simulations obtained with the 2-P model were consistent with the experimental observations.

The results were also compared to the predictions of the model recently proposed by (Ni et al., 2014) based on multiple production pathways and intracellular electron carriers. The model was combined with gas liquid transfer equations and batch experiments were simulated (Figure 36). With original calibration, this model predicted NO emissions higher than N_2O emissions, which was not in agreement with our observation and those mentioned in the literature (Ahn et al., 2011; Marlies J. Kampschreur et al., 2008; Rodriguez-Caballero and Pijuan, 2013). In fact, the multiple pathway model was initially developed without modeling NO stripping by (Ni et al., 2014) assuming that the NO consumption mainly occurred inside AOB cells without any bulk accumulation (or emission). For this reason, this multiple pathway model should be considered with more attention if the objective is to predict realistic NO emissions in the gas phase. In its present form it was possible only after considerable calibration effort, but these changes could completely modify the prediction capabilities of the model concerning other compounds. To conclude, more work would be necessary to evaluate whether both the NO and the N_2O emissions could be described appropriately with Ni's multiple pathway model or not.

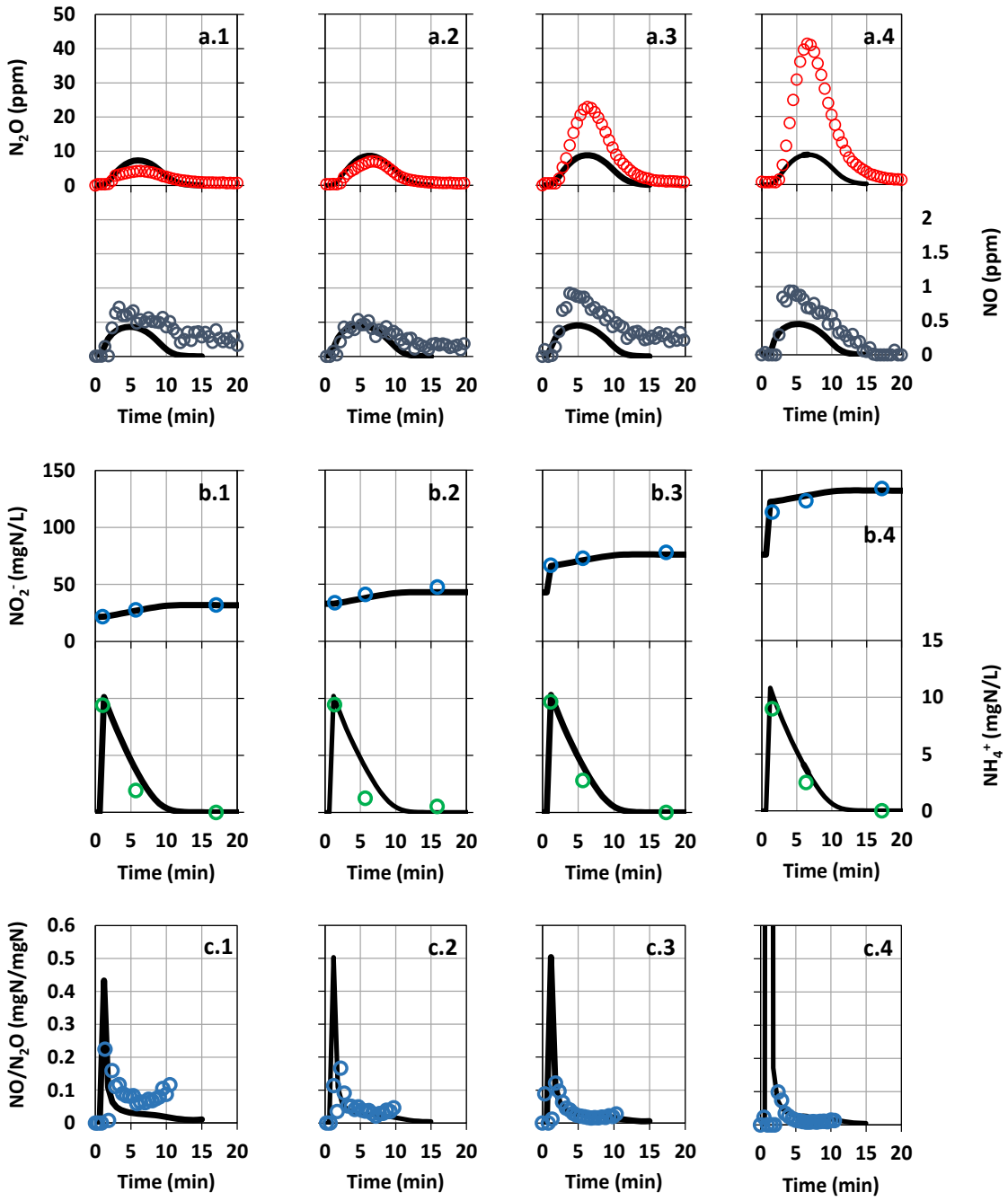

Figure 34. Experimental data (points) and simulation with the NN single pathway model from (Ni et al., 2013b) (lines) during four batch experiments of ammonia oxidation to nitrite with different nitrite concentrations. (a) NO and N_2O concentration in the gas phase (ppm); (b) Ammonia and nitrite concentrations; (c) NO/N_2O ratio. Time of ammonia/nitrite injections: 1 minute.

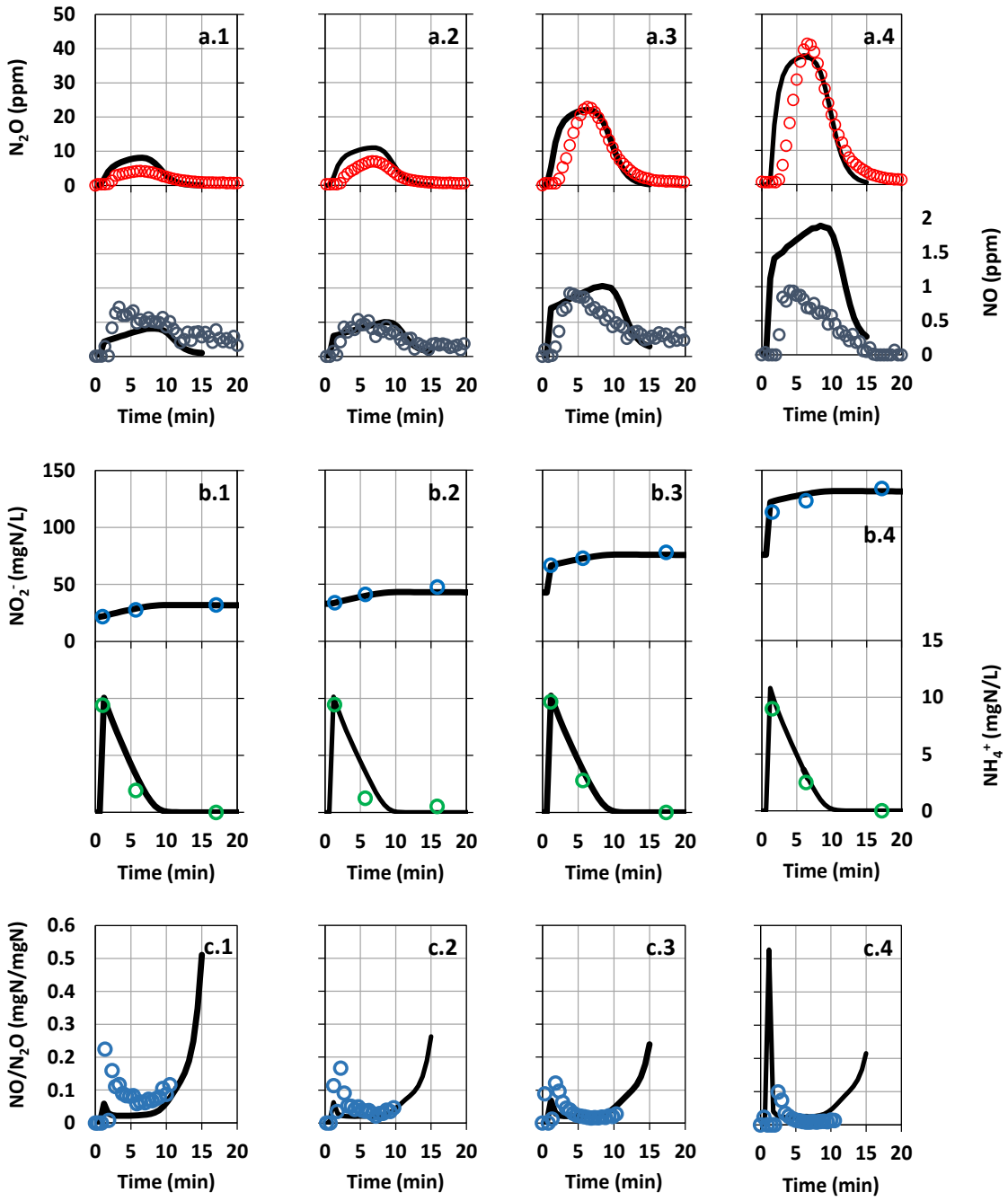

Figure 35. ND single pathway model simulation (lines) (Mampaey et al., 2013) and experimental (points) data for four batch experiments of ammonia oxidation to nitrite with different nitrite concentrations. (a) NO and N_2O concentration in the gas phase (ppm); (b) Ammonia and nitrite concentrations; (c) NO/N_2O ratio. Time of ammonia/nitrite injections: 1 minute.

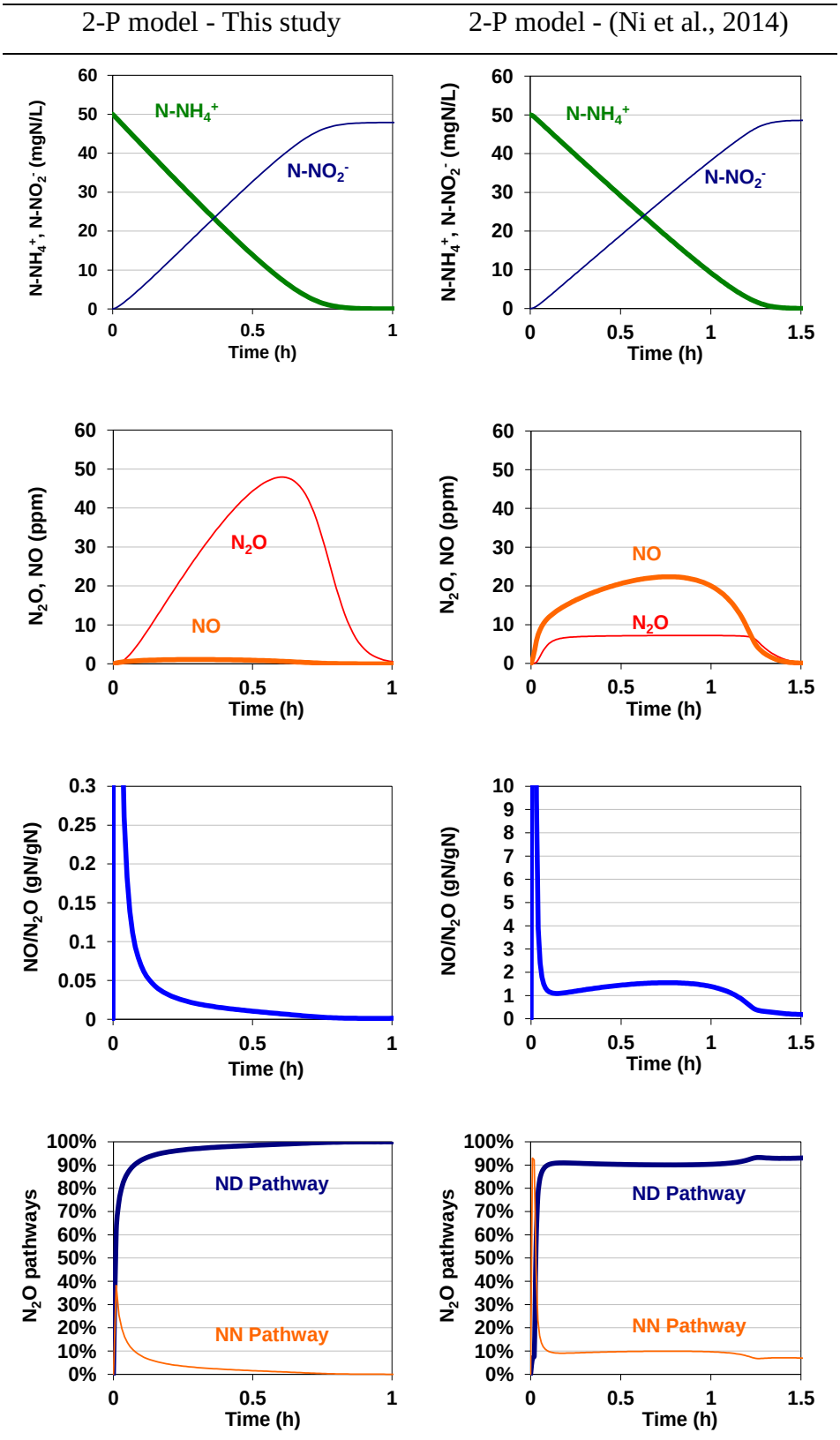

Figure 36. Comparison of the 2-P models proposed in this work and the multiple pathway model by (Ni et al., 2014)

4 Discussion

4.1 Capabilities of the two pathways model to predict NO and N_2O ratio and the pathways regulation

The two pathway model developed in this work is to date the only model that has been validated on both NO and N_2O measurements monitored during batch experiences experiments and long long-term operation of an SBR. The 2-P model successfully predicts the variation of the NO/N_2O ratio as well as the emission factors. The variation of the NO/N_2O ratio predicted by the model is related to a variation of the contribution of each pathway in the N_2O production, the maximum NO/N_2O ratio being predicted when the N_2O is produced by the NN pathway.

The 2-P model predicts a dynamic variation of the contribution of each pathway to the N_2O emissions as shown in Figure 37 (simulation of a batch experiment). Initially the contribution of the ND pathway accounted for about 60% but increased rapidly, reaching 100% at the end. This is in full agreement with the studies based on measurement of the site preference (SP) in isotopomers of N_2O to distinguish the pathways (Peng et al., 2014; Toyoda et al., 2011; Wunderlin et al., 2013). In similar batch experiments, (Wunderlin et al., 2013) found that the contribution of the ND pathway increased with time from around 75% to 100%. The same authors also demonstrated that the contribution of the NN pathway was dominant when hydroxylamine was used as the nitrogen source, and the 2-P model also predicts a maximum contribution by the NN process in case of hydroxylamine injection associated with high NO accumulation (not shown). On the one hand, the N_2O production rate through the ND pathway increases with time in relation with nitrite (or HNO_2). On the other hand, the N_2O produced by the NN pathway is stimulated by hydroxylamine and NO accumulation due to the unbalanced situation observed between AMO and HAO reaction rates in batch conditions. As NO was assumed to be mainly related to that hydroxylamine oxidation (HAO) in the model, it was not influenced by nitrite. This explains the decrease of the NO/N_2O ratio with time and with nitrite accumulation. In absence of nitrite (no accumulation at all, or if the ND pathway is artificially switched off), the calibrated model predicts an NO/N_2O ratio close to 0.6 for pure production by the NN pathway. Therefore the model tends to confirm the possible relation between NO/N_2O and pathway contributions, which still need to be further demonstrated in future work. Finally the capability of the 2-P model for predicting N_2O

emissions was demonstrated in that study but more work would be necessary to demonstrate that capability for predicting fluctuation of NO emissions. Further analysis of NN and ND contributions to NO emission with isotope analysis may be used to confirm the assumptions related to NO emission pathway.

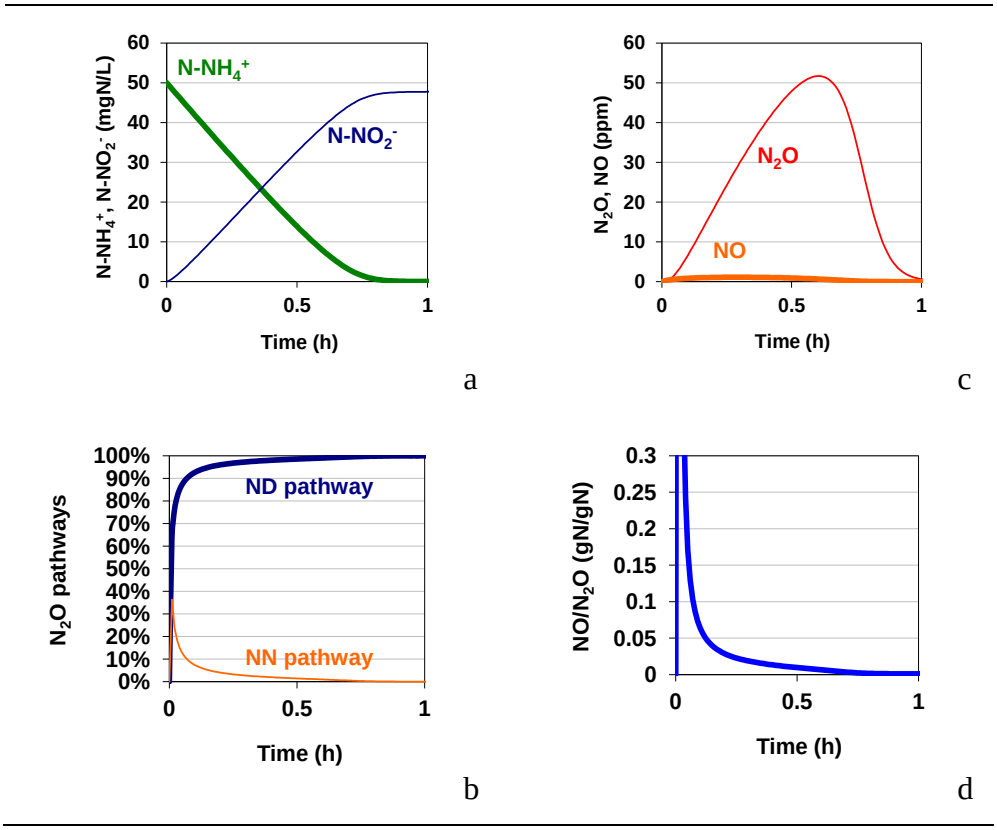

Figure 37. Simulated NO, N2O, NO/N2O ratio and contributions from the ND and NN pathways during a batch experiment.

4.2 Combined effect of operating parameters on emissions

In this work, the experimental data indicated that N_2O emission rate and emission factor were correlated to the variations of nitrite, pH, and dissolved oxygen. The effect of nitrite and pH were combined in the model by the use of free nitrous acid as the substrate for AOB denitrification. In the range of pH explored in the SBR, good agreement was observed. The variations of N_2O emissions with nitrite or slight pH change were predicted correctly by the model.

Peng et al., (2015) recently demonstrated the combined effect of DO and nitrite on the N_2O emission and pathway regulation. A simulation of the influence of HNO_2 and DO on NO and

N_2O emission factors, NO-EF/N_2O-EF ratio, and the contribution of pathways is presented in Figure 38. The simulations based on the 2-P model confirm a combined effect of HNO_2 and DO on the N_2O emission pathways. For a constant DO (2 $mgO_2.L^{-1}$), an increase in the HNO_2 concentration leads to an increase in the N_2O emission factor, an increase in the ND contribution and a decrease in the NO-EF/N_2O-EF ratio. For a similar HNO_2 concentration (0.7 µgN-$HNO_2.L^{-1}$) the increase of DO leads to a decrease of the N_2O-EF, a small decrease of the ND contribution associated with a small increase of the NN contribution, and a slight increase of the NO-EF/N_2O-EF. This effect of DO is in good agreement with the recent work of (Peng et al., 2014), who found that the ND pathway was the main contributor to N_2O production during ammonia oxidation (95% - 73% of N_2O from the ND pathway) and that an increase of the dissolved oxygen (DO) concentration from 0.2 to 3 $mgO_2.L^{-1}$ led to an increase of the NN pathway contribution from 5% to 27%. Finally, the highest predicted N_2O emission factors are observed for high HNO_2 concentration and relatively low DO (0.5-1 mgO_2/L). This is also in good agreement with our practical observations as the maximal peak in the SBR process was observed when high HNO_2 (0.9µgN/L) occurred at the same time as low DO (1.0 mg/L). This is also in good agreement with the study by Peng et al., (2015) on the combined effect of DO and nitrite. As the independent effect of DO was not fully tested in this work (more focused on nitrite effect) conclusion about oxygen effect should be considered with caution. A future analysis will be dedicated to the confrontation of 2-P models on data with combined DO and nitrite effect.

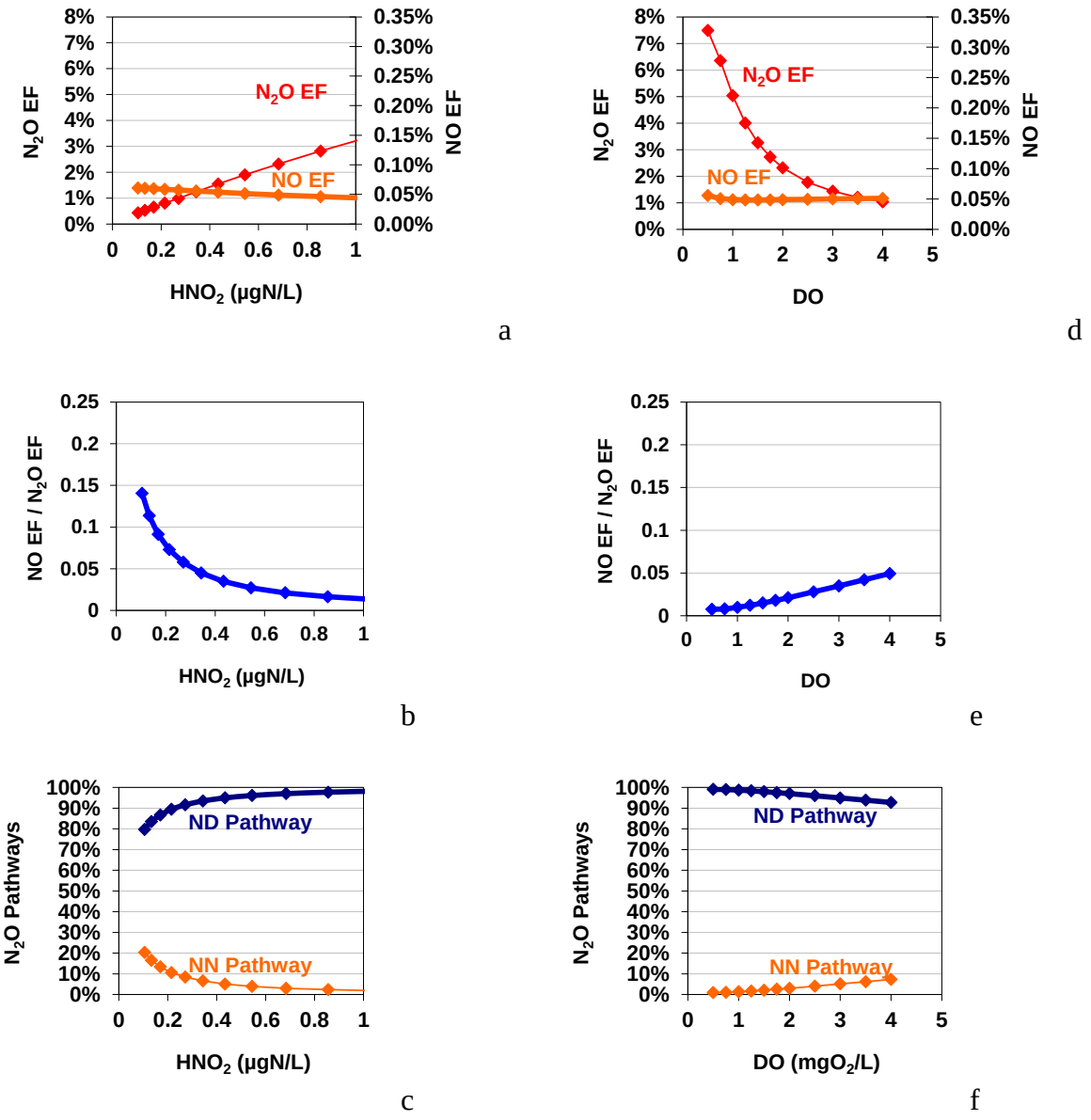

Figure 38. Simulations obtained for different HNO2 and DO concentrations. The HNO2 range was explored at a constant DO (2 mgO2.L-1) and, similarly, the range of DO was explored at a constant HNO2 concentration (0.7 µgN-HNO2.L-1)

4.3 Comparison of the 2-P model with other existing models and future use of the models

None of the AOB models based on a single pathway were able to describe the NO/N_2O ratio variation obtained experimentally. Moreover multiple pathway models were able to describe a difference in the effect of an operating parameter (DO for example) depending on the contribution of the pathway. For that reason the use of single pathway models should be limited to a given zone of experimental conditions. (Peng et al., 2015b) recently tested the predictive ability of a single pathway model to describe the N_2O data generated by a multiple pathway model. The conclusion was that the AOB denitrification model can be applied at low DO (<0.5 mg/L) or at high DO with significant nitrite accumulation (DO > 0.5 and NO_2^- > 1 mg N/L). The latter situation corresponds to the present work and our study confirms that the ND model was the best single pathway model to describe N_2O emission. This is logical as the contribution of this pathway to N_2O emission has been demonstrated to be major in the conditions of this study, due to the significant accumulation of nitrite. However it was also shown that the 2-P model was much better for predicting N_2O emissions as well as NO tendency. It was expected that the ND model would not be able to describe N_2O emissions in a system with low nitrite level (high NOB activity), leading to N_2O emissions by the NN pathway (Ni et al., 2013b). As previously demonstrated, ND models (Guo and Vanrolleghem, 2014; Mampaey et al., 2013; Pocquet et al., 2013) were able to describe experimental data in different systems but needed a significant and sometimes unrealistic adjustment of key parameters (η_{AOB}) to be able to describe a system with a low nitrite level (Spérandio et al., 2015). This was probably needed to compensate for the fact that the hydroxylamine pathway was not considered.

In contrast, in this study, it was shown that the NN model was capable of describing the NO emissions but did not match the N_2O emissions. The calibration of the two pathway model indicated that the N_2O emission rate (and emission factor) due to the NN pathway was likely to be low in the reactor studied. Indeed the maximum specific rate for N_2O production by the NN pathway ($q_{AOB,N2O,NN}$) was 3.10^{-4} mgN.mgCODX^{-1}.h^{-1}, i.e. 180 times lower than the maximum specific rate for N_2O production by the ND pathway ($q_{AOB,N2O,ND}$ = 0.0542 mgN.mgCODX^{-1}.h^{-1}). The last rate was also 4 times lower than the maximum specific rate of HAO reaction with oxygen ($q_{AOB,HAO}$=0.2167 mgN.mgCODX^{-1}.h^{-1}). Consequently, during a typical ammonia batch experiment, predictions indicated that about 96.7% of N_2O would be produced by the ND pathway and only 3.3% by the NN pathway. The last study by (Peng et

al., 2015b) suggested that the hydroxylamine oxidation model could be applied under high DO (DO>1.5mg/L) and nitrite concentration between 0 and 5.0 mgN/L. Our study revealed that, in a larger range of nitrite concentrations, this model was not able to predict the observations.

Finally the model proposed in this study was also compared to the multiple pathway model recently proposed by (Ni et al., 2014). Further work would be necessary to compare the predictive abilities of these two approaches. Our first comparison indicates that comparable prediction of N_2O emissions could be obtained but the 2-P model proposed in this study gave more realistic predictions for NO emissions, in agreement with experiments and previous literature (Ahn et al., 2011; Marlies J. Kampschreur et al., 2008; Rodriguez-Caballero and Pijuan, 2013). This is possibly due to the fact that the variable NO in the electron based model is likely to represent a local intracellular concentration instead of the concentration present in the bulk (which would be lower). Additional work will be necessary to determine which of these different concepts would be recommended for use in each specific situation. NO measurements from different experimental systems could be useful in order to test the proposed models and evaluate more in deep their ability to predict NO emission.

5 Conclusion

NO and N_2O emissions during nitritation were both used for calibration of single pathway AOB models and a two pathway AOB model. None of the models based on a single pathway could describe the variation of NO/N_2O ratio. In contrast the proposed model which includes the two pathways predicted a decrease of NO/N_2O ratio with the HNO_2 accumulation (due to nitrite or pH variation) which was in good agreement with the experimental observations.

The model confirmed the assumption that the decrease of the NO/N_2O ratio is explained by an increase of the contribution of the ND pathway which was the dominant pathway in the studied system. Inversely, the highest NO/N_2O corresponded to the situation of maximal contribution of the NN pathway. Thus the measurement of NO/N_2O ratio is an interesting tool for calibration of a model which includes two pathways.

The predicted combined effects of nitrite and dissolved oxygen on pathways regulation were in agreement with our practical observations and in accordance with literature.

Chapter VII Conclusions & Perspectives

1 Effect of operating conditions on NO and N_2O emissions during nitritation

The investigation of mechanisms of NO and N_2O emissions by AOB has been performed with experimental data that had been collected on a lab-scale SBR treating an ammonium rich effluent by nitrification/denitrification over nitrite. The aerobic period of SBR cycles was analyzed and for each of them, the average DO, the maximum HNO_2 concentration and NO and N_2O emission factors were calculated. In addition, designed batch experiments have been carried out in this study. The effects of HNO_2 and DO concentrations on NO and N_2O emissions during nitrification were investigated.

The N_2O emission factor (N_2O-EF) appeared to be exponentially correlated to the maximum HNO_2 concentration At HNO_2 concentration lower than 0.50 $\mu gN.L^{-1}$ the N_2O-EF remained relatively low and below 1%. Higher HNO_2 concentration resulted in a significant increase of N_2O-EF. At the maximum HNO_2 tested (around 0.9 $\mu gN.L^{-1}$), the N_2O-EF varied from 3% to 11%. The relation between DO and N_2O EF indicates that the lowest N_2O emission factors (<1%) were obtained at high DO (from 2.5 to 6.0 $mgO_2.L^{-1}$) whereas a large variation from 1% to 11% was observed at DO between 1 and 2 $mgO_2.L^{-1}$. In this range, the highest N_2O emissions have been observed for cycles with simultaneously the highest HNO_2 concentration whereas a low HNO_2 accumulation (lower than 0.5 $\mu N.L^{-1}$) led to N_2O-EF around 1%. These observations indicate a combined effect of DO and HNO_2 on N_2O-EF and match with the assumption that the activation of AOB denitrification pathway (ND) is exacerbated at a low DO when nitrite is present, DO and HNO_2 both of them playing the role of electron acceptors during nitritation. In contrast, NO-EF did not show such a tendency neither with the DO nor with the HNO_2 concentration. The NO-EF varied between 0.004% and 0.078% for all SBR cycles.

2 SBR control and reduction of NO and N_2O emissions

The specificity of the SBR process was to control the aerobic and anoxic periods of cycles with the automatic detection of the ends of nitrification and denitrification using DO and ORP signals respectively. This automatic phase length control based on DO bending point has the advantages to repress efficiently the NOB activity. It results in full conversion of ammonia to nitrite, leading to a reduction in oxygen consumption by NOB and the reduction of COD

needs for the reduction of nitrite to nitrogen gas by heterotrophic denitrification. Obviously, this accurate adaptation of aerobic phase length minimizes the energy needs of the process.

The development of this control strategy, which has been patented (EP 14196087), was realized in collaboration with the technological center CRITT GPTE of Toulouse. The control system was also optimized for the reduction of N_2O emissions. As a result, several recommendations can be proposed to limit significantly the environmental impact of a SBR with nitrification/denitrification over nitrite:

- Limit the presence of readily biodegradable COD during nitrification which impacts the competition between nitrifiers and heterotrophs for oxygen, decreasing the DO and possibly the pH during nitrification and leading to a higher HNO_2 concentration. These conditions lead to a higher activity of the ND pathway. Moreover, simultaneous nitrification and denitrification could take place with possibly a higher amount of N_2O emitted due to denitrification.

- Limit the accumulation of HNO_2 below 0.50 $\mu gN\text{-}HNO_2.L^{-1}$. This can be realized by limiting the amount of ammonium to be removed during nitrification (step-feed, reduction of the volumetric exchange ratio) or increasing the pH. If the HNO_2 concentration can not be reduced below this threshold value, the reduction of N_2O emissions can be achieved by maintaining a DO higher than 2.0 $mgO_2.L^{-1}$ during the nitrification.

3 Calibration of N_2O models based on a single pathway

Experimental observations have been confronted to N_2O models based on a single pathway. Four models describing the N_2O production by the ND pathway with different hypothesis and one model describing the NN pathway have been considered in this study. The calibration of these models to experimental data has been realized using a systematic approach based on a sensitivity analysis and a calibration procedure, depending on the experimental data set considered. For all models, parameters with the same physical meaning have been set at the same value considering that their values reflect the behaviour of the microbial culture. Thus, their values have to be independent of the mathematical structure considered. The general strategy was, firstly, to calibrate the models for an accurate description of the dynamics of

ammonia consumption and nitrite accumulation. Thereafter, the most influencing parameters for NO and N_2O production were automatically calibrated. Depending on the data set, different set of parameters were identified. This variability in estimated parameter values has two main explanations:

The experimental data set does not always involve the same measurements, which implies that the focus of the calibration may differ. In addition, the range of operating conditions can be different from one set to another one, and can lead to identifiability problems for the most influencing parameters or impact the set of parameter values identified.

The model structure does not accurately describe biological mechanisms such as the contribution of both NN and ND pathways on the N_2O production or the dynamic response of the enzymatic pool to changing environmental conditions.

The calibration of these single pathway models on continuous long-term data sets collected from four different biological processes has illustrated this variability of parameter values. Indeed, none of the models were able to describe with a unique set of parameter values the data obtained in systems with high and low nitrite concentrations. A significant calibration effort has been necessary for each system, leading in some cases to extreme and controversial values for parameters. On the other hand, all the collected N_2O data has been described by at least one (or several) model(s) considered in this study. Concerning the two different model concepts for N_2O production by AOB, the NN pathway model was able to describe most of the data except those which were obtained from a system with transient high accumulation of nitrite. The models based on the ND pathway were able to fit most of the data but needed a significant and sometimes unrealistic adjustment of key parameters (η_{AOB}) for systems with low nitrite accumulation. In these works the calibration performed with these single pathway models was focused especially on the N_2O emissions but not on NO measurements which probably also leads to uncertainties.

Using experimental data obtained with the SBR, these models had been subsequently confronted with both NO and N_2O emissions obtained under contrasted operating conditions. The ND pathway models were able to predict the increase of the N_2O-EF with the increase of the HNO_2 concentration which was not possible with the NN model. On the other hand, ND models showed an inappropriate NO tendency whereas the NN pathway model allowed a

sastisfying NO prediction. These results suggested that NO emissions were related mostly to the contribution of the NN pathway in comparison to the contribution of the ND pathway. On the other hand, it was suspected that the ND pathway was responsible for N_2O emissions, with an insignificant contribution of the NN pathway to the overall N_2O emissions in our conditions. These assumptions have been investigated using the variation of the NO/N_2O ratio with changing environmental conditions.

4 NO/N_2O ratio and regulation of AOB N_2O production pathways

The variation of the NO/N_2O ratio during nitritation, in relation with operating conditions, has been investigated. A possible relation between this ratio and the regulation between NO and N_2O production pathways has been revealed. The NO/N_2O ratio showed a clear decreasing trend with increasing HNO_2 concentration both during the dynamic of ammonia oxidation in batch experiments or considering all SBR cycles. During the dynamic of nitritation in batch, the NO/N_2O ratio decreased from 0.29 gN-NO/gN-N_2O to 0.02 gN-NO/gN-N_2O with an increase of nitrite in the bulk. Considering NO and N_2O emission factors of SBR cycles, the maximal NO-EF/N_2O-EF value (around 0.20 gN-NO/gN-N_2O) was observed for the lowest HNO_2 concentrations and a very low value (around 0.002 gN-NO/gN-N_2O) was obtained for the highest HNO_2 concentrations. In contrast, its variation with DO was different depending on operating conditions. Indeed, the highest values of the NO-EF/N_2O-EF ratio were obtained for cycles with a low level of HNO_2 but its variation was poorly correlated with the DO. In contrast, very low ratios were obtained for low DO and high nitrite levels. As a result, the variation of the NO-EF/N_2O-EF ratio appeared to be related to the contributions of the different N_2O production pathways. The decrease of this ratio reflects the increase of the ND pathway contribution to N_2O emissions with the increase of the HNO_2 concentration exacerbated at a low DO concentration.The contribution of the NN pathway is likely to be higher for cycles with a high NO/N_2O ratio associated to a low HNO_2 accumulation. These experimental observations have been confronted again to N_2O models based on a single pathway and none of them were able to predict the variation of NO/N_2O ratios observed. Both NN and ND models predicted a constant NO/N_2O ratio due to their mathematical structure.

Therefore, a new two-pathway N_2O model was proposed in this work. This model was constructed considering both NN and ND pathways and has been confronted to experimental

data as well as to the models based on a single pathway. These confrontations indicate that the two-pathway model combines the predictive capacities of ND models for N_2O and NN model for NO. In addition, the simulations of the NO/N_2O variations with this new model were in agreement with our experimental data obtained during the dynamic of ammonia oxidation or considering the overall variation of this ratio within all SBR cycles. The two-pathway model was able to catch the significant variations of the NO/N_2O ratio obtained with various operating conditions. This capacity is based on the assumption that NO emissions are mainly related to the NN pathway whereas N_2O is produced by both NN and ND pathway in the studied system. Indeed, the maximal NO/N_2O ratio is predicted when the N_2O is mainly produced by the NN pathway and vice versa. This variation of the NO/N_2O ratio is consequently related to a variation of the contribution of each pathway in the overall N_2O production confirming initial assumptions. Finally, the contribution of each pathway in the N_2O production predicted by the two-pathway model was in agreement with several recent works based on isotopic methods.

5 Perspectives

5.1 Validation of the two-pathway model

The new N_2O model presented in this thesis, based on the two main AOB N_2O production pathways, has been developed with the help of experimental data obtained in this study. These data allowed exploring an interesting range of operating conditions such as HNO_2 or DO concentrations. However the model has to be evaluated with other experimental data in order to explore its predictive capacity and extend its validity. Indeed, all experimental data presented in this work has been obtained under high transient nitrite accumulation. It would be thus interesting to analyze the capacity of the model to predict N_2O emissions for systems with little or no nitrite accumulation. In such conditions the contribution of the NN pathway is expected to be significant. These kinds of conditions are generally observed in municipal wastewater treatment systems, and, thus the model should also be confronted to N_2O emissions of treatment systems with daily variations of the influent composition. The exploration of such contrasted conditions could also be coupled to isotopic methods in order to quantify with accuracy and quantify the contribution of each AOB pathway involved in the N_2O production, thus improving the validity of the model for different systems and different

environmental conditions. Obviously this model should also be compared more in detail to the two-pathway model recently proposed by (Ni et al., 2014). More work is necessary to evaluate if the description of internal electron transport would extend the predictive capabilities and facilitate the calibration of multiple pathway models.

5.2 Potential openings of experimental and modeling findings

In this thesis the measurement of both NO and N_2O emissions highlighted the AOB N_2O production pathway regulation through the NO/N_2O ratio with the change of operating conditions. However, this new method to track N_2O production pathways is not a quantifying method and is only supported by the confrontation to the two-pathway model. Thus, it appears necessary to confirm its validity with the help of isotopic techniques as from now, the measurement of site preference is the only way to quantify the contribution of each N_2O pathway. Once validated, the measurement of the NO/N_2O ratio could constitute an interesting alternative, easier to implement than isotopic techniques, to evaluate pathways involved in N_2O emissions observed in either lab or full-scale systems. This identification of N_2O pathways could help the practitioners to analyze the origin of the emissions and reduce the climate footprint of these treatment systems. In this context, the use of a new validated N_2O model would also be useful for life cycle assessment (LCA) and benchmark simulations. Providing an accurate prediction of N_2O emissions in relation to operational conditions for different systems should improve the quality of the LCA for the comparison between contrasted treatment scenarios.

References

Ahn, J.H., Kim, S., Park, H., Rahm, B., Pagilla, K., Chandran, K., 2010. N2O emissions from activated sludge processes, 2008-2009: results of a national monitoring survey in the United States. Environ. Sci. Technol. 44, 4505–4511. doi:10.1021/es903845y

Ahn, J.H., Kwan, T., Chandran, K., 2011. Comparison of Partial and Full Nitrification Processes Applied for Treating High-Strength Nitrogen Wastewaters: Microbial Ecology through Nitrous Oxide Production. Environ. Sci. Technol. 45, 2734–2740. doi:10.1021/es103534g

Anderson, I.C., Levine, J.S., 1986. Relative Rates of Nitric Oxide and Nitrous Oxide Production by Nitrifiers, Denitrifiers, and Nitrate Respirers. Appl. Environ. Microbiol. 51, 938–945.

Anderson, I.C., Poth, M., Homstead, J., Burdige, D., 1993. A comparison of NO and N2O production by the autotrophic nitrifier Nitrosomonas europaea and the heterotrophic nitrifier Alcaligenes faecalis. Appl. Environ. Microbiol. 59, 3525–3533.

Anthonisen, A.C., Loehr, R.C., Prakasam, T.B.S., Srinath, E.G., 1976. Inhibition of Nitrification by Ammonia and Nitrous Acid. J. Water Pollut. Control Fed. 48, 835–852. doi:10.2307/25038971

Beaumont, H.J.E., Lens, S.I., Reijnders, W.N.M., Westerhoff, H.V., Van Spanning, R.J.M., 2004a. Expression of nitrite reductase in Nitrosomonas europaea involves NsrR, a novel nitrite-sensitive transcription repressor. Mol. Microbiol. 54, 148–158. doi:10.1111/j.1365-2958.2004.04248.x

Beaumont, H.J.E., Schooten, B. van, Lens, S.I., Westerhoff, H.V., Spanning, R.J.M. van, 2004b. Nitrosomonas europaea expresses a Nitric Oxide Reductase during Nitrification. J. Bacteriol. 186, 4417–4421. doi:10.1128/JB.186.13.4417-4421.2004

Blanco, G., Gerlagh, R., Suh, S., Barrett, J., de Coninck, H., Diaz Morejon, C.F., Mathur, R., Nakicenovic, N., Ofosu Ahenkora, A., Pan, J., Pathak, H., Rice, J., Richels, R., Smith, S.J., Stern, D.I., Toth, F.L., Zhou, P., 2014. Drivers, Trends and Mitigation, in: Climate Change 2014: Mitigation of Climate Change. Contribution of Working Group III to the Fifth Assessment Report of the Intergovernmental Panel on Climate Change [Edenhofer, O., R. Pichs-Madruga, Y. Sokona, E. Farahani, S. Kadner, K. Seyboth, A. Adler, I. Baum, S. Brunner, P. Eickemeier, B. Kriemann, J. Savolainen, S. Schlömer, C. von Stechow, T. Zwickel and J.C. Minx (eds.)]. Cambridge University Press, Cambridge, United Kingdom and New York, NY, USA.

Bock, E., Schmidt, I., Stüven, R., Zart, D., 1995. Nitrogen loss caused by denitrifying Nitrosomonas cells using ammonium or hydrogen as electron donors and nitrite as electron acceptor. Arch. Microbiol. 163, 16–20. doi:10.1007/BF00262198

Castro-Barros, C.M., Daelman, M.R.J., Mampaey, K.E., van Loosdrecht, M.C.M., Volcke, E.I.P., 2015. Effect of aeration regime on N2O emission from partial nitritation-anammox in a full-scale granular sludge reactor. Water Res. 68, 793–803. doi:10.1016/j.watres.2014.10.056

Chain, P., Lamerdin, J., Larimer, F., Regala, W., Lao, V., Land, M., Hauser, L., Hooper, A., Klotz, M., Norton, J., Sayavedra-Soto, L., Arciero, D., Hommes, N., Whittaker, M., Arp, D., 2003. Complete Genome Sequence of the Ammonia-Oxidizing Bacterium and Obligate Chemolithoautotroph Nitrosomonas europaea. J. Bacteriol. 185, 2759–2773. doi:10.1128/JB.185.9.2759-2773.2003

Chandran, K., Stein, L.Y., Klotz, M.G., van Loosdrecht, M.C.M., 2011. Nitrous oxide production by lithotrophic ammonia-oxidizing bacteria and implications for

engineered nitrogen-removal systems. Biochem. Soc. Trans. 39, 1832–1837. doi:10.1042/BST20110717

Colliver, B.B., Stephenson, T., 2000. Production of nitrogen oxide and dinitrogen oxide by autotrophic nitrifiers. Biotechnol. Adv. 18, 219–232.

Crutzen, P.J., 1979. The Role of NO and NO2 in the Chemistry of the Troposphere and Stratosphere. Annu. Rev. Earth Planet. Sci. 7, 443–472. doi:10.1146/annurev.ea.07.050179.002303

Czepiel, P., Crill, P., Harriss, R., 1995. Nitrous Oxide Emissions from Municipal Wastewater Treatment. Environ. Sci. Technol. 29, 2352–2356. doi:10.1021/es00009a030

Daelman, M.R.J., van Voorthuizen, E.M., van Dongen, L.G.J.M., Volcke, E.I.P., van Loosdrecht, M.C.M., 2013. Methane and nitrous oxide emissions from municipal wastewater treatment - results from a long-term study. Water Sci. Technol. J. Int. Assoc. Water Pollut. Res. 67, 2350–2355. doi:10.2166/wst.2013.109

Daelman, M.R.J., van Voorthuizen, E.M., van Dongen, U.G.J.M., Volcke, E.I.., van Loosdrecht, M.C.M., 2013. Full-scale evaluation of process conditions leading to the emission of nitrous oxide from municipal wastewater treatment plants, in: In: Proceedings WEF/IWA Nutrient Removal and Recovery 2013: Trends in Resource Recovery and Use.

Desloover, J., De Clippeleir, H., Boeckx, P., Du Laing, G., Colsen, J., Verstraete, W., Vlaeminck, S.E., 2011. Floc-based sequential partial nitritation and anammox at full scale with contrasting N2O emissions. Water Res. 45, 2811–2821. doi:10.1016/j.watres.2011.02.028

Fischedick, M., Roy, J., Abdel-Aziz, A., Acquaye, A., Allwood, J.M., Ceron, J.-P., Geng, Y., Kheshgi, H., Lanza, A., Perczyk, D., Price, L., Santalla, E., Sheinbaum, C., Tanaka, K., 2014. Industry, in: Climate Change 2014: Mitigation of Climate Change. Contribution of Working Group III to the Fifth Assessment Report of the Intergovernmental Panel on Climate Change [Edenhofer, O., R. Pichs-Madruga, Y. Sokona, E. Farahani, S. Kadner, K. Seyboth, A. Adler, I. Baum, S. Brunner, P. Eickemeier, B. Kriemann, J. Savolainen, S. Schlömer, C. von Stechow, T. Zwickel and J.C. Minx (eds.)]. Cambridge University Press, Cambridge, United Kingdom and New York, NY, USA.

Foley, J., de Haas, D., Yuan, Z., Lant, P., 2010. Nitrous oxide generation in full-scale biological nutrient removal wastewater treatment plants. Water Res. 44, 831–844. doi:10.1016/j.watres.2009.10.033

Goreau, T.J., Kaplan, W.A., Wofsy, S.C., McElroy, M.B., Valois, F.W., Watson, S.W., 1980. Production of NO2- and N2O by Nitrifying Bacteria at Reduced Concentrations of Oxygen. Appl. Environ. Microbiol. 40, 526–532.

Guo, L., Lamaire-Chad, C., Bellandi, G., Daelman, M., Amerlinck, Y., Maere, T., Nous, J., Flameling, T., Weijers, S., van Loosdrecht, M.C.M., Volcke, E.I.P., Nopens, I., Vanrolleghem, P.A., 2013a. High-Frequency Field Measurement of Nitrous oxide (N2O) Gas Emissions and Influencing Factors at WWTPs under Dry and Wet Weather Conditions. Proc. WEFIWA Nutr. Remov. Recovery 2013 Trends Resour. Recovery Use Vancouver, British Columbia, Canada, July 28-31.

Guo, L., Vanrolleghem, P.A., 2014. Full-scale simulation of N2O emissions with ASMG2d and elucidation of its different production and emission sources in nitrogen (N) and phosphorus (P) removed systems. Rev.

Guo, L., Vanrolleghem, P.A., 2013b. Calibration and validation of an activated sludge model for greenhouse gases no. 1 (ASMG1): prediction of temperature-dependent N2O emission dynamics. Bioprocess Biosyst. Eng. doi:10.1007/s00449-013-0978-3

Hauduc, H., Rieger, L., Takács, I., Héduit, A., Vanrolleghem, P.A., Gillot, S., 2010. A systematic approach for model verification: application on seven published activated sludge models. Water Sci. Technol. 61, 825. doi:10.2166/wst.2010.898

Henze, M., 2000. Activated Sludge Models: ASM1, ASM2, ASM2d and ASM3. IWA Publishing.

Hiatt, W.C., Grady, C.P.L., 2008. An Updated Process Model for Carbon Oxidation, Nitrification, and Denitrification. Water Environ. Res. 80, 2145–2156. doi:10.2175/106143008X304776

Hooper, A.B., Terry, K.R., 1979. Hydroxylamine oxidoreductase of Nitrosomonas. Production of nitric oxide from hydroxylamine. Biochim. Biophys. Acta 571, 12–20.

Hooper, A.B., Vannelli, T., Bergmann, D.J., Arciero, D.M., 1997. Enzymology of the oxidation of ammonia to nitrite by bacteria. Antonie Van Leeuwenhoek 71, 59–67. doi:10.1023/A:1000133919203

Houweling, D., Wunderlin, P., Dold, P., Bye, C., Joss, A., Siegrist, H., 2011. N2O emissions: modeling the effect of process configuration and diurnal loading patterns. Water Environ. Res. Res. Publ. Water Environ. Fed. 83, 2131–2139.

Juliette, L.Y., Hyman, M.R., Arp, D.J., 1993. Inhibition of Ammonia Oxidation in Nitrosomonas europaea by Sulfur Compounds: Thioethers Are Oxidized to Sulfoxides by Ammonia Monooxygenase. Appl. Environ. Microbiol. 59, 3718–3727.

Kampschreur, M.J., Tan, N.C.G., Kleerebezem, R., Picioreanu, C., Jetten, M.S.M., Van Loosdrecht, M.C.M., 2008. Effect of dynamic process conditions on nitrogen oxides emission from a nitrifying culture. Environ. Sci. Technol. 42, 429–435.

Kampschreur, M.J., Temmink, H., Kleerebezem, R., Jetten, M.S.M., Van Loosdrecht, M.C.M., 2009. Nitrous oxide emission during wastewater treatment. Water Res. 43, 4093–4103. doi:10.1016/j.watres.2009.03.001

Kampschreur, M.J., van der Star, W.R.L., Wielders, H.A., Mulder, J.W., Jetten, M.S.M., van Loosdrecht, M.C.M., 2008. Dynamics of nitric oxide and nitrous oxide emission during full-scale reject water treatment. Water Res. 42, 812–826. doi:10.1016/j.watres.2007.08.022

Kester, R.A., De Boer, W., Laanbroek, H.J., 1997. Production of NO and N(inf2)O by Pure Cultures of Nitrifying and Denitrifying Bacteria during Changes in Aeration. Appl. Environ. Microbiol. 63, 3872–3877.

Kim, S.-W., Miyahara, M., Fushinobu, S., Wakagi, T., Shoun, H., 2010. Nitrous oxide emission from nitrifying activated sludge dependent on denitrification by ammonia-oxidizing bacteria. Bioresour. Technol. 101, 3958–3963. doi:10.1016/j.biortech.2010.01.030

Krey, V., Masera, O., Blanford, G., Bruckner, T., Cooke, R., Fisher-Vanden, K., Haberl, H., Hertwich, E., Kriegler, E., Müller, D.B., Paltsev, S., Price, L., Schlömer, S., Ürge-Vorsatz, D., van Vuuren, D.P., Zwickel, T., 2014. Annex II: Metrics & Methodology, in: Climate Change 2014: Mitigation of Climate Change. Contribution of Working Group III to the Fifth Assessment Report of the Intergovernmental Panel on Climate Change [Edenhofer, O., R. Pichs-Madruga, Y. Sokona, E. Farahani, S. Kadner, K. Seyboth, A. Adler, I. Baum, S. Brunner, P. Eickemeier, B. Kriemann, J. Savolainen, S. Schlömer, C. von Stechow, T. Zwickel and J.C. Minx (eds.)]. Cambridge University Press, Cambridge, United Kingdom and New York, NY, USA.

Law, Y., Lant, P., Yuan, Z., 2013. The confounding effect of nitrite on N2O production by an enriched ammonia-oxidizing culture. Environ. Sci. Technol. 47, 7186–7194. doi:10.1021/es4009689

Law, Y., Ni, B.-J., Lant, P., Yuan, Z., 2012a. N2O production rate of an enriched ammonia-oxidising bacteria culture exponentially correlates to its ammonia oxidation rate. Water Res. 46, 3409–3419. doi:10.1016/j.watres.2012.03.043

Law, Y., Ye, L., Pan, Y., Yuan, Z., 2012b. Nitrous oxide emissions from wastewater treatment processes. Philos. Trans. R. Soc. B Biol. Sci. 367, 1265–1277. doi:10.1098/rstb.2011.0317

Lemaire, R., Chauzy, J., Veuillet, F., DiMassimo, R., Sorensen, K., Deleris, S., 2011a. Advanced Control System to Reduce N2O Emission and Improve Performance of an SBR Treating N-Rich Effluent Via Nitrite Pathway. Proc. Water Environ. Fed. 2011, 6480–6493. doi:10.2175/193864711802766399

Lemaire, R., Chauzy, J., Veuillet, F., DiMassimo, R., Sorensen, K., Deleris, S., 2011b. Advanced control system to treat ammonia-rich effluent and reduce N2O emission by using an SBR operating via nitrite pathway. Proc. 84th Annu. Water Environ. Fed. Tech. Expo. Conf. CD-ROM Los Angeles, California, Oct 15-19; Water Environment Federation: Alexandria, Virginia.

Mampaey, K.E., Beuckels, B., Kampschreur, M.J., Kleerebezem, R., van Loosdrecht, M.C.M., Volcke, E.I.P., 2013. Modelling nitrous and nitric oxide emissions by autotrophic ammonia-oxidizing bacteria. Environ. Technol. 34, 1555–1566.

Ni, B.-J., Peng, L., Law, Y., Guo, J., Yuan, Z., 2014. Modeling of nitrous oxide production by autotrophic ammonia-oxidizing bacteria with multiple production pathways. Environ. Sci. Technol. 48, 3916–3924. doi:10.1021/es405592h

Ni, B.-J., Ruscalleda, M., Pellicer-Nàcher, C., Smets, B.F., 2011. Modeling nitrous oxide production during biological nitrogen removal via nitrification and denitrification: extensions to the general ASM models. Environ. Sci. Technol. 45, 7768–7776. doi:10.1021/es201489n

Ni, B.-J., Ye, L., Law, Y., Byers, C., Yuan, Z., 2013b. Mathematical Modeling of Nitrous Oxide (N2O) Emissions from Full-Scale Wastewater Treatment Plants. Environ. Sci. Technol. 47, 7795–7803. doi:10.1021/es4005398

Ni, B.-J., Yuan, Z., Chandran, K., Vanrolleghem, P.A., Murthy, S., 2013a. Evaluating four mathematical models for nitrous oxide production by autotrophic ammonia-oxidizing bacteria. Biotechnol. Bioeng. 110, 153–163. doi:10.1002/bit.24620

NIST Chemistry WebBook [WWW Document], 2005. URL http://webbook.nist.gov/chemistry/

Pan, Y., Ni, B.-J., Yuan, Z., 2013. Modeling Electron Competition among Nitrogen Oxides Reduction and N2O Accumulation in Denitrification. Environ. Sci. Technol. 47, 11083–11091. doi:10.1021/es402348n

Peng, L., Ni, B.-J., Erler, D., Ye, L., Yuan, Z., 2014. The effect of dissolved oxygen on N2O production by ammonia-oxidizing bacteria in an enriched nitrifying sludge. Water Res. 66, 12–21. doi:10.1016/j.watres.2014.08.009

Peng, L., Ni, B.-J., Ye, L., Yuan, Z., 2015a. The combined effect of dissolved oxygen and nitrite on N2O production by ammonia oxidizing bacteria in an enriched nitrifying sludge. Water Res. 73, 29–36. doi:10.1016/j.watres.2015.01.021

Peng, L., Ni, B.-J., Ye, L., Yuan, Z., 2015b. Selection of mathematical models for N2O production by ammonia oxidizing bacteria under varying dissolved oxygen and nitrite concentrations. Chem. Eng. J. 281, 661–668. doi:10.1016/j.cej.2015.07.015

Pijuan, M., Torà, J., Rodríguez-Caballero, A., César, E., Carrera, J., Pérez, J., 2014. Effect of process parameters and operational mode on nitrous oxide emissions from a nitritation reactor treating reject wastewater. Water Res. 49, 23–33. doi:10.1016/j.watres.2013.11.009

Pocquet, M., Queinnec, I., Spérandio, M., 2013. Adaptation and identification of models for nitrous oxide (N2O) production by autotrophic nitrite reduction. Proc. 11th IWA Conf. Instrum. Control Autom. ICA2013 Narbonne, France, September 18-20.

Poth, M., Focht, D.D., 1985. 15N Kinetic Analysis of N2O Production by Nitrosomonas europaea: an Examination of Nitrifier Denitrification. Appl. Environ. Microbiol. 49, 1134–1141.

Poughon, L., Dussap, C.-G., Gros, J.-B., 2001. Energy model and metabolic flux analysis for autotrophic nitrifiers. Biotechnol. Bioeng. 72, 416–433. doi:10.1002/1097-0290(20000220)72:4<416::AID-BIT1004>3.0.CO;2-D

Rathnayake, R.M.L.D., Song, Y., Tumendelger, A., Oshiki, M., Ishii, S., Satoh, H., Toyoda, S., Yoshida, N., Okabe, S., 2013. Source identification of nitrous oxide on autotrophic partial nitrification in a granular sludge reactor. Water Res. 47, 7078–7086. doi:10.1016/j.watres.2013.07.055

Reichert, P., 1998. User manual, computer program for the identification and simulation of aquatic systems.

Ritchie, G.A.F., Nicholas, D.J.D., 1972. Identification of the sources of nitrous oxide produced by oxidative and reductive processes in Nitrosomonas europaea. Biochem. J. 126, 1181–1191.

Rodriguez-Caballero, A., Pijuan, M., 2013. N2O and NO emissions from a partial nitrification sequencing batch reactor: exploring dynamics, sources and minimization mechanisms. Water Res. 47, 3131–3140. doi:10.1016/j.watres.2013.03.019

Schlegel, H.G., Bowien, B., 1989. Autotrophic Bacteria. Springer-Verlag.

Schulthess, R.V., Gujer, W., 1996. Release of nitrous oxide (N2O) from denitrifying activated sludge: Verification and application of a mathematical model. Water Res. 30, 521–530. doi:10.1016/0043-1354(95)00204-9

Shaw, L.J., Nicol, G.W., Smith, Z., Fear, J., Prosser, J.I., Baggs, E.M., 2006. Nitrosospira spp. can produce nitrous oxide via a nitrifier denitrification pathway. Environ. Microbiol. 8, 214–222. doi:10.1111/j.1462-2920.2005.00882.x

Shiskowski, D.M., Mavinic, D.S., 2006. The influence of nitrite and pH (nitrous acid) on aerobic-phase, autotrophic N2O generation in a wastewater treatment bioreactor. J. Environ. Eng. Sci. 5, 273–283. doi:10.1139/s05-034

Simon, J., Klotz, M.G., 2013. Diversity and evolution of bioenergetic systems involved in microbial nitrogen compound transformations. Biochim. Biophys. Acta BBA - Bioenerg., The evolutionary aspects of bioenergetic systems 1827, 114–135. doi:10.1016/j.bbabio.2012.07.005

Spérandio, M., Paul, E., 1997. Determination of carbon dioxide evolution rate using on-line gas analysis during dynamic biodegradation experiments. Biotechnol. Bioeng. 53, 243–252. doi:10.1002/(SICI)1097-0290(19970205)53:3<243::AID-BIT1>3.0.CO;2-I

Spérandio, M., Pocquet, M., Guo, L., Ni, B.-J., Vanrolleghem, P.A., Yuan, Z., 2015. Calibration of five candidate nitrous oxide production models with four continuous long-term wastewater treatment process data series. Bioprocess Biosyst. Eng.

Stein, L.Y., 2011. Surveying N2O-producing pathways in bacteria. Methods Enzymol. 486, 131–152. doi:10.1016/B978-0-12-381294-0.00006-7

Stein, L.Y., Arp, D.J., 1998. Loss of Ammonia Monooxygenase Activity in Nitrosomonas europaea upon Exposure to Nitrite. Appl. Environ. Microbiol. 64, 4098–4102.

Stüven, R., Vollmer, M., Bock, E., 1992. The impact of organic matter on nitric oxide formation by <i>Nitrosomonas europaea</i> Arch. Microbiol. 158, 439–443. doi:10.1007/BF00276306

Sümer, E., Weiske, A., Benckiser, G., Ottow, J.C.G., 1995. Influence of environmental conditions on the amount of N2O released from activated sludge in a domestic waste water treatment plant. Experientia 51, 419–422. doi:10.1007/BF01928908

Sutka, R.L., Ostrom, N.E., Ostrom, P.H., Breznak, J.A., Gandhi, H., Pitt, A.J., Li, F., 2006. Distinguishing Nitrous Oxide Production from Nitrification and Denitrification on the Basis of Isotopomer Abundances. Appl. Environ. Microbiol. 72, 638–644. doi:10.1128/AEM.72.1.638-644.2006

Suzuki, I., Dular, U., Kwok, S.C., 1974. Ammonia or Ammonium Ion as Substrate for Oxidation by Nitrosomonas europaea Cells and Extracts. J. Bacteriol. 120, 556–558.

Tallec, G., Garnier, J., Billen, G., Gousailles, M., 2006. Nitrous oxide emissions from secondary activated sludge in nitrifying conditions of urban wastewater treatment plants: Effect of oxygenation level. Water Res. 40, 2972–2980. doi:10.1016/j.watres.2006.05.037

Terada, A., Sugawara, S., Yamamoto, T., Zhou, S., Koba, K., Hosomi, M., 2013. Physiological characteristics of predominant ammonia-oxidizing bacteria enriched from bioreactors with different influent supply regimes. Biochem. Eng. J. 79, 153–161. doi:10.1016/j.bej.2013.07.012

Toyoda, S., Suzuki, Y., Hattori, S., Yamada, K., Fujii, A., Yoshida, N., Kouno, R., Murayama, K., Shiomi, H., 2011. Isotopomer analysis of production and consumption mechanisms of N2O and CH4 in an advanced wastewater treatment system. Environ. Sci. Technol. 45, 917–922. doi:10.1021/es102985u

Vadivelu, V.M., Keller, J., Yuan, Z., 2007. Free ammonia and free nitrous acid inhibition on the anabolic and catabolic processes of Nitrosomonas and Nitrobacter. Water Sci. Technol. J. Int. Assoc. Water Pollut. Res. 56, 89–97. doi:10.2166/wst.2007.612

Vadivelu, V.M., Keller, J., Yuan, Z., 2006. Effect of free ammonia and free nitrous acid concentration on the anabolic and catabolic processes of an enriched Nitrosomonas culture. Biotechnol. Bioeng. 95, 830–839. doi:10.1002/bit.21018

Vanhooren, H., Meirlaen, J., Amerlinck, Y., Claeys, F., Vangheluwe, H., Vanrolleghem, P.A., 2003. WEST: modelling biological wastewater treatment. [WWW Document]. URL http://www.iwaponline.com/jh/005/jh0050027.htm (accessed 11.29.14).

Wrage, N., Velthof, G.., van Beusichem, M.., Oenema, O., 2001. Role of nitrifier denitrification in the production of nitrous oxide. Soil Biol. Biochem. 33, 1723–1732. doi:10.1016/S0038-0717(01)00096-7

Wunderlin, P., Lehmann, M.F., Siegrist, H., Tuzson, B., Joss, A., Emmenegger, L., Mohn, J., 2013. Isotope signatures of N2O in a mixed microbial population system: constraints on N2O producing pathways in wastewater treatment. Environ. Sci. Technol. 47, 1339–1348. doi:10.1021/es303174x

Wunderlin, P., Mohn, J., Joss, A., Emmenegger, L., Siegrist, H., 2012. Mechanisms of N2O production in biological wastewater treatment under nitrifying and denitrifying conditions. Water Res. 46, 1027–37.

Ye, L., Ni, B.-J., Law, Y., Byers, C., Yuan, Z., 2014. A novel methodology to quantify nitrous oxide emissions from full-scale wastewater treatment systems with surface aerators. Water Res. 48, 257–268. doi:10.1016/j.watres.2013.09.037

Yu, R., Chandran, K., 2010. Strategies of Nitrosomonas europaea 19718 to counter low dissolved oxygen and high nitrite concentrations. BMC Microbiol. 10, 70. doi:10.1186/1471-2180-10-70

Yu, R., Kampschreur, M.J., Loosdrecht, M.C.M. van, Chandran, K., 2010. Mechanisms and Specific Directionality of Autotrophic Nitrous Oxide and Nitric Oxide Generation during Transient Anoxia. Environ. Sci. Technol. 44, 1313–1319. doi:10.1021/es902794a

Zacharia, I.G., Deen, W.M., 2005. Diffusivity and solubility of nitric oxide in water and saline. Ann. Biomed. Eng. 33, 214–222.

Appendix

Appendix A

Appendix A. Automatic control of aerobic and anoxic periods of the SBR

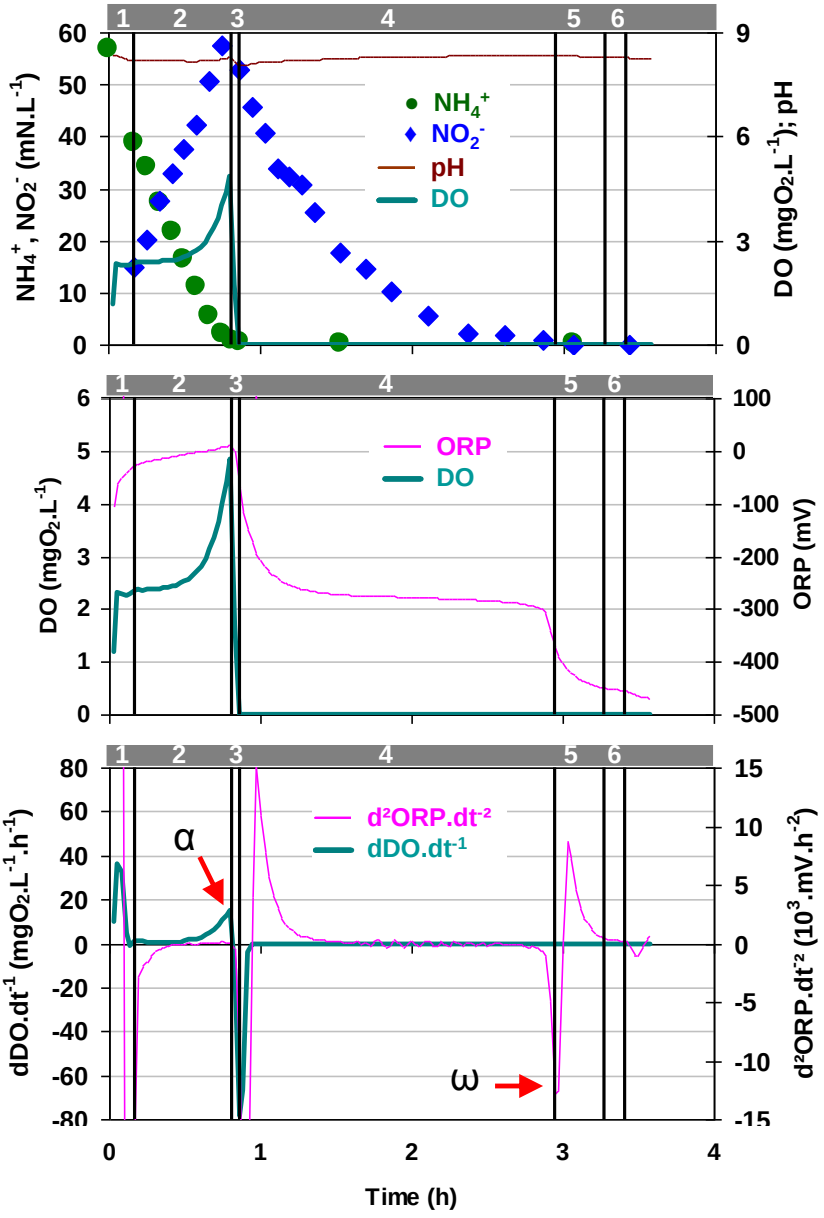

Phase	Description	Aerated	Length (minutes)
1	Ammonia feeding	YES	10
2	Nitrification	YES	Controlled with $dDO.dt^{-1}$
3	COD feeding	NO	5
4	Denitrification	NO	Controlled with $d^2ORP.dt^{-2}$
5	Settling	NO	20
6	Withdrawal	NO	8

Ammonium is fed during the first 10 minutes (period 1) of the aerobic period. The nitrification takes place as soon as period 1 begins. Aeration is maintained (period 2) until the depletion of ammonium (49 minutes later). All the nitrified ammonium was converted to nitrite. Nitrite Oxidising Bacteria (NOB) were outcompeted due to simultaneous effect of ammonium inhibition, substrate privation (aeration is stopped after ammonia depletion) and high temperature (growth rate of ammonium oxidizing bacteria becoming higher than those of NOB).

Aeration is interrupted from periods 3 to 6 maintaining anoxic condition. Period 3 corresponds to the introduction of the secondary solution (organic carbon source) into the reactor. Then, nitrite was removed in 129 minutes by heterotrophic denitrification (periods 3 and 4). After the exhaustion of nitrite, a settling period (period 5) of 20 minutes was followed by a last decanting period (period 6) of 8 minutes for treated supernatant withdrawal.

Evolution of DO, ORP, the first derivative of DO and the second derivative of ORP are presented below. DO increases rapidly as soon as the cycle begins until reach 2.3 $mgO_2.L^{-1}$. During 20 minutes, the consumption of oxygen by AOB for the oxidation of ammonium to nitrite remains constant as indicated by the first derivative of DO which is constant and close to 0. After 30 minutes of nitrification, the nitrification rate decreases, decreasing the rate of oxygen consumption which leads to an augmentation of DO, therefore, an augmentation of the rate of DO accumulation in the reactor (i.e. $dDO.dt^{-1}$), until reach 4.8 $mgO_2.L^{-1}$ at the end of period 2. The COD feeding in period 3 coupled to the shutdown of aeration lead to a quick decrease of DO induced by the oxygen consumption of heterotrophic bacteria to oxidize a small part of the organic matter. After that, DO remains below the detection limit of the probe until the end of the cycle, assigning a zero value to the first derivative of DO and allowing anoxic conditions for denitrification during the period 4.

When oxygen is present in the liquid medium, the evolution of ORP is directly related to the evolution of DO. Indeed, redox systems which include ammonium, nitrite and nitrate (such as NO_3^- / NO_2^-, NO_3^- / NH_4^+ or NO_2^- / NH_4^+) have a low electroactivity, and a significant variation of these species has an insignificant impact on ORP. The logarithmic relationship between ORP and DO leads to a more pronounced effect on ORP when the DO concentration tends towards zero. That explains the dynamic of ORP observed during the cycle. When

aeration starts (period 1), ORP increases rapidly to a value close to those observed at the end of the aerobic period (end of period 2). The significant variation of DO the last 20 minutes before the end of nitrification didn't have a significant impact on ORP profile. The quick decrease of DO when the system switches to the period 3 explains the quick decrease of ORP. When the DO concentration falls below the limit of detection, the probe returns a zero value. In reality, the shape of DO concentration likely bends due to an oxygen concentration significantly below the half-saturation coefficient. As a results, the ORP profile trends to a negative slope, reflecting the decrease of DO following a line with a slope close to zero until the exhaustion of nitrite few minutes before the end of period 4. When the nitrite concentration is close to zero, ORP decreases rapidly with a slower diminution during periods 5 and 6. The bending point of this break in the slope, also visible on the second derivative of ORP, indicates indirectly the end of denitrification. Indeed, as previously underlined, couples involving nitrogen species have an insignificant impact on the variation of ORP. When nitrite and/or nitrate are depleted, sulfate-reducing bacteria will use sulfates as final electron acceptor for the carbon consumption. As a consequence, sulfates (SO_4^{2-}) are reduced to sulfides (HS^-, H_2S) which have a strong influence on ORP. Thus, the inhibitory effect of oxygen, nitrite and nitrate on the sulfate-reducing activity allows observing this bending point on the ORP curve which indicates the end of denitrification.

The automatic control system is based on these biological activities in order to detect the end of nitrification and denitrification, thus control the length of these periods. During nitrification, the exhaustion of ammonium induces an augmentation of DO in the liquid medium which leads to an augmentation of the first derivative of DO. When this rate of oxygen accumulation reaches a threshold value (noted α), the system automatically moves to the next period of the cycle, thereby detecting the end of nitrification. At the end of denitrification, the establishment of sulfate-reducing activity induces a bending point on ORP which leads to a quick decrease of the second derivative of ORP. When this acceleration reach a threshold value (noted ω), the end of denitrification is detected by the system which moves to the next period. Threshold values used for the control of the cycle presented in this example are 14 $mgO_2.L^{-1}.h^{-1}$ and -12000 $mV.h^{-2}$ for α and ω respectively. For periods automatically controlled by the system, a timeout period is applied during which the system didn't detect values higher than α and ω, making the control system not active. Indeed, perturbations can be observed on $dDO.dt^{-1}$ and $dORP.dt^{-2}$ at the beginning of nitrification and denitrification and these signals can exceed threshold values which didn't correspond to the

end of biological nitrogen removal. The fact that the sensor derivatives were used as an indicator makes the system insensitive to signal drift and calibration error. This is a very important property which reduces time for maintenance and improves the robustness.

Appendix B

Appendix B. Parameter values related to heterotrophs and gas transfert

Name	Description	Unit	Value	Source
b_{AOB}	Endogenous respiration rate for X_{AOB}	d^{-1}	0.15	(Henze, 2000)
b_H	Endogenous respiration rate for X_{OHO}	d^{-1}	0.20	(Henze, 2000)
b_{NOB}	Endogenous respiration rate for X_{NOB}	d^{-1}	0.15	(Henze, 2000)
f_{XI}	Fraction of inert biomass generated during endogenous respiration	$gX_I.gX_{Bio}^{-1}$	0.2	(Henze, 2000)
$i_{N,XI}$	Nitrogen content of inert biomass	$gN.gX_{Bio}^{-1}$	0.02	(Henze, 2000)
$K_{O2,OHO}$	Half-saturation coefficient for O_2 - Heterotrophs	$mgO_2.L^{-1}$	0.2	(Henze, 2000)
ρ_{N2O}	Partial pressure of N_2O	atm of $N\text{-}N_2O$	1.60E-07	Calculated
ρ_{NO}	Partial pressure of NO	atm of NO	5.00E-06	Calculated
$S_{O2,Max}$	Maximum oxygen concentration in the liquid medium (20°C)	$mgO_2.L^{-1}$	9.2	Empirical
D_{N2O}	Gas-liquid diffusivity coefficient of N_2O	$m^2.d^{-1}$	1.77E-09	(Schulthess and Gujer, 1996)
D_{NO}	Gas-liquid diffusivity coefficient of NO	$m^2.d^{-1}$	2.21E-09	(Zacharia and Deen, 2005)
D_{O2}	Gas-liquid diffusivity coefficient of O_2 (20°C)	$m^2.d^{-1}$	2.08E-09	Roustan
$K_{H,N2O}$	Henry's law constant for N_2O	$mgN\text{-}N_2O.L^{-1}.atm^{-1}$	172.79	Calculated with NIST value
$K_{H,NO}$	Henry's law constant for NO	$mgN\text{-}NO.L^{-1}.atm^{-1}$	26.26	NIST

Appendix C

Appendix C. Parameters of the models A, A1, B, B1, and C used in chapter IV and chapter VI

Name	Description	Unit	A	A1	B	B1	C	Source
η_{AOB}	N_2O emission factor	Dimensionless	0.86	0.38	0.15	0.13	0.05	Estimated
$\mu_{AOB,AMO}$	Maximum AOB growth rate - AMO	h^{-1}	0.216	0.216	-	-	0.216	Calculated*
$\mu_{AOB,HAO}$	Maximum AOB growth rate - HAO	h^{-1}	0.0325	0.0325	-	-	-	Calculated*
$\mu_{AOB,HAO,1}$	Maximum AOB growth rate - HAO1 (C)	h^{-1}	-	-	-	-	0.0325	Calculated*
$\mu_{AOB,HAO,2}$	Maximum AOB growth rate - HAO2 (C)	h^{-1}	-	-	-	-	0.216	Calculated*
μ_{AOB}	Maximum AOB growth rate	h^{-1}	-	-	0.0325	0.0325	-	Calculated*
$K_{HNO2,AOB}$	AOB affinity constant for HNO_2	$mgN.L^{-1}$	-	0.004	0.004	0.004	-	Estimated
$K_{NO2,AOB}$	AOB affinity constant for NO_2^-	$mgN.L^{-1}$	300	-	-	-	-	Estimated
$K_{I,NH3,AOB}$	AOB inhibition constant for NH_3	$mgN.L^{-1}$	-	16	-	16	-	(Vadivelu et al., 2006)
$K_{I,HNO2,AOB}$	AOB inhibition constant for HNO_2	$mgN.L^{-1}$	-	-	-	0.4	-	(Vadivelu et al., 2006)
$K_{NH2OH,AOB}$	AOB affinity constant for NH_2OH	$mgN.L^{-1}$	0.9	0.9	-	-	0.9	Estimated
$K_{NH3,AOB}$	AOB affinity constant for NH_3	$mgN.L^{-1}$	-	0.2	0.2	0.2	-	Estimated
$K_{NH3,AOB,den}$	AOB affinity constant for NH_3 for AOB den	$mgN.L^{-1}$	-	-	-	0.2	-	Considered similar to $K_{NH3,AOB}$
$K_{NH4,AOB}$	AOB affinity constant for NH_4^+	$mgN.L^{-1}$	2	-	-	-	2	Estimated
$K_{NO,AOB}$	AOB affinity constant for NO	$mgN.L^{-1}$	0.008	0.008	0.008	0.008	-	Estimated
$K_{O2,AOB,1}$	AOB affinity constant for O_2 - AMO	$mgO_2.L^{-1}$	1	1	-	-	1	Estimated
$K_{O2,AOB,2}$	AOB affinity constant for O_2 - HAO	$mgO_2.L^{-1}$	0.6	0.6	-	-	0.6	(Ni et al., 2013a)
$K_{O2,AOB}$	AOB affinity constant for O_2	$mgO_2.L^{-1}$	-	-	1	1	-	Estimated
$K_{O2,AOB,den}$	AOB affinity constant for O_2 for AOB den	$mgO_2.L^{-1}$	-	-	-	1	-	Considered similar to $K_{O2,AOB}$
$K_{I,O2,AOB}$	AOB inhibition constant for O_2 for AOB den	$mgO_2.L^{-1}$	2	-	-	2	-	Estimated
$i_{N,BM}$	Nitrogen content of biomass	$mgN.mgCODX^{-1}$	0.07	0.07	0.07	0.07	0.07	(Henze, 2000)
Y_{AOB}	AOB growth yield	$mgCODX.mgN^{-1}$	0.15	0.15	0.15	0.15	0.15	(Ni et al., 2013a)
$Y_{AOB,den}$	AOB growth yield for AOB denitrification	$mgCODX.mgN^{-1}$	0.15	0.15	0.15	0.15	0.15	Considered similar to Y_{AOB}
$K_{NO,AOB,nor}$	AOB affinity constant for NO	$mgN.L^{-1}$	-	-	-	-	0.008	Estimated
$K_{NO,AOB,HAO}$	AOB affinity constant for NO	$mgN.L^{-1}$	-	-	-	-	0.0003	Estimated

*Calculated using values of (Hiatt and Grady, 2008) and considering that $\mu_{AOB}=\mu_{AOB,AMO}=\mu_{AOB,HAO}$

Appendix D

Appendix D. Parameter sets for ASMN model (heterotrophs, denitrification, NOB, growth and decay). Rate values at 20 ºC.

Name	Description	Unit	SBR1	OD	SBR2	UCT
μ_{OHO}	Maximum OHO growth rate	d^{-1}	6.2	6.2	6.2	1.24
Y_{OHO}	OHO growth yield	$mgCODX.mgCOD^{-1}$	0.6	0.6	0.6	0.625
η_Y	Anoxic yield factor	Dimensionless	0.9	0.9	0.9	0.9
b_{OHO}	Decay coefficient - OHO	d^{-1}	0.41	0.41	0.41	0.42
$\eta_{g2,OHO}$	Anoxic growth factor – NO_3^- reduction	Dimensionless	0.28	0.28	0.28	0.3/0.3/0.5
$\eta_{g3,OHO}$	Anoxic growth factor – NO_2^- reduction	Dimensionless	0.16	0.16	0.16	0.3/0.3/0.5
$\eta_{g4,OHO}$	Anoxic growth factor – NO reduction	Dimensionless	0.35	0.35	0.35	0.8/0.8/0.8
$\eta_{g5,OHO}$	Anoxic growth factor – N_2O reduction	Dimensionless	0.35	0.35	0.35	0.6/0.8/0.6
K_{S1}	OHO affinity constant for COD – Aerobic growth	$mgCOD.L^{-1}$	2	20	20	20*
K_{S2}	OHO affinity constant for COD – NO_3^- reduction	$mgCOD.L^{-1}$	2	20	20	10*
K_{S3}	OHO affinity constant for COD – NO_2^- reduction	$mgCOD.L^{-1}$	2	20	20	10*
K_{S4}	OHO affinity constant for COD – NO reduction	$mgCOD.L^{-1}$	2	20	20	10*
K_{S5}	OHO affinity constant for COD – N_2O reduction	$mgCOD.L^{-1}$	2	40	40	10*
k_h	Maximum hydrolysis rate	d^{-1}	3.5	3.5	3.5	3.5
$K_{O2,OHO,1}$	OHO affinity constant for O_2 – Aerobic growth	$mgO_2.L^{-1}$	0.1	0.1	0.1	1
$K_{O2,OHO,2}$	OHO affinity constant for O_2 – NO_3^- reduction	$mgO_2.L^{-1}$	0.1	0.1	0.1	1
$K_{O2,OHO,3}$	OHO affinity constant for O_2 – NO_2^- reduction	$mgO_2.L^{-1}$	0.1	0.1	0.1	1
$K_{O2,OHO,4}$	OHO affinity constant for O_2 – NO reduction	$mgO_2.L^{-1}$	0.1	0.1	0.1	1
$K_{O2,OHO,5}$	OHO affinity constant for O_2 – N_2O reduction	$mgO_2.L^{-1}$	0.1	0.1	0.1	1
$K_{NO3,OHO}$	OHO affinity constant for NO_3^-	$mgN.L^{-1}$	0.2	0.2	0.2	4/1.5/2
$K_{NO2,OHO}$	OHO affinity constant for NO_2^-	$mgN.L^{-1}$	0.2	0.2	0.2	1/0.1/0.1
$K_{NO,OHO}$	OHO affinity constant for NO	$mgN.L^{-1}$	0.05	0.05	0.05	0.1
$K_{N2O,OHO}$	OHO affinity constant for N_2O	$mgN.L^{-1}$	0.05	0.05	0.05	0.2/0.1/0.2
$K_{I,NO,OHO,3}$	OHO inhibition constant for NO – NO_2^- reduction	$mgN.L^{-1}$	0.5	0.5	0.5	0.5
$K_{I,NO,OHO,4}$	OHO inhibition constant for NO – NO reduction	$mgN.L^{-1}$	0.3	0.3	0.3	0.3
$K_{I,NO,OHO,5}$	OHO inhibition constant for NO – N_2O reduction	$mgN.L^{-1}$	0.075	0.075	0.075	0.2
b_{AOB}	Decay coefficient - AOB	d^{-1}	0.13	0.054	0.13	0.05
μ_{NOB}	Maximum NOB growth rate	d^{-1}	-	1.4	1.4	1.03
b_{NOB}	Decay coefficient - NOB	d^{-1}	-	0.06	0.06	0.05
Y_{NOB}	NOB growth yield	$mgCODX.mgN^{-1}$	-	0.041	0.041	0.06
$K_{O2,NOB}$	NOB affinity constant for O_2	$mgO_2.L^{-1}$	-	2.2	2.2	1.0/1.2/0.5
$K_{HNO2,NOB}$	NOB affinity constant for HNO_2	$mgN.L^{-1}$	-	-	-	10^{-6}
$K_{NO2,NOB}$	NOB affinity constant for NO_2^-	$mgN.L^{-1}$		5.5	5.5	-

Appendix E

Appendix E. Other parameters used in UCT process: extension to phosphorus removal (based on ASM2).

Parameter	Description	Unit	Value
$K_{Alk,PAO}$	Saturation coefficient for alkalinity (HCO3-)	mmol HCO3-.L-1	0.1
$K_{NH4,PAO}$	Saturation coefficient for ammonia (nutrient)	mg N.L-1	0.05
$K_{P,PAO}$	Saturation coefficient for phosphorus (nutrient)	mg P.L-1	0.01
μ_{PAO} *	Maximum NOB growth rate	d-1	1.02
Y_{PAO}	Yield coefficient	mg COD.mg COD-1	0.625
Y_{PHA}	PHA requirement for XPP storage	mg COD.mg P-1	0.1
η_{YPAO}	Anoxic reduction factor for yield	-	0.9
η_{YPHA}	Anoxic reduction factor for XPP storage	-	0.9
b_{PAO} *	Maximum XPAO lysis rate	d-1	0.20
b_{PHA}*	Maximum XPHA lysis rate	d-1	0.20
b_{PP} *	Maximum XPP lysis rate	d-1	0.20
q_{PHA}^{*}	Maximum X_{PHA} storage rate	d^{-1}	3
$K_{A,PHAstor}$	Saturation coefficient for S_A in X_{PHA} storage	mg $COD.L^{-1}$	5
K_{PP}	Saturation coefficient for X_{PP}/X_{PAO} ratio in X_{PHA} storage	mg P.mg COD^{-1}	0.01
Y_{PO}	S_{PO4} released per X_{PHA} stored	mg P.mg COD^{-1}	0.2
q_{PP}^{*}	Maximum X_{PP} storage rate	d^{-1}	3
$K_{P,PPstor}$	Saturation coefficient for S_{PO4} in X_{PP} storage	mg $P.L^{-1}$	0.2
K_{IPP}	Inhibition coefficient for X_{PP}/X_{PAO} ratio in X_{PP} storage	mg P.mg COD^{-1}	0.02
K_{MAX}	Maximum limit for X_{PP}/X_{PAO} ratio in X_{PP} storage	mg P.mg COD^{-1}	0.34
$K_{O,PAO}$	Saturation coefficient for oxygen	mg $O_2.L^{-1}$	0.2
K_{PHA}	Saturation coefficient for X_{PHA}	mg $COD.L^{-1}$	2
$K_{I3NO,PAO}$	Inhibition coefficient for NO in denitrification of $NO_2^- \rightarrow NO$	mg $N.L^{-1}$	0.5
$K_{I4NO,PAO}$	Inhibition coefficient for NO in denitrification of $NO \rightarrow N_2O$	mg $N.L^{-1}$	0.3
$K_{I5NO,PAO}$	Inhibition coefficient for NO in denitrification of $N_2O \rightarrow N_2$	mg $N.L^{-1}$	0.2
$K_{N2O,PAO}$	Saturation coefficient for N_2O in denitrification of $N_2O \rightarrow N_2$	mg $N.L^{-1}$	0.2/0.1/0.2
$K_{NO,PAO}$	Saturation coefficient for NO in denitrification of $NO \rightarrow N_2O$	mg $N.L^{-1}$	0.1
$K_{NO2,PAO}$	Saturation coefficient for nitrite in denitrification of $NO_2^- \rightarrow NO$	mg $N.L^{-1}$	1/0.1/0.1
$K_{NO3,PAO}$	Saturation coefficient for nitrate in denitrification of $NO_3^- \rightarrow NO_2^-$	mg $N.L^{-1}$	4/1.5/2
η_{PAO2}	Anoxic reduction factor for denitrification of $NO_3^- \rightarrow NO_2^-$	-	0.3/0.3/0.5
η_{PAO3}	Anoxic reduction factor for denitrification of $NO_2^- \rightarrow NO$	-	0.3/0.3/0.5
η_{PAO4}	Anoxic reduction factor for denitrification of $NO \rightarrow N_2O$	-	0.8
η_{PAO5}	Anoxic reduction factor for denitrification of $N_2O \rightarrow N_2$	-	0.6

Appendix F

Appendix F. Other parameters used in UCT process: temperature corrections with Ratkowsky equation.

Parameter	Description	Unit	Value
$b_{\mu H}$	Coefficient b for Ratkowsky equation	-	0.031
$c_{\mu H}$	Coefficient c for Ratkowsky equation	-	0.3
$T_{Max,H}$	Maximum temperature for Ratkowsky equation	ºC	50
$T_{Min,H}$	Minimum temperature for Ratkowsky equation	ºC	-20
θ_{bH}	Coefficient θ for lysis rate equation with temperature dependency	-	1.072
$K_{NOx,H,b}$	Saturation coefficient for nitrate in lysis	mg $N.L^{-1}$	0.5
$K_{O,H,b}$	Saturation/Inhibition coefficient for oxygen in lysis	mg $O_2.L^{-1}$	0.2
$\eta_{H,b}$	Anoxic reduction factor for lysis	-	0.33
θ_{kh}	Coefficient θ for hydrolysis rate equation	-	1.041
K_X	Maximum saturation coefficient for X_S	mg COD.mg COD^{-1}	10
θ_{KX}	Coefficient θ for K_X temperature-dependency equation	-	0.896
$K_{NOx,Hyd}$	Saturation/Inhibition coefficient for nitrate in hydrolysis	mg $N.L^{-1}$	2
$K_{O,Hyd}$	Saturation/Inhibition coefficient for oxygen in hydrolysis	mg $O_2.L^{-1}$	0.2
η_{Hyd}	Anoxic reduction factor for hydrolysis	-	0.6
η_{fe}	Anaerobic reduction factor for hydrolysis	-	0.4
$b_{\mu NOB}$	Coefficient b for Ratkowsky equation of NOB growth	-	0.0235
$c_{\mu NOB}$	Coefficient c for Ratkowsky equation of NOB growth	-	0.1
$T_{Max,NOB}$	Maximum temperature for Ratkowsky equation of NOB growth	ºC	57
$T_{Min,NOB}$	Minimum temperature for Ratkowsky equation of NOB growth	ºC	-25
θ_{bAOB}	Coefficient θ for AOB lysis rate equation with temperature dependency	-	1.116
θ_{bNOB}	Coefficient θ for NOB lysis rate equation with temperature dependency	-	1.116
$\eta_{AOB,b}$	Anoxic reduction factor for AOB lysis	-	0.33
$\eta_{NOB,b}$	Anoxic reduction factor for NOB lysis	-	0.33
$K_{NOx,AOB,b}$	Saturation coefficient for nitrate in AOB lysis	mg N.L-1	0.5
$K_{NOx,NOB,b}$	Saturation coefficient for nitrate in NOB lysis	mg N.L-1	0.5
$K_{O,AOB,b}$	Saturation/Inhibition coefficient for oxygen in AOB lysis	mg O2.L-1	0.2
$K_{O,NOB,b}$	Saturation/Inhibition coefficient for oxygen in NOB lysis	mg O2.L-1	0.2
bμAOB	Coefficient b for Ratkowsky equation of AOB growth	-	0255
cμAOB	Coefficient c for Ratkowsky equation of AOB growth	-	0.15
$T_{Max,AOB}$	Maximum temperature for Ratkowsky equation of AOB growth	ºC	50
$T_{Min,AOB}$	Minimum temperature for Ratkowsky equation of AOB growth	ºC	-15
$b_{\mu AOB,AMO}$	Coefficient b for Ratkowsky equation of AOB growth-AMO	-	0.04
$b_{\mu AOB,HAO}$	Coefficient b for Ratkowsky equation of AOB growth-HAO	-	0.04
$c_{\mu AOB,AMO}$	Coefficient c for Ratkowsky equation of AOB growth-AMO	-	0.15
$c_{\mu AOB,HAO}$	Coefficient c for Ratkowsky equation of AOB growth-HAO	-	0.15
$T_{Max,AOB,AMO}$	Maximum temperature for Ratkowsky equation of AOB growth-AMO	ºC	50
$T_{Max,AOB,HAO}$	Maximum temperature for Ratkowsky equation of AOB growth-HAO	ºC	50
$T_{Min,AOB,AMO}$	Minimum temperature for Ratkowsky equation of AOB growth-AMO	ºC	-15
$T_{Min,AOB,HAO}$	Minimum temperature for Ratkowsky equation of AOB growth-HAO	ºC	-15
$b_{\mu PAO}$	Coefficient b for Ratkowsky equation	-	0.0256
$c_{\mu PAO}$	Coefficient c for Ratkowsky equation	-	0.17
$T_{Max,PAO}$	Maximum temperature for Ratkowsky equation	ºC	50
$T_{Min,PAO}$	Minimum temperature for Ratkowsky equation	ºC	-20
θ_{bPAO}	Coefficient θ for XPAO lysis rate equation	-	1.072
θ_{bPHA}	Coefficient θ for XPHA lysis rate equation	-	1.072
θ_{bPP}	Coefficient θ for XPP lysis rate equation	-	1.072
$K_{NOx,PAO,b}$	Saturation coefficient for nitrate in lysis	mg N.L-1	0.5
$K_{O,PAO,b}$	Saturation/Inhibition coefficient for oxygen in lysis	mg O2.L-1	0.2
$\eta_{PAO,b}$	Anoxic reduction factor for lysis	-	0.33
θ_{qPHA}	Coefficient θ for XPHA storage rate equation	-	1.041
θ_{qPP}	Coefficient θ for XPP storage rate equation	-	1.041

Appendix G

Appendix G. Other parameters used in UCT process (based on ASM2).

Parameter	Description	Unit	Value
f_{SI}	Production of S_I in hydrolysis	-	0
f_{XI}	Fraction of X_I generated in biomass lysis	-	0.1
$i_{N,SF}$	N content of S_F	mg N.mg COD^{-1}	0.03
$i_{N,SI}$	N content of S_I	mg N.mg COD^{-1}	0.01
$i_{N,XI}$	N content of X_I	mg N.mg COD^{-1}	0.02
$i_{N,XS}$	N content of X_S	mg N.mg COD^{-1}	0.04
$i_{P,BM}$	P content of biomass	mg P.mg COD^{-1}	0.02
$i_{P,SF}$	P content of S_F	mg P.mg COD^{-1}	0.01
$i_{P,SI}$	P content of S_I	mg P.mg COD^{-1}	0
$i_{P,XI}$	P content of X_I	mg P.mg COD^{-1}	0.01
$i_{P,XS}$	P content of X_S	mg P.mg COD^{-1}	0.01
$i_{TSS,BM}$	TSS to COD ratio for biomass	mg TSS/mg COD^{-1}	0.9
$i_{TSS,XI}$	TSS to COD ratio for X_I	mg TSS/mg COD^{-1}	0.75
$i_{TSS,XS}$	TSS to COD ratio for X_S	mg TSS.mg COD^{-1}	0.75
$K_{Alk,H}$	Saturation coefficient for alkalinity (HCO_3^-)	mmol $HCO_3^-.L^{-1}$	0.1
$K_{NH4,H}$	Saturation coefficient for ammonia (nutrient)	mg $N.L^{-1}$	0.05
$K_{P,H}$	Saturation coefficient for phosphorus (nutrient)	mg $P.L^{-1}$	0.01
q_{fe}^{*}	Maximum fermentation rate	d^{-1}	3
θ_{qfe}	Coefficient θ for fermentation rate equation	-	1.072
K_{fe}	Saturation coefficient for fermentation of S_F	mg $COD.L^{-1}$	20
$K_{NOx,Ferm}$	Inhibition coefficient for nitrate in fermentation	mg $N.L^{-1}$	0.1
$K_{O,Ferm}$	Inhibition coefficient for oxygen in fermentation	mg $O_2.L^{-1}$	0.2
$K_{Alk,Aut}$	Saturation coefficient for alkalinity (HCO3-)	mmol HCO3-.L-1	0.5
$K_{P,Aut}$	Saturation coefficient for phosphorus (nutrient)	mg P.L-1	0.01
k_{PRE}	P precipitation rate	[mg Fe(OH)3 ×d]-1	1
k_{RED}	P redissolution rate	d-1	0.6
$K_{Alk,RED}$	Saturation coefficient for alkalinity	mmol HCO3-.L-1	0.5

Appendix H

Appendix H. Two-pathway model of (Ni et al., 2014).

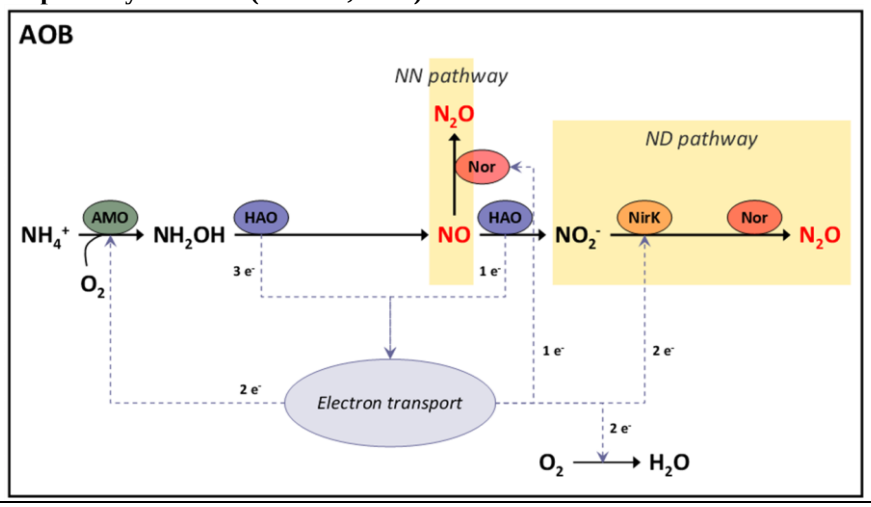

	Model Components – NN + ND Pathways (Ni et al., 2014)							
Process	S_{O_2}	S_{NH}	S_{NH_2OH}	S_{NO_2}	S_{NO}	S_{N_2O}	S_{Mox}	S_{Mred}
1	-1	-1	1				1	-1
2			-1		1		$-\frac{3}{2}$	$\frac{3}{2}$
3				1	-1		$-\frac{1}{2}$	$\frac{1}{2}$
4					-1	$\frac{1}{2}$	$\frac{1}{2}$	$-\frac{1}{2}$
5	$-\frac{1}{2}$						1	-1
6				-1		$\frac{1}{2}$	1	-1

Process	Kinetic rate expressions – NN + ND Pathways (Ni et al., 2014)
1	$r_{NH_3,ox} \cdot \frac{S_{O_2}}{S_{O_2}+K_{O_2,NH_3}} \cdot \frac{S_{NH_3}}{S_{NH_3}+K_{NH_3}} \cdot \frac{S_{Mred}}{S_{Mred}+K_{Mred,1}} \cdot X_{AOB}$
2	$r_{NH_2OH,ox} \cdot \frac{S_{NH_2OH}}{S_{NH_2OH}+K_{NH_2OH}} \cdot \frac{S_{Mox}}{S_{Mox}+K_{Mox}} \cdot X_{AOB}$
3	$r_{NO,ox} \cdot \frac{S_{NO}}{S_{NO}+K_{NO,ox}} \cdot \frac{S_{Mox}}{S_{Mox}+K_{Mox}} \cdot X_{AOB}$
4	$r_{NO,red} \cdot \frac{S_{NO}}{S_{NO}+K_{NO,red}} \cdot \frac{S_{Mred}}{S_{Mred}+K_{Mred,2}} \cdot X_{AOB}$
5	$r_{O_2,red} \cdot \frac{S_{O_2}}{S_{O_2}+K_{O_2,red}} \cdot \frac{S_{Mred}}{S_{Mred}+K_{Mred,3}} \cdot X_{AOB}$
6	$r_{NO_2^-,red} \cdot \frac{S_{NO_2^-}}{S_{NO_2^-}+K_{NO_2^-}} \cdot \frac{S_{Mred}}{S_{Mred}+K_{Mred,4}} \cdot X_{AOB}$
7	$S_{Mred}+S_{Mox}=C_{tot}$